

AD-A042 917

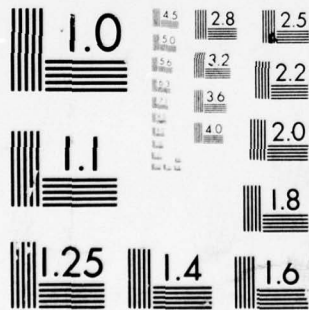
SYSTEMS RESEARCH LABS INC NEWPORT NEWS VA RASA DIV F/G 20/4
A THEORETICAL AND EXPERIMENTAL INVESTIGATION OF VORTEX FLOW CON--ETC(U)
DEC 76 R P WHITE, S T GANGWANI, J C BALCERAK N00014-74-C-0091
RASA/SRL-14-77-2 ONR-CR212-223-3 NL

UNCLASSIFIED

1 OF 2
AD
A042 917



0429



MICROCOPY RESOLUTION TEST CHART
NATIONAL BUREAU OF STANDARDS-1963-A

AD A 042917

12



A THEORETICAL AND EXPERIMENTAL INVESTIGATION OF
VORTEX FLOW CONTROL FOR HIGH LIFT GENERATION

Richard P. White, Jr.
Santu T. Gangwani
John C. Balcerak

RASA Division of
SYSTEMS RESEARCH LABORATORIES, INC.
1055 J. Clyde Morris Boulevard
Newport News, Virginia 23602



CONTRACT N00014-74-C-0091
ONR TASK 212-223
December 1976

Interim Report for the Period 1 January - 31 December 1976

Approved for public release; distribution unlimited.

DDC FILE COPY



PREPARED FOR THE

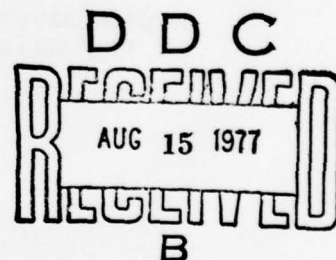
OFFICE OF NAVAL RESEARCH • 800 N. QUINCY ST. • ARLINGTON • VA • 22217



A THEORETICAL AND EXPERIMENTAL INVESTIGATION OF
VORTEX FLOW CONTROL FOR HIGH LIFT GENERATION

Richard P. White, Jr.
Santu T. Gangwani
John C. Balcerak

RASA Division of
SYSTEMS RESEARCH LABORATORIES, INC.
1055 J. Clyde Morris Boulevard
Newport News, Virginia 23602



CONTRACT N00014-74-C-0091
ONR TASK 212-223
December 1976

Interim Report for the Period 1 January - 31 December 1976

Approved for public release; distribution unlimited.



PREPARED FOR THE

OFFICE OF NAVAL RESEARCH • 800 N. QUINCY ST. • ARLINGTON • VA • 22217

Change of Address

Organizations receiving reports on the initial distribution list should confirm correct address. This list is located at the end of the report. Any change of address or distribution should be conveyed to the Office of Naval Research, Code 211, Arlington, Virginia 22217.

Disposition

When this report is no longer needed, it may be transmitted to other organizations. Do not return it to the originator or the monitoring office.

Disclaimer

The findings and conclusions contained in this report are not to be construed as an official Department of Defense or Military Department position unless so designated by other official documents.

Reproduction

Reproduction in whole or in part is permitted for any purpose of the United States Government.

19. REPORT DOCUMENTATION PAGE		READ INSTRUCTIONS BEFORE COMPLETING FORM	
1. REPORT NUMBER	2. GOVT ACCESSION NO.	3. RECIPIENT'S CATALOG NUMBER	
ONR CR212-223-3		(9)	
4. TITLE (and Subtitle)		5. TYPE OF REPORT & PERIOD COVERED	
A THEORETICAL AND EXPERIMENTAL INVESTIGATION OF VORTEX FLOW CONTROL FOR HIGH LIFT GENERATION.		Interim Report. 1 January - 31 December 1976	
7. AUTHOR(s)		6. PERFORMING ORG. REPORT NUMBER	
Richard P. White, Jr., Santu T. Gangwani John C. Balcerak		(14) RASA/SRL Report 14-77-2	
8. PERFORMING ORGANIZATION NAME AND ADDRESS		9. CONTRACT OR GRANT NUMBER(s)	
RASA DIVISION OF SYSTFMS RESEARCH LABORATORIES, INC. 1055 J. Clyde Morris Boulevard Newport News, Virginia 23602		(15) N00014-74-C-0091	
11. CONTROLLING OFFICE NAME AND ADDRESS		10. PROGRAM ELEMENT, PROJECT, TASK AREA & WORK UNIT NUMBERS	
Department of the Navy, Office of Naval Research Flight Vehicles Technology Division Vehicles and Propulsion Program, Code 211 Arlington, Virginia 22217		62241N RF 41-411-801 NR 212-223	
14. MONITORING AGENCY NAME & ADDRESS (if different from Controlling Office)		12. REPORT DATE	
(16) F41411		(11) December 1976	
		13. NUMBER OF PAGES	
		176 (12) 190	
		15. SECURITY CLASS. (of this report)	
		Unclassified	
		15a. DECLASSIFICATION/DOWNGRADING SCHEDULE	

16. DISTRIBUTION STATEMENT (of this Report)			
(17) RF41411801			
Approved for public release; distribution unlimited.			
17. DISTRIBUTION STATEMENT (of the abstract entered in Block 20, if different from Report)			
18. SUPPLEMENTARY NOTES			

19. KEY WORDS (Continue on reverse side if necessary and identify by block number)			
vortex lift vortex flow stall flow		wing-vortex interactions leading edge vortex generators	
20. ABSTRACT (Continue on reverse side if necessary and identify by block number)			
A theoretical and experimental program was conducted to investigate the effects of vortex flow control on the performance characteristics of a low aspect ratio, highly-swept lifting surface. Experimentally, it was determined that the lift-curve slope and the maximum lift coefficient could be increased above that of a basic planform by the use of leading edge separators.			
(over)			

409 781

red)

△ A theoretical prediction technique based on a modification of a doublet vortex lattice approach to account for flow separation and external interacting vortices was found to realistically predict the measured lifting characteristics of the airfoil at high angles of attack. Favorable correlation between measured and predicted results was shown both in the total lift and in the pressure distributions. The theoretical results suggest that modest refinements can make the analysis a versatile tool for the study of the performance and maneuverability characteristics of low aspect ratio aircraft at high angles of attack. ↗

SUMMARY

A theoretical and experimental program was conducted to investigate the effects of vortex flow control on the performance characteristics of a low aspect ratio, highly-swept lifting surface. Experimentally, it was determined that the lift-curve slope and the maximum lift coefficient could be increased above that of a basic planform by the use of leading edge separators. In addition, it was found that various planform changes could effect significant changes in the pressure distributions over the lifting surface by means of the strong vortex flows they created.

A theoretical prediction technique based on a modification of a doublet vortex lattice approach to account for flow separation and external interacting vortices could realistically predict the measured lifting characteristics of the airfoil at high angles of attack. Favorable correlation between measured and predicted results was shown both in the total lift and in the pressure distributions. The theoretical results suggest that modest refinements can make the analysis a versatile tool for the study of means by which the performance and maneuverability characteristics of low aspect ratio aircraft can be improved at high angles of attack.

ACCESSION for	
NTIS	White Section <input checked="" type="checkbox"/>
DDC	Buff Section <input type="checkbox"/>
UNANNOUNCED	<input type="checkbox"/>
JUSTIFICATION _____	
BY _____	
DISTRIBUTION/AVAILABILITY CODES	
Dist. AVAIL. and/or SPECIAL	
A	

FOREWORD

The work described in this technical report was performed by RASA Division of Systems Research Laboratories, Inc., for the Department of the Navy, Office of Naval Research, Arlington, Virginia under Contract Number N00014-74-C-0091. The research program was undertaken under the technical cognizance of Dr. Robert E. Whitehead of the Flight Vehicles Technology Division of ONR.

TABLE OF CONTENTS

REPORT DOCUMENTATION PAGE	ii
SUMMARY	iii
FOREWORD	iv
TABLE OF CONTENTS	v
LIST OF TABLES	vi
LIST OF ILLUSTRATIONS	vii
LIST OF SYMBOLS	xi
I. INTRODUCTION	1
II. DESCRIPTION OF MODEL AND INSTRUMENTATION	4
A. Model	4
B. Instrumentation	5
C. Performance and Pressure Measurements	6
III. WIND TUNNEL TESTS	8
IV. DEVELOPMENT OF THE THEORETICAL PREDICTION TECHNIQUE	9
V. DISCUSSION OF RESULTS	21
A. Experimental Performance and Pressure Data	21
B. Correlation of Predicted and Measured Results	40
VI. CONCLUSIONS AND RECOMMENDATIONS	45
VII. REFERENCES	47
VIII. APPENDIX - Balance Data for Various Configurations	137

LIST OF TABLES

<u>Table</u>		<u>Page</u>
I	SUMMARY OF TEST CONFIGURATIONS	49
II	GENERAL CLASSIFICATION OF TEST CONFIGURATIONS	51
III	SUMMARY OF DATA OBTAINED FOR THE TEST CON- FIGURATIONS	52

LIST OF ILLUSTRATIONS

<u>Figure</u>		<u>Page</u>
1.	Model Planform.	53
2.	Planforms of various test configurations.	54
3.	Coordinate system for balance measurements.	57
4.	Wind tunnel model installation (Configuration 7A shown)	58
5.	Lift coefficient vs angle of attack (Configuration 1)	59
6.	Drag coefficient vs angle of attack (Configuration 1)	60
7.	Pitching moment coefficient vs angle of attack (Configuration 1)	61
8.	Upper surface pressure coefficient vs semispan (Configuration 1, $\alpha = 13.1^\circ$)	62
9.	Upper surface pressure coefficient vs semispan (Configuration 1, $\alpha = 21.6^\circ$)	63
10.	Upper surface pressure coefficient vs semispan (Configuration 1, $\alpha = 27.7^\circ$)	64
11.	Lift coefficient vs angle of attack (Configuration 3A)	65
12.	Drag coefficient vs angle of attack (Configuration 3A)	66
13.	Pitching moment coefficient vs angle of attack (Configuration 3A)	67
14.	Upper surface pressure coefficient vs angle of attack (Configuration 3A, $\alpha = 13.1^\circ$)	68
15.	Upper surface pressure coefficient vs semispan (Configuration 3A, $\alpha = 13.1^\circ$)	69
16.	Upper surface pressure coefficient vs semispan (Configuration 3A, $\alpha = 26.1^\circ$)	70
17.	Lift coefficient vs angle of attack (Configuration 5C)	71

LIST OF ILLUSTRATIONS

<u>Figure</u>	<u>Page</u>
18. Drag coefficient vs angle of attack (Configuration 5C).	72
19. Pitching moment coefficient vs angle of attack (Configuration 5C).	73
20a&b. Upper surface pressure coefficient vs semispan (Configuration 5C, $\alpha = 13.1^\circ$)	74 75
21a&b. Upper surface pressure coefficient vs semispan (Configuration 5C, $\alpha = 21.7^\circ$)	76 77
22a&b. Upper surface pressure coefficient vs semispan (Configuration 5C, $\alpha = 26.1^\circ$)	78 79
23. Lift coefficient vs angle of attack (Configuration 6)	80
24. Drag coefficient vs angle of attack (Configuration 6)	81
25. Pitching moment coefficient vs angle of attack (Configuration 6)	82
26a&b. Upper surface pressure coefficient vs semispan (Configuration 6, $\alpha = 13.1^\circ$)	83 84
27a&b. Upper surface pressure coefficient vs semispan (Configuration 6, $\alpha = 17.4^\circ$)	85 86
28a&b. Upper surface pressure coefficient vs semispan (Configuration 6, $\alpha = 21.7^\circ$)	87 88
29a&b. Upper surface pressure coefficient vs semispan (Configuration 6, $\alpha = 26.1^\circ$)	89 90
30. Lift coefficient vs angle of attack (Configuration 9C-1).	91
31. Drag coefficient vs angle of attack (Configuration 9C-1).	92
32. Pitching moment coefficient vs angle of attack (Configuration 9C-1).	93
33a&b. Upper surface pressure coefficient vs semispan (Configuration 9C-1, $\alpha = 13.1^\circ$)	94 95

LIST OF ILLUSTRATIONS

Figure	Page
34a&b. Upper surface pressure coefficient vs semispan (Configuration 9C-1, $\alpha = 17.4^\circ$)	96 97
35a&b. Upper surface pressure coefficient vs semispan (Configuration 9C-1, $\alpha = 21.7^\circ$)	98 99
36a&b. Upper surface pressure coefficient vs semispan (Configuration 9C-1, $\alpha = 26.1^\circ$)	100 101
37. Lift coefficient vs angle of attack (Configura- tion 19).	102
38. Drag coefficient vs angle of attack (Configura- tion 19).	103
39. Pitching moment coefficient vs angle of attack (Configuration 19).	104
40a&b. Upper surface pressure coefficient vs semispan (Configuration 19, $\alpha = 13.1^\circ$)	105 106
41a&b. Upper surface pressure coefficient vs semispan (Configuration 19, $\alpha = 17.4^\circ$)	107 108
42a&b. Upper surface pressure coefficient vs semispan (Configuration 19, $\alpha = 21.7^\circ$)	109 110
43a&b. Upper surface pressure coefficient vs semispan (Configuration 19, $\alpha = 26.1^\circ$)	111 112
44a&b. Upper surface pressure coefficient vs semispan (Configuration 20, $\alpha = 12.0^\circ$)	113 114
45a&b. Upper surface pressure coefficient vs semispan (Configuration 20, $\alpha = 20.0^\circ$)	115 116
46a&b. Upper surface pressure coefficient vs semispan (Configuration 20, $\alpha = 24.0^\circ$)	117 118
47. Effect of vortex induced velocities on angle of attack.	119
48. Comparison of measured and predicted lift coef- ficient vs angle of attack.	120
49. Predicted vortex geometry, $\alpha = 19.4^\circ$	121

LIST OF ILLUSTRATIONS

<u>Figure</u>	<u>Page</u>
50. Tuft flow visualization, $\alpha = 19.4^{\circ}$	122
51a-e. Comparison of measured and predicted spanwise pressure distribution at (5%) (10%) (15%) (20%) (40%) chord, $\alpha = 19.4^{\circ}$	123- 127
52. Predicted vortex geometry, $\alpha = 27.7^{\circ}$	128
53. Tuft flow visualization $\alpha = 27.7^{\circ}$	129
54a-g. Comparison of measured and predicted spanwise pressure distributions at (5%) (10%) (15%) (20%) (25%) (40%) (70%) chord, $\alpha = 27.7^{\circ}$	130- 136

LIST OF SYMBOLS

α	Angle of attack of wing
A_{mnij}	Influence coefficient of box mn with respect to box ij
B_{mnj}	Influence coefficient of box mn with respect to wake element j
C_c	Empirically obtained crossflow coefficient
C_D	Drag coefficient
C_L	Lift coefficient
C_M	Moment coefficient
C_{pu}	Static pressure coefficient on the upper wing surface (theoretical)
C_{pl}	Static pressure coefficient on the lower wing surface (theoretical)
C_{PU}	Static pressure coefficient on the upper wing surface (experimental)
D_{ij}	Doublet strength at box ij of the wing
D_j^m	Strength of jth element of wake vortex number m
h	Vertical displacement of the vortex relative to upper surface of the wing
h_∞	A parameter describing the initial position of the vortex and it is obtained empirically
r	Characteristic length parameter in coordinate transformation
l_{mn}	Local lift at box mn
l_c	Local lift of stalled box
n	Unit vector normal to the wing surface
N	Number of boxes representing the wing surface
p	Static pressure
P_n	Pressure measured at wing surface pressure tap
P_s	Static pressure at the tunnel centerline

P_t	Tunnel total pressure
p_∞	Free stream static pressure
q	Dynamic pressure
r	Radial coordinate
r_c	Vortex core radius
r_1	Dummy integral variable
U	Free stream velocity
U_{mn}	Velocity at box mn on wing in the free stream direction
V	Velocity on the surface of the wing in the vicinity of vortex along an axis parallel to the vortex centerline
V_c	Axial velocity at the centerline of vortex
V_ϕ	Swirl velocity due to vortex
V_∞	Free stream velocity
\vec{V}	Velocity vector
W_{mn}	Induced velocity component normal to wing surface at box mn
x, y, z	Cartesian coordinate system fixed to the wing
X, Y, Z	Modified Cartesian coordinate system
α	Geometric angle of attack of wing
α_a	Aerodynamic angle of attack
α_{mn}	Geometric angle of attack of box mn
Γ	Circulation strength of interacting vortex
Γ_k^p	Circulation of kth element of wake vortex number p
ΔC_p	Suction pressure coefficient in the vicinity of vortex
ΔC_{pv}	Total pressure coefficient
ΔP	Pressure difference
ϕ	Velocity potential
Φ	Modified velocity potential
ρ	Density of air

I. INTRODUCTION

A three-year research program was conducted to investigate the feasibility and practicality of using controlled vortex flows to improve the performance characteristics of low aspect ratio swept wing fighter-type aircraft. In the first year's effort, the research program was theoretical, and investigated the feasibility of improving the aerodynamic lift and drag characteristics of a highly loaded lifting surface through the use of appropriately located line vortices (Reference 1). A simplified analytical model was developed which included both the near-field pressure and far-field downwash/upwash, wing-vortex interaction effects. On the basis of the simplified model, it was concluded that vortices generated in the pressure field of a lifting surface would be more efficient in producing incremental lift than free vortices. This result stemmed from the observation that the suction field generated by wing-vortex interaction with vortices generated in the pressure field was far greater than that associated with an isolated vortex of the same strength.

As also described in Reference 1, the vortex interaction effects for the noted vortex generating devices were not always beneficial at low angles of attack, but when the basic wing began to stall, the vortex suction lift increased markedly with further increase in angle of attack. This phenomenon was attributed to the fact that at low angles of attack where unseparated potential flow exists, the vortex interaction effects were dominated by the induced effects of the vortex. At angles of attack above stall, the vortex flows are stronger, and the suction effect begins to dominate. In view of the positive aspects of the theoretical research, an experimental program was conducted in the second year in order to verify whether the potential

benefits predicted by the theoretical model were realizable and to obtain data which could be used to remove the limitations associated with the vortex model. In this experimental program, a 1/4-scale model typical of an F-4 wing planform was tested with various vortex-generating devices such as snags and strakes either singly or in combination.

The results of the second year's effort (Reference 2) demonstrated that the maximum lift coefficient of the wing with the various vortex generating devices could be increased significantly over that of the basic wing. The most significant effect was demonstrated by the addition of a strake at the wing root. While the vortex generated by the strake did not have a large lifting effect by itself, it effected a significant increase in the suction effect of the leading edge vortex. The addition of a snag farther outboard on the surface in combination with the strake resulted in a further beneficial change in the performance characteristics.

In the theoretical aspects of the program, the analysis of the experimental pressure and flow-visualization data showed that the simplified wing-vortex interaction model developed during the first year's effort would be totally inadequate in representing the observed phenomena, as the flow field was much more complex than originally assumed. Thus, although the simplified vortex interaction model was adequate qualitatively, it did not possess the capability to predict the effects of multiple vortex interactions and their effects on the lifting surface.

From the effort that was conducted through the second year, it was evident that insofar as the experimental aspects of the phenomena were concerned, an apparent limit had been reached on the maximum lift coefficient that could be attained by the vortex flow-control devices attached near the wing root. Thus, further improvements in the performance

capabilities would need to be achieved by modifying the flow characteristics over the outboard wing sections. As regards theoretical aspects, it was evident that a more sophisticated representation of the flow field would be required to represent the detailed effects of the interacting multi-vortex flows adequately. Thus a two-pronged effort was undertaken in the third year of the program whose objectives were to (1) experimentally investigate whether changes could be effected in the lift-curve slope of the lifting surface and whether the flow on the outboard section of the lifting surface could be stabilized and (2) theoretically represent the complex flow field over the lifting surface in a more comprehensive, yet concise manner. The results of this third year of effort are the subject of this report.

II. DESCRIPTION OF MODEL AND INSTRUMENTATION

A. Model

The panel model used in the experimental program was similar in geometry to the F-4 Phantom wing planform, but had no outboard dihedral. A detailed description of the model construction is given in Reference 1. A planform sketch of the basic model with the root strake, listing dimensional data is shown in Figure 1, while planform sketches of the various types of configurations derived by retrofit vortex flow generation devices to this planform are shown in Figure 2. Table I lists a brief description of each of the test configurations and Table II presents a classification of the configurations based on the types of vortex flow devices utilized, that is, strakes, separators or combinations thereof.

The root strake consisted of a triangular-shaped leading edge extension. The base of the triangular strake increased the root chord of the basic planform by 38%, and its leading edge was swept 75% with respect to the free stream. The outboard strakes were geometrically similar to the root strakes and the base chord of the strakes also comprised 38% of the local coincident chord of the basic wing planform. As noted in Table I, some configurations were devised in which the strakes were shifted spanwise or inverted such that these configurations comprised exceptions to these general test configuration parameters. None of these configuration showed any significant results, and only limited data were obtained for them (see Table III).

In addition to the strakes, the other type of leading edge vortex flow control device utilized was a leading edge separator plate. The separators were a flat plate extension with a sharp leading edge which, in general, extended the

local chord by 5% along the entire leading edge or a fraction of it. In two cases (Configurations 19 and 20) the separators extended the leading edge by 10 to 15 percent, respectively.

Pressure taps were installed at 220 locations on one side of the panel model. The locations of the pressure taps are shown and listed in Reference 1. For the purpose of this report, the detailed upper surface pressure data were plotted versus the semispan along constant chordlines. As listed in Table III, only limited pressure data were obtained for some of the test configurations for the reasons discussed in Section III of this report.

B. Instrumentation

Forces and moments on the semispan model were measured by a six-component, yoke-type balance located beneath the floor of the test section at the University of Maryland wind tunnel facility (Reference 3). The balance measurements were monitored on-line prior to off-line computer processing into the lift, drag, and side force, and the pitch, roll, and yawing moment coefficients. The forces and moments were resolved into a wind-axes coordinate system. The pitching moment was taken about an axis which passed through the quarter chord line of the mean aerodynamic chord, and the rolling and yawing moments were taken about the wing root. A sketch of the coordinate system is shown as Figure 3.

The pressure at the 220 pressure taps located on the semispan model were recorded from pressure transducers housed in five 48-port scanivalves. Three ports on each scanivalve monitored the tunnel total, static and tunnel centerline static pressures. The pressure transducers were calibrated in the range of $\pm 2.5 \text{ lb/in}^2$. The pressure measurements were recorded on punched cards and were converted to coefficient

form, $\Delta P/q$. as follows:

$$\Delta P/q = (P_S - P_n) / |P_t - P_S|$$

where P_S is the static pressure at the tunnel centerline, P_n is the pressure measured at each port and P_t is the tunnel total pressure.

Flow visualization of the vortex flow was provided by tufts and the helium-bubble technique (cf. Reference 4). Although the helium-bubble technique has generally provided a good qualitative description of the external flow field, it was not adequate in visualizing the flow next to the wing surface. Therefore to obtain indication of the flow characteristics over the surface of the wing, tufts were mounted on the upper surface of the model at each of the pressure tap locations, and photographs of the surface flow field as depicted by the tufts were taken at various angles of attack for configurations noted in Table III.

C. Performance and Pressure Measurements

The balance system at the University of Maryland Wind Tunnel has the following accuracy:

Lift	± 0.5 lb
Drag	± 0.1 lb
Side Force	± 0.2 lb
Pitching Moment	± 0.2 ft-lb
Rolling Moment	± 0.2 ft-lb
Yawing Moment	± 0.2 ft-lb

Corrections were applied to the balance measurements to account for wind tunnel wall and blockage interference effects according to the following relationships, which were derived from References 5 and 6.

$$\begin{aligned}
 \alpha &= \alpha_m + 1.57008 C_L \\
 C_D &= C_{D_M} + 0.02247 C_L^2 \\
 C_M &= C_{M_m} + 0.004646 C_L
 \end{aligned}$$

The performance data in this report have been non-dimensionalized with their respective planform area and have been modified by the "standard" wind tunnel wall and blockage interference corrections as noted above. Further appropriate corrections to the data as described in Reference 2 were not made as the tests were conducted primarily on a comparative basis of a given configuration versus a reference configuration.

For the pressure measurements, the transducers in each scanivalve were calibrated against the central manometer system of the University of Maryland Wind Tunnel. The wind tunnel total, static and the centerline static pressure were monitored from three ports in each scanivalve. The normal sensitivity of the pressure measurement system yielded a resolution of $\Delta P/q = \pm 0.01$. Since the system measures the steady pressures instantaneously, the mean rms pressures may not always be measured, particularly for stalled flow.

III. WIND TUNNEL TESTS

The model was installed in the wind tunnel such that the vertical centerline of the wind tunnel passed through the quarterchord of the mean aerodynamic chord (see Figure 4). Figure 4 is a photograph showing the installation of a double-strake configuration with a full span separator plate (Conf. 7A).

As described in Reference 2, consideration was given to the effects of Reynolds number and model asymmetries in the test program, and neither of these parameters were found to have any significant effect on the results. The current tests were conducted at a nominal Reynolds number of 2.5×10^6 based on the wing MAC and a nominal dynamic pressure of 12 lbf/ft^2 . The primary purpose of the test program conducted under this phase of the research effort was to try to further enhance the performance characteristics of the more promising configurations tested previously. In this approach, variations in this test program were made primarily to Configuration 3A of Reference 2. These variations consisted of the inclusion of additional leading edge strakes and/or in leading edge separator plates so as to improve the performance characteristics of the lifting surface at lower angles of attack. In the first part of the test program a series of configurations were tested to determine their performance characteristics in comparison to those of Configuration 3A. Limited pressure data were also obtained for these configurations. These data were along the 5 and 10 percent chord lines of the model, and some at the 15 percent chordline. From these initial tests, the most promising configurations were selected for detailed pressure surveys over the entire planform of the lifting surface and for flow visualization studies. A description of the configurations selected for detailed testing is given in Table III and sketches of the configurations are shown in Figure 2.

IV. DEVELOPMENT OF THE THEORETICAL PREDICTION TECHNIQUE

In the last decade, the prediction of aerodynamic loads on lifting surfaces of various shapes by lifting surface theory has been developed rather extensively (e.g. References 7, 8, and 9). The simplest lifting surface methods for predicting aerodynamic loads are limited to flows at low angles of attack (linear methods). In these cases, the lattice representing the surface (and the wake, if the wake effects are included) consists of elements which are parallel and normal to the free-stream velocity. In the nonlinear methods, this constrained representation is relaxed so as to account for leading edge and tip vortex systems. Nonlinear lifting surface methods vary in their formulation principally (1) in the method of satisfying the no-flow conditions, (2) of accounting for the detailed effects of vortex flows, (3) of applying separation criteria, and (4) in the aerodynamic representation of separated flow regions.

The complexity with which the nonlinear prediction of aerodynamic loads on a lifting surface are formulated can be based on several considerations. For the application to swept, low-aspect ratio lifting surfaces being considered herein, the formulation was governed by two major considerations, namely; (1) the inclusiveness of the pertinent flow phenomena at high angles of attack, and (2) a directed simplicity for practical use and application. Under these considerations, the analysis for predicting the effect of vortex flows over the lifting surface that was formulated is an extension of that developed in References 10 and 11. The

formulation differs from most contemporary nonlinear methods for predicting aerodynamic loads on lifting surfaces (e.g. Reference 12) in that it includes the suction effect of the free vortices and accounts for vortex bursting and lift due to separated flow. Briefly, the analysis considers the following force components that make up the total lift of the wing: potential flow lift, crossflow lift and suction lift. In the potential flow regions of the lifting surface, a doublet-lattice method is utilized for computing the lift, and the no-flow boundary conditions are satisfied over the mean-cambered plane of the airfoil. In the crossflow regions of the lifting surface where the flow is fully separated, the lift is computed in terms of the components of the normal force acting on the crossflow region. Once the vortex locations, with respect to the lifting surface have been determined, the spatial distribution of the vortex suction lift is computed by determining the suction pressure required to balance the centrifugal force of the swirling vortex flows and adding those pressures to those suction pressures developed by the axial flows. The analysis can account for up to six vortices, each of which can interact with the others and the wing surface in reaching an equilibrium position in space. This phase of the analysis obviously involves an iterative solution in which the primary unknowns are: (1) the circulation strengths and the spatial positions of the vortices, (2) regions of potential flow and (3) regions of separated flow.

The wing was modeled by representing the lifting surface by 100 boxes having ten equally spaced segments both along the chord and span of the surface. In this representation, regions of potential and separated flow are mutually exclusive, while the vortex suction effect is superposed on each region. A description of the predictive technique developed

for each of the three types of lift will be presented in the following paragraphs. Following this discussion a description of the manner by which these separate predictive techniques were combined to yield the total analysis procedure as a computer program will be given.

(1) Potential Flow Analysis

The potential flow field is assumed to be replaced by a distribution of doublets of strength

$$D(X, Y, Z) = \phi_u - \phi_\ell \quad (1)$$

corresponding to the discontinuity in the modified velocity potential over the appropriate region of the lifting surface. For convenience, the modified potential ϕ and the modified coordinate X, Y, Z are related to the coordinates x, y, z as follows

$$x = \ell X; \quad y = \ell Y; \quad z = \ell Z \quad (2)$$

and the velocity potential ϕ (excluding the effects of compressibility) by

$$\phi(x, y, z) = U\ell\phi(X, Y, Z) \quad (3)$$

where ℓ is a reference length which is taken as the semispan of the lifting surface and U is the free-stream velocity, and where the vertical coordinate is included to account for the effects of camber.

Since $\phi(x, y, z)$ is a solution of Laplace's equation

$$\nabla^2 \phi = 0 \quad (4)$$

it is obvious that ϕ is also a solution of Laplace's equation, that is

$$\nabla^2 \phi = 0 \quad (5)$$

Equation (4) is based on potential flow theory which implies that the velocity vector \vec{V} can be expressed by the gradient of a velocity potential ϕ , that is,

$$\vec{V} = \vec{\nabla} \phi \quad (6)$$

Equation (4) is obtained by combining the continuity equation $\vec{\nabla} \cdot \vec{V} = 0$ with Equation (6). Since the doublet strength $D(X, Y, Z) = \phi_u - \phi_l$, the solution of the problem consists in the determination of a modified velocity potential $D(X, Y, Z)$ by solving Equation (5) in conjunction with the boundary condition on the airfoil which requires flow tangency over its surface.

The numerical procedure involved in applying this theory to the lifting surface consists in dividing the surface into a number of appropriately shaped boxes. While the shape and the number of these boxes is arbitrary, as will be noted later, the boxes should be concentrated in regions where three-dimensional flow gradients are large so as to represent the flow field more adequately in these regions.

The magnitude of the doublet strength D over each box is assumed to be uniform. The total velocity induced perpendicular to the surface at a box consists of that due to the vorticity of all other boxes on the surface, the effects of the concentrated vortices (such as the leading edge vortex, strake vortex, tip vortex, etc.) and that due to all the vorticity in the wake starting at the trailing edge or at the point of separation from the lifting surface. When the flow

tangency requirements on the surface are satisfied, the problem of calculating the doublet strengths is reduced to one of solving a set of N linear equations, where N is the number of boxes on the lifting surface. Specifically, if A_{mnij} is the aerodynamic influence coefficient at the center of the box mn due to the effect of the box ij and its image, and if B_{mnj} is the aerodynamic influence coefficient at the box mn due to the wake trailer j and its image, then the normal component of velocity induced at box mn by the doublet distribution over the lifting surface D_{ij} and by its wake D_j^W is

$$w_{mn} = \sum_i \sum_j A_{mnij} D_{ij} + \sum_j B_{mnj} D_j^W \quad (7)$$

where A_{mnij} and B_{mnj} are evaluated by Biot-Savart's law.

When the geometry of the wake (including the concentrated vortices) is known, B_{mnj} can be evaluated directly. In general, the strength of the wake D_j^W is not known explicitly but is computed simultaneously with the lifting surface loads. Therefore, D_j^W can be expressed in terms of unknown D_{ij} of the lifting surface. For example, the strength the wake elements starting at the trailing edge can be expressed in terms of D_{ij} of the trailing edge boxes, by application of Kutta condition at the trailing edge. Similarly, the D_j^W of the various segments of the leading edge vortex may be expressed as the linear combination of the D_{ij} corresponding to the leading edge boxes by application of a simplified rollup assumption. Thus the second term on the right hand side of the Equation (7) involves the same unknowns (D_{ij}) as the first term.

Where both the strength and geometry of the wake elements are known at the conclusion of an iteration loop, the second term on the right hand side of the Equation (7) can be computed directly.

The total free-stream velocity relative to the wing surface at box mn is defined as U_{mn} . If α_{mn} is the geometric angle of attack with respect to U_{mn} , then the tangential flow condition requires that the total induced velocity perpendicular to the surface be equal and opposite to $U_{mn} \sin \alpha_{mn}$, or

$$\vec{\nabla} \phi \cdot \hat{n} = U_{mn} \frac{\partial D}{\partial Z} = U_{mn} \sin \alpha_{mn} \quad (8)$$

where \hat{n} is a unit vector normal to the surface at box mn . Combining Equations (7) and (8) yields the following relationships:

$$U_{mn} \sin \alpha_{mn} = \sum_i \sum_j A_{mnij} D_{ij} + \sum_j B_{mnj} D_j^w \quad (9)$$

Once the solution of the simultaneous Equation (9) is obtained, the lift at any box is given by

$$l_{mn}(X, Y, Z) = \rho U_{mn}^2 \frac{\partial D}{\partial X} \quad (10)$$

and the total (potential) lift is obtained by summing the local lift over all the boxes.

(2) Separated Flow Analysis

When the flow field is separated, the lift can no longer be computed from the doublet lattice potential flow analysis of (1) above. The criterion used for determining whether separation has occurred is a comparison of the net aerodynamic angle of attack (the geometric angle of attack minus the induced angle of attack) versus an empirically defined angle of attack above which the section is assumed to be stalled. Specifically, the angle α_a is determined at each control point mn on the wing surface from the

following relation:

$$U_{mn} \sin \alpha_a = U_{mn} \sin \alpha_{mn} - \sum_p \sum_k B_{mnk}^p D_k^p \quad (11)$$

where α_{mn} is the geometric angle of attack of the wing. The evaluation as to whether or not separation has occurred is conducted on a box-by-box basis so that at various geometric angles of attack, the lifting surface may have different regions of separated flow. If a control box is determined to be separated on the basis of this criterion, the lift is computed from the expression

$$l_c = C_c \cdot 1/2 \rho U^2 \sin \alpha \quad (12)$$

where C_c is usually considered in the range of 0.8 to 1.3 depending on the location of the control box with respect to a free edge.

(3) Vortex Suction Lift

Suction lift is the component of the lift which results from the low pressure region within the vortices when they are in proximity of a lifting surface. When the force-free positions of vortices are determined, this component of lift is superimposed on the potential and separated flow lift components to obtain the total loading distribution over the wing.

If (ΔC_p) is the suction pressure on the wing surface in the vicinity of the vortex due to the swirl velocity V_ϕ ,

$$(\Delta C_p)_{\text{swirl}} = (p_\infty - p) / \frac{1}{2} \rho V_\infty^2 \quad (13)$$

Then, based on quasi-cylindrical assumption, it can be easily shown that

$$(\Delta C_p)_{\text{swirl}} = V_\phi^2 / V_\infty^2 \quad (14)$$

This is an approximate result obtained from the relation

$$p = p_\infty - \int_r^\infty \rho \frac{V_\phi^2(r_1)}{r_1} dr_1 \quad (15)$$

by assuming a Rankine vortex swirl velocity distribution for the isolated vortex and utilizing the method of images to satisfy the condition of no flow on the mean chordline of the wing.

The effect of the variation of axial velocity within the vortex on the suction pressure peaks must also be determined. The variation in axial velocity in the core can be determined by utilizing conservation of mass and the appropriate variation in core diameter of the vortex. Bernoulli's equation is utilized for this computation. If p_v is the pressure on the wing surface in the vicinity of vortex (but outside the vortex core where most of the viscous effects are confined) and p_s is the static pressure, the following relationship can be written

$$\frac{p_s - p_v}{\frac{1}{2} \rho V_\infty^2} = \frac{V_\phi^2}{V_\infty^2} + \frac{V^2 - V_\infty^2}{V_\infty^2} \quad (16)$$

In equation (16) V is the axial velocity on the surface of the wing due to the axial flow in the vortex.

$$\text{If } \Delta C_{pv} = \frac{P_s - P_v}{\frac{1}{2}\rho V_\infty^2} \quad (17)$$

the following relationship results

$$\Delta C_{pv} = \frac{V_\phi^2}{V_\infty^2} + \frac{V^2 - V_\infty^2}{V_\infty^2} \quad (18)$$

The axial velocity at the center of the Vortex V_c is a function of the strength of the vortex (Γ), core radius of the vortex (r_c), and the relative distance of vortex from the wing (h). Since Γ , r_c , and h , in general, vary along the lengths of the vortex, the axial flow at each segment of the vortex has to be determined. A simple balance of momentum due to axial flow and momentum of the vortex with respect to wing results in the following expression

$$V_c = V_\infty + \frac{\Gamma(h_\infty - h)}{\pi r_c^2} \quad (19)$$

Here h_∞ is a constant related to the vortex and has to be established empirically. A preliminary estimate of h_∞ indicates it is a function of the angle of attack. Also, for the present analysis, the point at which the vortex bursts is dependent on the value of h_∞ . In Equation 19 it is assumed that the radial distribution of axial velocity varies as e^{-r^2/r_c^2} . Thus, V can be obtained at any point of the wing surface once V_c is obtained from Equation (19).

The amount of vortex suction achieved (Equation 18) is very strongly dependent on the axial flow in the core of the vortex besides the strength of the vortex. The magnitude of the vortex core axial flow and the subsequent computation of the suction pressure peaks were found to be very sensitive to the distance of the vortices from the wing surface. Therefore, it became necessary to include the thickness and curvature of the airfoil for the correct determination of these suction pressure peaks.

The analysis described above for the computation of wing loads in the presence of vortices includes some additional features which are summarized below.

(4) Force-Free Positions of Vortices

For the computation of the correct pressure distributions over the surface of a wing in the presence of vortices, it is essential that the force-free positions of the vortices be determined. In the present analysis, control points are described along the length of each of the vortices. At each of these control points the following components of velocities are predicted:

- a. the velocities induced by the distribution of bound circulation,
- b. the self-induced velocities due to vortex curvature,
- c. the free-stream velocity, and
- d. the axial velocity in the vortex core.

Since a force-free vortex allows for only the flow along its axis, the vortex is considered stationary when this condition is satisfied. It is obvious that since these above velocity components are dependent upon the unknowns being solved for, the force-free position of the vortices must be determined in an iterative manner.

(5) Vortex Bursting

The phenomenon of vortex bursting is included in the present analysis using a simple criterion that is, a vortex is assumed to have burst when there is a velocity defect at the center of the vortex.

With respect to equation (19), a vortex is assumed to burst when h is greater than h_{∞} . This simple criterion appears to agree reasonably well with the experimental observation of the leading edge vortex bursting.

A computer program was written for the analysis outlined above to predict the pressure distributions and the total lift developed by the low aspect ratio wing-strake configuration that was tested in the wind tunnel at moderate to high angles of attack. Since the analysis is directed toward the prediction of lift at moderate to high angles of attack, it must consider the mixed potential-separated and vortex flows over the surface of the wing. In general, the wing-vortex system represented by the computer program allows for six vortices over the surface of the wing, but the program was exercised using three vortices; that is, the strake vortex, the leading edge vortex, and the tip vortex. The primary unknowns in the solution were the circulation strengths at each of the control points and the force-free positions of the vortices.

For the predictions that were undertaken, the lifting surface was divided into 100 boxes obtained by partitioning the surface into ten equal percentage fractions of the chord and span. Initially, the magnitude of the doublet strength at each control point was assumed, as well as the force-free positions of the vortices. In the procedure, the aerodynamic influence coefficients A_{mnij} (Equation 7) were computed by using Biot-Savart's law, and each of the free vortices was represented by a finite number of segments. The strengths Γ_j^p of the various free vortex elements are expressed in terms of the unknowns Γ_{mnij} at the edges of the wing. Thus, inclusion of the free vortices does not introduce any additional unknowns. As the positions of the free vortices are known (either from initial estimates or from the computation within an iteration loop), the influence coefficients B_{mnj} are also computed using Biot-Savart's law. At each control point a test is made to determine whether the flow is separated.

The flow is considered to be separated on the basis of the relation given in Equation (11). If α_a in Equation (11) exceeds the assumed (input) stall angle at any control point, the box corresponding to that control point is considered separated and Γ_{ij} corresponding to that box is taken to be zero in the set of Equation (7). The pressure coefficients are then determined at the separated flow points by using empirically derived cross-flow force coefficients.

Once the circulation strengths of the doublet lattice system on the lifting surface (and hence the circulation strengths of the free vortices) as well as the force-free positions of the free vortices are determined from the iterative solution of the equations, the component of lift due to the suction effect of the free vortices is superimposed on the potential and separated flow component of lift.

V. DISCUSSION OF RESULTS

A. Experimental Performance and Pressure Data

Table III summarizes the data that were obtained for each of the configurations that were tested. The configurations listed in the upper half of the table are those which will be discussed in more detail in this report. Table II lists the configurations tested by general classifications. From these classifications the discussion of results will concentrate on the results obtained with the following configurations: single strake, double strake, single strake with leading edge separator plate and a partial leading edge plate.

The experimental research program that will be discussed herein had a two fold approach (1) to obtain some quantitative results on the effects of vortex control devices and (2) to gain further insight into the controlling parameters which effect positive vortex generation and interaction with a lifting surface at high angles of attack.

As the experimental program developed, greater emphasis was placed on the latter purpose as the additional predesigned configurations for which quantitative data was to be obtained did not yield positive benefits much greater than those which had been tested previously (Reference 2). Since the reasons for this lack of additional benefits were determined early during the test program, various configuration changes were quickly constructed from sharp edge flat plates and tested to evaluate vortex configurations that might provide additional benefits if they were incorporated with smooth aerodynamic section profiles. Therefore, much of the quantitative data that will be presented for these additional configurations should be evaluated primarily on the basis of the vortex flow field that was generated and not on the absolute magnitude of the balance forces and pressure distributions.

(1) Previous Test Results

In order that the reader might fully understand the approach of choosing the various configurations for test during the present program, a brief review of some of the pertinent results obtained during the preceding year will be presented first to provide the proper background. It is noted that the previously obtained results, as well as all the new results presented in this report, have been non-dimensionalized by the planform area for the configuration for which the data is presented.

During the previous test program conducted under this contract, various wing-strake-snag configurations were tested to evaluate the effects of vortex flows generated by these modifications on the performance characteristics of the basic lifting surface at high angles of attack (Reference 2). Figures 5, 6 and 7 present the lift, drag and pitching moment characteristics respectively, for the basic low aspect ratio swept lifting surface that was used as the basic configuration during the research program.

From the results presented in Figures 5 and 6, no unusual lift-drag characteristics were noted for the basic 6% thick lifting surface over the angle of attack range for which data was obtained. As can be seen, a constant lift curve slope was obtained up to an angle of attack of approximately 15 degrees. At that angle of attack leading edge separation was initiated and as more of the airfoil stalled with increasing angle of attack, the slope of the lift curve decreased and became zero at an angle of attack of approximately 25 degrees at which a maximum C_L of 1.00 was obtained. As the angle of attack was increased further, the C_L decreased and the rate of increase of the drag with angle of attack decreased as might be expected (Figure 6). The variation of the pitching moment about the MAC of the basic lifting surface with angle of attack, however, (Figure 7) did indicate a somewhat unusual characteristic. At an angle of attack of approximately 13 degrees, the rate of increase of the pitching moment

with angle of attack showed a discontinuity that might not be expected. As previously noted, at this angle of attack the flow of the 6% thick swept lifting surface starts to separate at the leading edge. At an angle of attack of approximately 25 degrees, the rate of increase of the pitching moment is again approximately that which was measured in the angle of attack range of 0 to 13 degrees. Analysis of the pressure data taken over the surface of the wing indicated a reason for the unusual behavior of the pitching moment with angle of attack. Figure 8 presents spanwise plots, along constant chord lines, of the pressures over the basic lifting surface at an angle of attack of 13.1 degrees. On the basis of these pressure distributions and flow visualization, it was concluded that a weak leading edge vortex had formed as well as a small secondary vortex due to the flow separation along the leading edge. The peaks in the spanwise pressure distributions trace the path of the vortex across the lifting surface as shown in the insert. As shown in the sketch, it is estimated that the vortices burst at the 40 to 50% chord location. This location was chosen because of the radical drop in the peak pressure along the axis of the vortex. The formation of this leading edge vortex, although rather large and rather weak, formed a low pressure region on the leading edge ahead of the MAC thus creating a nose up pitching moment in opposition to the nose down pitching generated by the rest of the lifting surface. It is believed that the incremental nose up pitching moment generated by the leading edge vortex is the reason for the discontinuity in the pitching moment curve at this angle of attack.

At an angle of attack of approximately 22 degrees, the pressure distributions shown in Figure 9 indicate that the primary leading edge vortex has moved inboard on the lifting surface, has become better correlated, but turns into the

streamwise direction more rapidly and bursts earlier as indicated on the insert drawing. Because the pressure peaks due to the vortex are further forward from the MAC than they were at 13.1 degrees, due to the inward movement of the vortex, the incremental nose up pitching moment is larger. At an angle of attack of approximately 28 degrees however, the pressure distributions presented in Figure 10 indicate that the leading edge vortex has moved extremely far inboard and bursts soon after its formation thus minimizing its effects. It can also be seen from the data presented in Figure 10 that the entire lifting surface is completely stalled as indicated by an upper surface pressure coefficient $-C_p \approx 1.00$. At angles of attack higher than 28 degrees the C_L lift and pitching moment are primarily due to separated flow and thus the characteristic trend of the pitching moment with angle of attack as shown in Figure 7 would be expected.

The addition of a beveled edge highly swept flat plate strake to the root of the lifting surface radically altered the performance characteristics of the basic lifting surface as shown in Figures 11 through 13. It can be seen from the data presented in Figure 11 that the addition of the strake, while not effecting any change in the lifting characteristics of the basic wing below an angle of attack of 15 degrees, created a flow field that enabled the lifting surface to maintain almost a linear lift curve slope up to an angle of attack of approximately 28 degrees before abruptly stalling. The maximum C_L obtained by this configuration was approximately 45% greater than that of the basic lifting surface.

As would be expected, the drag also increased due to the increased lift, but not to the extent that might be expected (Figure 12). Because of this, the turning radius of an aircraft having the strake attached and operating at maximum power would be approximately 30% less than the basic wing configuration. Reference 2 has a fuller discussion of

this point. The pitching moment characteristics of the wing strake when compared to that of the basic wing (Figure 13), showed a similar and also a different characteristic than that of the basic wing.

As can be seen from the data presented in Figure 13, the similar characteristic is that at an angle of attack of approximately 13 degrees there is a discontinuity in the pitching moment curve. The different characteristic is that for angles of attack above 13 degrees, the slope of the pitching moment curve has a different sign for the wing strake configuration than it had for the basic wing. This trend of the data indicates that the leading edge vortex tends to dominate the pitching moment above an angle of attack of 13 degrees and at an angle of attack of approximately 30 degrees the pitching moment due to the vortices is approximately one and one half times the magnitude of that generated by the rest of the lifting surface.

The pressure distributions measured for this lifting surface configuration are shown at three angles of attack in Figures 14 through 16. It is noted that the pressure distributions measured at 13.1 degrees (Figure 14) are significantly different for the wing-strake configuration than they were for the basic wing. Analysis of the pressure distribution shows that the leading edge vortex is formed further out on the span than it was for the basic wing configuration and had the characteristic of a concentrated vortex instead of a diffused vortex like that generated by the basic wing. The strake vortex, while relatively weak at this angle of attack, is noticeable as it passes over the chord near the wing root. Since the presence of the strake moved the formation of the

leading edge vortex outboard, the strake vortex was too far removed to interact with the leading edge vortex. At an angle of attack of approximately 20 degrees the initial formation point of the leading edge vortex has moved inboard and the strength of the vortex has increased markedly (Figure 15). Due to the increased strength of the strake vortex at this angle of attack, its induced effect increases the angle of attack near the leading edge which is the reason the leading edge vortex is strengthened and is formed at a more inboard location. Since the two vortices (strake and leading edge) are in closer proximity to each other, their mutually induced effects change the paths of the vortices over the surface of the lifting surface.

As the angle of attack is increased to that at which the maximum C_L was obtained, the leading edge and strake vortices continue to be strengthened and to interact more noticeably. It can be noted from the pressure distributions presented in Figure 16 for an angle of attack of 26.1 degrees, that the peak suction pressure of the leading edge vortex is approximately 50% more than it was at an angle of attack of 20 degrees. It can also be seen that the strong interaction of the strake and leading edge vortices cause the strake vortex to sweep out the span and under the burst leading edge vortex as it crosses the chord.

It is apparent from the data presented in Figures 14 through 16 the manner by which the additional lift is obtained and why the pitching moment characteristics of the basic wing are altered so radically when the leading edge strake is added at the wing root. The increased lift is obviously due to the strong suction pressures generated by the vortices and the increasing nose up pitching moment with angle of attack is because these suction pressures are generated on the leading edge ahead of the MAC. It is also obvious from the

results that as the angle of attack increases, the leading edge vortex bursts sooner and more and more of the outboard section of the lifting surface becomes stalled.

It was hypothesized that if a similar type of vortex flow pattern could be generated over the outboard sections of the lifting surface as it had been over the inboard sections of the lifting surface, then it should be possible to obtain a higher C_L at a given angle of attack and a higher C_L maximum. In addition, if such a flow pattern could be established over the outboard wing sections aft of the MAC, the large variation in the pitching moment about the MAC could be minimized.

The experimental investigations conducted this last year were undertaken to determine if this could be accomplished by additional vortex generating and control devices. The remainder of the discussions of the experimental investigations that were conducted will present the results that were obtained for the various configurations that were tested in an attempt to generate a more favorable vortex flow pattern over the surface of the wing.

(2) Effect of Configuration Changes on Vortex Flows

As previously mentioned, in order to accomplish as many configuration changes as possible during a short tunnel test time and realizing that a primary intent of the program was to determine how best to generate the types of vortex flows that would be beneficial, it was decided to make the configuration changes by means of flat plate additions that had beveled leading edges. While it was realized that such an approach might cause undue separation over the airfoil surface and possibly degrade rather than enhance the performance characteristic, it was believed that as regards vortex flows, significant information could be obtained concerning the

effects of planform modification on the generation and interactions of the various vortices over the surface of the wing. A discussion of the results obtained with the various configurations follows:

(a) Multiple Strake Configurations

Since the root strake generated a favorable interaction with the leading edge vortex of the basic wing, an attempt to create similar flow pattern over the outer wing panel by means of an outboard strake seemed to be a logical approach. Strakes with the same leading edge sweep as the root strake were constructed for placement at the 50%, 60% and 68% span stations. The chordwise dimension of each strake was such that its relationship to the local wing chord was the same as the root strake had to the wing root chord. The root chord or inboard edge of the strake had a partial end plate that had zero height at the nose (point) and was tangent to the wing section contour where the strake was attached to the wing surface.

Figures 17 through 19 present the basic performance characteristics measured for Configuration 5c which had an additional strake located at the 68% span station. The results measured for this configuration are compared with Configuration 3A, the basic wing strake configuration. As can be seen from the data presented in Figures 17 through 19, the basic performance characteristics were almost identical for the two configurations. On the basis of these results it might be concluded that the outboard strake had no effect on the aerodynamic flow over the wing surface. Flow visualization studies of this configuration indicated however that a concentrated strake type leading edge vortex was formed as well as a very turbulent diffuse vortex about the inboard edge (root edge) of the strake. Comparison of the pressure distribution measured for this configuration at three angles

of attack (Figures 20 through 22) with those obtained for Configuration 3A (Figures 14 through 16) indicate that there are significant differences in the pressure distribution caused by the outboard strake. For example, at an angle of attack of 13.1 degrees, it is obvious that the effect of the vortex flow generated by the outboard strake moved the leading edge vortex inboard thus weakening it and turning it into the free stream sooner. The distribution of the suction pressures generated by the outboard strake vortex is also very apparent in the data presented in Figure 20 indicating that the outboard strake vortices had both a significant induced and suction effect over the outer wing span. While the additional vortex flows altered the distribution of loading, the total integrated loading was not altered except for the pitching moment about the MAC which was altered slightly due to the inward and thus forward movement of the leading edge vortex.

As the angle of attack was increased with Configuration 5c, the effect of the outboard strake vortex became less due to separation and bursting of the vortices and the pressure distributions were controlled by the root strake and leading edge vortices as they were with Configuration 3A. The corresponding pressure distributions were therefore almost identical (Figures 22 and 16) as were the integrated results.

On the basis of the results that were obtained with Configuration 5c when compared with those obtained with 3A, it was concluded that:

- (1) The slight increase in lift over the wing directly behind the outboard strake, due to the induced effects of the two vortices, was nullified by the loss in lift outboard and inboard of the strake which was due to induced effects of the two vortices of opposite rotation.

- (2) The induced flow effects of the outboard strake vortices moved the leading edge vortex inward and reduced its strength.
- (3) The outboard strake vortex field while generating additional lift over the outboard sections of the lifting surface due to suction effects, did not stabilize the flow in this same region so that a second leading edge vortex could be formed in the tip region of the airfoil; and
- (4) While the addition of a second strake redistributed the airfoil loading, the integrated performance results were not altered.

Inspection of the results obtained for the outboard strake located at other spanwise stations indicated that they were essentially the same as those that were presented and will therefore not be discussed.

(b) Leading Edge Separator Plate

Since, in addition to a minimum sweep angle, the formation of a leading edge vortex is due to local separation at the leading edge of the airfoil section, it was thought that if leading edge separation could be initiated at angles of attack lower than that at which the normal airfoil section started to separate, the leading edge vortex would form at lower angles of attack and would also be stronger. During the tests reported in Reference 2, the results obtained with a sharp edge flat plate snag indicated that such a beneficial flow mechanism might be realized. In order to evaluate this possibility a 5% chord sharp edge flat plate was attached to the leading edge of Configuration 3A. The performance results obtained for this configuration (Configuration 6) compared to those of Configuration 3A are presented in Figures 23 through 25. As indicated in Figure 23, additional lift

was generated in the angle of attack range of 5 to 22 degrees with the maximum increment of 17% occurring at an angle of attack of approximately 13 degrees, which is the angle at which the first beneficial effects of vortex flow was noted for Configuration 3A. At angles of attack above approximately 25 degrees however, the lift generated by Configuration 6 was less than that developed by 3A. This difference was probably due to the more extensive separation caused by the sharp edge plate at high angles of attack.

As might be expected in the angle of attack region, where additional lift was obtained, additional drag was also obtained (Figure 24). The pitching moment characteristics of Configuration 6, when compared to those measured for Configuration 3A, (Figure 25), indicate that the center of pressure of the vortex suction peaks is further forward at all angles of attack for Configuration 6 than it was for Configuration 3A. While an explanation for these significant changes in the performance characteristics is not apparent from the performance data, it is believed that one can be formulated by analyzing the pressure data presented for Configuration 6 in Figures 26 through 29. The spanwise pressure distributions shown in Figure 26 for Configuration 6 at 13.1 degrees angle of attack indicate that the flow field is dominated by the vortex flows generated by the lifting surface. In comparing these pressure distributions with those measured for Configuration 3A (Figure 14), it is apparent that the leading edge vortex is formed much further inboard and affects much more of the wing surface than it did for Configuration 3A at the same angle of attack. It is also noted that the leading edge vortex traverses the wing planform and interacts with the strake vortex far differently than it did with Configuration 3A. It is believed that the basic reason for this different behavior of the vortex flows is

that the separation caused by the leading edge separator plate not only initiates the formation of the leading edge vortex near the juncture of the strake but also angles the vortex centerline away from the leading edge. In addition, since the separator plate causes a more extensive leading edge separation, the forming vortex has characteristics more like a spiral vortex rather than that of a concentrated line vortex.

Because of the larger size of the leading edge vortex and the fact that its path has been moved inward, it interacts very quickly with the strake vortex to form a much larger single vortex. These three somewhat independent effects; early formation of the leading edge vortex, the sweeping aft of the vortex path, and the strong interaction of the leading edge and strake vortices, not only resulted in a stronger interaction of the vortices with the wing surface but also maintained this interaction over a larger portion of the wing surface than for Configuration 3A thus creating more suction lift.

As the angle of attack was increased with Configuration 6, the sweepback of the leading edge vortex became greater thus allowing it and the strake vortex to interact sooner. While these effects were beneficial at the lower angles of attack, they become detrimental at high angles of attack. At an angle of attack of 26.1 degrees for example, it can be seen from the pressure distributions (Figure 29), that the two vortices have combined into a single vortex near the leading edge of the lifting surface. This strong interaction has swept the weaker strake vortex under the stronger leading edge vortex raising it from the lifting surface and weakening the suction peak that is generated on the wing. In comparing the pressure distributions in Figure 29 for Configuration 6 with those of Configuration 3A in Figure 16 another detrimental aspect of the strong interaction of the leading edge

and strake vortex can be seen. For Configuration 6, the aft sweep of the combined vortices due to the strong leading edge separation caused by the flat plate has resulted in the lifting surface being completely stalled outboard of the 40-45% span because of the magnitude and direction of the induced effects of the combined vortices. For Configuration 3A, however, due to the forward location of the strong leading edge vortex, which is still independent of the strake vortex, the induced effect of the leading edge vortex tends to stabilize the flow over the wing in between the two vortices thus generating more lift in this area. In addition; because of the more outboard location and smaller sweepback angle of the leading edge vortex for Configuration 3A, complete flow separation over the wing does not occur inboard of the 70% span.

On the basis of the results obtained with a 5% chord sharp edge leading edge separator plate it was concluded that at low angles of attack beneficial vortex interaction was achieved in that the lift generated by the vortex suction effects was greater than that which was lost due to more of the wing surface being stalled. At high angles of attack, however, these same effects were detrimental as the additional lift obtained from the vortex suction effects was less than that which was lost due to more of the lifting surface being fully stalled due to the induced effects of the combined vortices. It is suggested that a much smaller leading edge separator plate might initiate the formation of the leading edge vortex at low angles of attack without generating such a large leading edge separation area which moves the vortex aft. If this could be accomplished, it might keep the leading edge and strake vortices separated at the high angles of attack and thus recover the lift lost with the current configuration.

(c) Combined Multiple Strake Leading Edge Separator Plate

In this configuration, the outboard strake of Configuration 5c was combined with the leading edge separator plate of Configuration 6 except that the separator plate from the outboard strake to the wing tip was eliminated. The integrated performance results for this configuration (Configuration 9C1) are presented in Figures 30 through 32. In comparing these results with those obtained for 5C (Figures 17 through 19) and those obtained for Configuration 6 (Figures 23 through 25), it can be seen that they correspond more to those of Configuration 6 than to those of Configuration 5C. In comparing the pressure distribution obtained for Configuration 9C1 (Figures 33 through 36) with those obtained for Configuration 6 it is noted that the distributions are nearly the same except for the suction pressures developed by the outboard strake, which were less than those developed by the same outboard strake of Configuration 5C. It is believed that the reduction in these pressure peaks was due to the flow separation of the separator plate which in turn caused an earlier separation of the outboard strake vortex.

(d) Extended Partial Leading Edge Separator Plate

The configurations that have been discussed previously had either local appendages added to the wing leading edge having two free edges, or had a continuous leading edge extension with no additional free edges. The last configuration to be discussed is one that had a leading edge appendage with only one free edge. This configuration was formulated by adding a beveled edge flat plate leading edge extension from the inboard strake to the 50% span station. The outboard edge of the leading edge extension was swept to the windstream at the same angle as the inboard strake (75 degrees). Two different leading edge extensions were tested, one with a 10% chord extension (Configuration 19) and the other with

a 15% chord extension (Configuration 20). The integrated performance results for Configuration 19 are presented in Figures 37 through 39. It can be seen from the data presented in Figure 37 that, like Configurations 6 and 9C1 (Figures 23 and 30 respectively), with respect to Configuration 3A, additional lift was obtained in the angle of attack range of approximately 10 to 25 degrees. While some lift was lost near C_L maximum, it was not as great with Configuration 19 as it was with Configuration 6 and 9C1. As with the other configuration, Configuration 19 had more drag than Configuration 3A in the angle of attack range over which the additional lift was obtained (Figure 38). The pitching moment characteristics presented in Figure 39 for Configuration 19 show that a significantly higher nose up pitching moment was generated by this configuration than for either Configurations 6 or 9C1 which indicates that the chordwise loading distribution was altered significantly by the partial leading edge separator plate. While, except for the pitching moment, the performance characteristics of Configuration 19 were not much different than they were for Configurations 6 and 9C1, the manner by which these characteristics were obtained were significantly different. Figure 40 presents the pressure distributions measured for Configuration 19 at an angle of attack of 13.1 degrees. It can be noted from the pressure distributions presented in Figure 40 that three distinct vortices have been formed by this planform configuration. The outboard vortex, formed by the loading discontinuity at the leading edge and strengthened by the induced effects of the leading edge vortex, seems to be the strongest of the three vortices. In comparing these pressure distributions and the paths of the vortices with those measured for Configuration 6 (Figure 26), it is noted that while the inboard strake and leading edge vortices combine in a very similar manner, the paths of the combined vortices over the surface of the wing

are significantly different. For Configuration 19 the outboard vortex turns the combined strake-leading edge vortex in the streamwise direction which causes it to burst and lose its beneficial suction effect. With Configuration 6, the combined vortex did not turn and burst and thus the suction effects of the combined vortex were obtained over more of the lifting surface. The loss in the suction lift from the combined vortex of Configuration 19 however, was partially made up by the suction effects of the outboard vortex.

As the angle of attack of Configuration 19 was increased, the inboard pair of vortices moved inboard as they mixed more rapidly and their combined strength increased in much the same manner as they did for Configuration 6. The outboard vortex seemed to decrease in strength and burst earlier with increasing angle of attack (Figures 41 through 43). At an angle of attack of 26.1 degrees, the pressure distributions from the root to the 40% span stations are almost identical for Configurations 19 and 6 (Figures 29 and 43 respectively). Outboard of the 40% span the pressure distributions are different. As for Configuration 6 the surface is completely stalled while Configuration 19 still has the outboard vortex and only the outboard 30% of the wing span is completely stalled.

When the leading edge plate was increased in size from 10% to 15% of the chord (Configuration 20), very similar pressure distributions were obtained (Figures 44 through 46).

While the paths of the vortices of Configuration 20 were nearly identical to those of Configuration 19, the strength of the outboard vortex seems to be slightly stronger for Configuration 20. It is also noted that the inboard vortex pair seemed to separate from the wing earlier for Configuration 20 than they did for Configuration 19, thus decreasing

the vortex suction lift effects over this area of the wing surface.

On the basis of what was observed from the results obtained for this basic configuration, it was concluded that a vortex formed from a single edge discontinuity of a lifting surface is stronger and more effective in generating a beneficial suction effect over the lifting surface than those that are generated from an attached three-dimensional surface.

As regards Configurations 19 and 20, it is hypothesized that the lifting characteristic due to vortex suction effects could be improved significantly by two basic changes. The first change that, it is believed, would have a significant beneficial effect is to replace the partial extended leading separator plate by an airfoil section having the same planform but contoured to the main wing section. This change should separate the leading edge and strake vortices so that they would not interact so strongly and therefore the higher vortex suction pressures realized by Configuration 3A over the inboard section could be obtained. In order to accomplish this however, the leading edge discontinuity would have to be moved somewhat outboard so that the outboard vortex would not force the inboard leading edge towards the strake vortex thus again enhancing vortex interaction. If these changes were made it is believed that higher lift would be obtained over the entire angle of attack range due to the outboard vortex.

While the outboard vortex formed from the leading edge discontinuity will be beneficial due to its suction effect, it will not stabilize the flow over the outboard section of the lifting surface as its induced effect is such as to promote stall over the outboard section of the lifting surface. The top sketch in Figure 47 illustrates the effect

of the vortex induced velocities over the surface of the wing for Configurations 19 and 20. The minus sign (-) indicates the area where the induced effect decreases the angle of attack and the plus sign (+) indicates an increase in the angle of attack. It can be seen that outboard of the vortex generated by the discontinuity, the angle of attack is increased due to the induced effect of the vortex. This induced effect plus the similar one due to the inboard leading edge vortex is what increases the lift in the angle of attack range of 5 to twenty degrees. At high angles of attack however, these same induced effects tend to reduce the lift generated by the wing and cause the vortices to separate from the lifting surface.

The sketch presented at the bottom of Figure 47 proposes a planform configuration that should enhance vortex and potential lift at high angles of attack as well as keeping the vortices closer to the lifting surface. As indicated on the sketch, the leading edge and large snag vortices are of different signs so they should repel each other and not intertwine as the strake and leading edge vortex do over the inboard portion of the lifting surface.

In addition, the mutually induced effects of the outboard vortices should keep them close to the wing surface as well as keeping the flow in between them as potential flow up to relatively high angles of attack. As indicated in the sketch, the inboard edge of the extended snag would be tapered like a delta wing so that a potential vortex would be generated instead of the turbulent vortex generated by the conventional snag having sharp edges.

The vortex pattern over the inboard sections of the planform should be very similar to that obtained for Configuration 3A. If the very favorable interactions obtained for Configuration 3A over the inboard sections could be

obtained as well as the expected benefits over the outboard sections, a significant increase in vortex lift control should be realizable.

B. Correlation of Predicted and Measured Results

The analysis procedure that was formulated during this program was utilized to predict the differential pressure distributions and the total integrated lift for the wing-strake configuration (Configuration 3A) at angles of attack of 13.1° , 19.4° , and 27.7° .

Comparison of the total measured and predicted lift coefficient in terms of the angle of attack is shown in Figure 48. The figure also shows the various components of lift as predicted by the analysis as well as the experimental variation of the lift coefficient of the basic quadrilateral planform. At 13.1 degrees it can be seen that, as might be expected, the lift is wholly potential and is predicted accurately by the lattice-doublet potential representation. At an angle of attack of 27.7 degrees the total predicted lift again agrees very well with the measured results. Of the total predicted lift at this angle of attack, approximately $3/4$ of the lift is due to cross-flow, and the other fourth of the lift is due to vortex suction. While the cross-flow and potential lift have been combined, over 90% of this lift was that due to separated flow. At an angle of attack of 19.4 degrees, the cross-flow and potential flow components of lift are about equal in magnitude, while the suction lift is about one-half of either of these components. It is also noted that the total predicted lift is approximately 7% less than the measured lift. On the basis of these and other results obtained in this angle of attack region, it was concluded that in flow regions in which there is a large mix of potential, separated and vortex flows, the theory was not adequately representing the effects of the mutual interactions. It might be concluded on the basis of the

results presented in Figure 48, however, that the prediction technique adequately represents the wing vortex flow field over the angle of attack range of interest. While, in fact, the integrated performance values are fairly well predicted, comparison of the measured and predicted pressure distributions is a more demanding evaluation and one that tends to show where the theoretical method is not adequately representing the wing-vortex flow fields, particularly in the angle of attack range $15 \leq \alpha \leq 23$ degrees.

As previously noted, at $\alpha = 13.1^\circ$, the total computed lift on the airfoil surface agreed very well with the measured lift. At this angle of attack, the flow is fully attached, and although the strake, leading edge, and tip vortices are distinctively formed, their suction effect is insignificant. As the angle of attack is increased; the vortices become more concentrated, and their suction effect becomes more predominant. The vortex geometry predicted by the analysis at $\alpha = 19.4^\circ$ is shown in Figure 49, and the comparable experimental vortex geometry as depicted by the tuft flow visualization is shown in Figure 50. The vortex paths along the planform as indicated by flow visualization have been superposed on the photographs manually for clarity. As can be seen by comparing the results in Figures 49 and 50, the predicted paths of the vortices agree fairly well with those that were indicated from the measurements.

A comparison between the predicted and measured spanwise differential pressure distributions along several constant chord lines for Configuration 3A at an angle of attack of 19.4 degrees are shown in Figure 51. Qualitatively, it is seen that the spanwise variation of the pressures are fairly well predicted. Although the pressures predicted by the analysis tend to overpredict the peak pressures near the leading edge, they are generally slightly less than the measured pressures,

which results in a slight under-prediction of the total integrated lift.

The predicted vortex geometry for Configuration 3A at an angle of attack $\alpha = 27.7^\circ$ is shown in Figure 52, and the comparable experimental vortex geometry as depicted by tuft flow visualization is shown in Figure 53. Here again, the vortex paths along the planform were superposed on the photographs manually for clarity. As can be seen by comparing the results in Figures 52 and 53, the predicted paths of the vortices also agree fairly well with those that were indicated from the flow visualization measurements. Comparisons of the differential pressures predicted by the analysis and the measured pressures for several constant chord lines along the span are shown in Figure 54. At this angle of attack the pressures predicted by the analysis again tend to overpredict the peak pressures near the leading edge, while overall the predicted pressures fall below the measured values. At this angle of attack, however, the differences tend to compensate each other, such that the total lift is near its measured value.

Inspection of the pressure distributions presented in Figures 51 and 54 indicate the following discrepancies between the predicted and measured values:

1. Over the 20 to 40 percent span near the leading edge, the predicted pressures are generally less than the measured values.
2. From the 50 percent chord aft, the predicted pressures are generally less than the measured values.
3. The peak vortex suction pressures are generally more than the measured values, and
4. The predicted spanwise pressure distributions indicate abrupt stalling whereas the measured

distributions indicate a gradual transition into the stalled portions of the lifting surface.

It is believed that a basic assumption of lifting surface theories, that is also inherent in the present program, is the reason for the discrepancies noted in 1 through 3 above. As is generally done in lifting surface theories, the no-flow conditions are satisfied along the mean camber line of the airfoil. For conventional flows this is probably a reasonable assumption, but for the type of flows being considered herein, it is believed that this assumption can seriously limit the prediction capabilities of the analysis. Because of this assumption, the inclusion of the airfoil thickness for the prediction of the vortex suction effects places the vortex flow too close to the airfoil surface, thus causing the peak pressures to be overpredicted. Over the 20 to 40 percent span area in the leading edge region, it is believed that this same assumption limits the predicted accuracy as the strong curvature effects of the airfoil suction within this region are neglected. For stations aft of the 50 percent chord, this same assumption limits the predicted accuracy because when it is determined that the upper surface stalls, the analysis also basically assumes that the lower surface stalls due to the cross-flow analogy.

It is thought that these limitations can be removed by applying the doublet-lattice lifting surface theory to both the upper and lower surfaces of the airfoil section contour. By satisfying the boundary conditions on both the upper and lower surfaces of the actual airfoil contour, the curvature effect in the leading edge region would be correctly represented, thus allowing the leading edge potential pressures to be predicted more accurately. In the airfoil region behind the 50 percent chord, when the flow separated off the upper surface, the potential flow over the lower surface

would be properly represented, thus enhancing the prediction of the pressures in the region of separated flow. This representation of the airfoil would also properly locate the attached vortex flows with respect to the surface of the airfoil, thus improving the prediction of the peak vortex pressures. In this regard it is believed that the inclusion of the radial flow component in the representation of the vortex flows, neglected in the present analysis, will also enhance the prediction of the distribution of vortex suction pressures over the surface of the wing, particularly in the leading edge region.

As regards the prediction of abrupt stalling of the lifting surface, it is believed that a finer grid of surface boxes in association with an improved three-dimensional stall criteria will result in a more gradual stall being predicted as indicated by the experimental results. In the present analysis, the wing surface was arbitrarily divided into 100 surface boxes along constant percentage lines in chord and span. Thus, based on a preset criteria when it was predicted that stall was present at the control point, the entire box was assumed stalled, thus creating an apparent abrupt stall. It is believed that this can be corrected by providing for an arbitrary location of the control points and concentrating more control points over the surface of the wing where vortex flows might be expected to occur.

It is believed that with the successful incorporation of these modifications to the prediction program that the discrepancies noted between predicted and measured pressure distributions will be minimized and the program can be used with confidence to predict the effects of attached vortex flows on the pressure distributions of low aspect ratio swept wings at high angles of attack.

VI. CONCLUSIONS AND RECOMMENDATIONS

On the basis of the experimental and theoretical results obtained in this research program, it is concluded that:

1. The lift curve slope in the angle of attack region of 5 to 15 degrees can be increased significantly by inducing leading edge separation by means of a sharp edge plate along the leading edge.
2. External appendages having two free edges which generated vortices of opposite sense outside of the pressure field of the lifting surface were not effective in enhancing the wing vortex field and thus the lift at high angles of attack.
3. Planform tailoring in the leading edge region such that only a single free vortex is formed within the wing pressure field has the greatest potential of increasing the lifting capabilities of a wing at high angles of attack due to favorable interacting vortex flows.
4. Since the suction fields generated by the enhanced leading edge vortex fields are ahead of the MAC quarter chord point, the pitching moment about the MAC quarter chord point becomes statically unstable.
5. A rather rudimentary lifting surface theory which includes the interaction effects between potential, separated, and vortex flows shows promise of predicting the performance characteristics of low-aspect ratio swept wings at high angles of attack.
6. Because of the mixed flows over the surface of the wing at high angles of attack, the lifting surface theory must be applied to both the upper and lower wing surfaces.

On the basis of the results obtained during this program, it is recommended that:

1. The effects of wing vortex flow control devices on the tailplane and the effects of the tailplane in relation to the overall performance characteristics of an aircraft be investigated.
2. The vortex flow field of a complete fullspan wing body configuration should be measured at high angles of attack to determine how the body vortex interacts with the modified wing vortex flow field.
3. Effort continue to further the development of the analytical procedure by removing some of its restrictions and by providing more versatility in the lattice representation over the surface.
4. The theoretical prediction technique should be expanded to include the body vortex flows so that it can be utilized to predict the performance characteristics of a complete aircraft.
5. The refined analysis which incorporates the modifications of 3 above, should be exercised to develop planforms which could optimize the use of vortex flow control to improve maneuverability of modern day aircraft.
6. The planforms developed in 5 above should be wind tunnel tested to verify their (improved) performance characteristics, and to verify the capability of the analysis in modelling vortex flows over various planforms.

VII. REFERENCES

1. White, R. P., Jr. and Zalay, A. D., "High Lift Generation by the Use of Vortices", RASA/SRL Report No. 74-12, Dec. 1974.
2. White, R. P., Jr. and Balcerak, J. C., "An Experimental Investigation of Vortex Flow Control for High Lift Generation", ONR CR212-223-2, Dec. 1975.
3. Pirello, C. J., Hardin, R. D., Heckart, M. V., and Brown, K. R., "An Inventory of Aeronautical Ground Research Facilities", NASA CR-1874, Nov. 1971.
4. Hale, R. W., Tan, P., Stowell, R. C., and Ordway, D. C., "Development of an Integrated System for Flow Visualization in Air Using Neutrally-Buoyant Bubbles", SA1-RR-7107, Dec. 1971.
5. Sevelles, J. C. and Salmi, R. M., "Jet Boundary Corrections for Complete and Semispan Wings in Circular Tunnels", NACA TN 2454, 1951.
6. Katzoff, S. and Hannah, M. E., "Calculation of Tunnel Induced Upwash Velocities for Swept and Yawed Wings", NACA TN 1748, 1948.
7. Ashley, H., Widnall, S. E., and Landahl, M. T., "New Directions in Lifting Surface Theory", AIAA Journal, Vol. 3, No. 1, January 1965, pp. 3-16.
8. Mook, D. T. and Maddox, S. A., "Extension of a Vortex-Lattice Method to Include Effects of Leading-Edge Separation", Journal of Aircraft, Vol. 11, pp. 127-128, February 1974.
9. Giesing, J. P., Kalman, T. P., and Roden, W. P., "Subsonic Unsteady Aerodynamics for General Configurations; Direct Application of the Nonplanar Doublet-Lattice Method", USAF FDL-TR-71-5, 1971.
10. Rao, B. M., "Application of a Simplified Aerodynamic Lifting Surface Theory for Wings in Steady and Unsteady Subsonic Flow", Presented at the 2nd AIAA North Texas Symposium, University of Texas at Arlington, February 1974.
11. Jones, W. P. and Moore, J. A., "Simplified Aerodynamic Theory of Oscillating Thin Surfaces in Subsonic Flow", AIAA Journal, Vol. 11, No. 9, September 1973, pp. 1305-1309.

12. Kandil, O. A., Mook, D. T., and Nayfeh, A. H., "Nonlinear Prediction of Aerodynamic Loads on Lifting Surfaces", Journal of Aircraft, Vol. 13, No. 1, January 1976.

TABLE I SUMMARY OF TEST CONFIGURATIONS

CONFIGU- RATION	PLANFORM AREA ft ²	m ²	DESCRIPTION
1*	16.45	(1.528)	Basic Wing
3A*	17.46	(1.622)	Wing with Root Strake
4A*	17.58	(1.633)	Conf. 3A plus 5% leading edge snag at the 68% semispan
5A	17.81	(1.655)	Conf. 3A plus strake at 50% semispan
5B	17.75	(1.649)	Conf. 3A plus strake at 60% semispan
5C	17.66	(1.641)	Conf. 3A plus strake at 68% semispan
6	18.29	(1.699)	Conf. 3A plus 5% undeflected leading edge separator plate from root strake to tip
7A	18.50	(1.719)	Conf. 5A plus Conf. 6
8AC	18.00	(1.672)	Conf. 5A plus Conf. 5C
9A1	18.13	(1.684)	Conf. 5A with 5% undeflected leading edge separator plate from the root strake to the strake at the 50% semispan
9A2	18.13	(1.684)	Conf. 5A with 5% undeflected leading edge separator plate from the strake at the 50% semispan to tip
9C1	18.13	(1.684)	Conf. 5C with 5% undeflected leading edge separator plate from the root strake to the strake at the 70% semispan
10	17.05	(1.584)	Conf. 1 with 5% undeflected leading edge separator from root strake position to tip (Conf. 6 with root strake removed)
11	16.80	(1.561)	Conf. 1 with the strake designed for the 50% semi-span

TABLE I CONTINUED:

CONFIGURATION	PLANFORM AREA ft ²	m ²	DESCRIPTION
12	18.27	(1.697)	Conf. 3A plus Conf. 11 plus 5% undeflected leading edge separator plate from the root strake to the strake at the 68% semispan
14	18.29	(1.699)	Conf. 3A plus 5% leading edge separator plate from the root strake to tip separator plate oriented at +10° with respect to the wing chordline
15	18.05	(1.677)	Conf. 4A plus undeflected separator plate from root strake to the snag at the 69% semispan
17	17.66	(1.641)	Conf. 5C with the outboard strake attached inversely in relation to Conf. 5C
18	18.29	(1.699)	Conf. 3A plus 5% leading edge separator plate from the root strake to the tip. Separator plate oriented at -20° with respect to the wing chordline
19	18.30	(1.700)	Conf. 3A plus 10% undeflected leading edge separator plate from the root strake to the 50% semispan
20	18.73	(1.740)	Conf. 3A plus 15% undeflected leading edge separator plate from the root strake to the 50% semispan

* Data for these configurations were obtained in tests conducted under the effort described in Reference 1. Configuration 3A was retested as a check case.

TABLE II GENERAL CLASSIFICATION OF
TEST CONFIGURATIONS

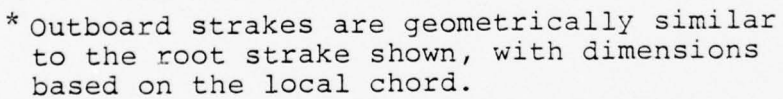
SINGLE STRAKE	DOUBLE STRAKE	TRIPLE STRAKE	SINGLE STRAKE WITH SEPARATOR PLATE	DOUBLE STRAKE WITH SEPARATOR PLATE	STRAKE SNAG AND SEPARATOR PLATE	SEPARATOR PLATE ONLY
3A	5A	8AC	6	7A	15	10
11	5B		14	9A1		
	5C		18	9A2		
	17		19	9C1		
			20	12		

TABLE III SUMMARY OF DATA OBTAINED
FOR THE TEST CONFIGURATIONS

CONFIGURATION	PERFORMANCE	LEADING EDGE PRESSURES	UPPER SURFACE PRESSURES	TUFT VISUALIZATION	HELIUM BUBBLE VISUALIZATION
3A	X*	X*	X*	X*	X*
5C	X	X	X	X	X
6	X	X	X	X	X
9C1	X	X	X	X	X
19	X		X		
20	X		X		

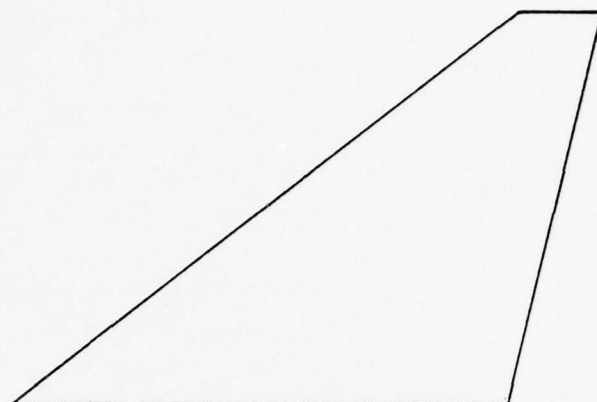
5A	X	X			
5B	X	X			
7A	X	X			
8AC	X	X			
9A1	X	X			
9A2	X	X			
10	X	X			
11	X				
12	X	X			
14	X		X		X
15	X	X			
17	X	X			
18	X	X	X	X	

* Data was obtained during the test program reported in Reference 2.



All dimensions are in inches.

53

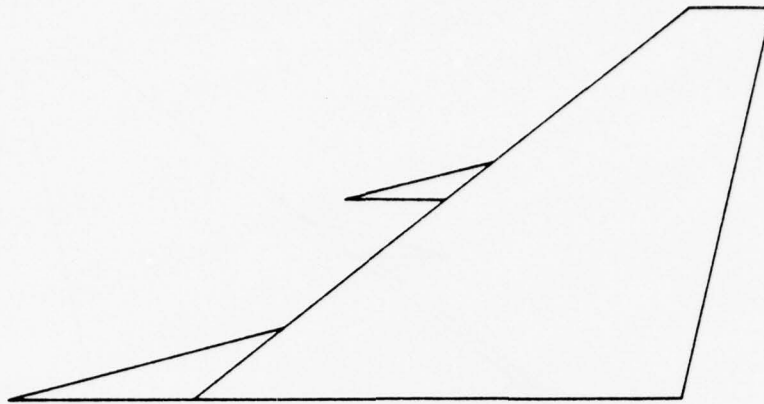


BASIC PLANFORM (CONF 1)

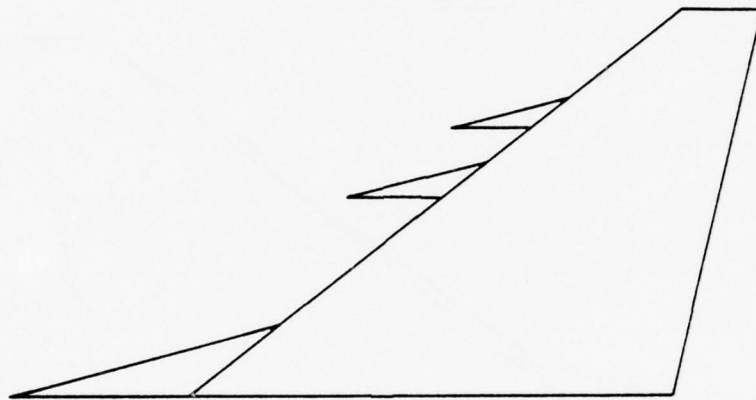


SINGLE STRAKE (CONF 3A)

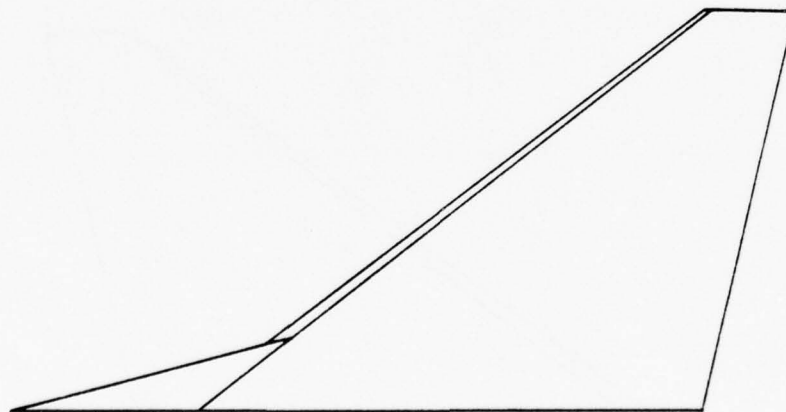
FIGURE 2. PLANFORMS OF VARIOUS TEST CONFIGURATIONS.



DOUBLE STRAKE (CONF 5A)

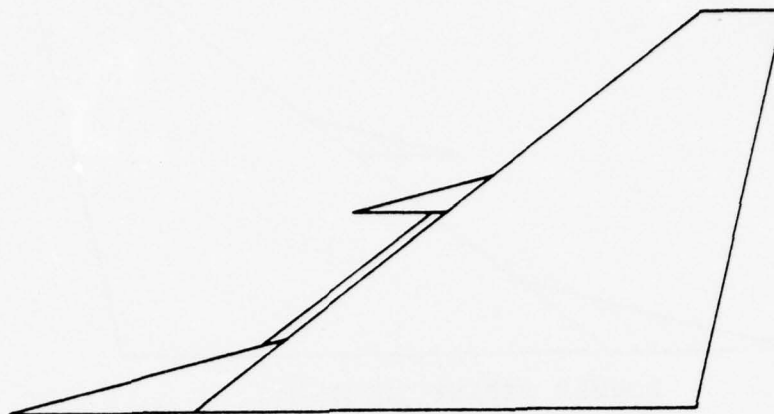


TRIPLE STRAKE (CONF 8AC)

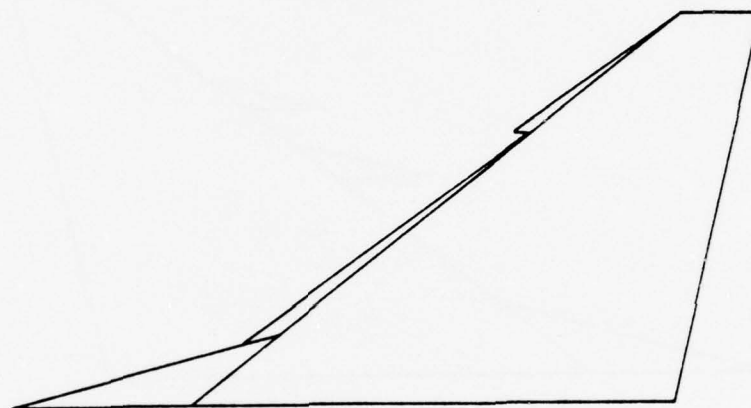


SINGLE STRAKE WITH SEPARATOR PLATE (CONF 6)

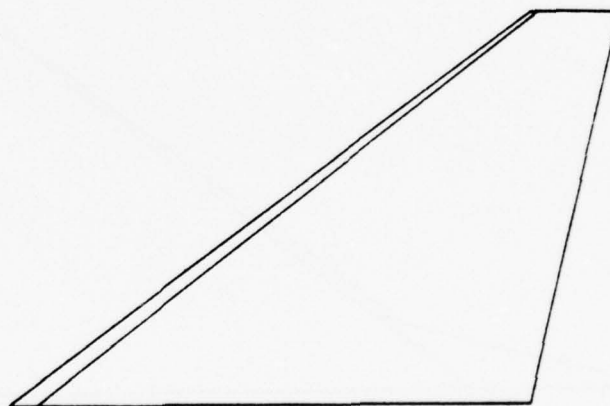
FIGURE 2. PLANFORMS OF VARIOUS TEST CONFIGURATIONS.
(CONTINUED)



DOUBLE STRAKE WITH SEPARATOR PLATE
(CONF 9A1)



STRAKE, SNAG AND SEPARATOR PLATE
(CONF 15)



SEPARATOR PLATE (CONF 10)

FIGURE 2. PLANFORMS OF VARIOUS TEST CONFIGURATIONS.
(CONTINUED)

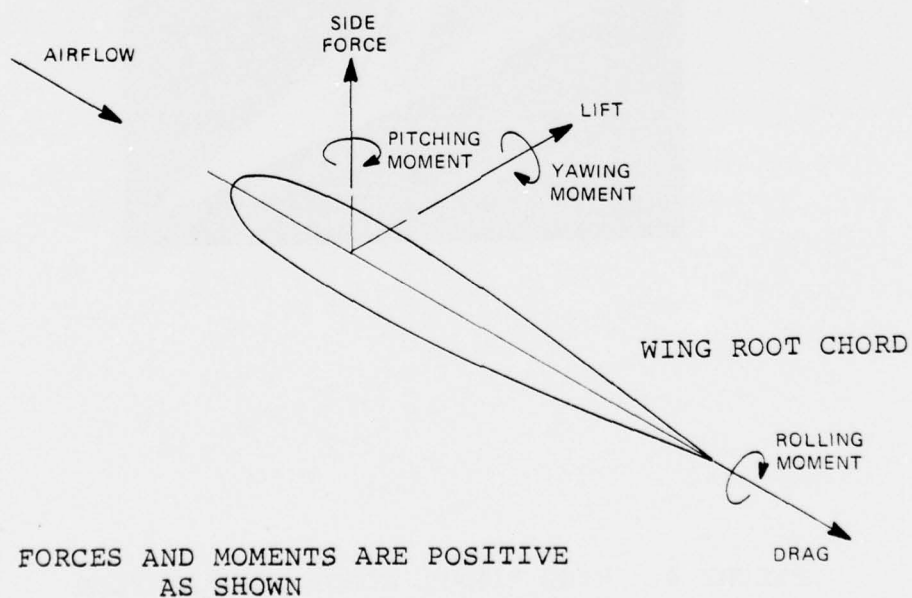
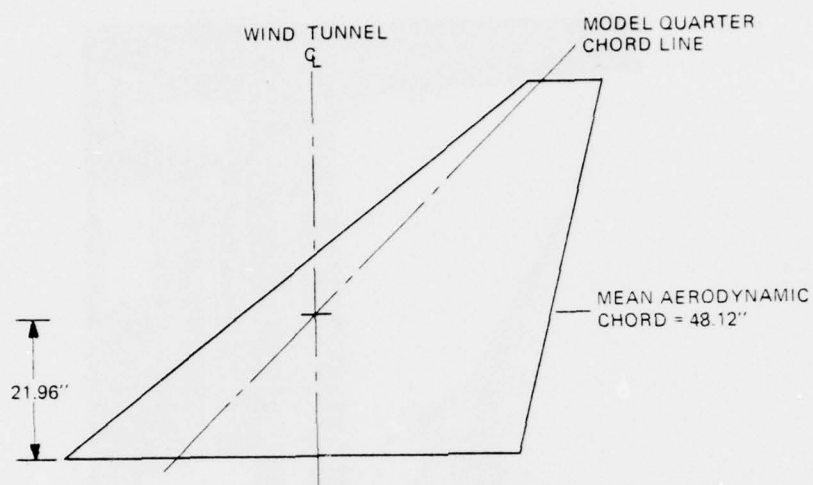


FIGURE 3. COORDINATE SYSTEM FOR BALANCE MEASUREMENTS



FIGURE 4. WIND TUNNEL MODEL INSTALLATION
(CONFIGURATION 7A SHOWN)

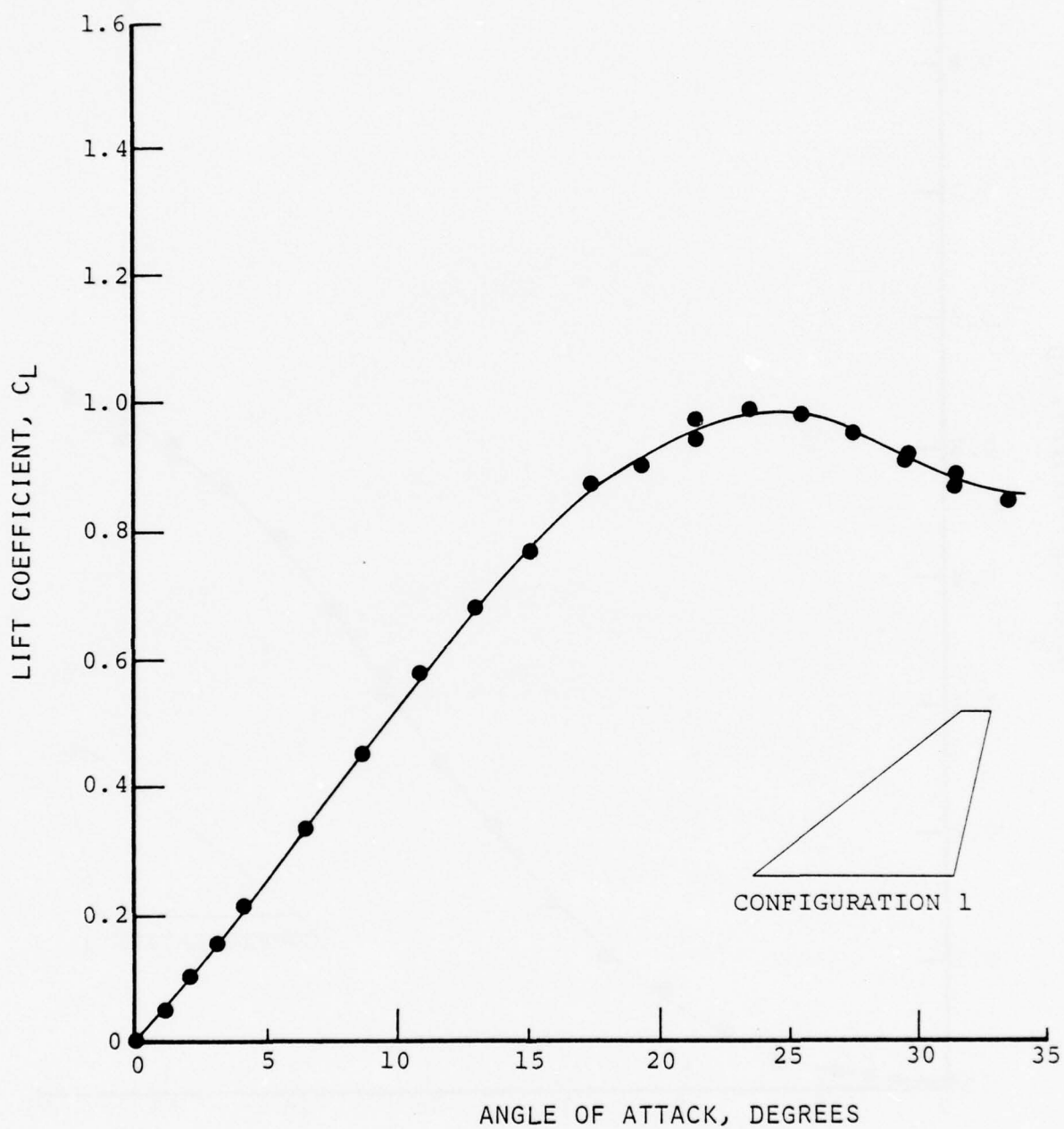


FIGURE 5. LIFT COEFFICIENT VS ANGLE OF ATTACK.
(CONFIGURATION 1)

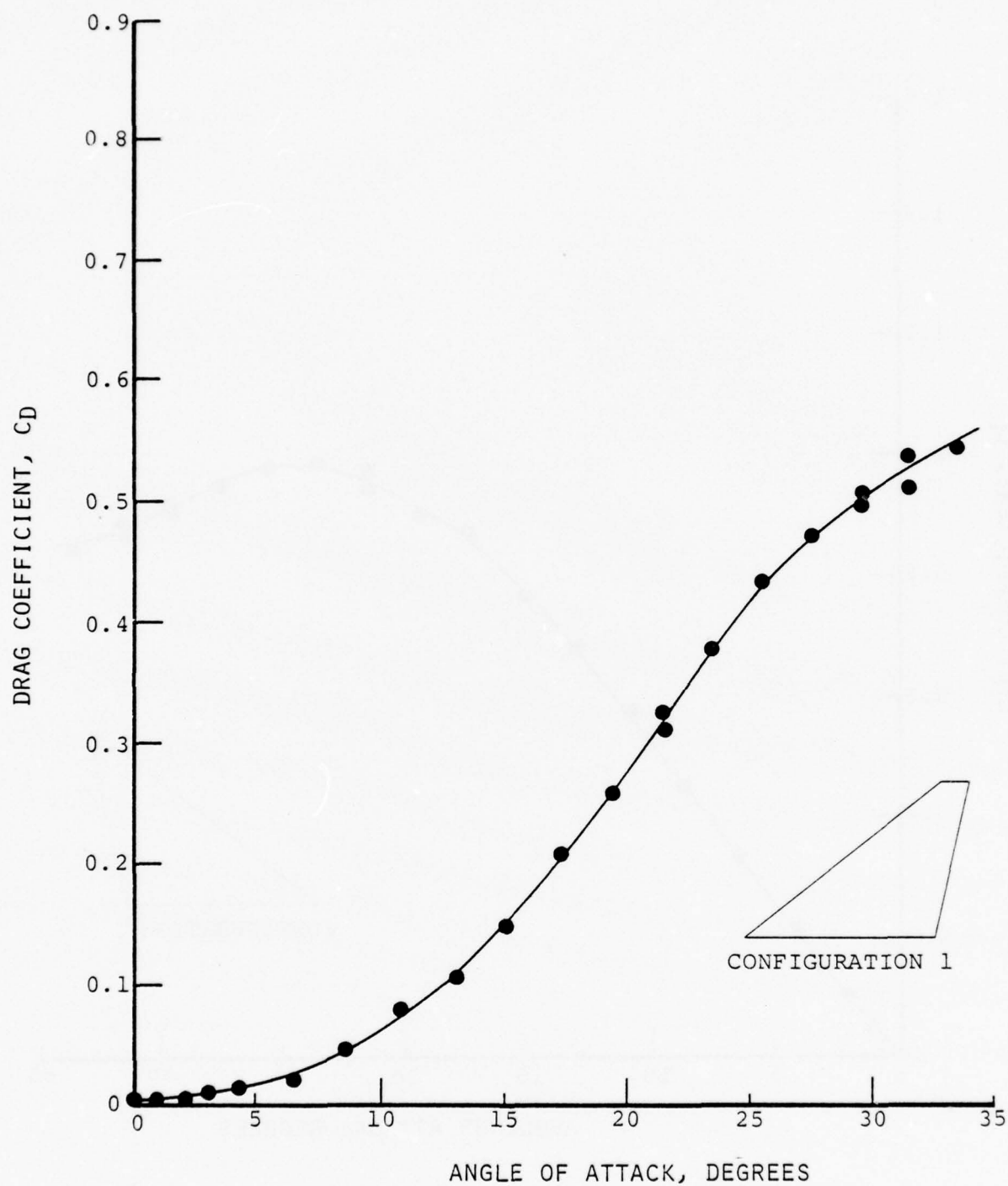


FIGURE 6. DRAG COEFFICIENT VS ANGLE OF ATTACK.
(CONFIGURATION 1)

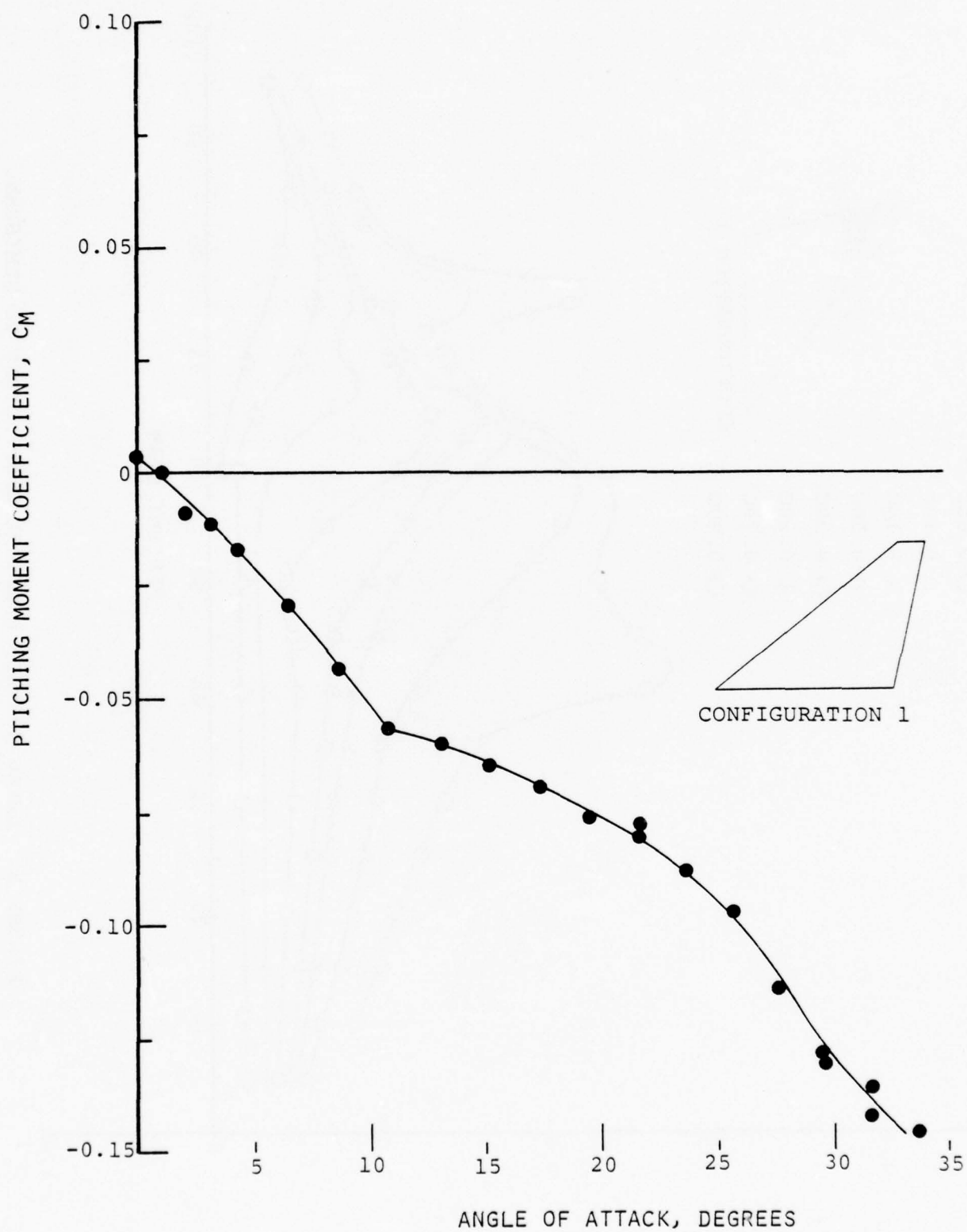


FIGURE 7. PITCHING MOMENT COEFFICIENT VS ANGLE OF ATTACK.
(CONFIGURATION 1)

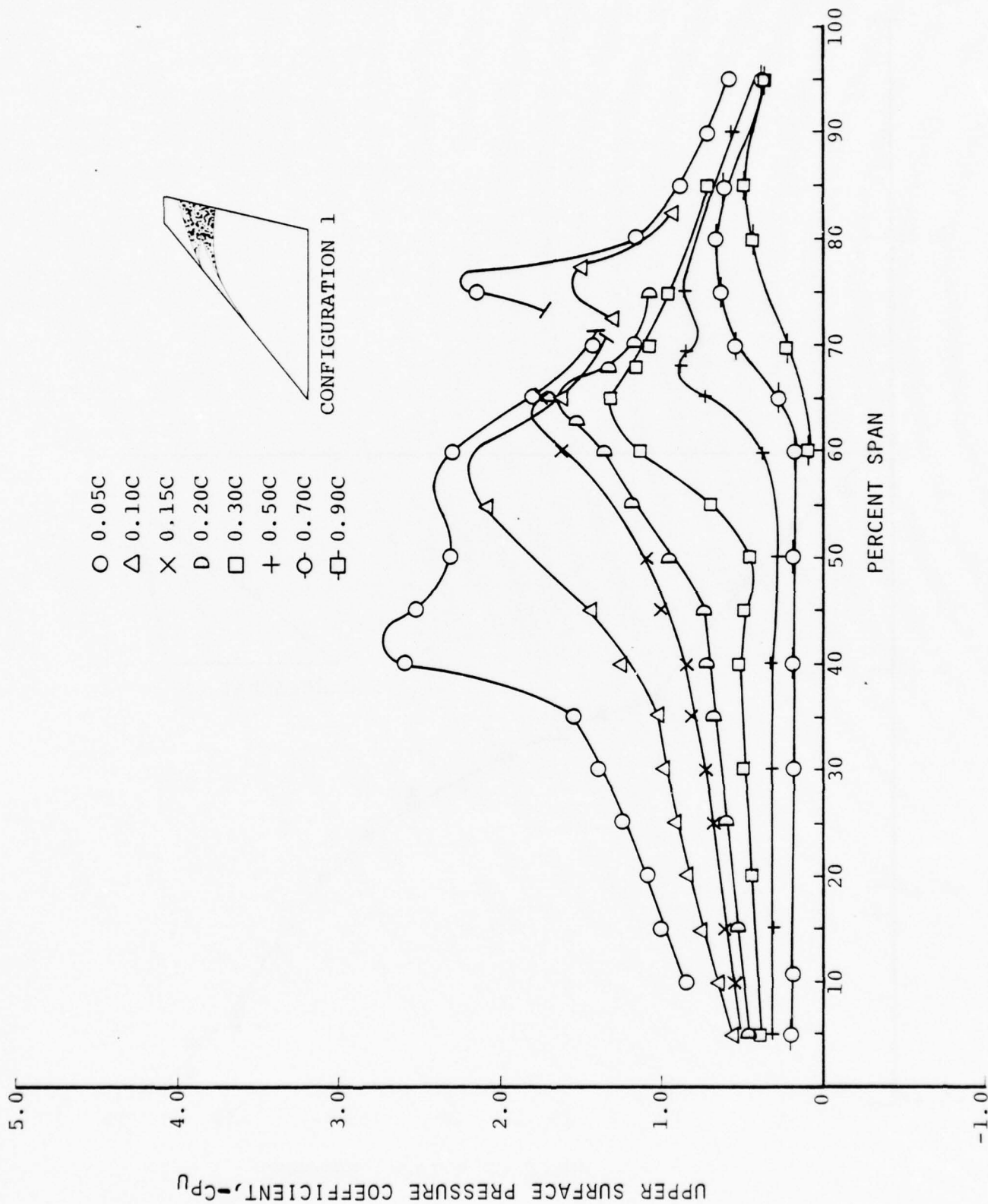


FIGURE 8. UPPER SURFACE PRESSURE COEFFICIENT VS SEMISPAN.
(CONFIGURATION 1, $\alpha = 13.1^\circ$)

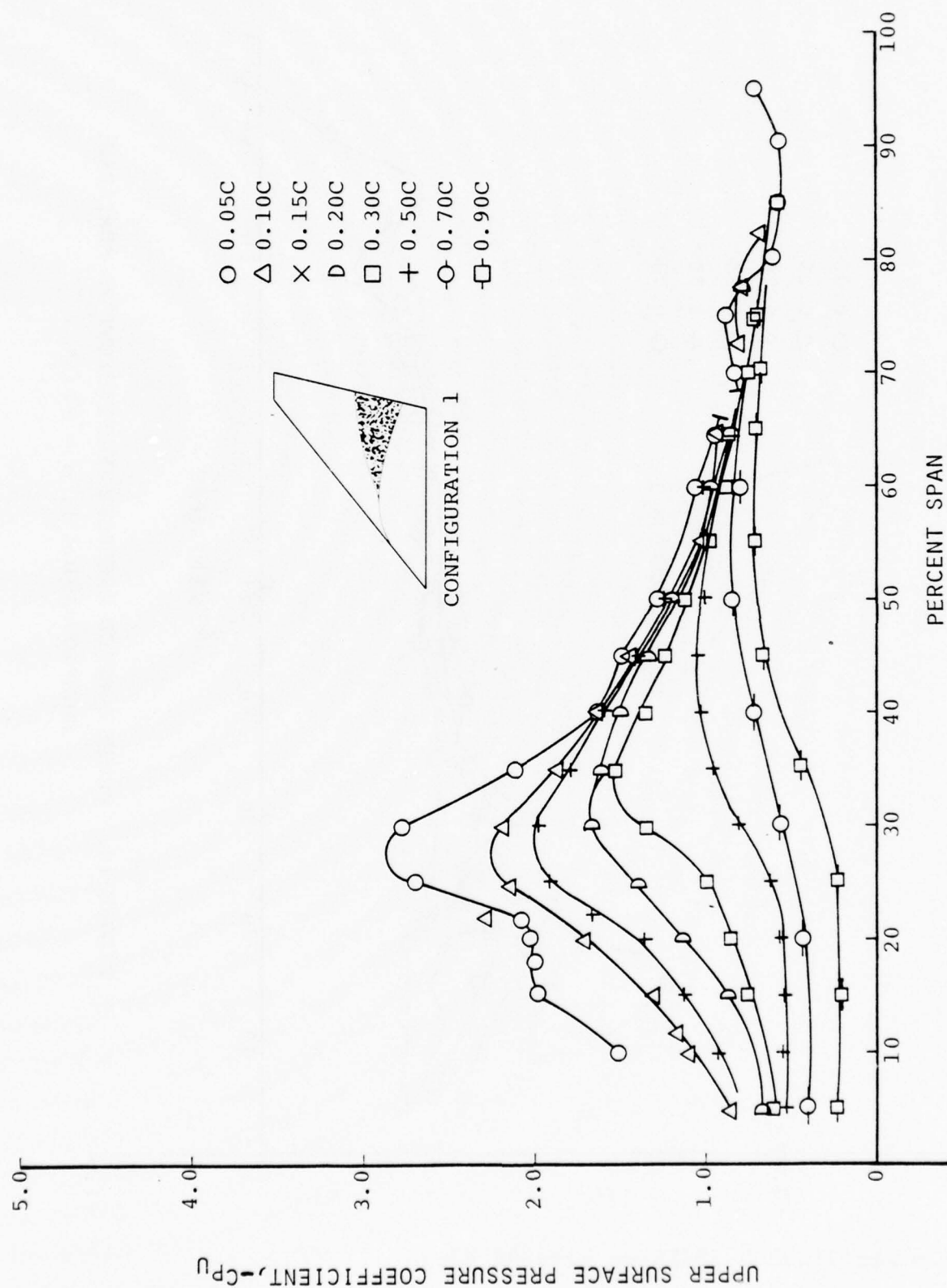


FIGURE 9. UPPER SURFACE PRESSURE COEFFICIENT VS SEMISPAN.
(CONFIGURATION 1, $\alpha = 21.6^\circ$)

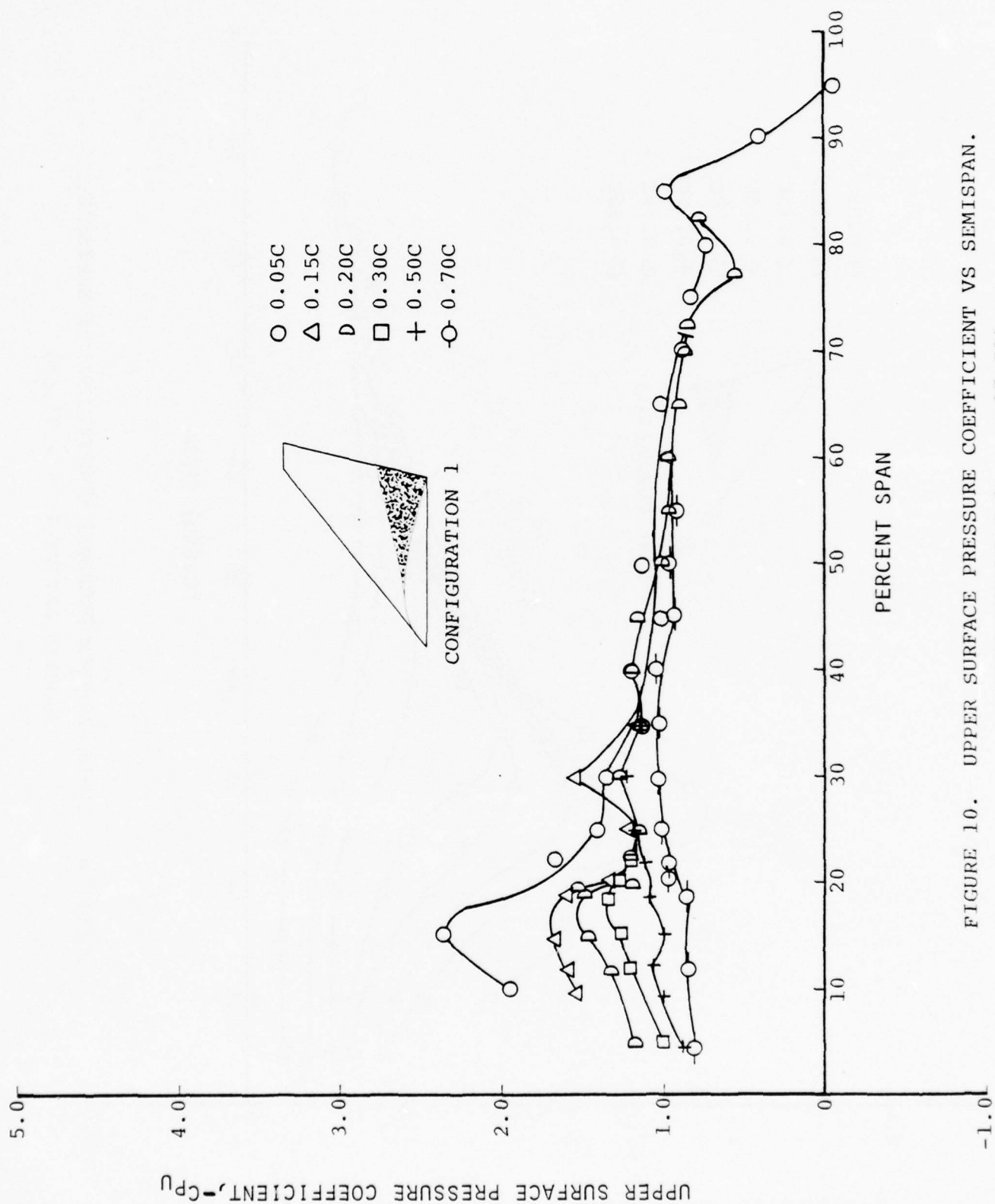


FIGURE 10. UPPER SURFACE PRESSURE COEFFICIENT VS SEMISPAN.

(CONFIGURATION 1, $\alpha = 27.7^\circ$)

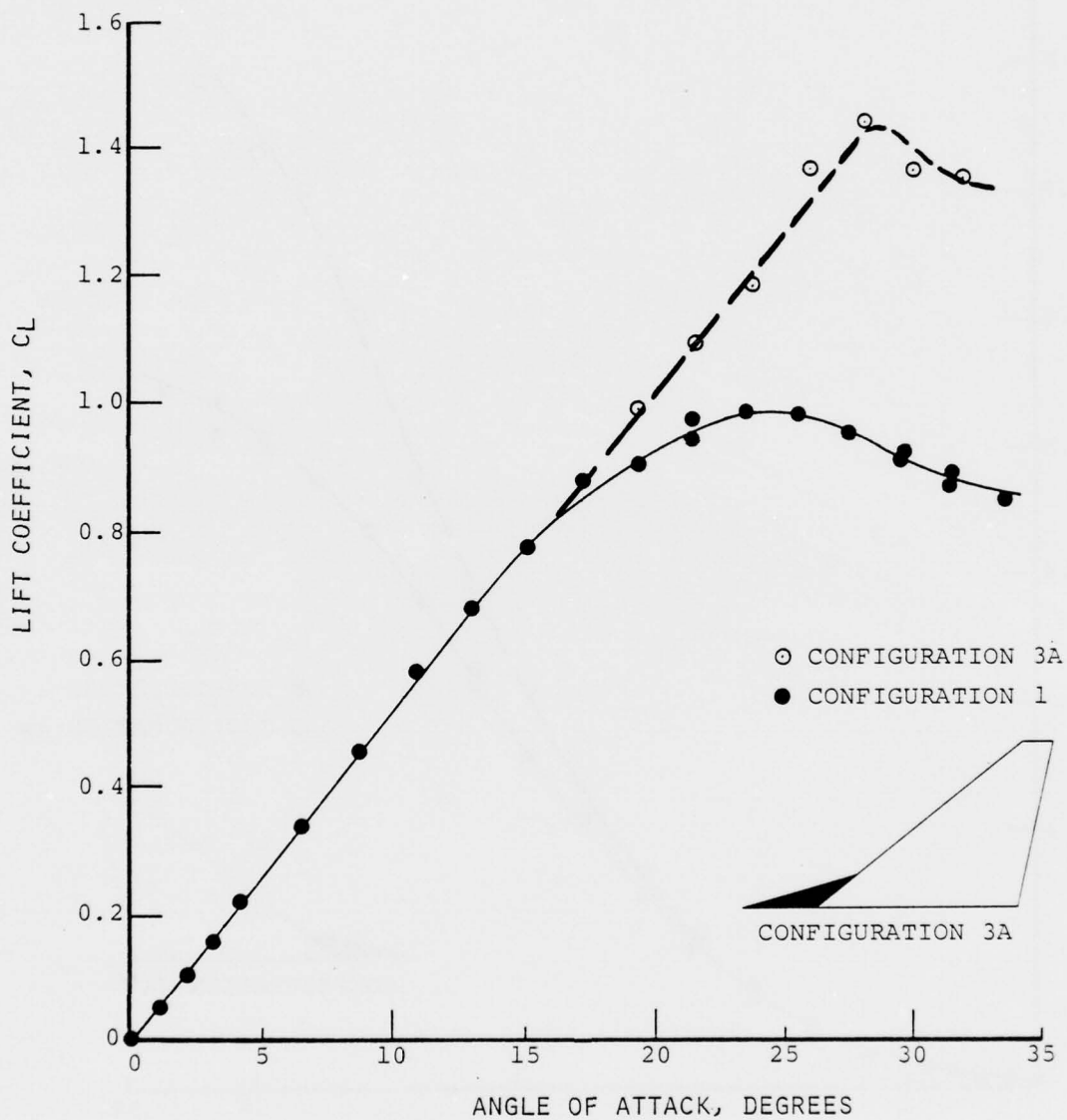


FIGURE 11. LIFT COEFFICIENT VS ANGLE OF ATTACK.
(CONFIGURATION 3A)

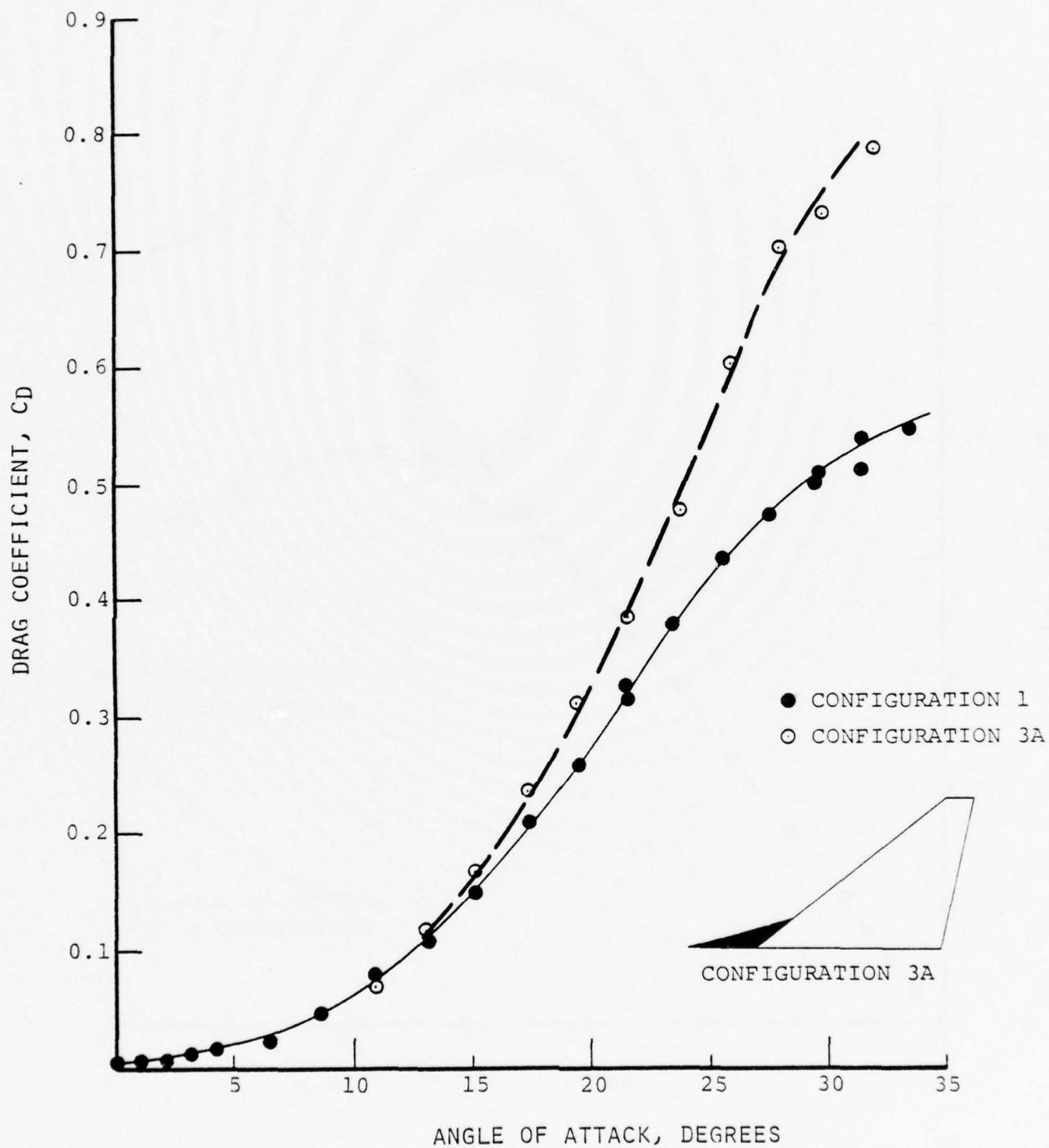


FIGURE 12. DRAG COEFFICIENT VS ANGLE OF ATTACK.
(CONFIGURATION 3A)

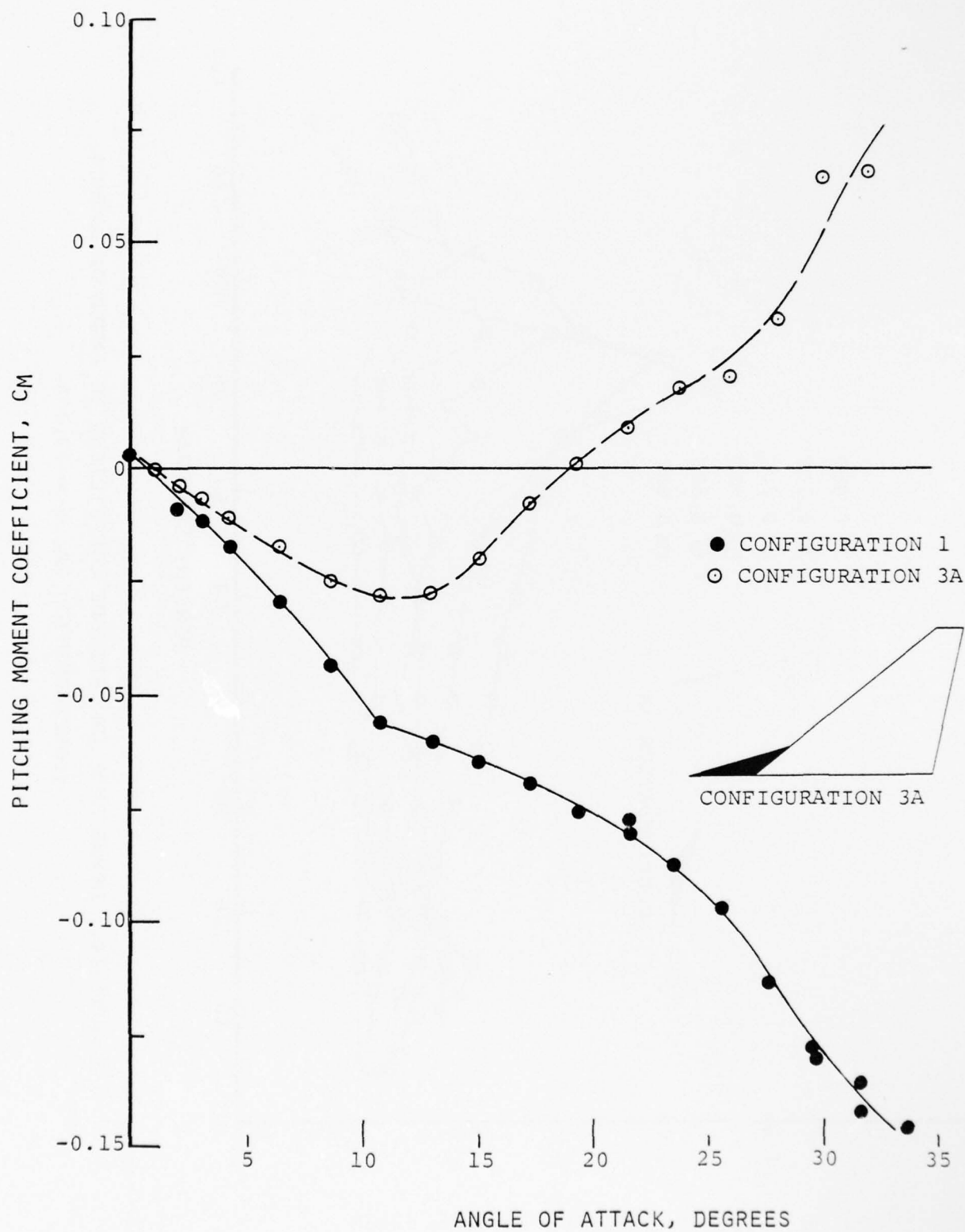


FIGURE 13. PITCHING MOMENT COEFFICIENT VS ANGLE OF ATTACK.
(CONFIGURATION 3A)

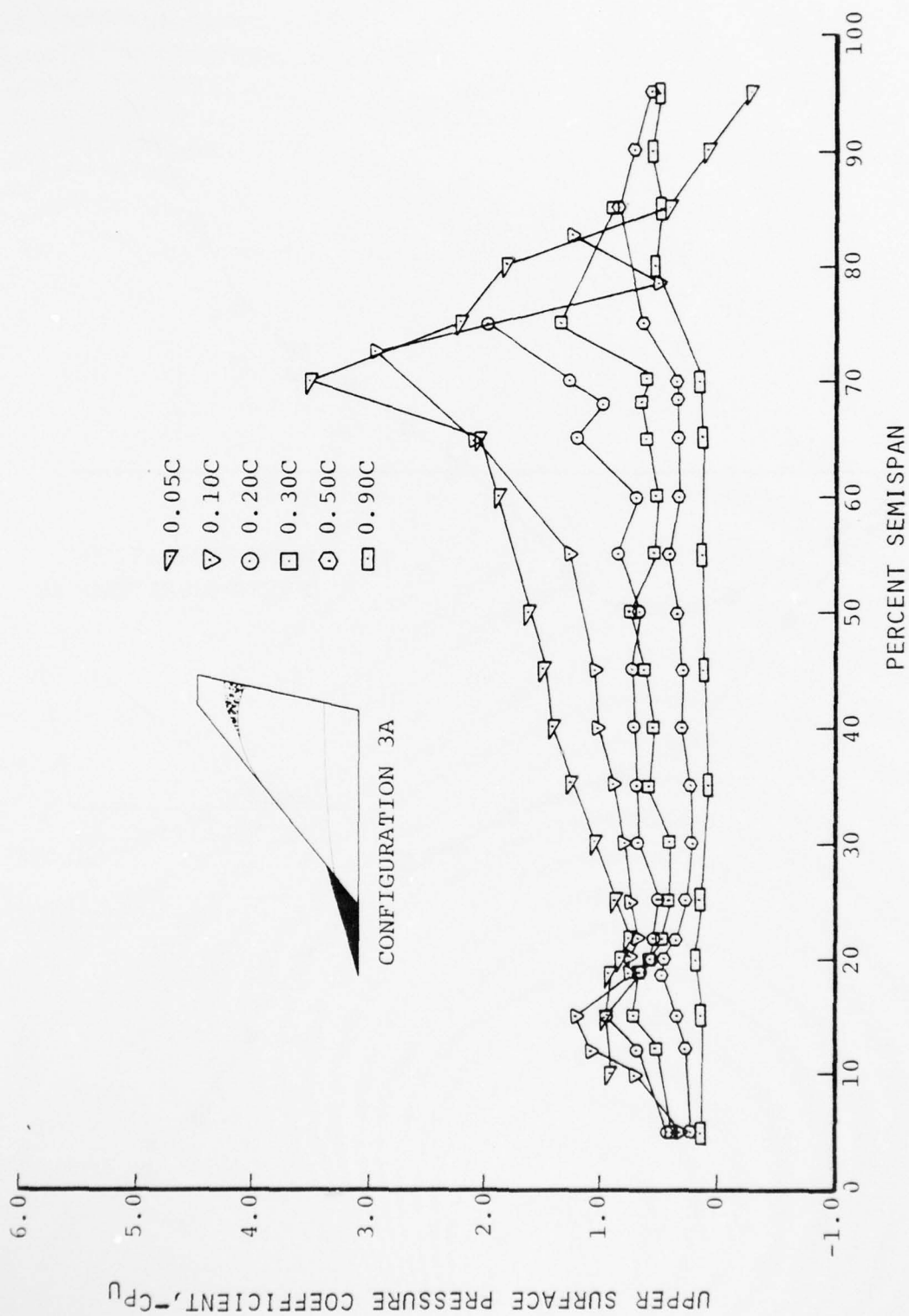


FIGURE 14. UPPER SURFACE PRESSURE COEFFICIENT VS ANGLE OF ATTACK.
(CONFIGURATION 3A, $\alpha = 13.1^\circ$)

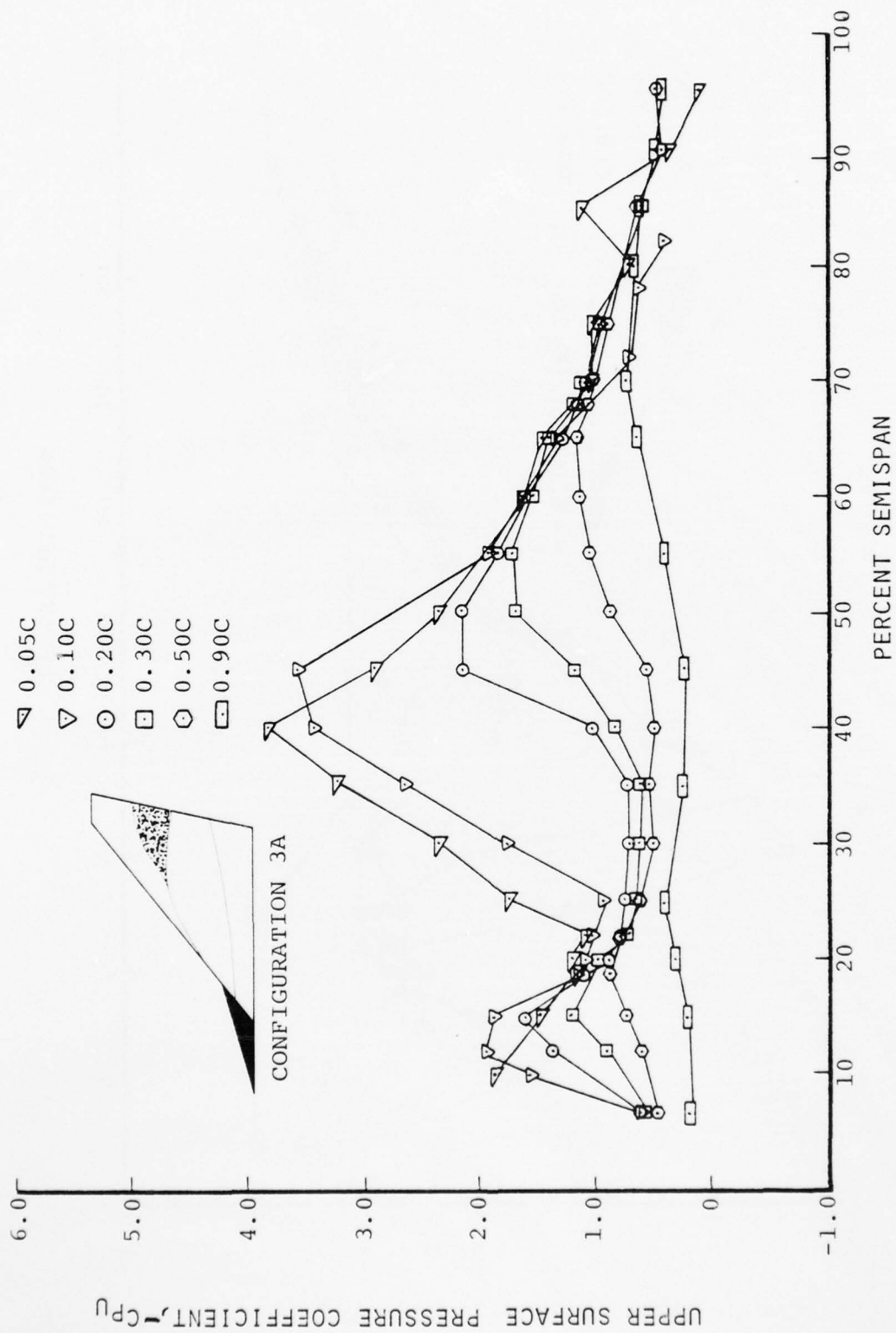


FIGURE 15. UPPER SURFACE PRESSURE COEFFICIENT VS SEMISPAN.

(CONFIGURATION 3A, $\alpha = 19.5^\circ$)

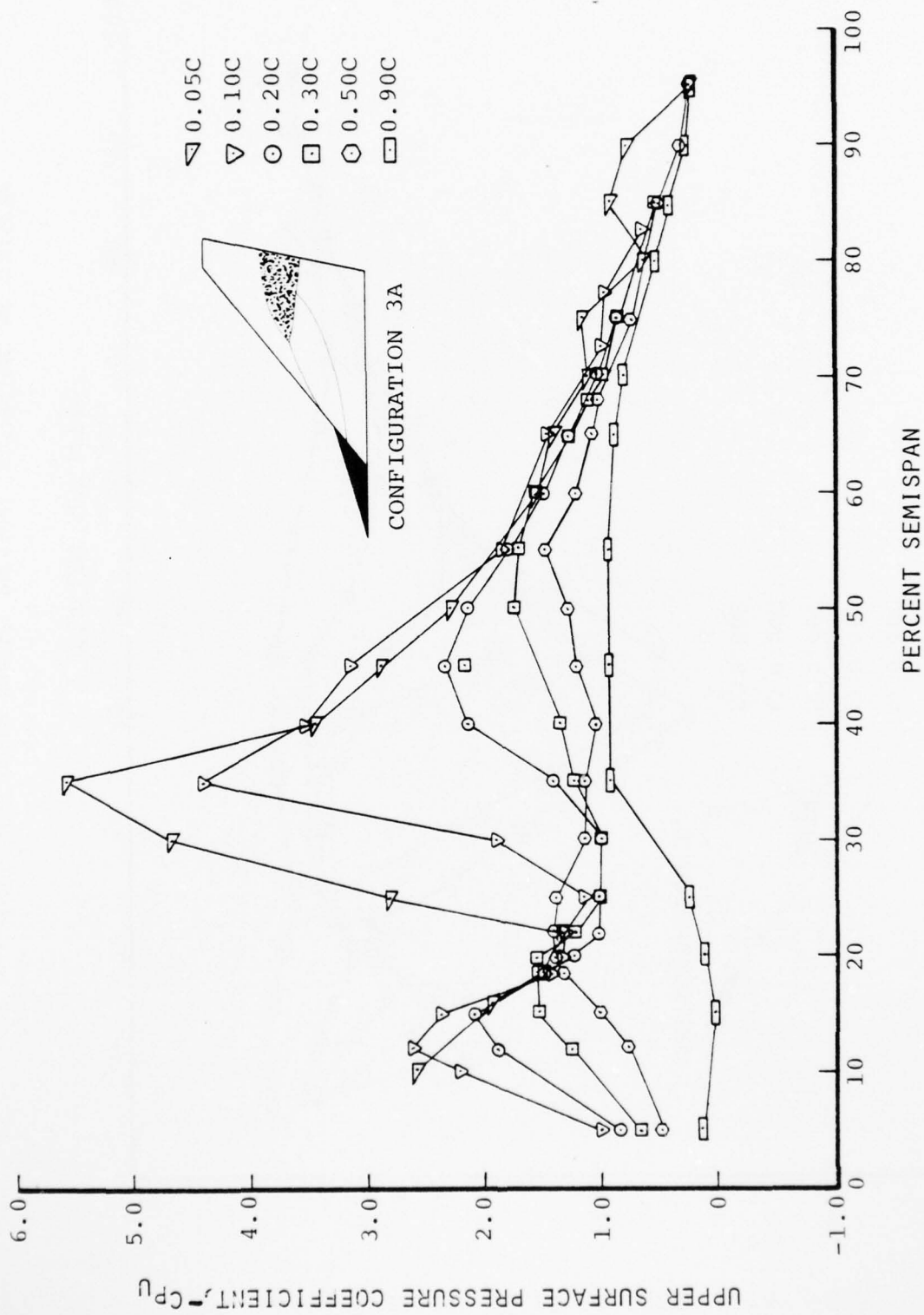


FIGURE 16. UPPER SURFACE PRESSURE COEFFICIENT VS SEMISPAN.

(CONFIGURATION 3A, $\alpha = 26.1^\circ$)

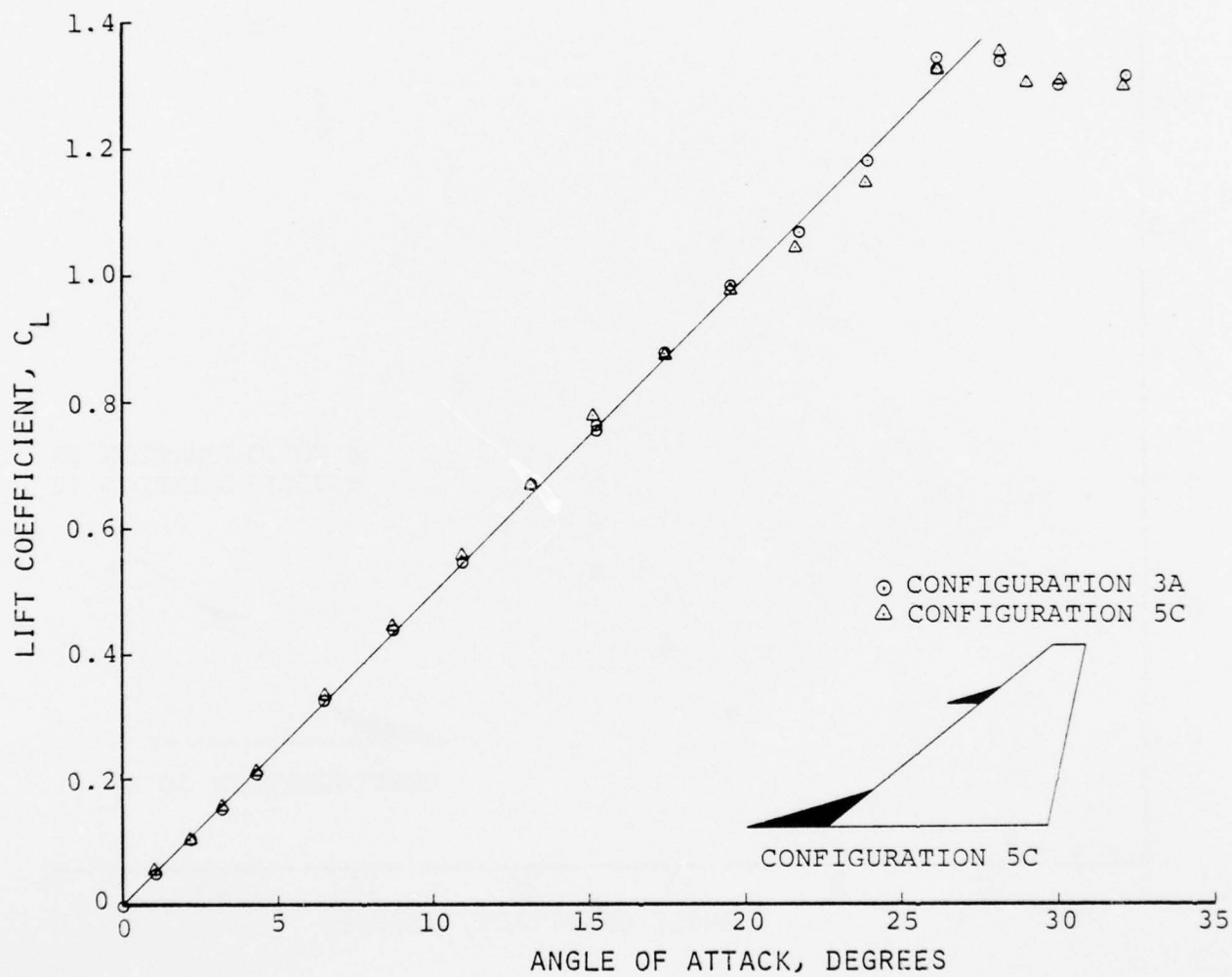


FIGURE 17. LIFT COEFFICIENT VS ANGLE OF ATTACK.
(CONFIGURATION 5C)

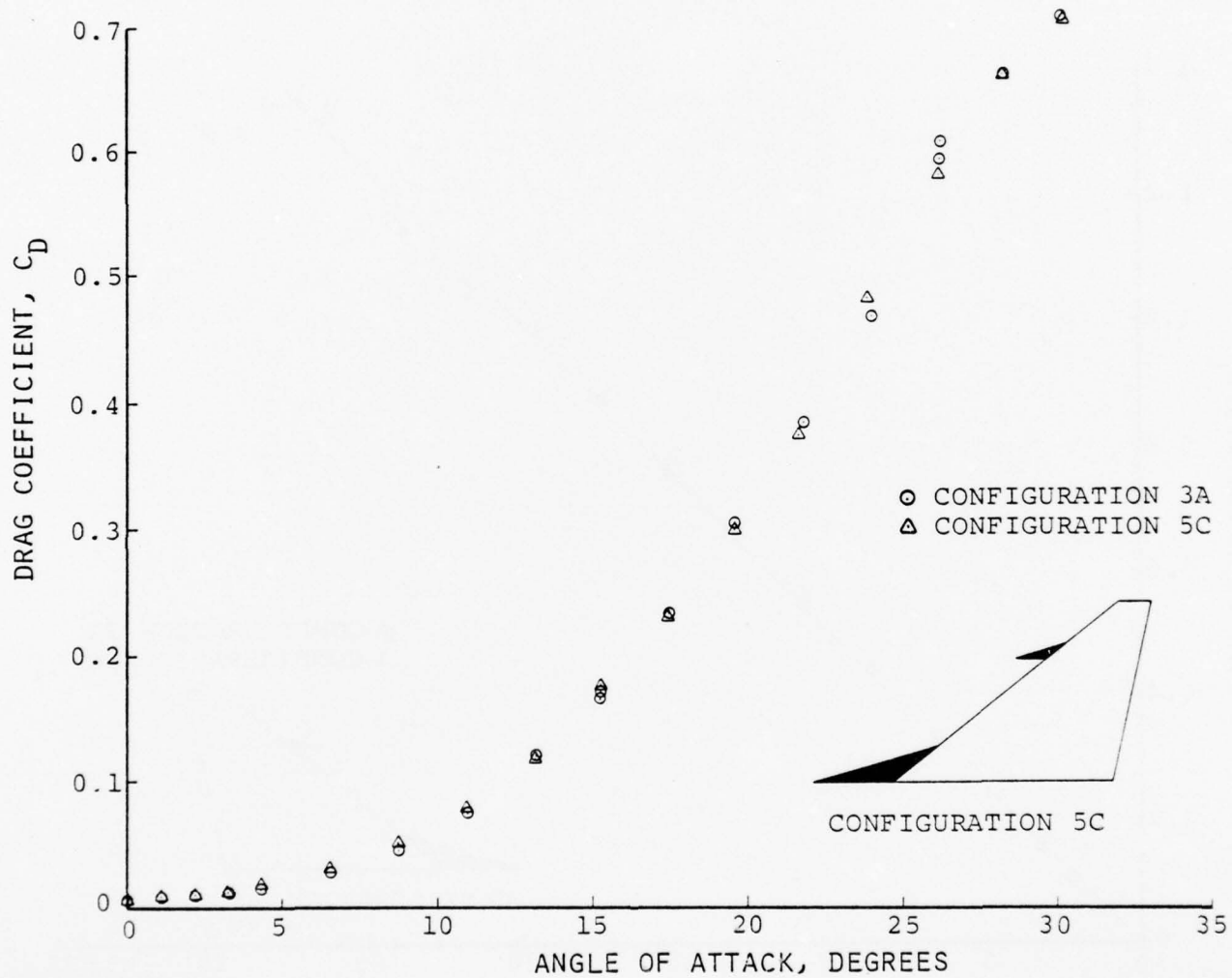


FIGURE 18. DRAG COEFFICIENT VS ANGLE OF ATTACK.
(CONFIGURATION 5C)

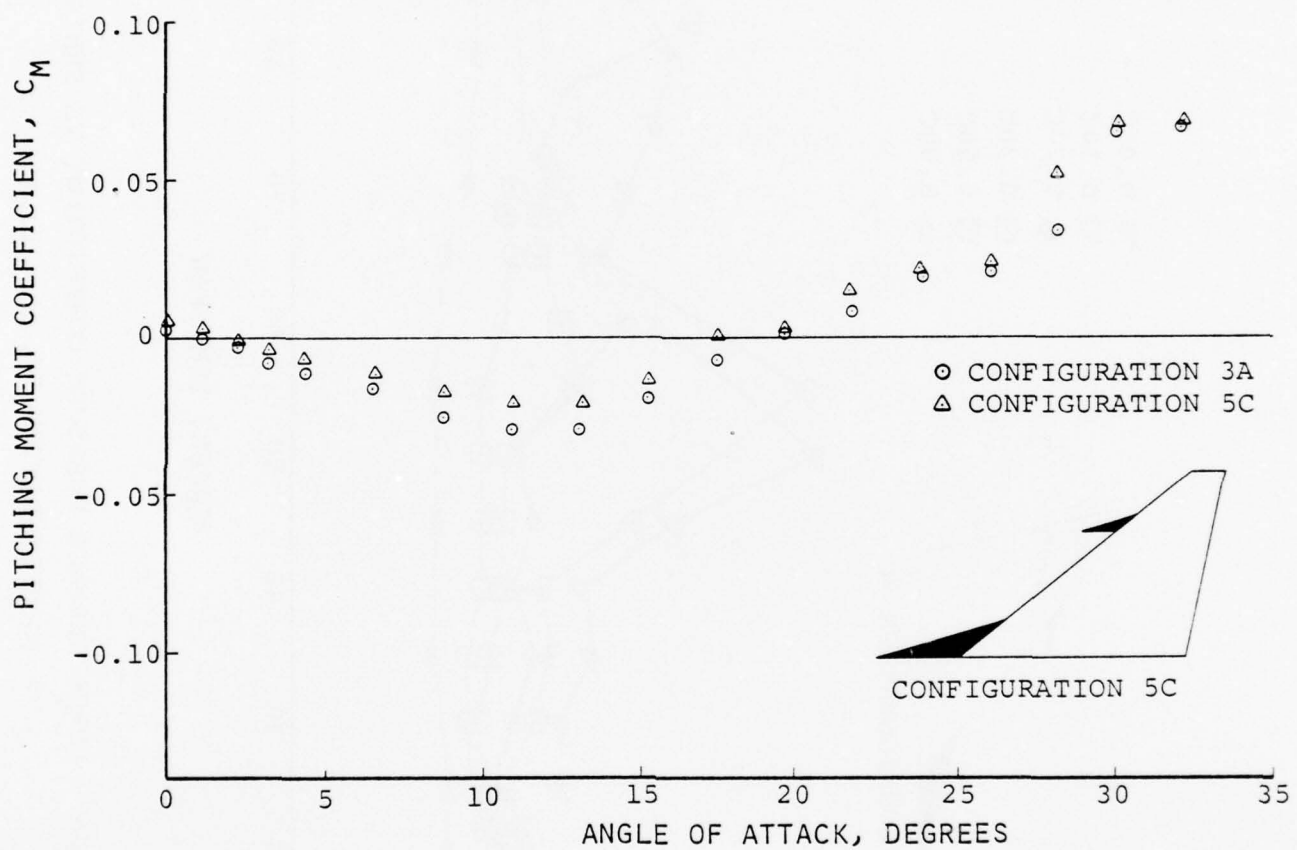


FIGURE 19. PITCHING MOMENT COEFFICIENT VS ANGLE OF ATTACK.
(CONFIGURATION 5C)

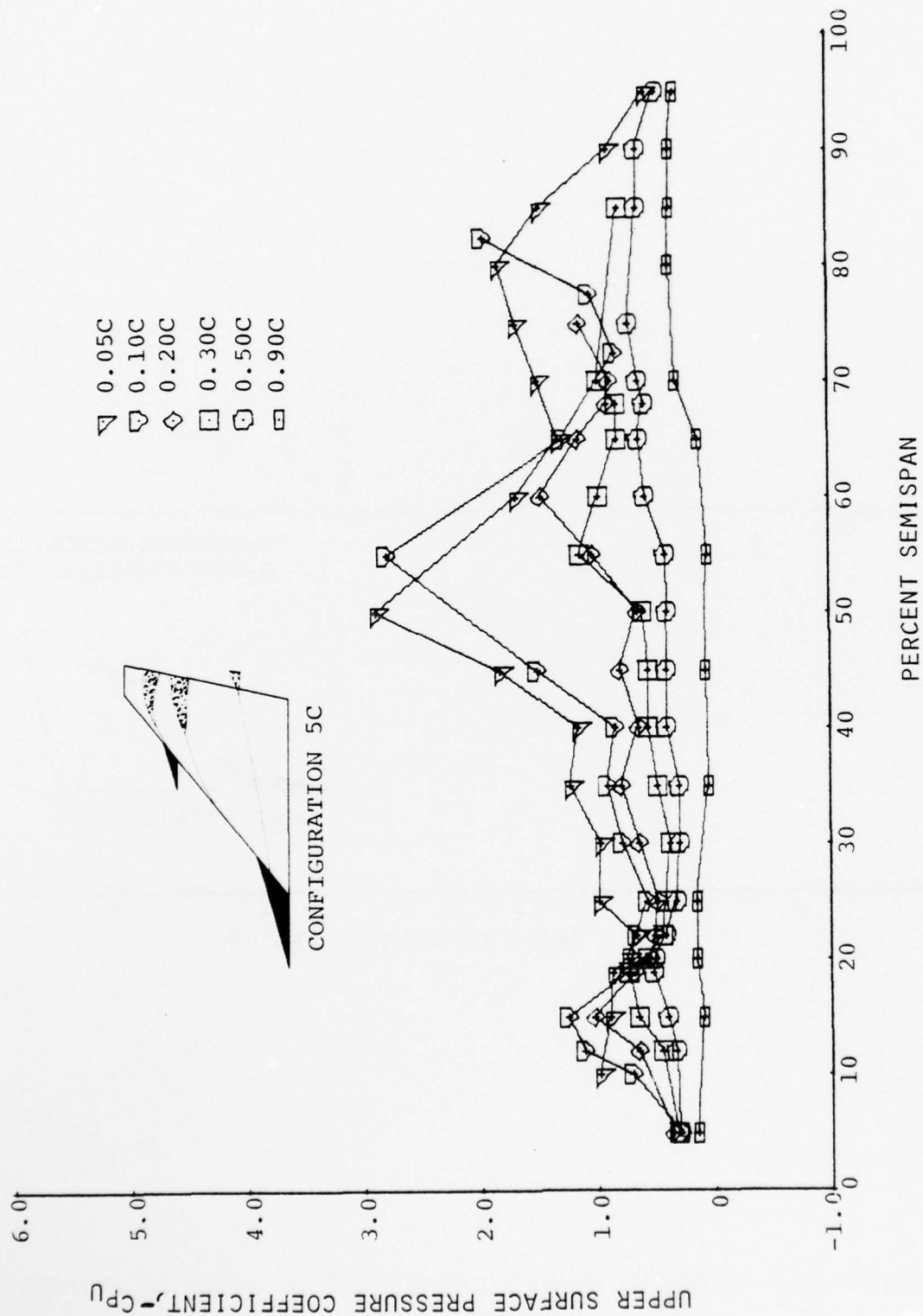


FIGURE 20a. UPPER SURFACE PRESSURE COEFFICIENT VS SEMISPAN.
(CONFIGURATION 5C, $\alpha = 13.1^\circ$)

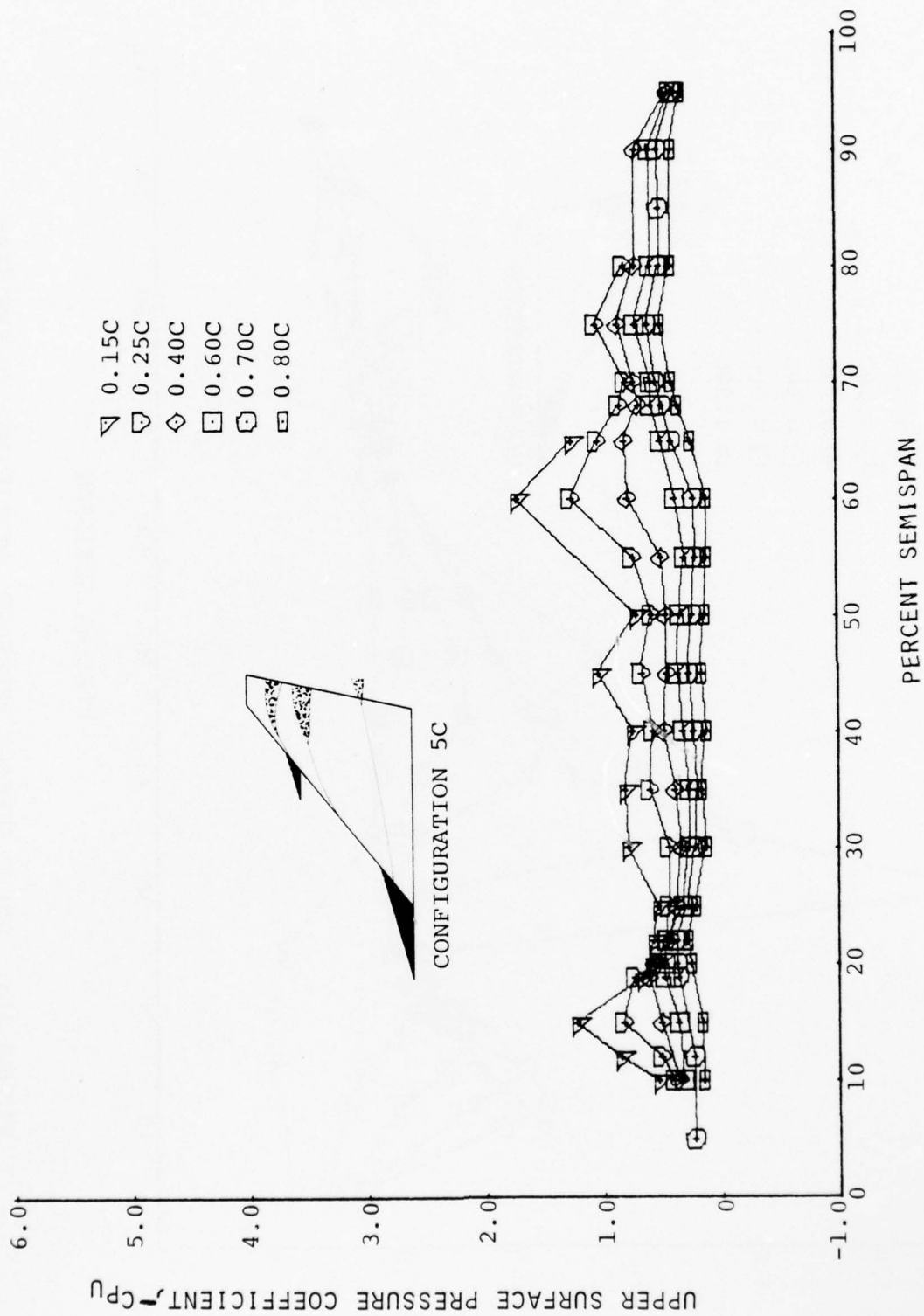


FIGURE 20b. UPPER SURFACE PRESSURE COEFFICIENT VS SEMISPAN.
(CONFIGURATION 5C, $\alpha = 13.1^\circ$)

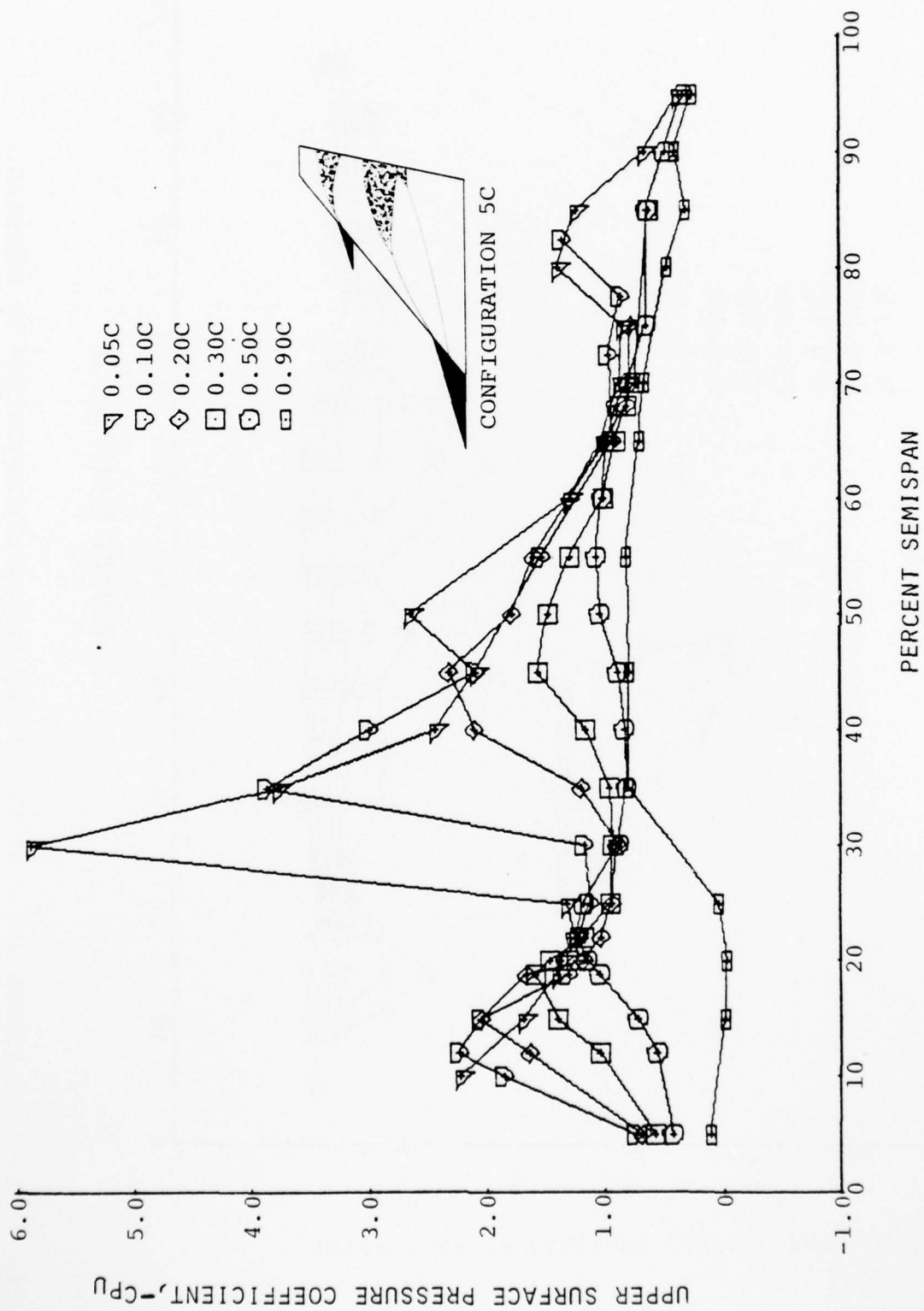


FIGURE 21a. UPPER SURFACE PRESSURE COEFFICIENT VS SEMISPAN.
(CONFIGURATION 5C, $\alpha = 21.7^\circ$)

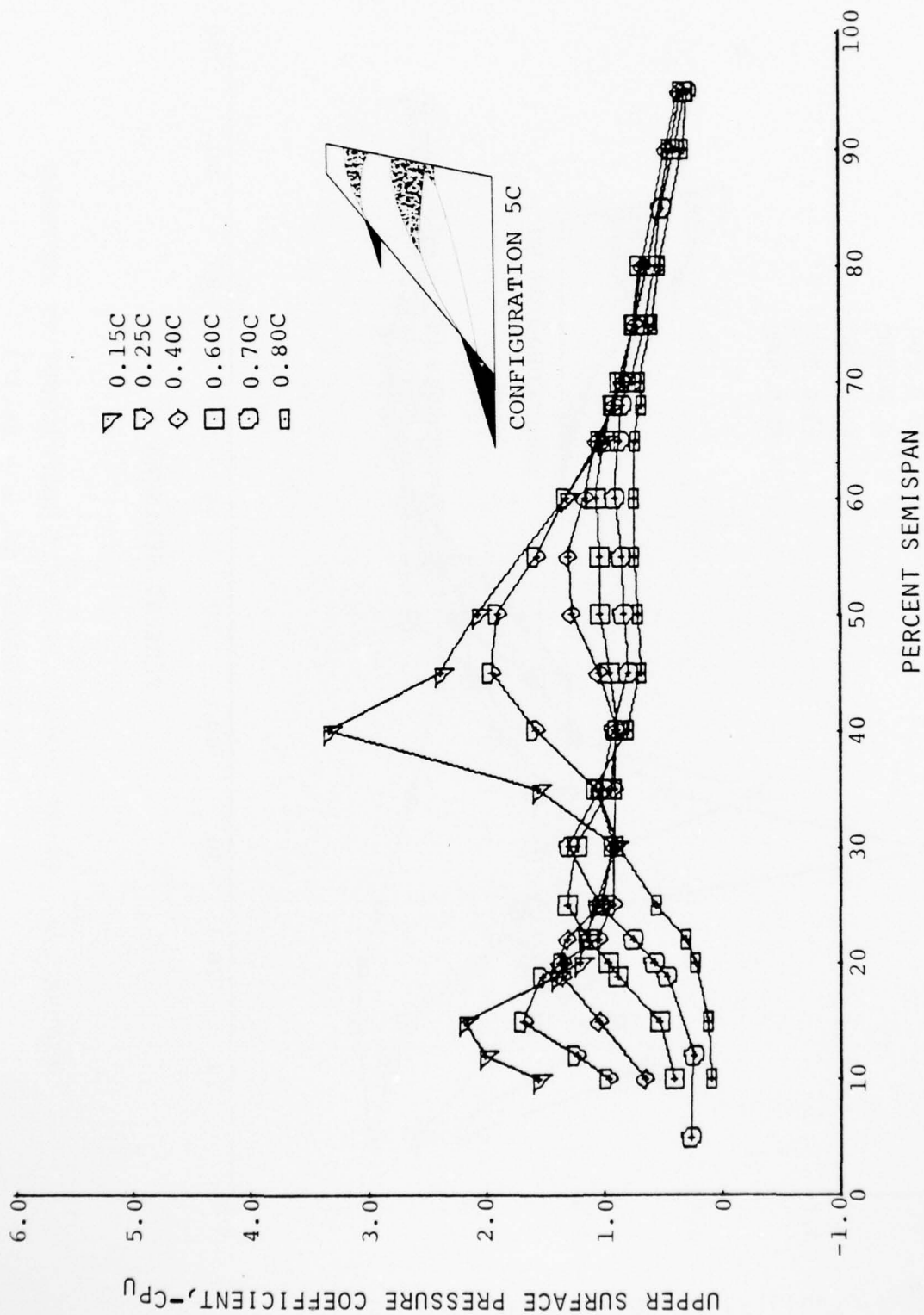


FIGURE 21b. UPPER SURFACE PRESSURE COEFFICIENT VS SEMISPAN.
(CONFIGURATION 5C, $\alpha = 21.7^\circ$)

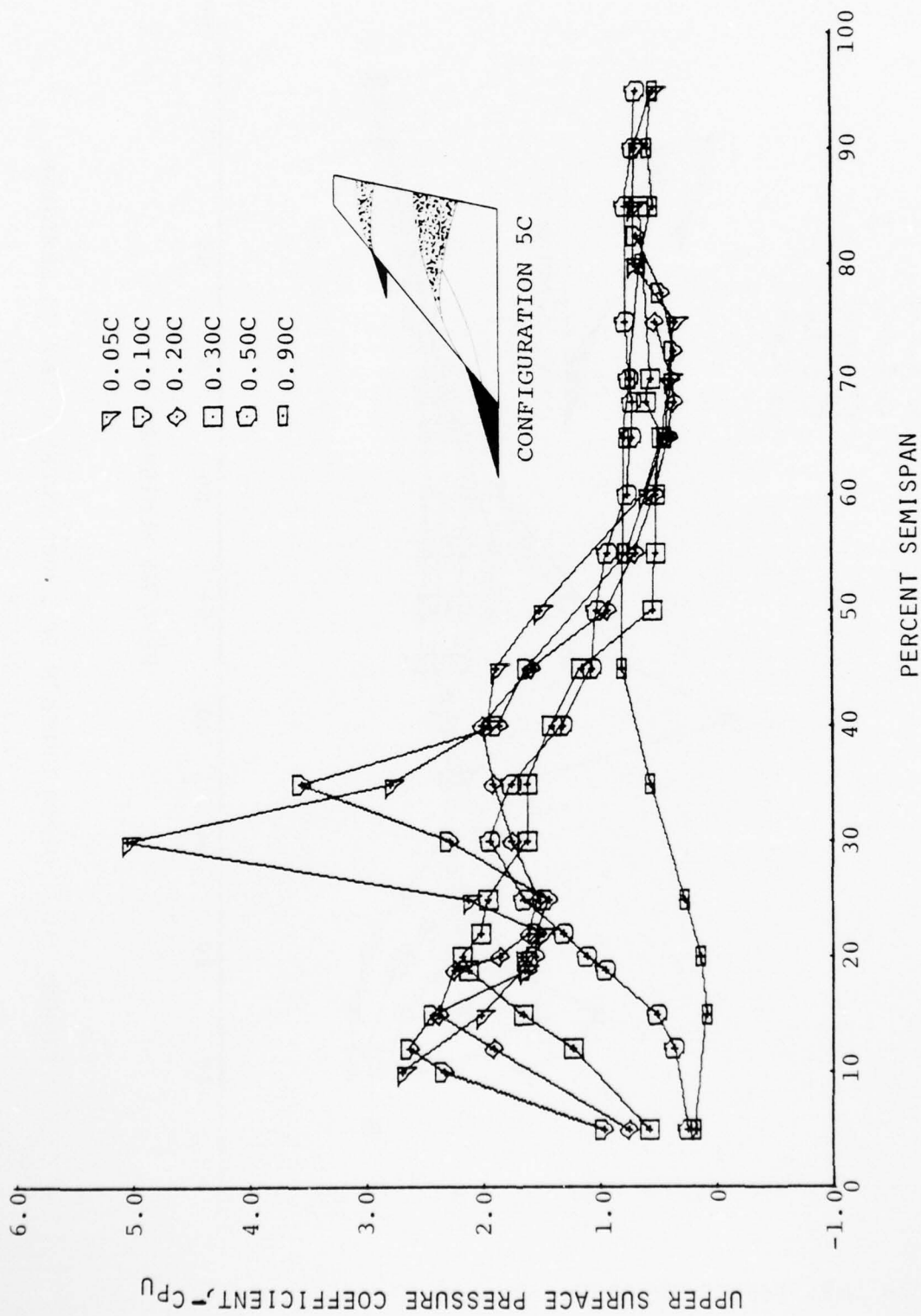


FIGURE 22a. UPPER SURFACE PRESSURE COEFFICIENT VS SEMISPAN.
(CONFIGURATION 5C, $\alpha = 26.1^\circ$)

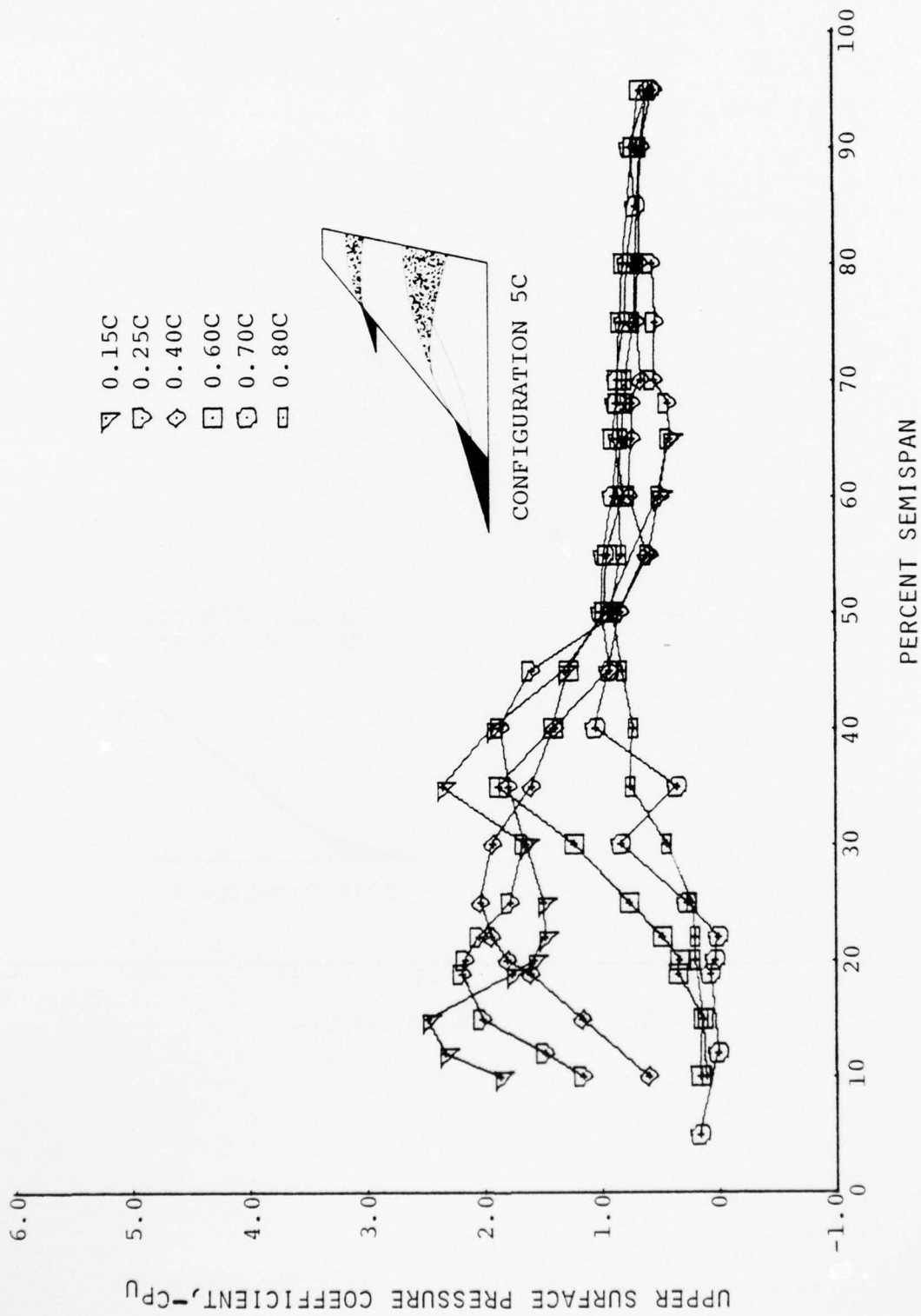


FIGURE 22b. UPPER SURFACE PRESSURE COEFFICIENT VS SEMISPAN.
(CONFIGURATION 5C, $\alpha = 26.1^\circ$)

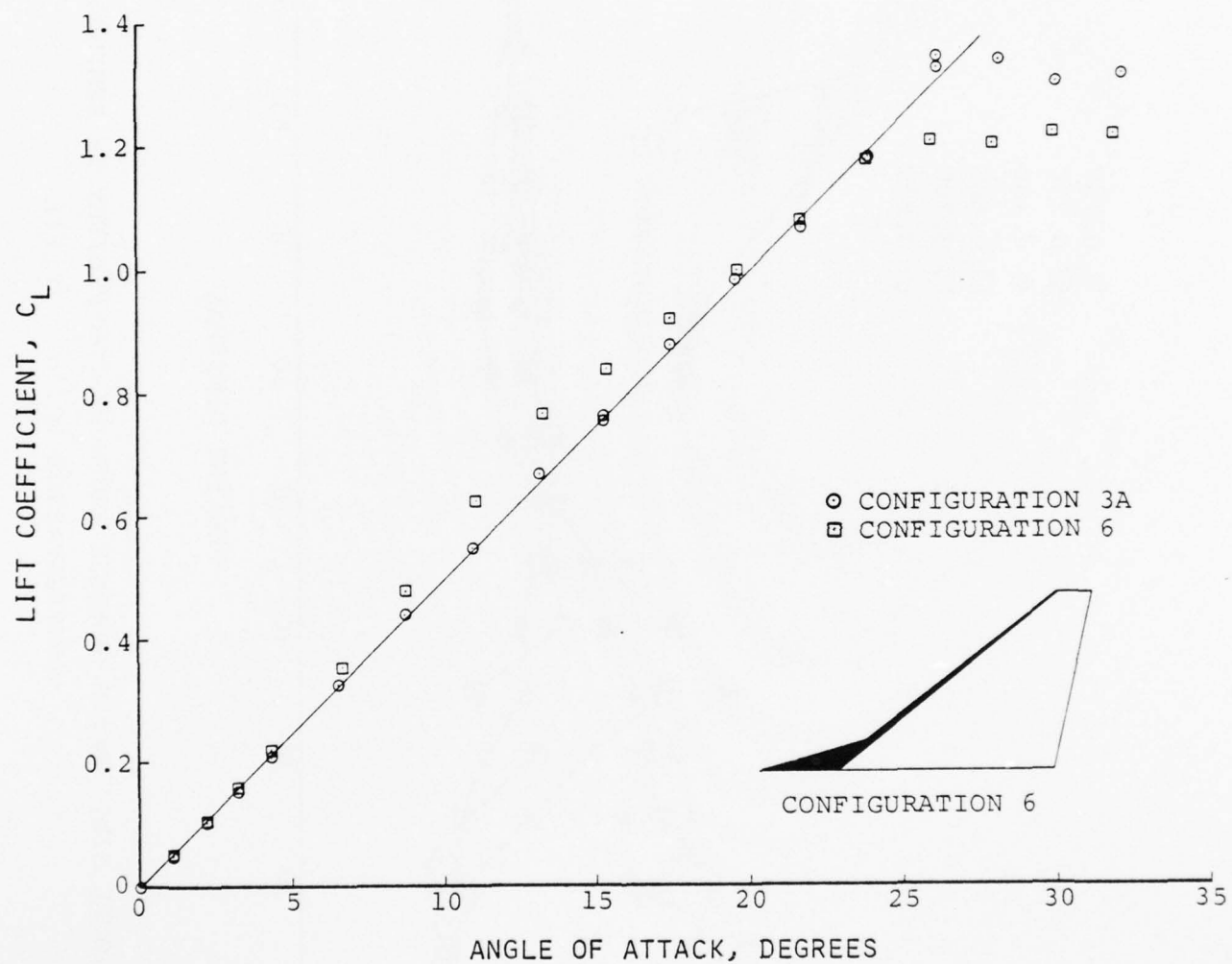


FIGURE 23. LIFT COEFFICIENT VS ANGLE OF ATTACK.
(CONFIGURATION 6)

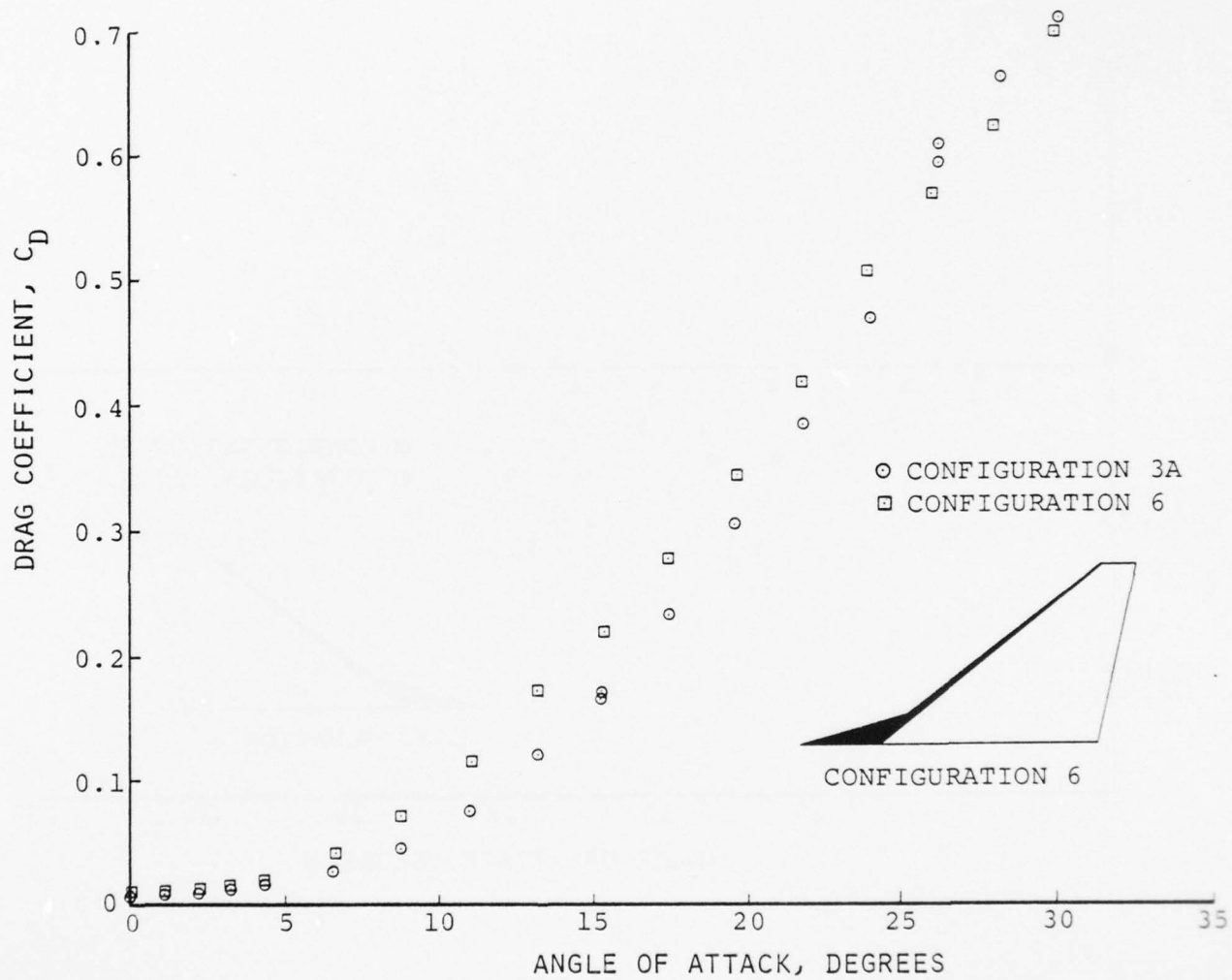


FIGURE 24. DRAG COEFFICIENT VS ANGLE OF ATTACK.
(CONFIGURATION 6)

AD-A042 917

SYSTEMS RESEARCH LABS INC NEWPORT NEWS VA RASA DIV F/G 20/4
A THEORETICAL AND EXPERIMENTAL INVESTIGATION OF VORTEX FLOW CON--ETC(U)
DEC 76 R P WHITE, S T GANGWANI, J C BALCERAK N00014-74-C-0091
RASA/SRL-14-77-2 ONR-CR212-223-3 NL

UNCLASSIFIED

2 OF 2
AD
A042 917



END
DATE
FILMED
9-77
DDC

042917

1.0 1.1 1.25 1.4 1.6 1.8 2.0 2.2 2.5 2.8 3.2 3.6 4.0 4.5 5.0 5.6 6.3 7.1 8.0 9.0 10 11 12.5 14 16 18 20 22.5 25 28 32 36 40 45 50 56 63 71 80 90 100

MICROCOPY RESOLUTION TEST CHART
NATIONAL BUREAU OF STANDARDS-1963-A

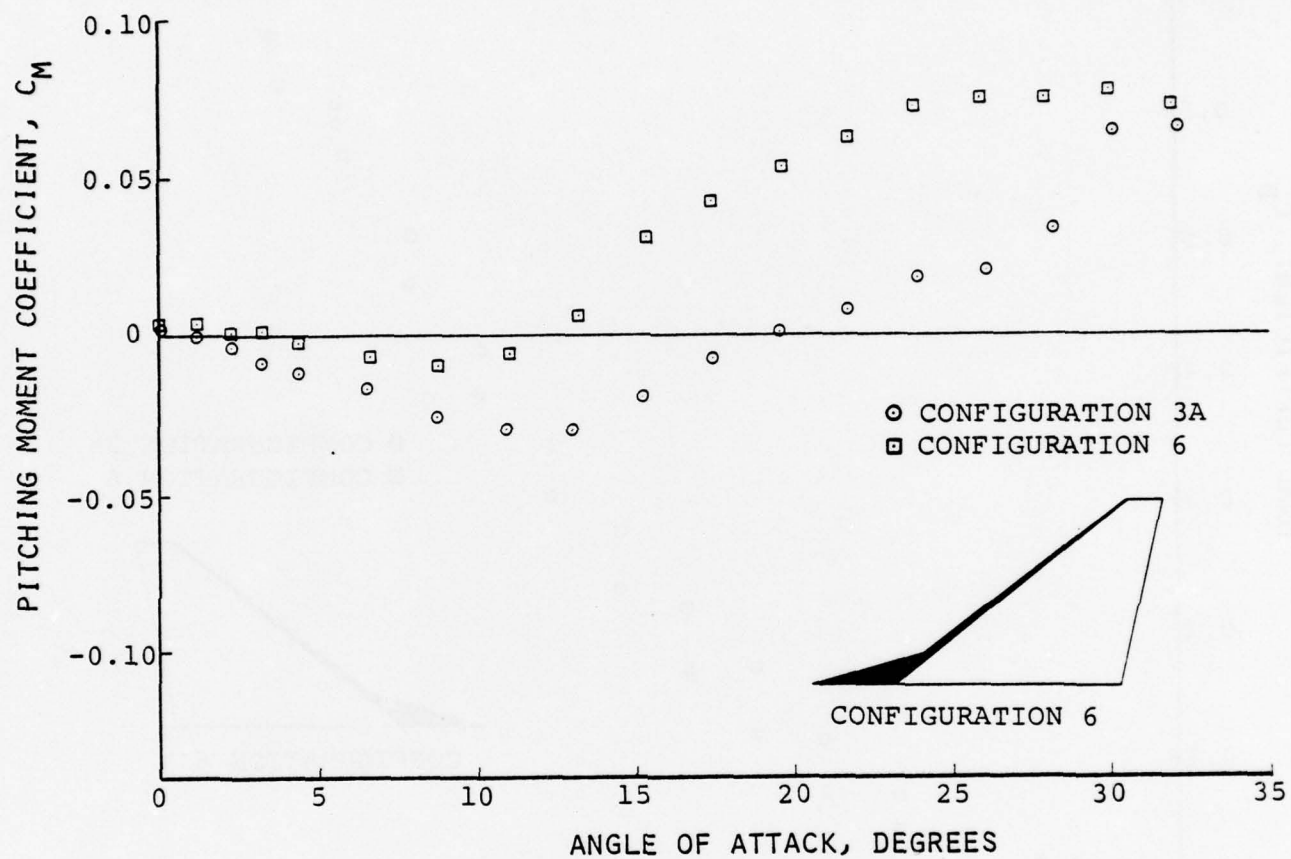


FIGURE 25. PITCHING MOMENT COEFFICIENT VS ANGLE OF ATTACK.
(CONFIGURATION 6)

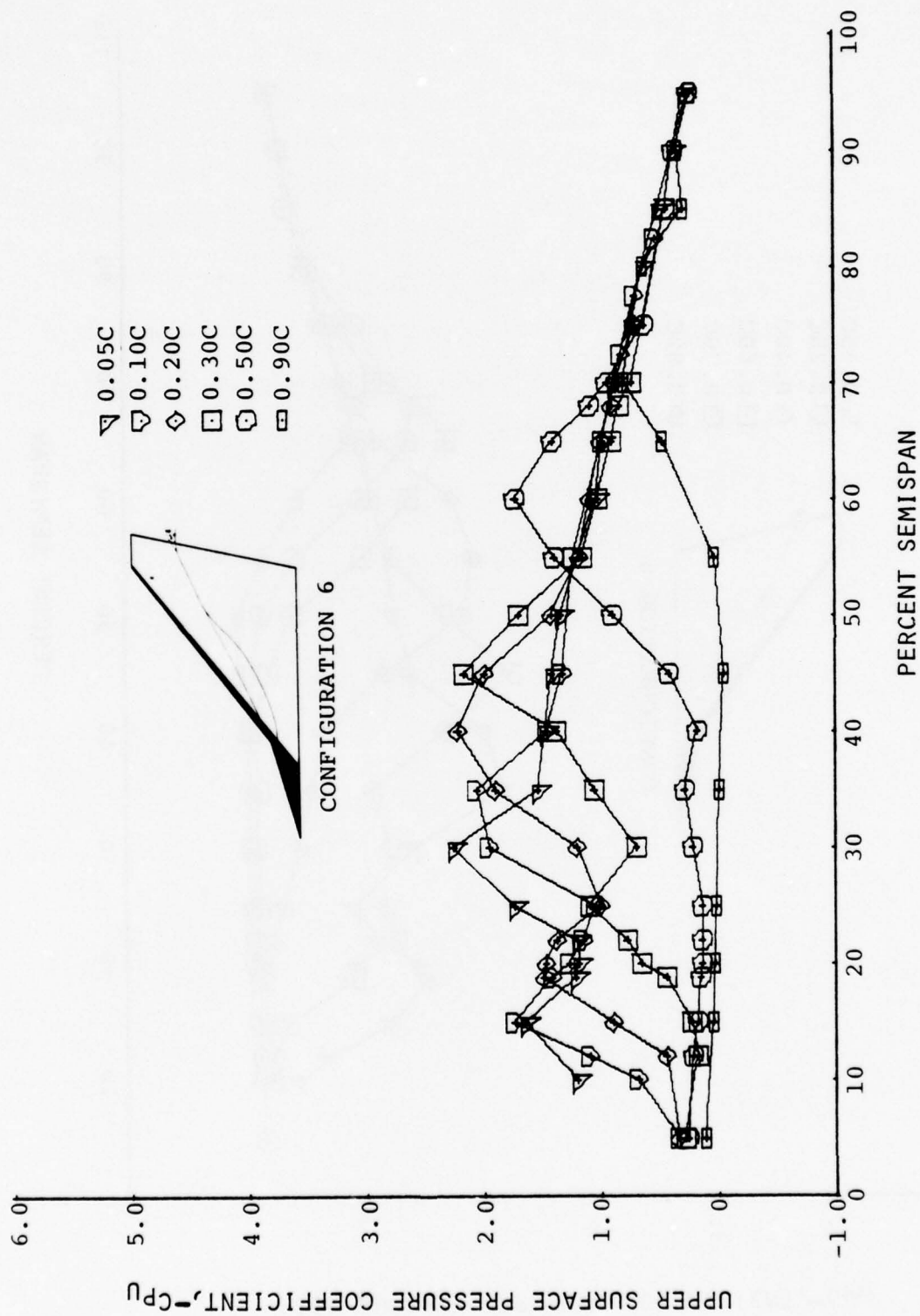


FIGURE 26a. UPPER SURFACE PRESSURE COEFFICIENT VS SEMISPAN.
(CONFIGURATION 6, $\alpha = 13.1^\circ$)

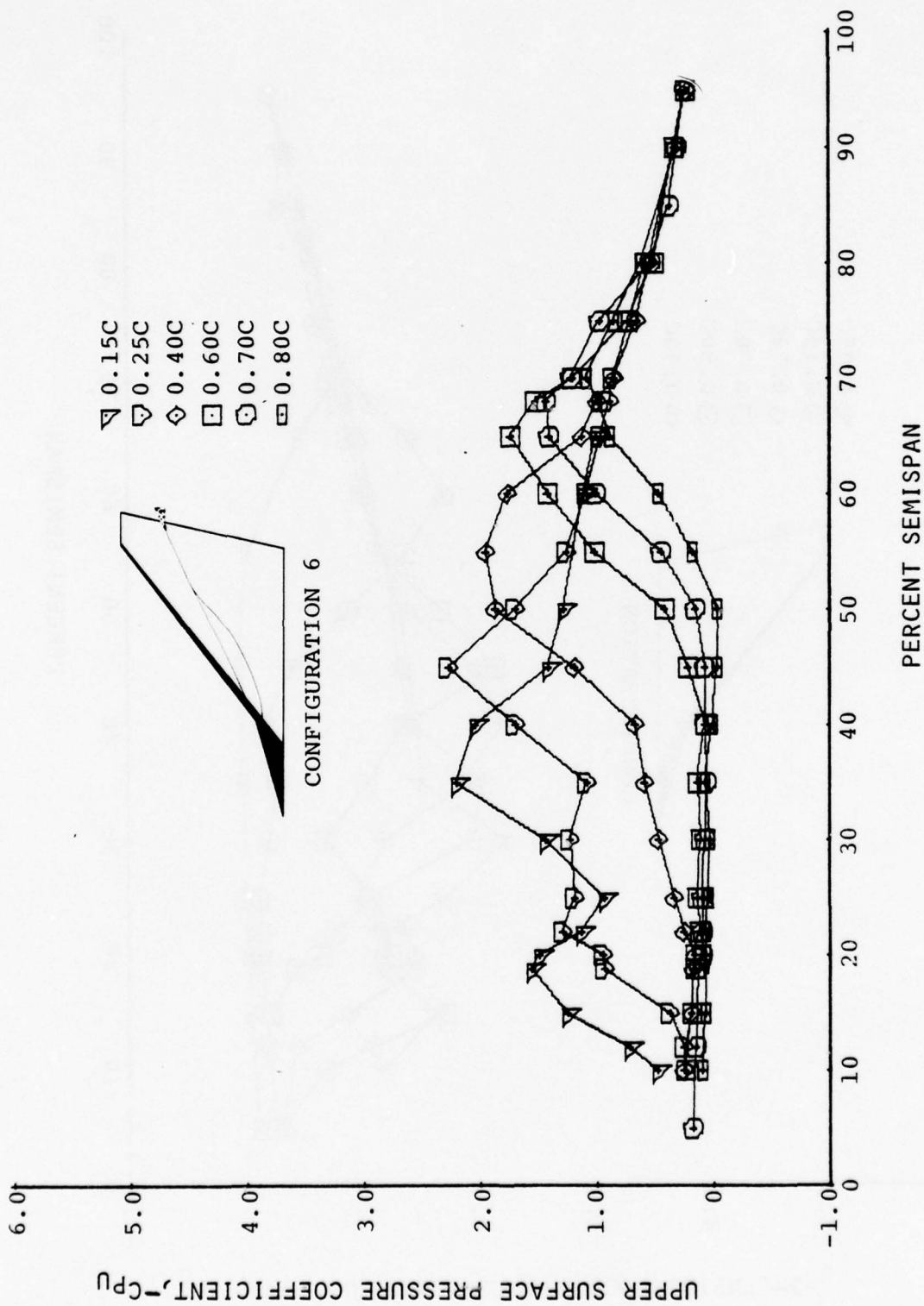


FIGURE 26b. UPPER SURFACE PRESSURE COEFFICIENT VS SEMISPAN.
(CONFIGURATION 6, $\alpha = 13.1^\circ$)

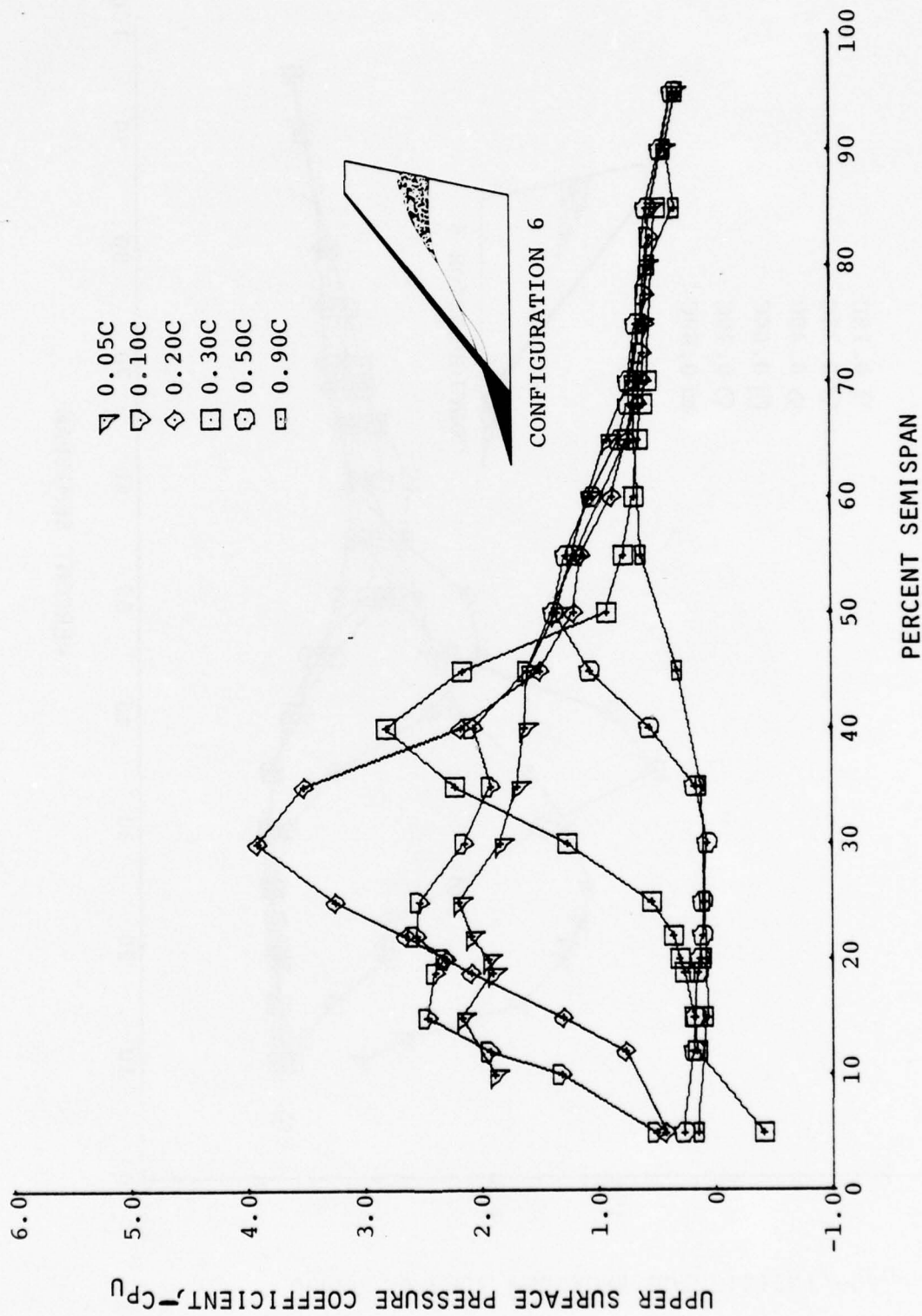


FIGURE 27a. UPPER SURFACE PRESSURE COEFFICIENT VS SEMISPAN.
(CONFIGURATION 6, $\alpha = 17.4^\circ$)

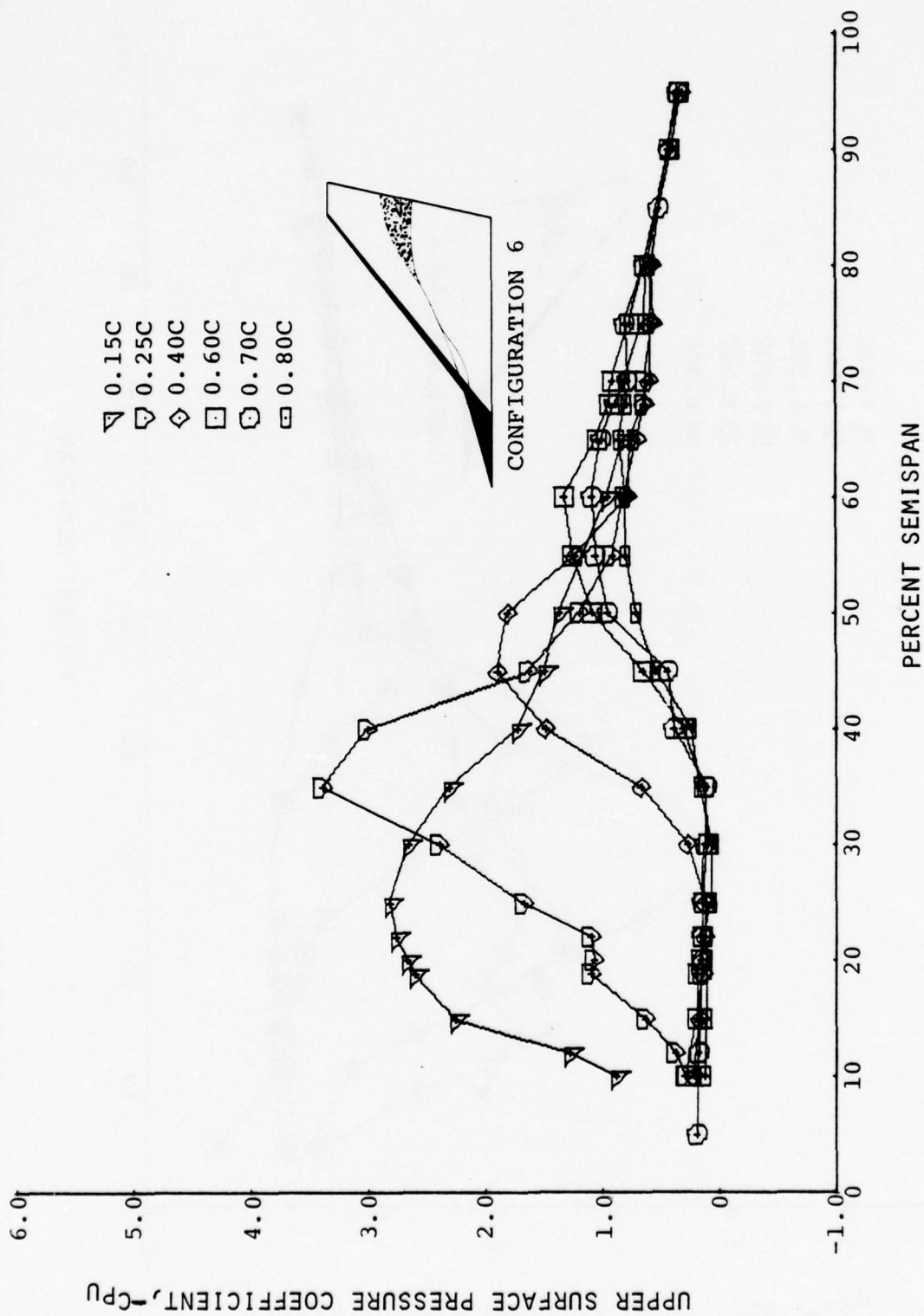


FIGURE 27b. UPPER SURFACE PRESSURE COEFFICIENT VS SEMISPAN.
(CONFIGURATION 6, $\alpha = 17.4^\circ$)

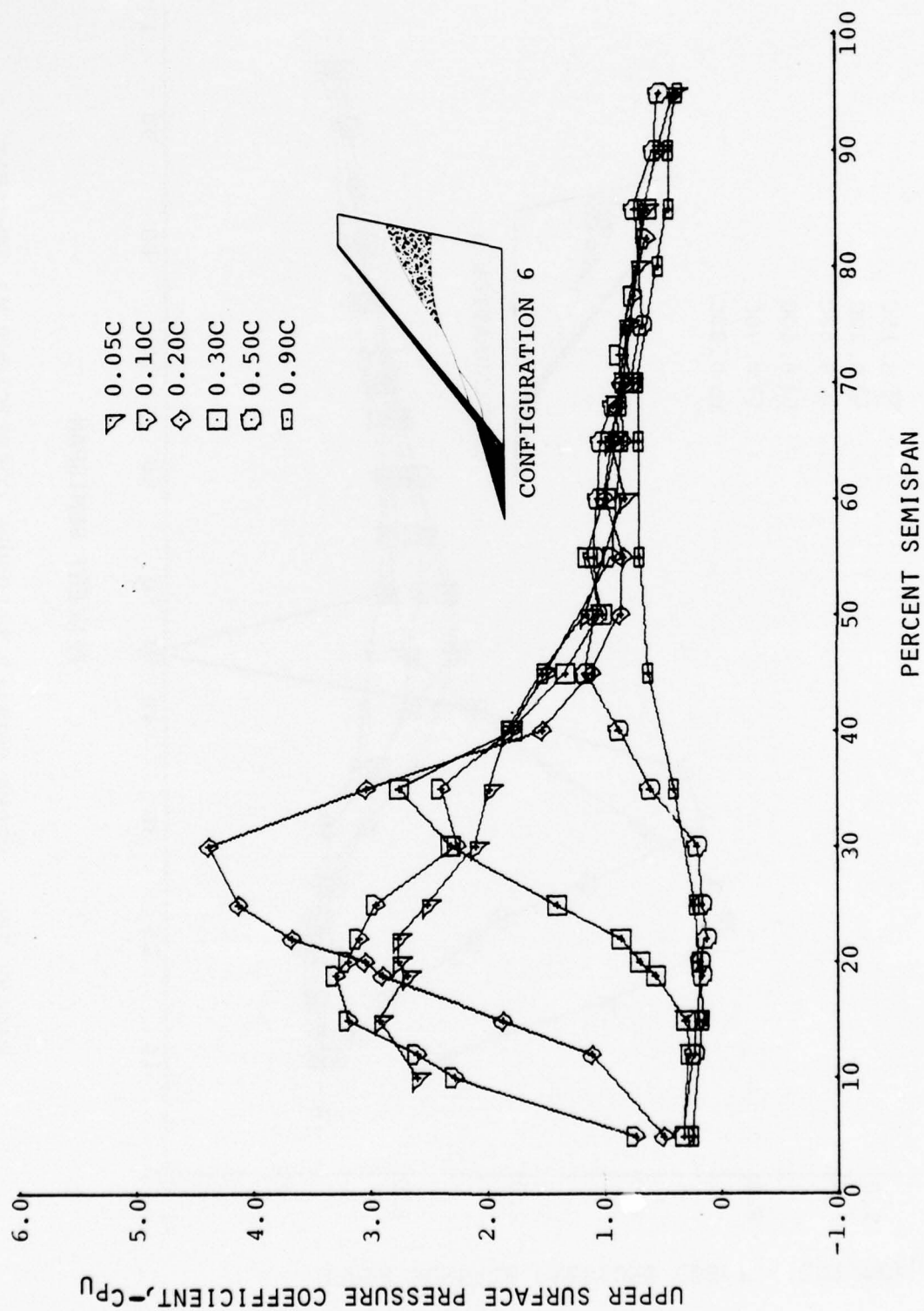


FIGURE 28a. UPPER SURFACE PRESSURE COEFFICIENT VS SEMISPAN.
(CONFIGURATION 6, $\alpha = 21.7^\circ$)

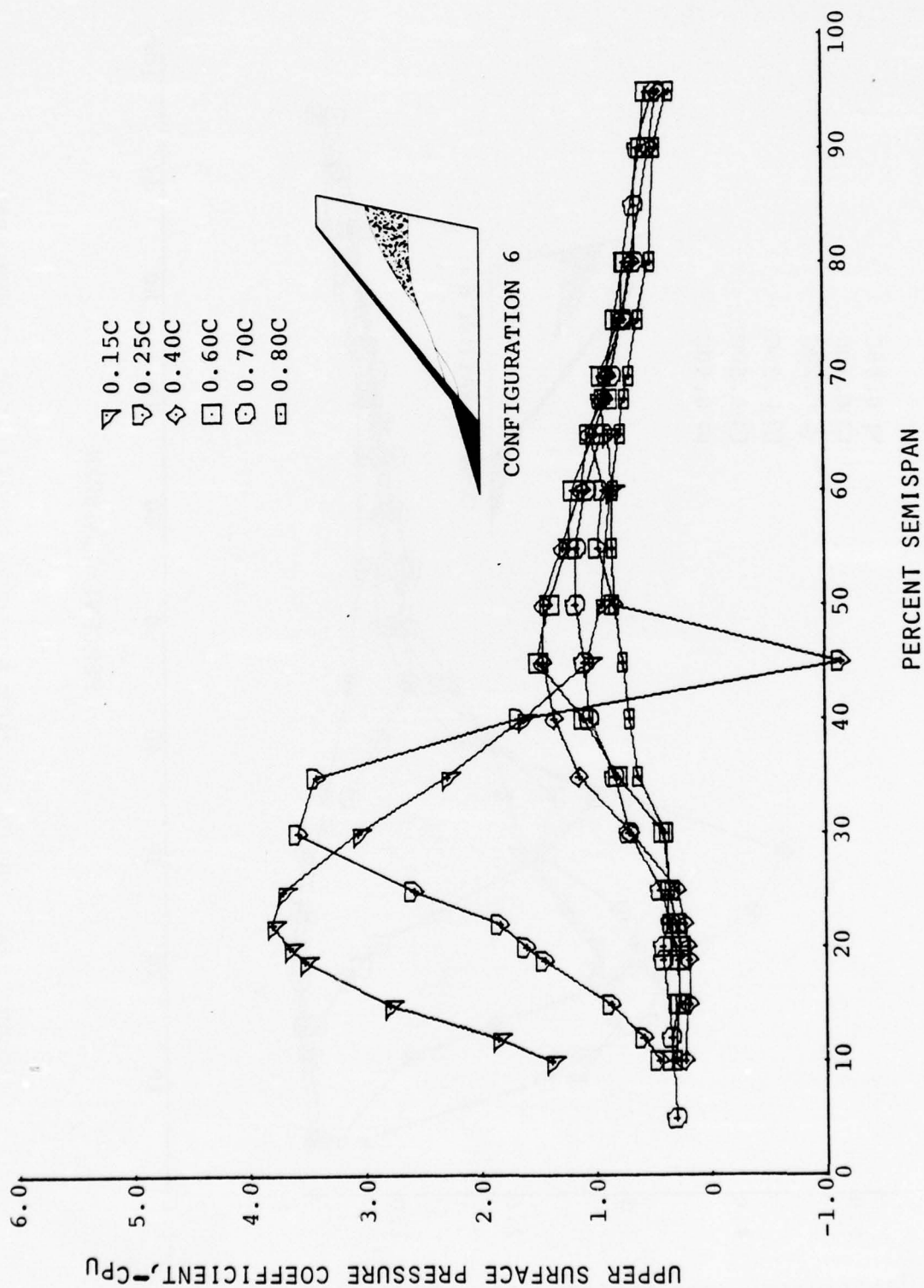


FIGURE 28b. UPPER SURFACE PRESSURE COEFFICIENT VS SEMISPAN.
(CONFIGURATION 6, $\alpha = 21.7^\circ$)

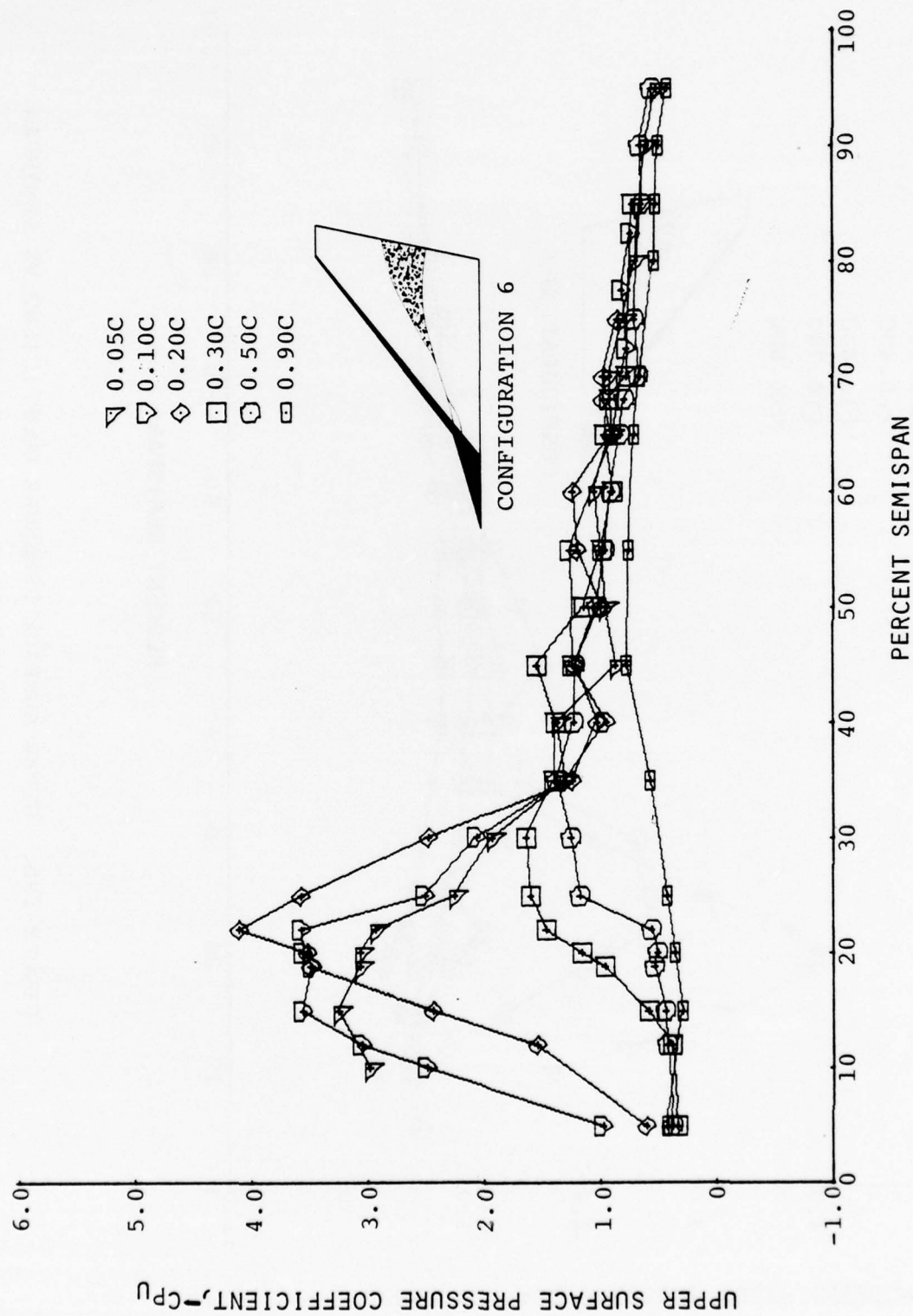


FIGURE 29a. UPPER SURFACE PRESSURE COEFFICIENT VS SEMISPAN.
(CONFIGURATION 6, $\alpha = 26.1^\circ$)

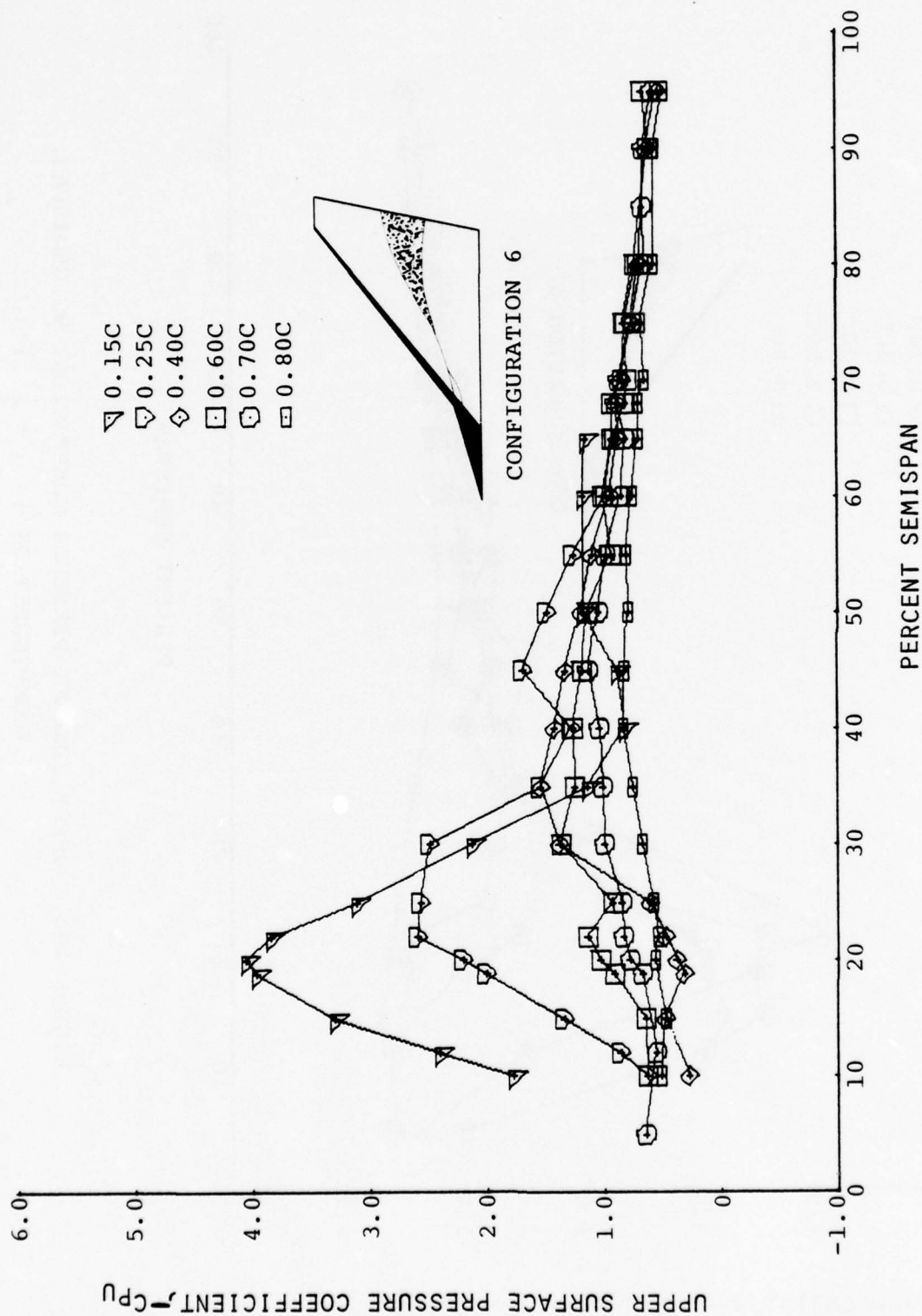


FIGURE 29b. UPPER SURFACE PRESSURE COEFFICIENT VS SEMISPAN.
(CONFIGURATION 6, $\alpha = 26.1^\circ$)

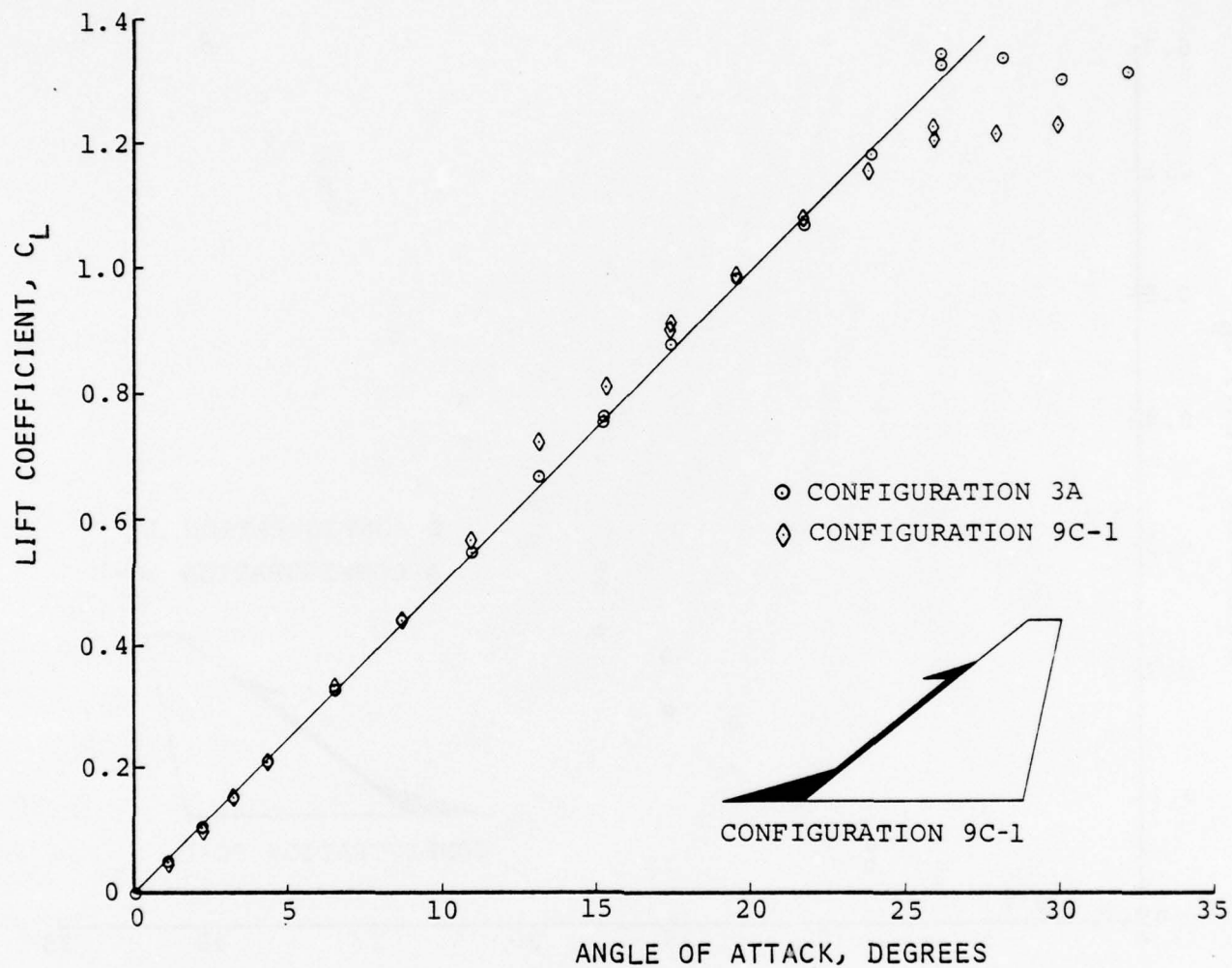


FIGURE 30. LIFT COEFFICIENT VS ANGLE OF ATTACK.
(CONFIGURATION 9C-1)

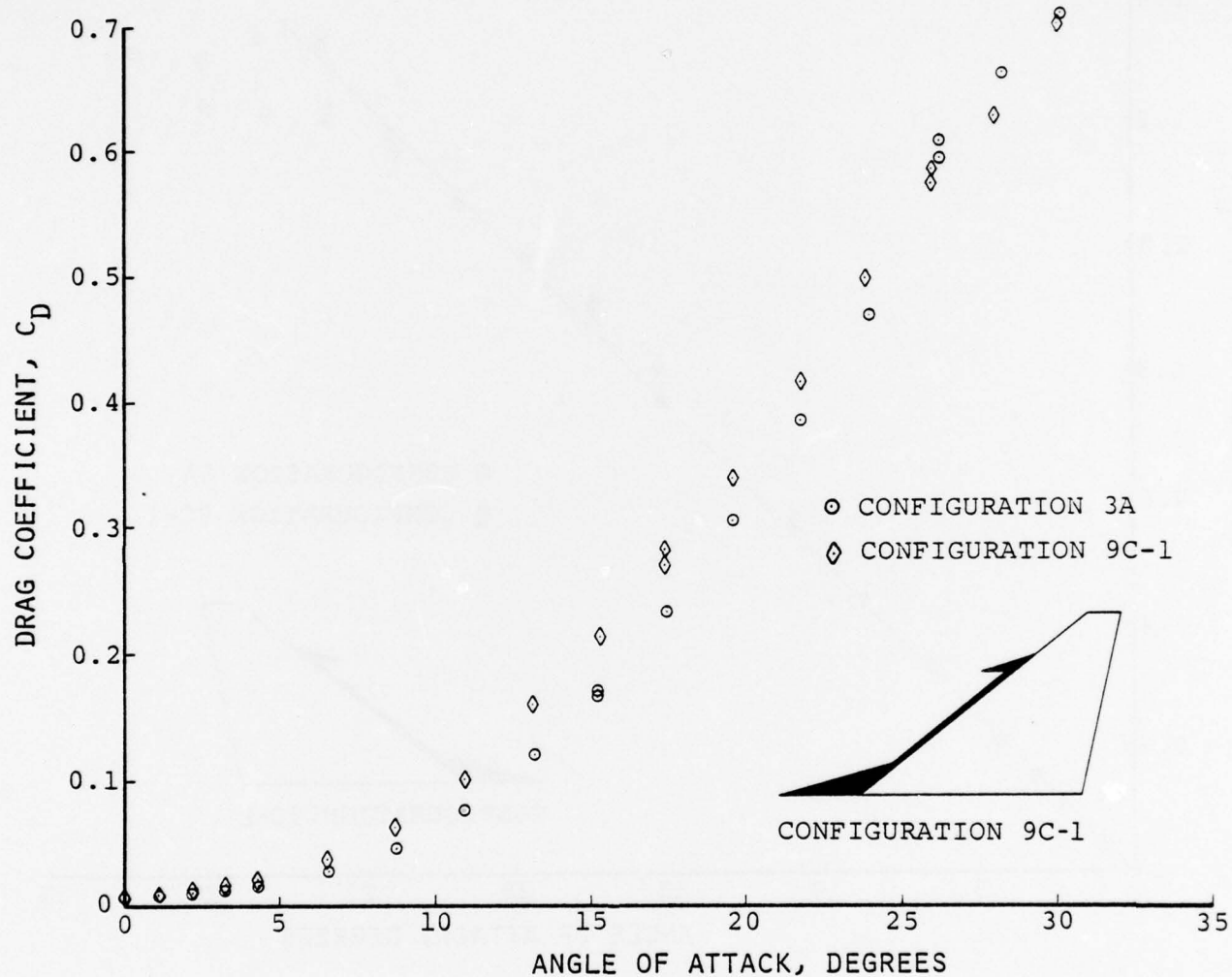


FIGURE 31. DRAG COEFFICIENT VS ANGLE OF ATTACK.
(CONFIGURATION 9C-1).

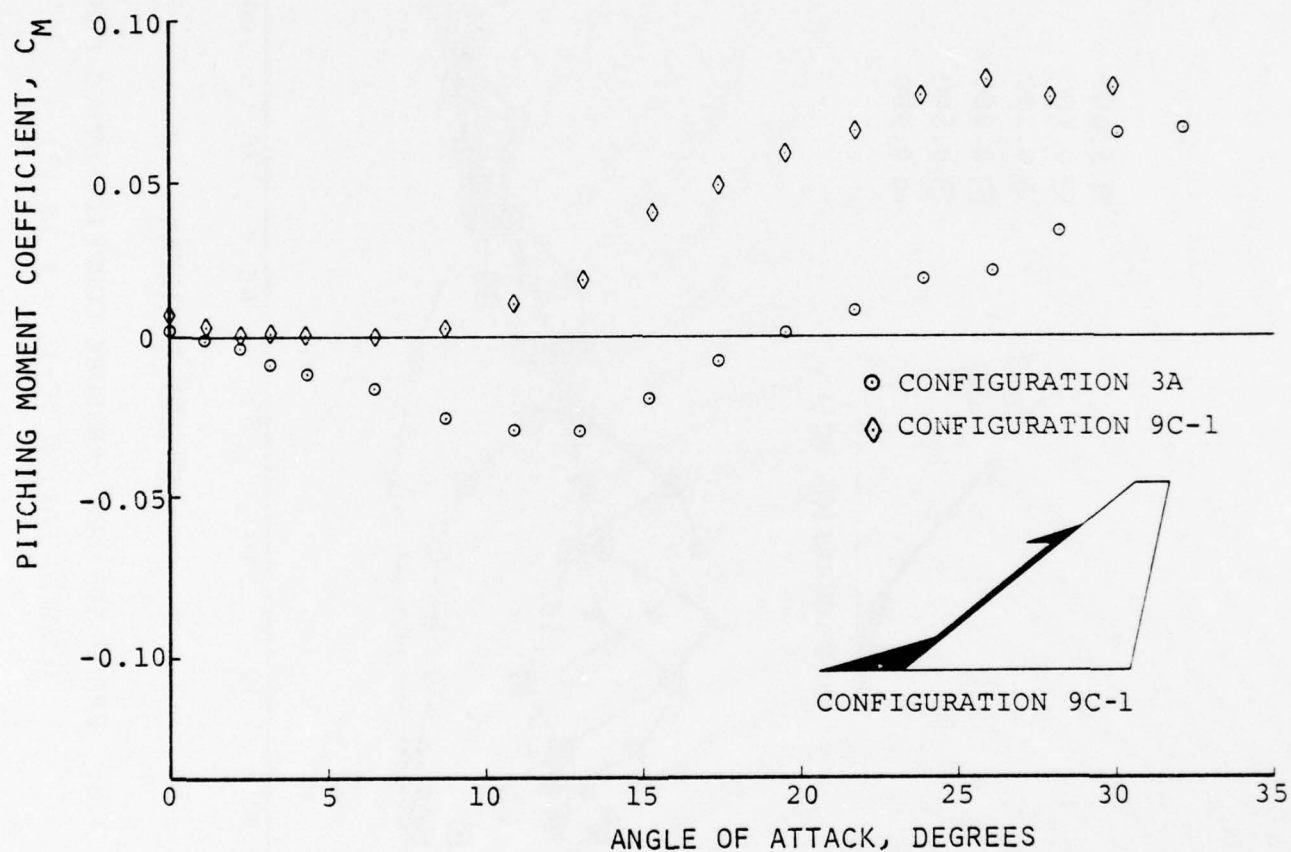


FIGURE 32. PITCHING MOMENT COEFFICIENT VS ANGLE OF ATTACK.
(CONFIGURATION 9C-1)

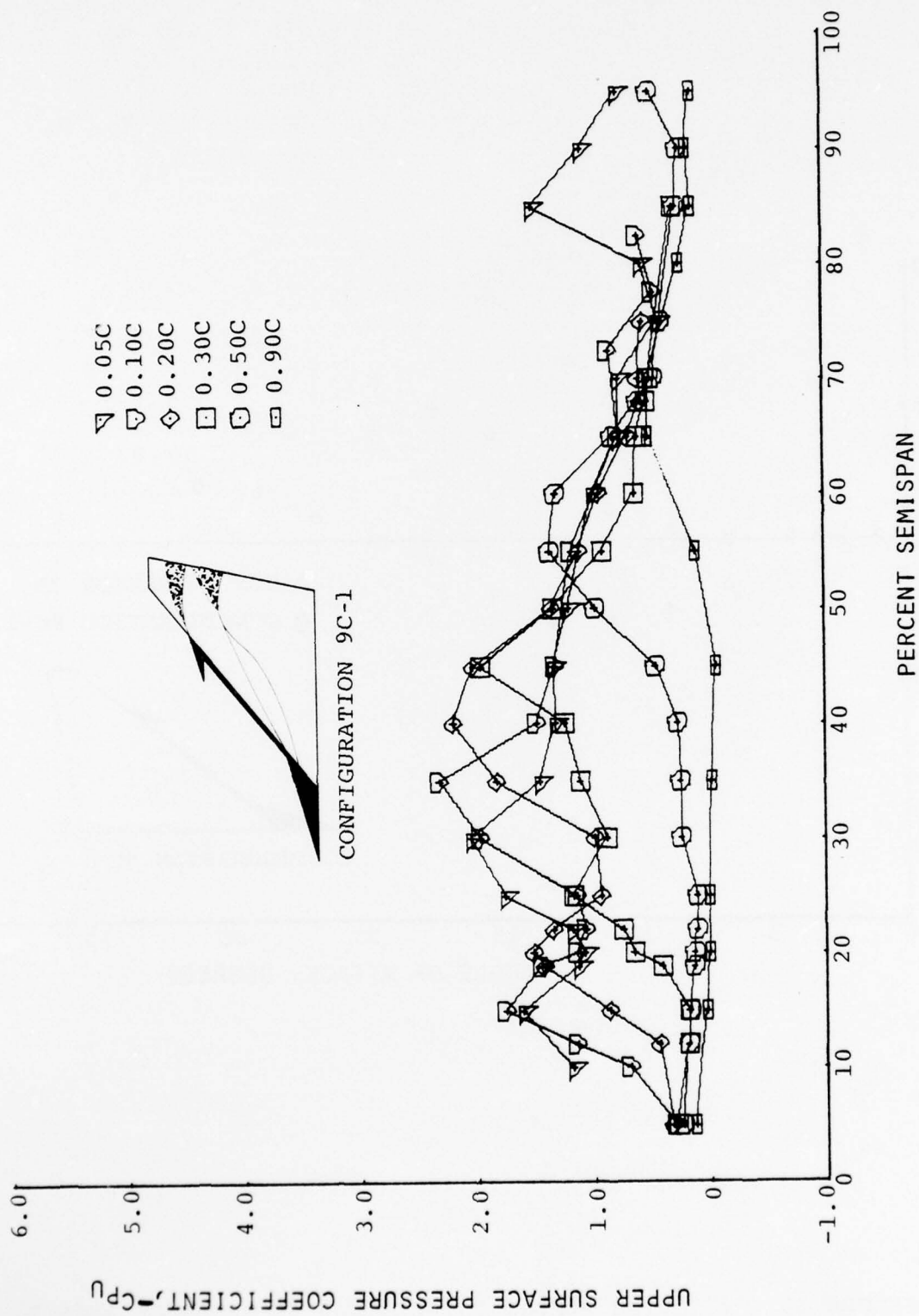


FIGURE 33a. UPPER SURFACE PRESSURE COEFFICIENT VS SEMISPAN.
(CONFIGURATION 9C-1, $\alpha = 13.1^\circ$)

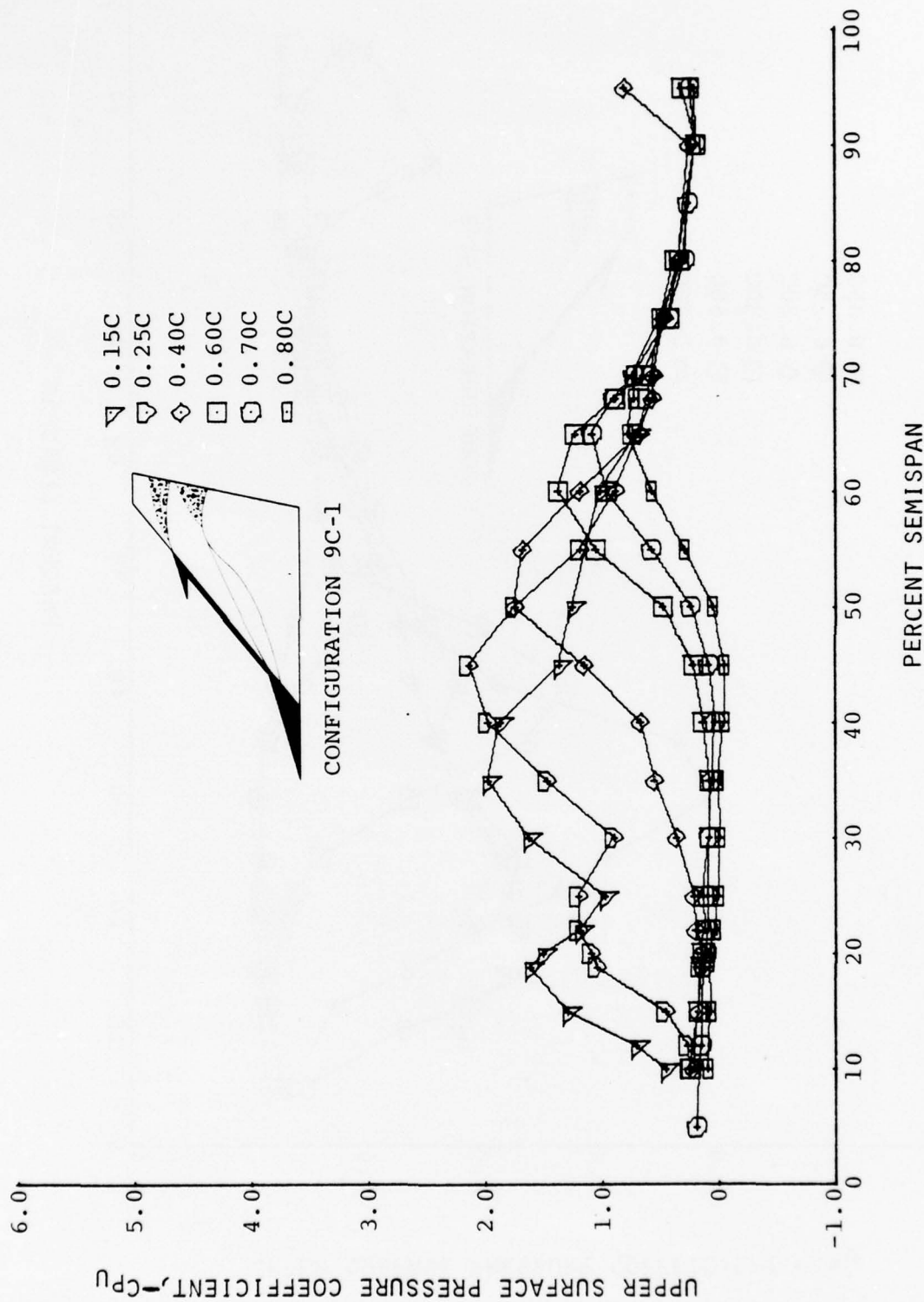


FIGURE 33b. UPPER SURFACE PRESSURE COEFFICIENT VS SEMISPAN.
(CONFIGURATION 9C-1, $\alpha = 13.1^\circ$)

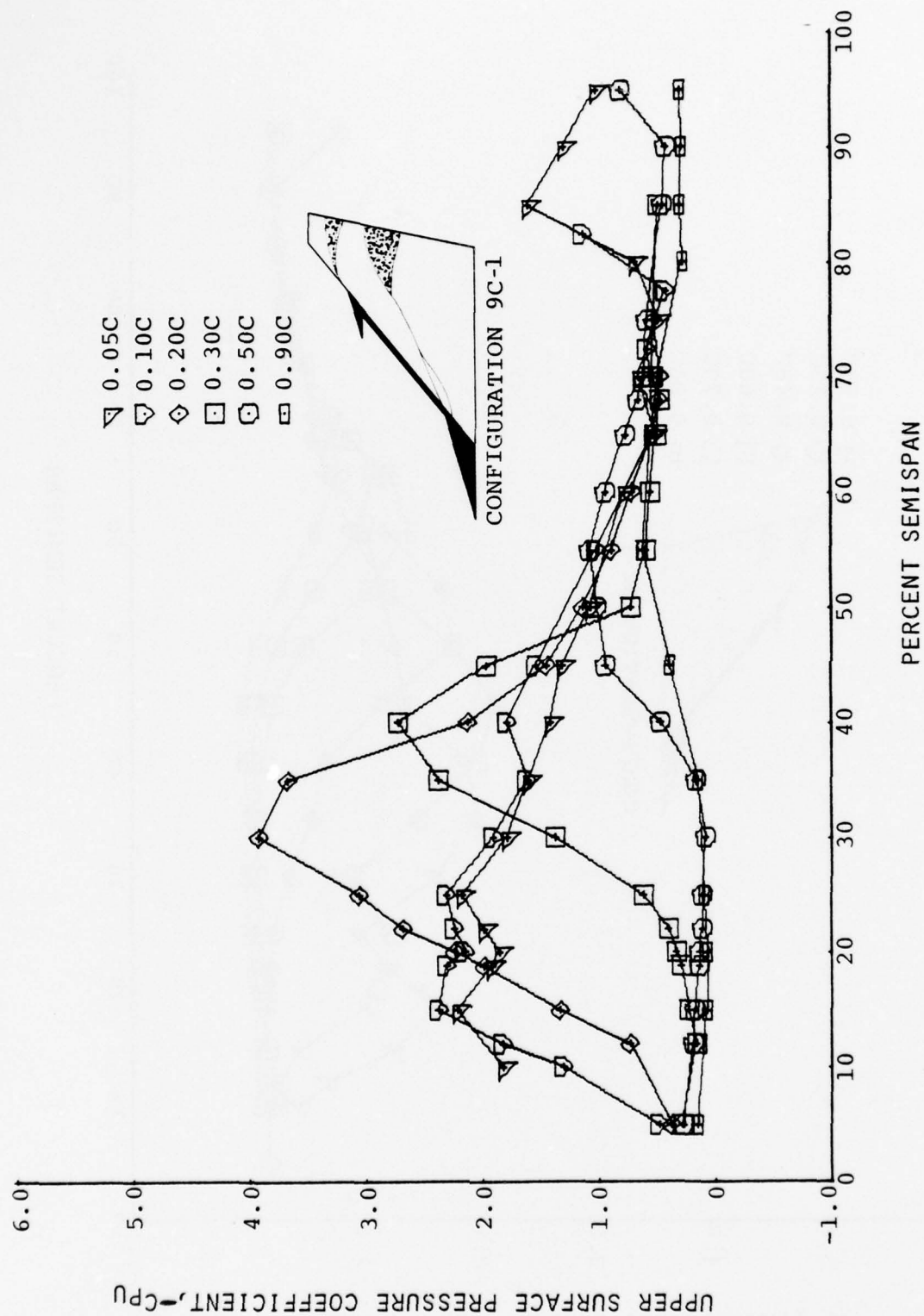


FIGURE 34a. UPPER SURFACE PRESSURE COEFFICIENT VS SEMISPAN.
(CONFIGURATION 9C-1, $\alpha = 17.4^\circ$)

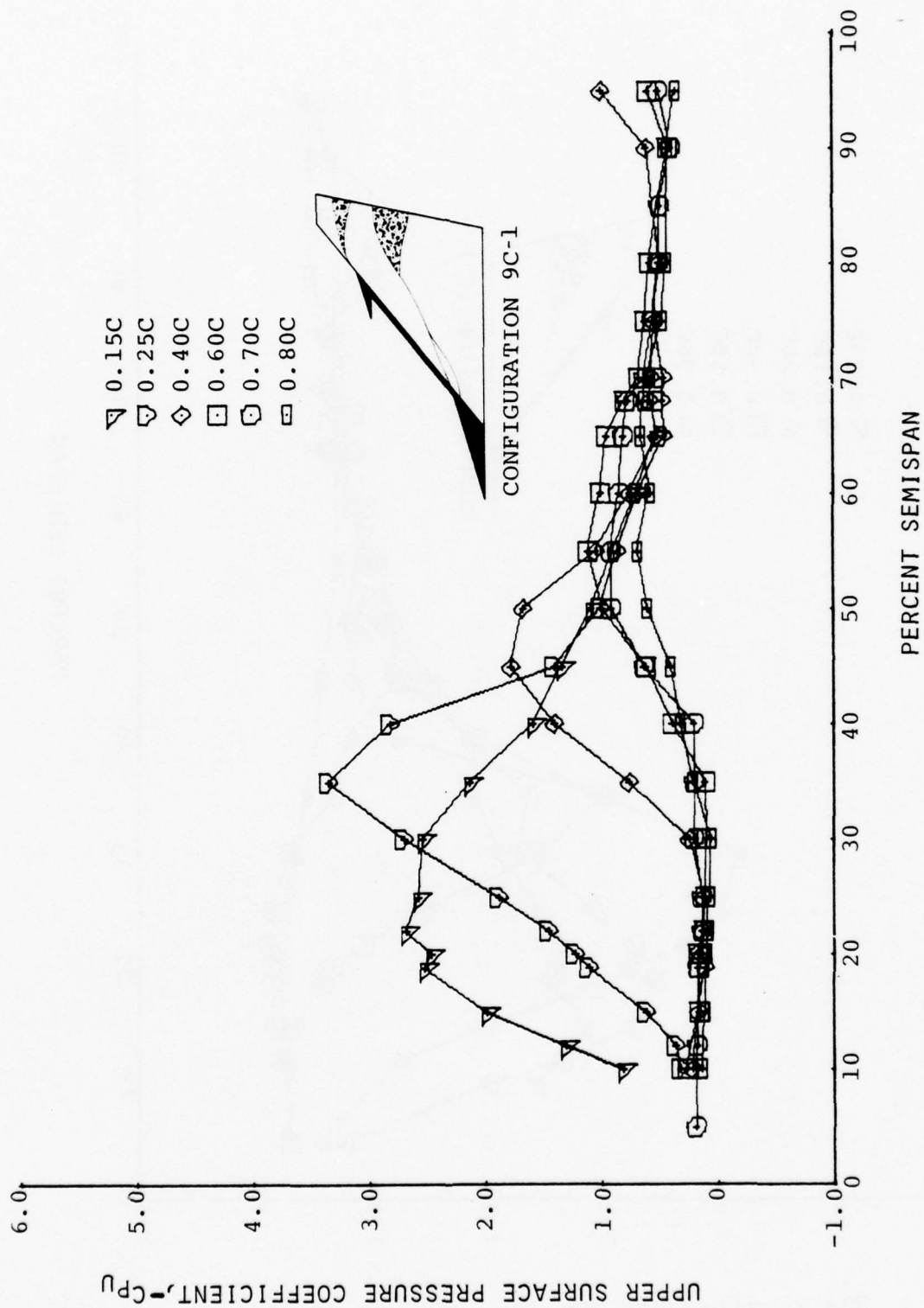


FIGURE 34b. UPPER SURFACE PRESSURE COEFFICIENT VS SEMISPAN.
(CONFIGURATION 9C-1, $\alpha = 17.4^\circ$)

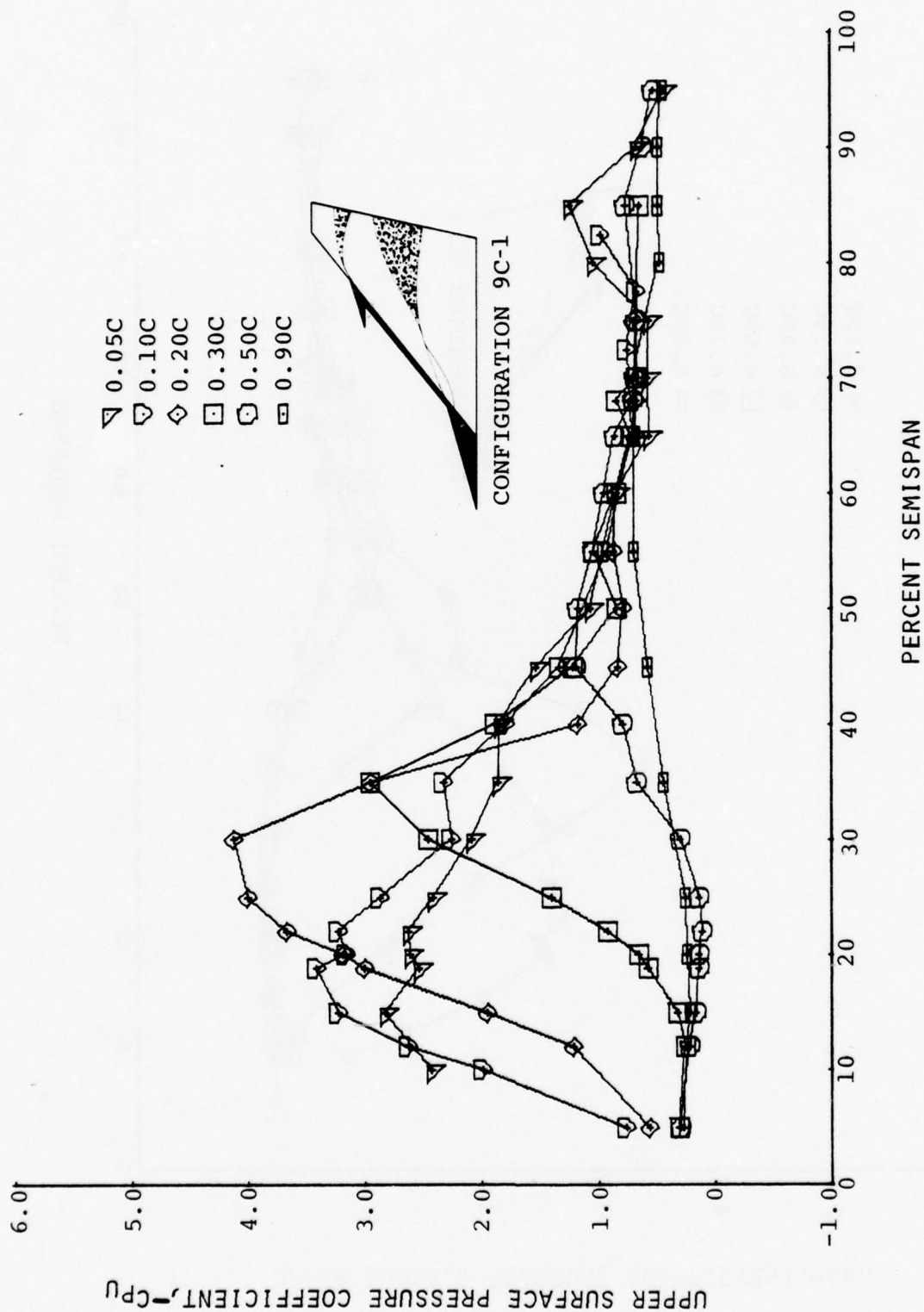


FIGURE 35a. UPPER SURFACE PRESSURE COEFFICIENT VS SEMISPAN.
(CONFIGURATION 9C-1, $\alpha = 21.7^\circ$)

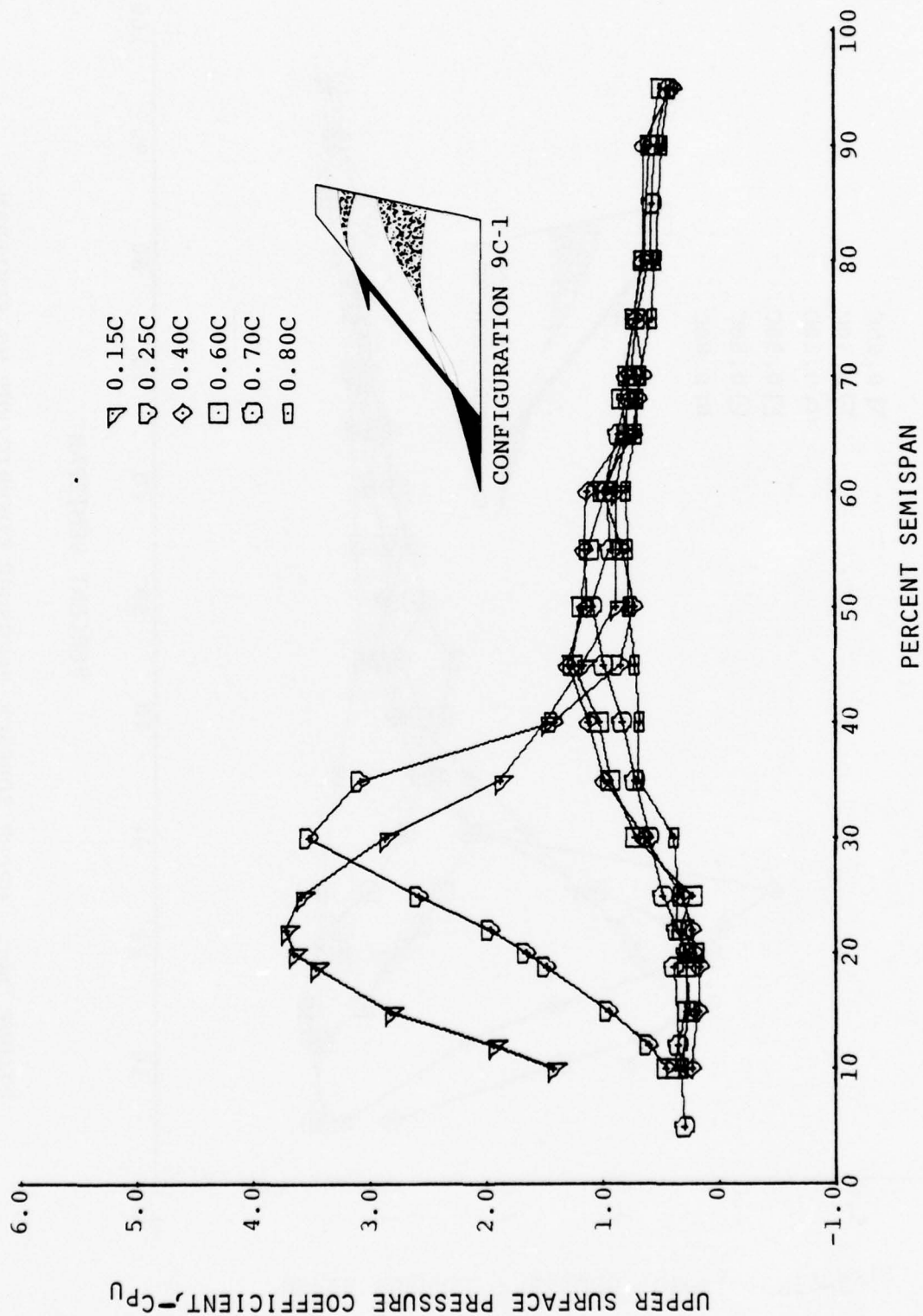


FIGURE 35b. UPPER SURFACE PRESSURE COEFFICIENT VS SEMISPAN.
(CONFIGURATION 9C-1, $\alpha = 21.7^\circ$)

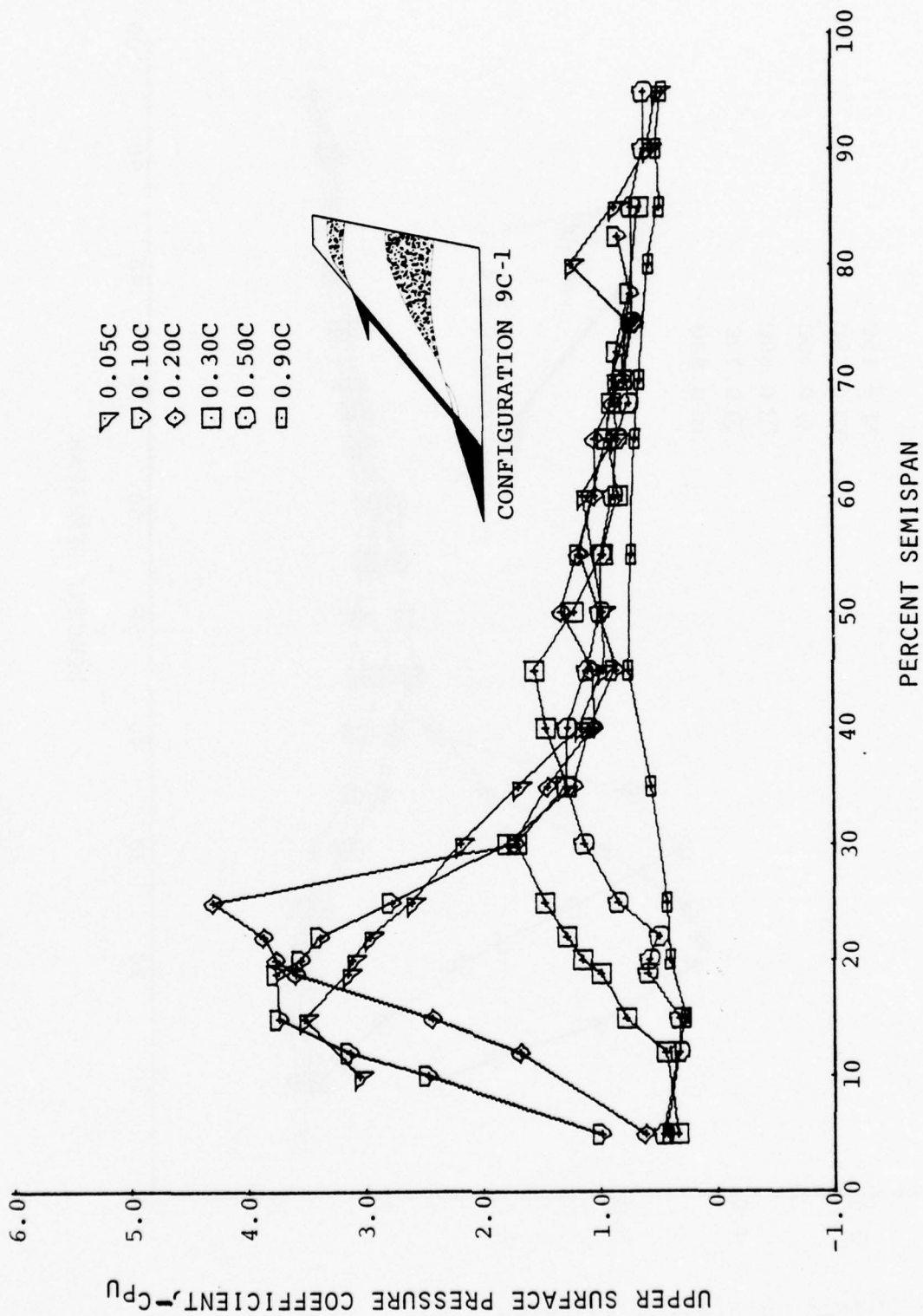


FIGURE 36a. UPPER SURFACE PRESSURE COEFFICIENT VS SEMISPAN.
(CONFIGURATION 9C-1, $\alpha = 26.1^\circ$)

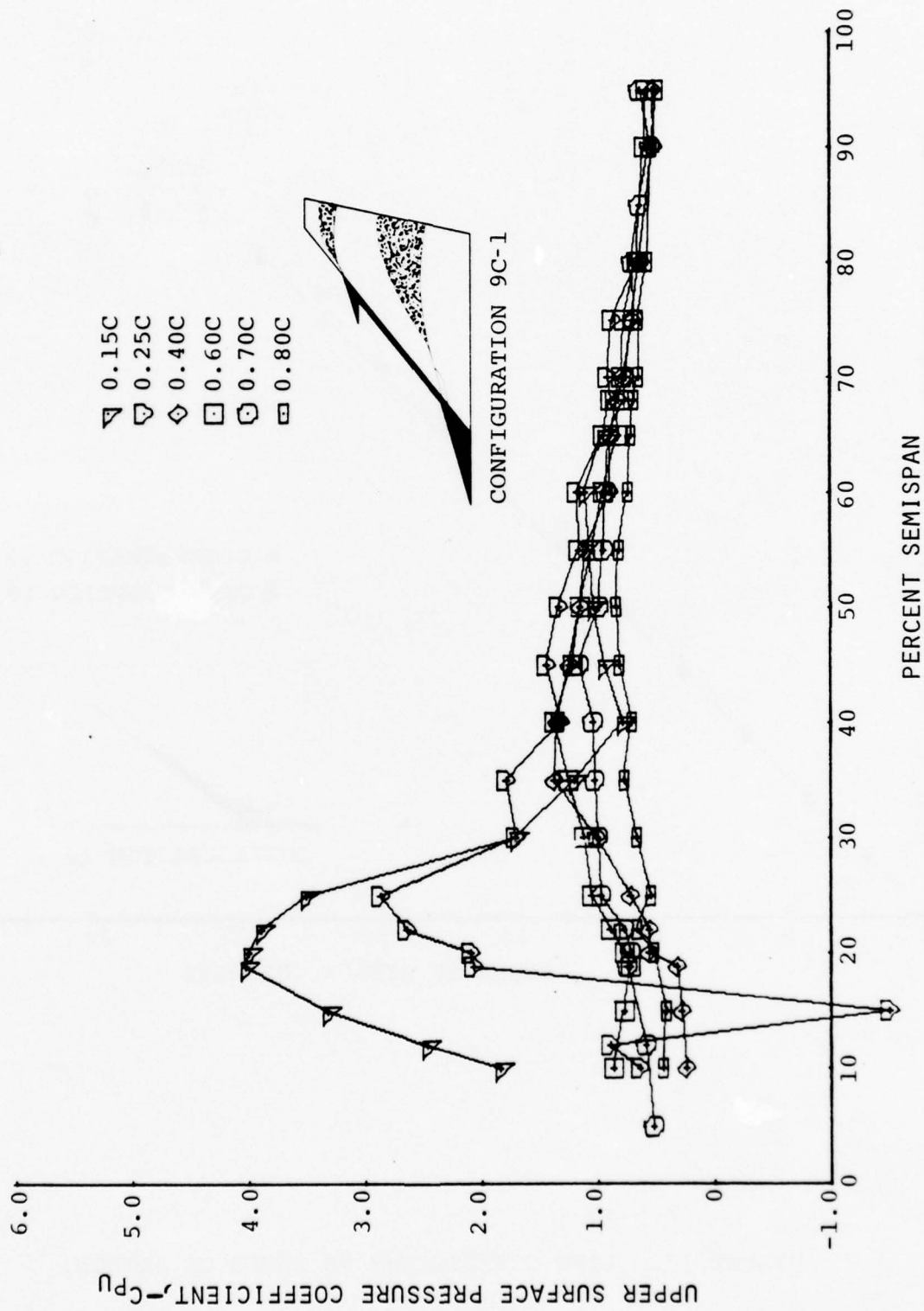


FIGURE 36b. UPPER SURFACE PRESSURE COEFFICIENT VS SEMISPAN.
(CONFIGURATION 9C-1, $\alpha = 26.1^\circ$)

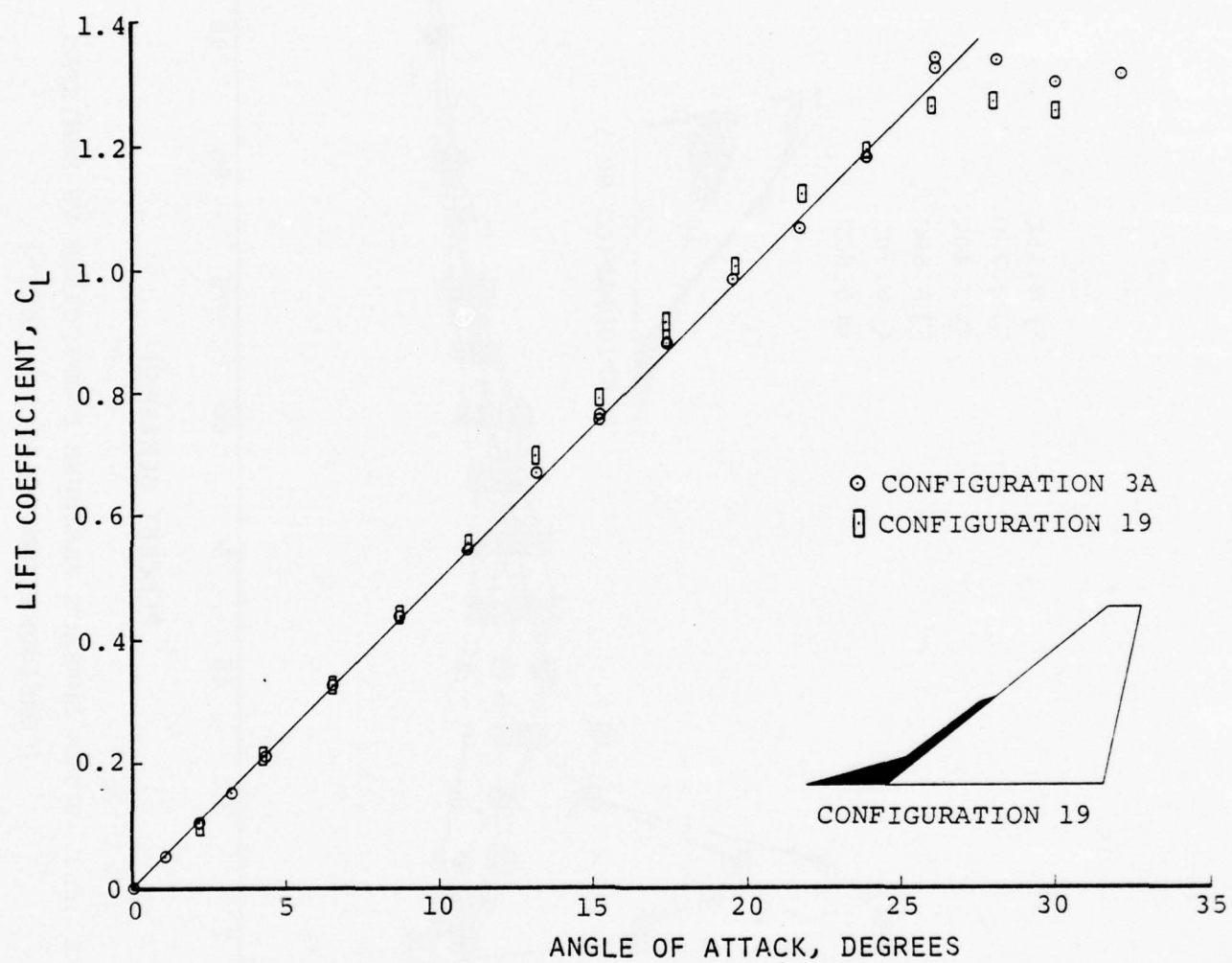


FIGURE 37. LIFT COEFFICIENT VS ANGLE OF ATTACK.
(CONFIGURATION 19)

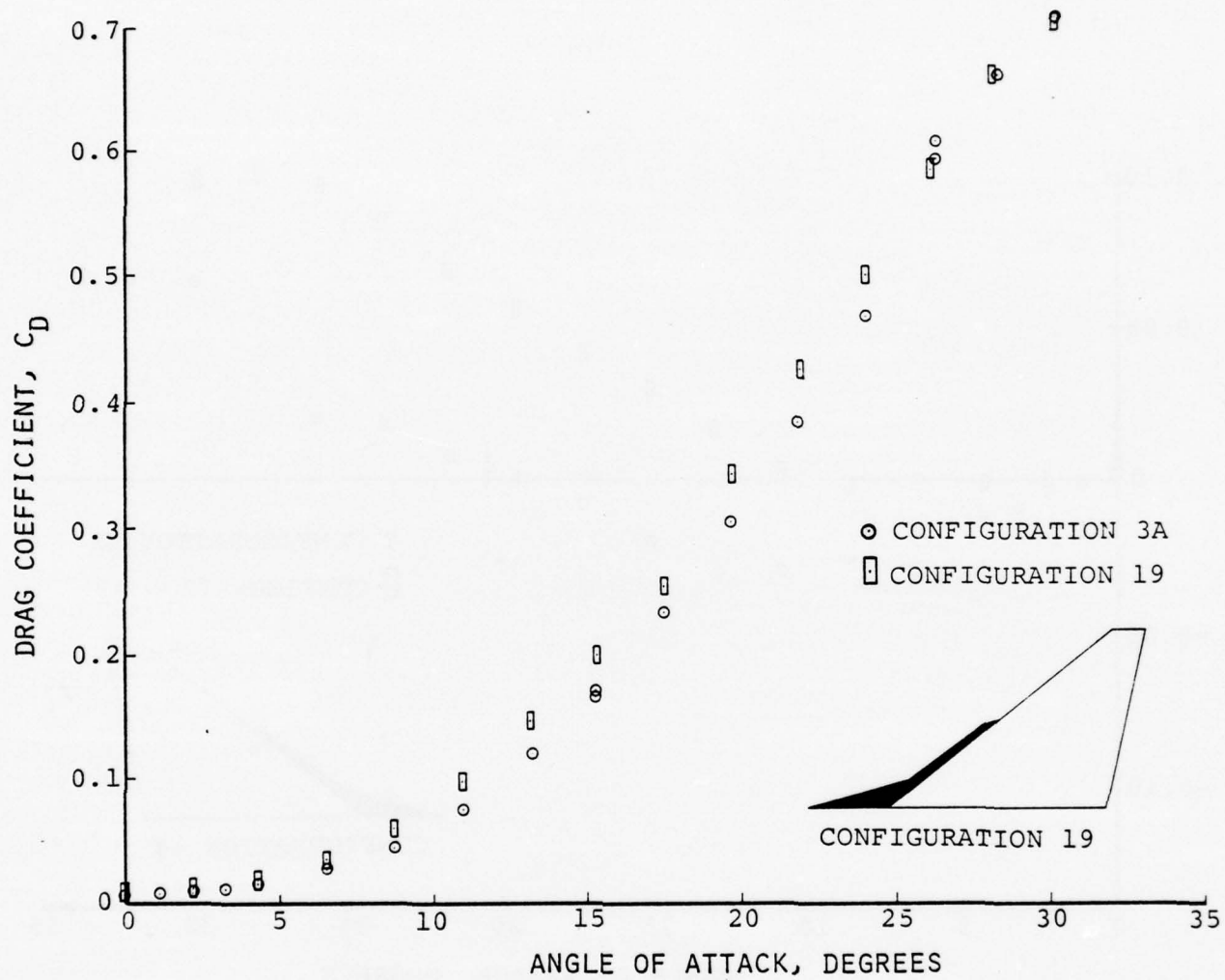


FIGURE 38. DRAG COEFFICIENT VS ANGLE OF ATTACK.
(CONFIGURATION 19)

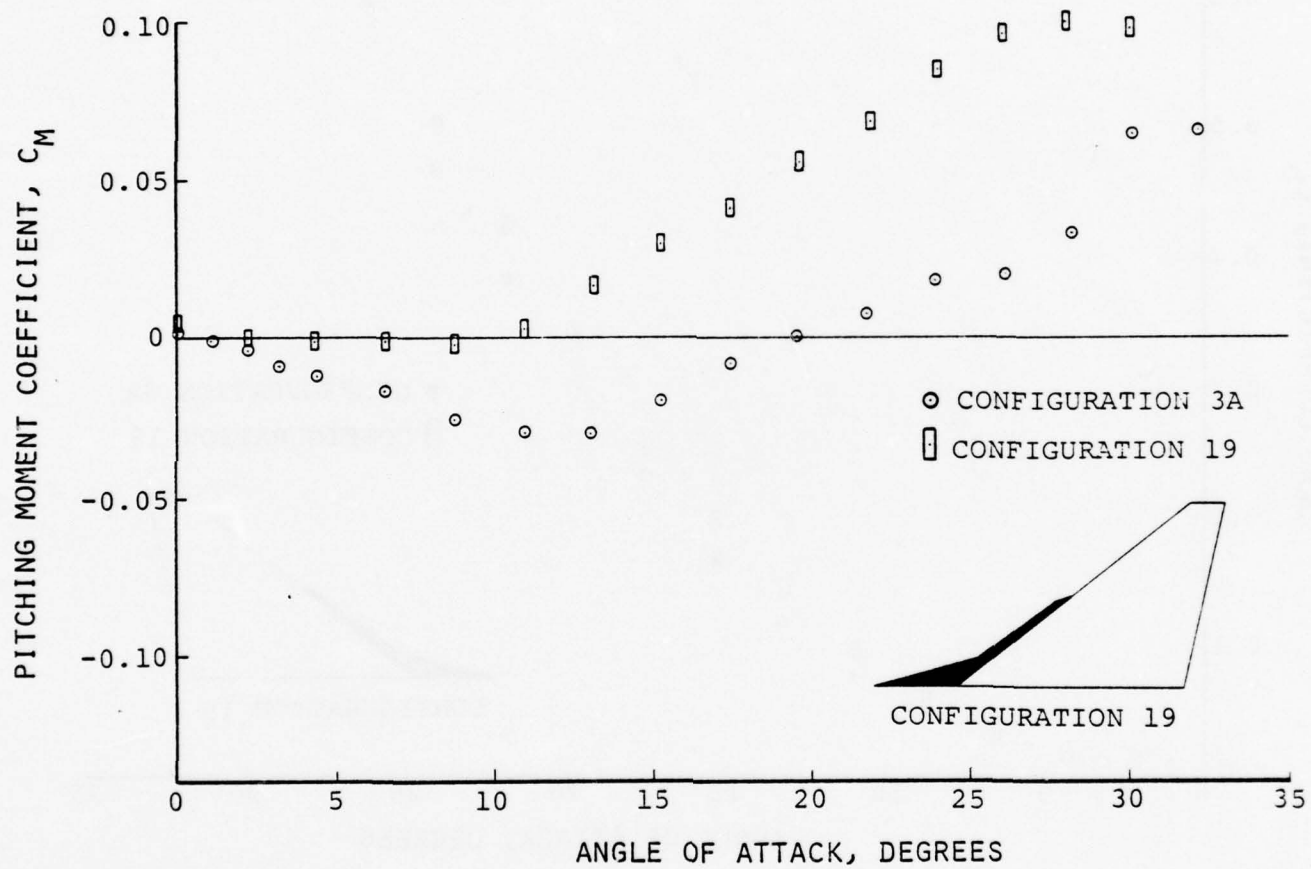


FIGURE 39. PITCHING MOMENT COEFFICIENT VS ANGLE OF ATTACK.
(CONFIGURATION 19)

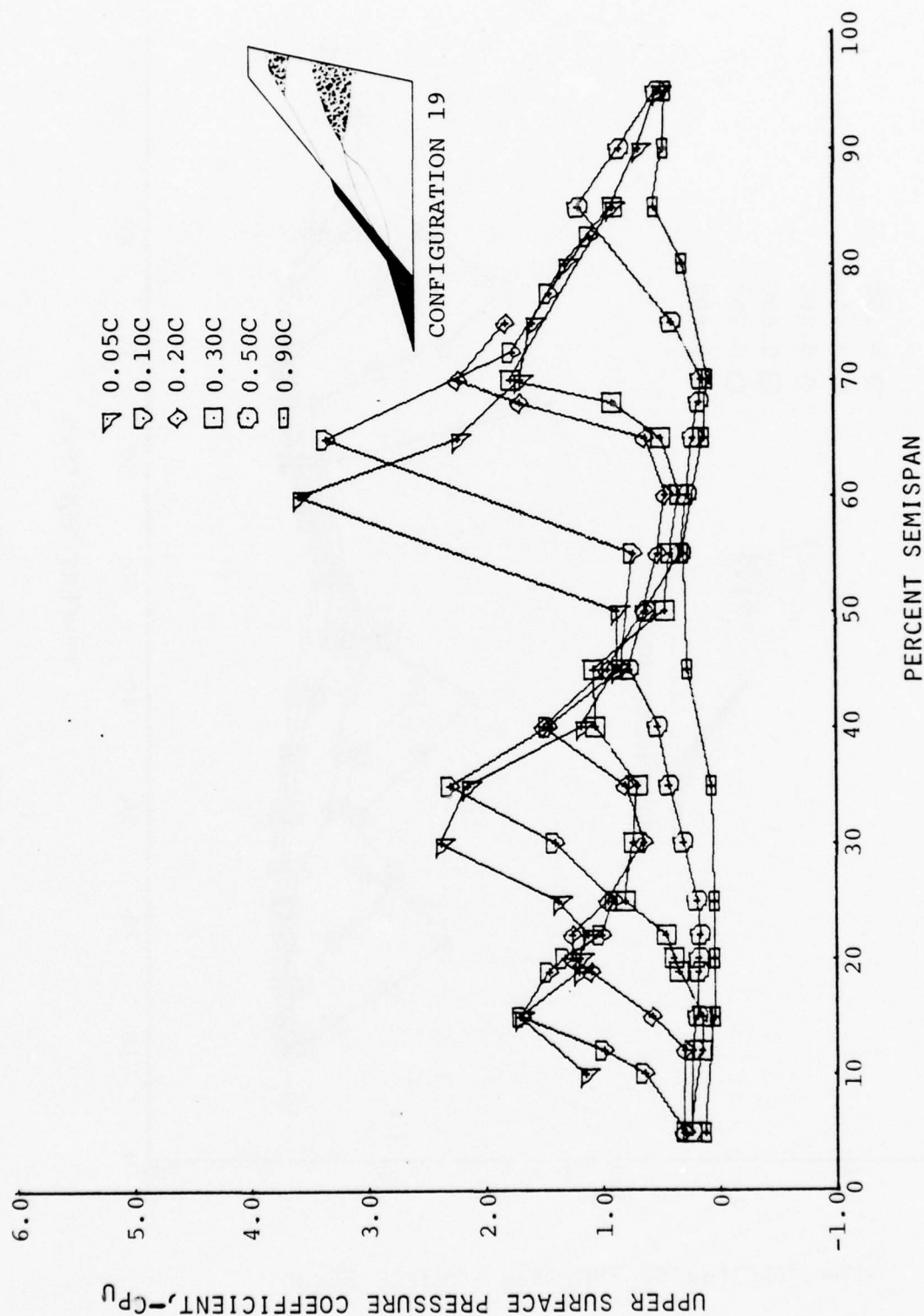


FIGURE 40a. UPPER SURFACE PRESSURE COEFFICIENT VS SEMISPAN.
(CONFIGURATION 19, $\alpha = 13.1^\circ$)

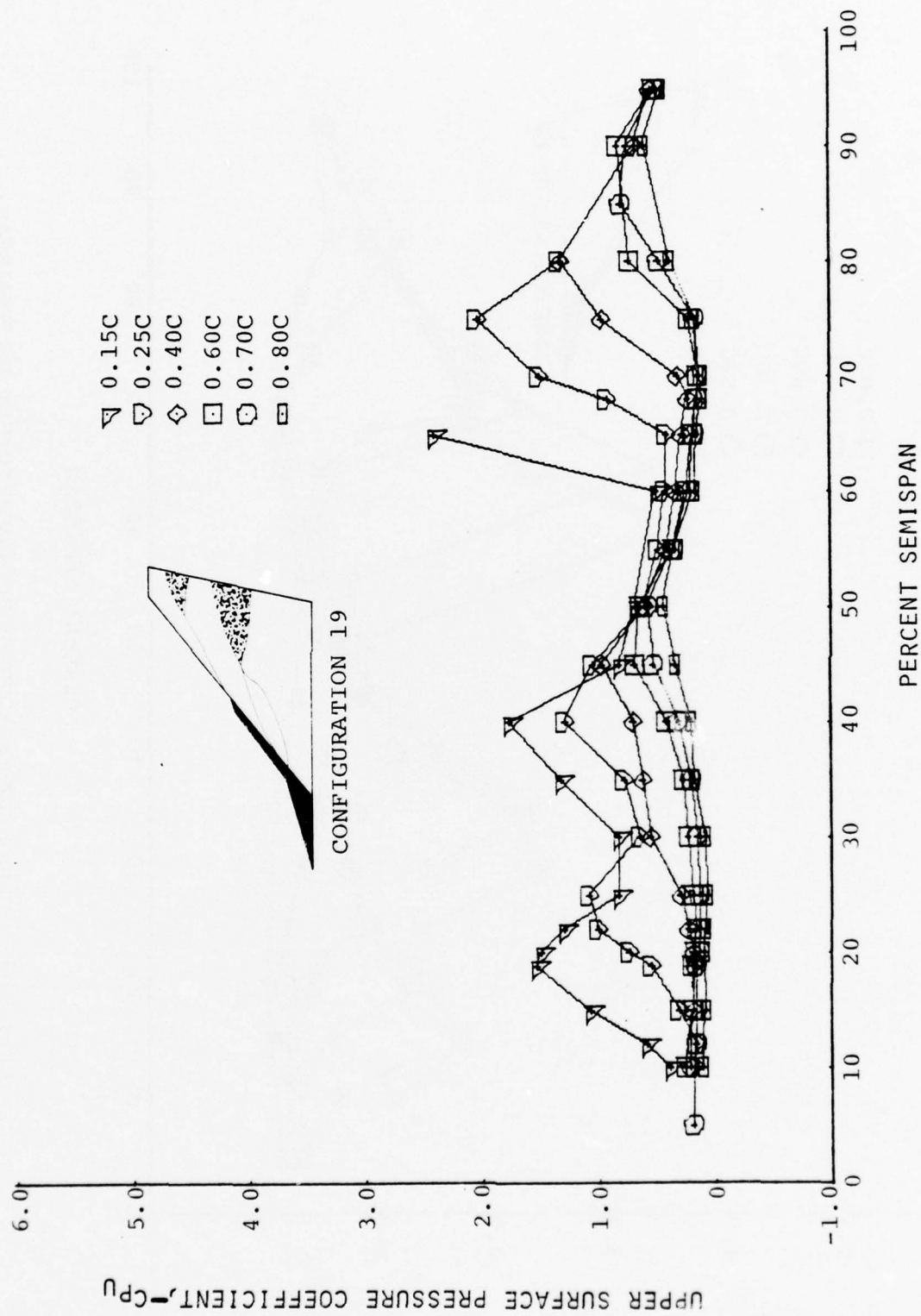


FIGURE 40b. UPPER SURFACE PRESSURE COEFFICIENT VS SEMISPAN.
(CONFIGURATION 19, $\alpha = 13.1^\circ$)

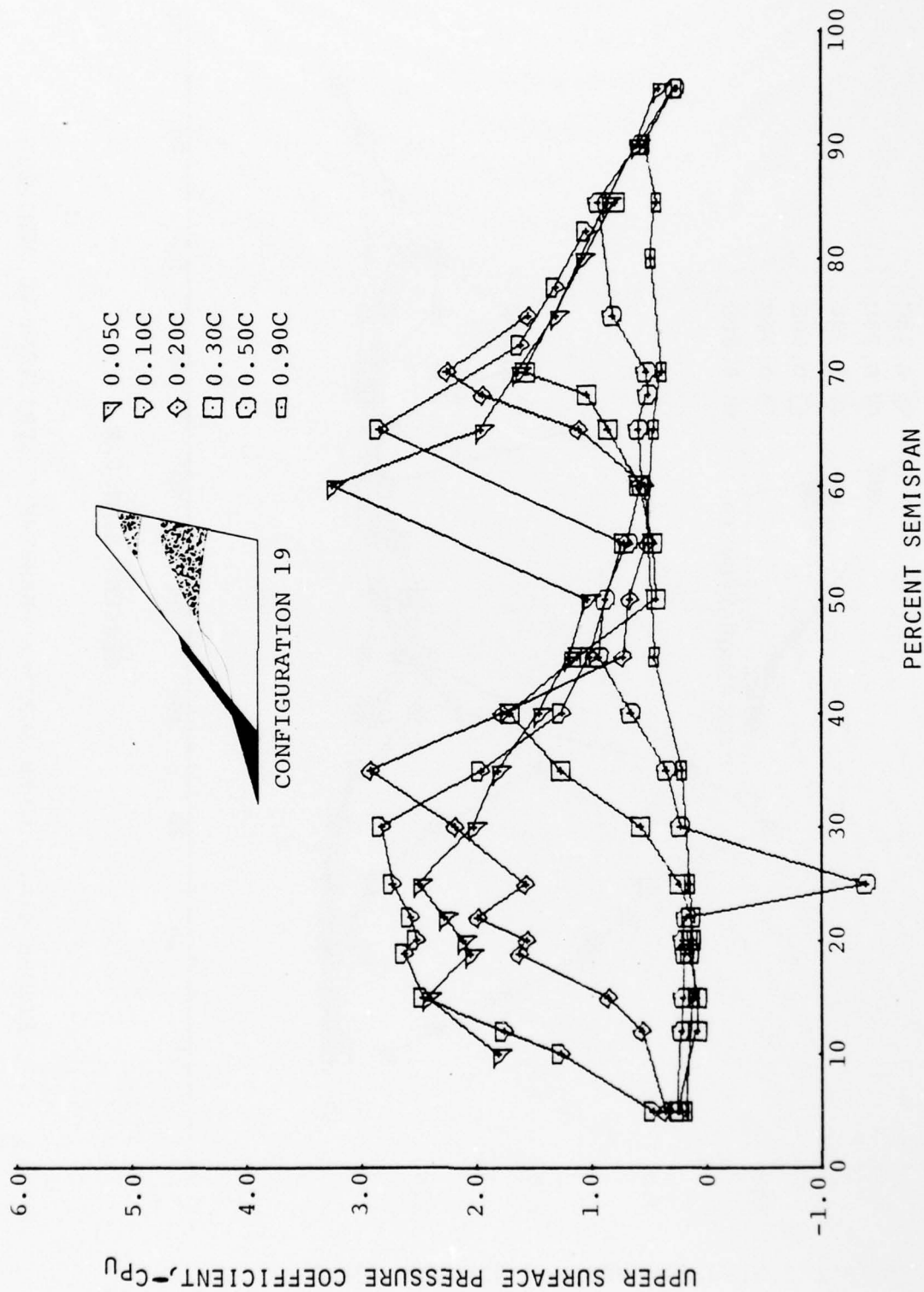


FIGURE 41a. UPPER SURFACE PRESSURE COEFFICIENT VS SEMISPAN.
(CONFIGURATION 19, $\alpha = 17.4^\circ$)

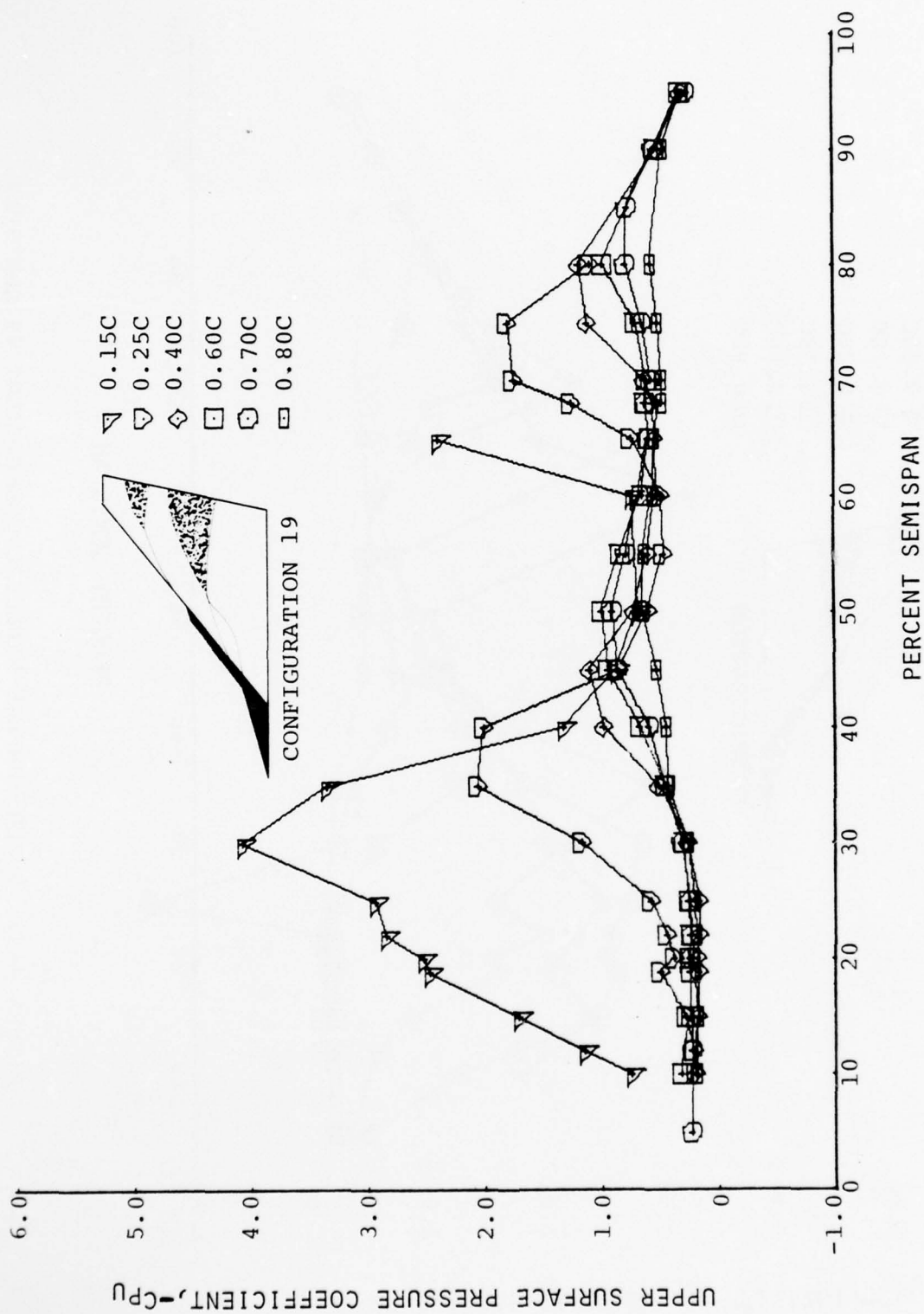


FIGURE 41b. UPPER SURFACE PRESSURE COEFFICIENT VS SEMISPAN.
(CONFIGURATION 19, $\alpha = 17.4^\circ$)

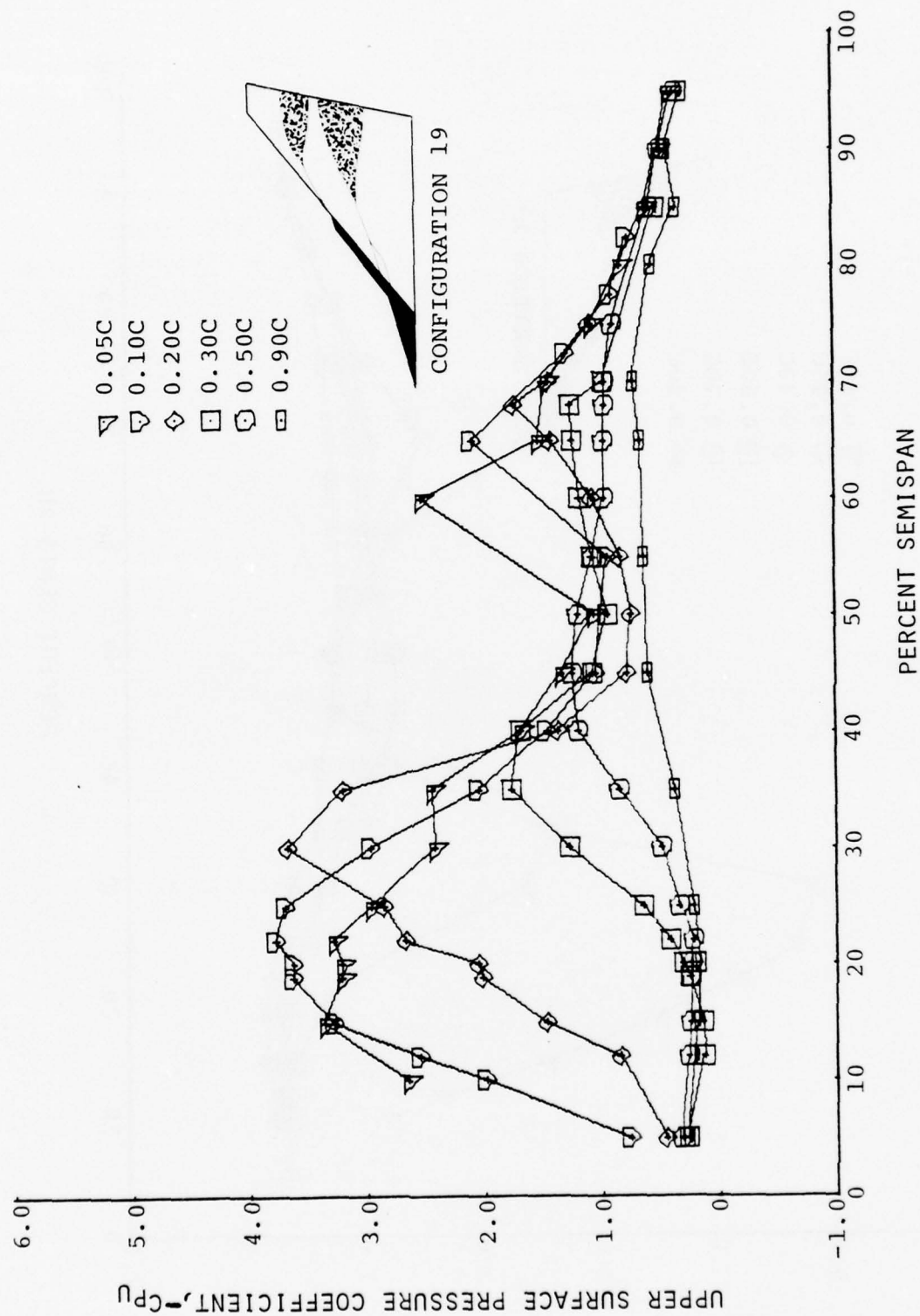


FIGURE 42a. UPPER SURFACE PRESSURE COEFFICIENT VS SEMISPAN.
(CONFIGURATION 19, $\alpha = 21.7^\circ$)

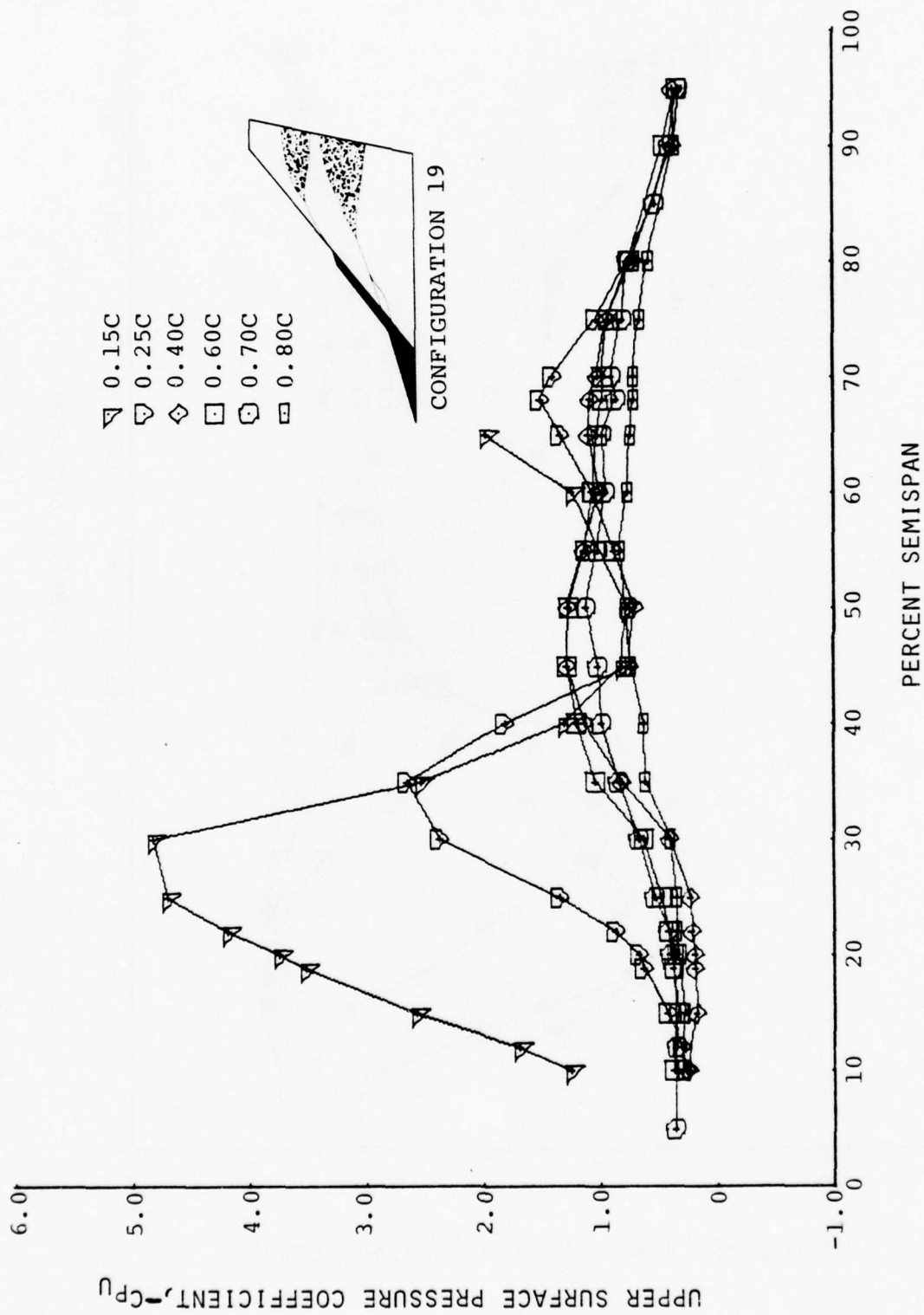


FIGURE 42b. UPPER SURFACE PRESSURE COEFFICIENT VS SEMISPAN.
(CONFIGURATION 19, $\alpha = 21.7^\circ$)

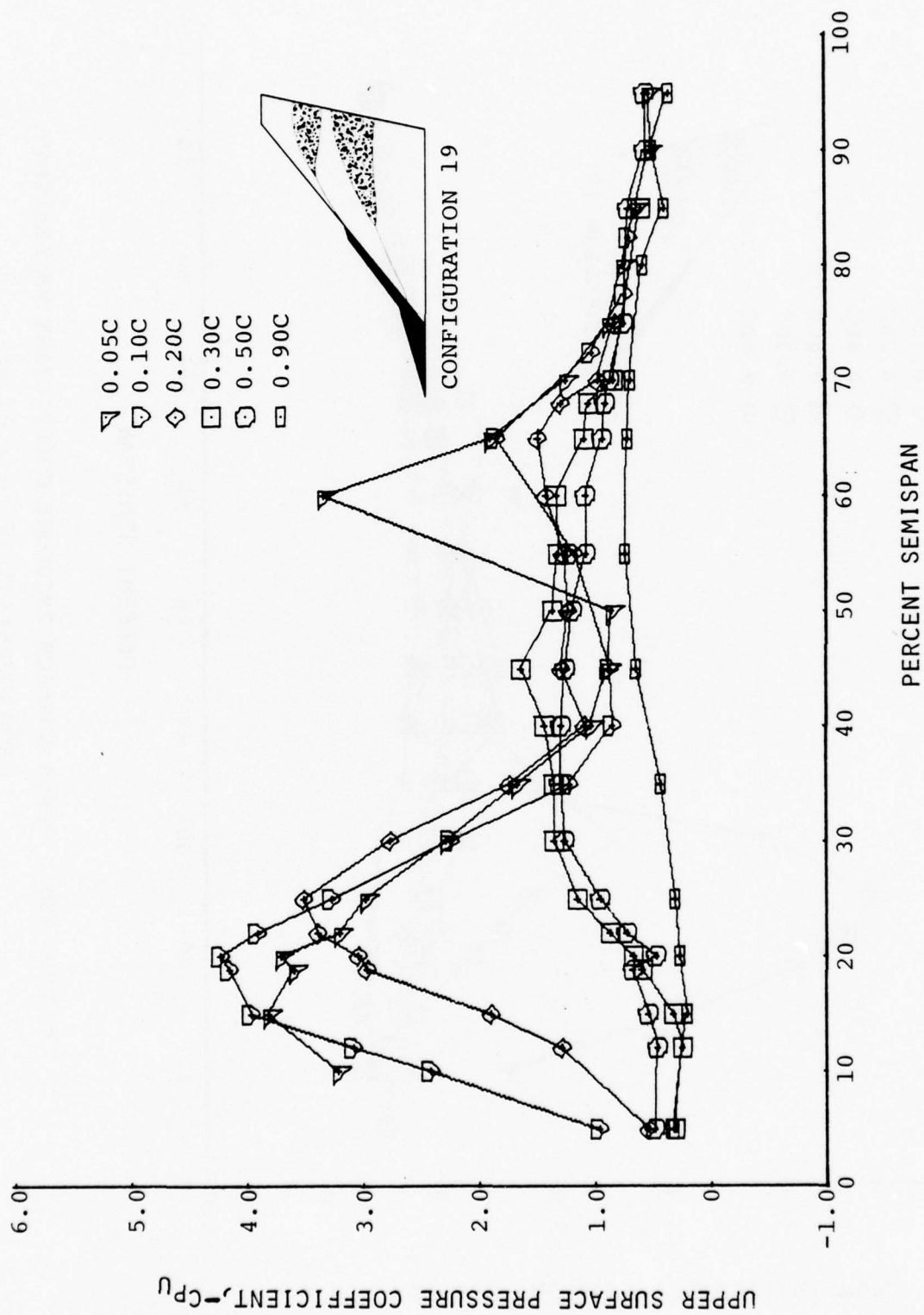


FIGURE 43a. UPPER SURFACE PRESSURE COEFFICIENT VS SEMISPAN.
(CONFIGURATION 19, $\alpha = 26.1^\circ$)

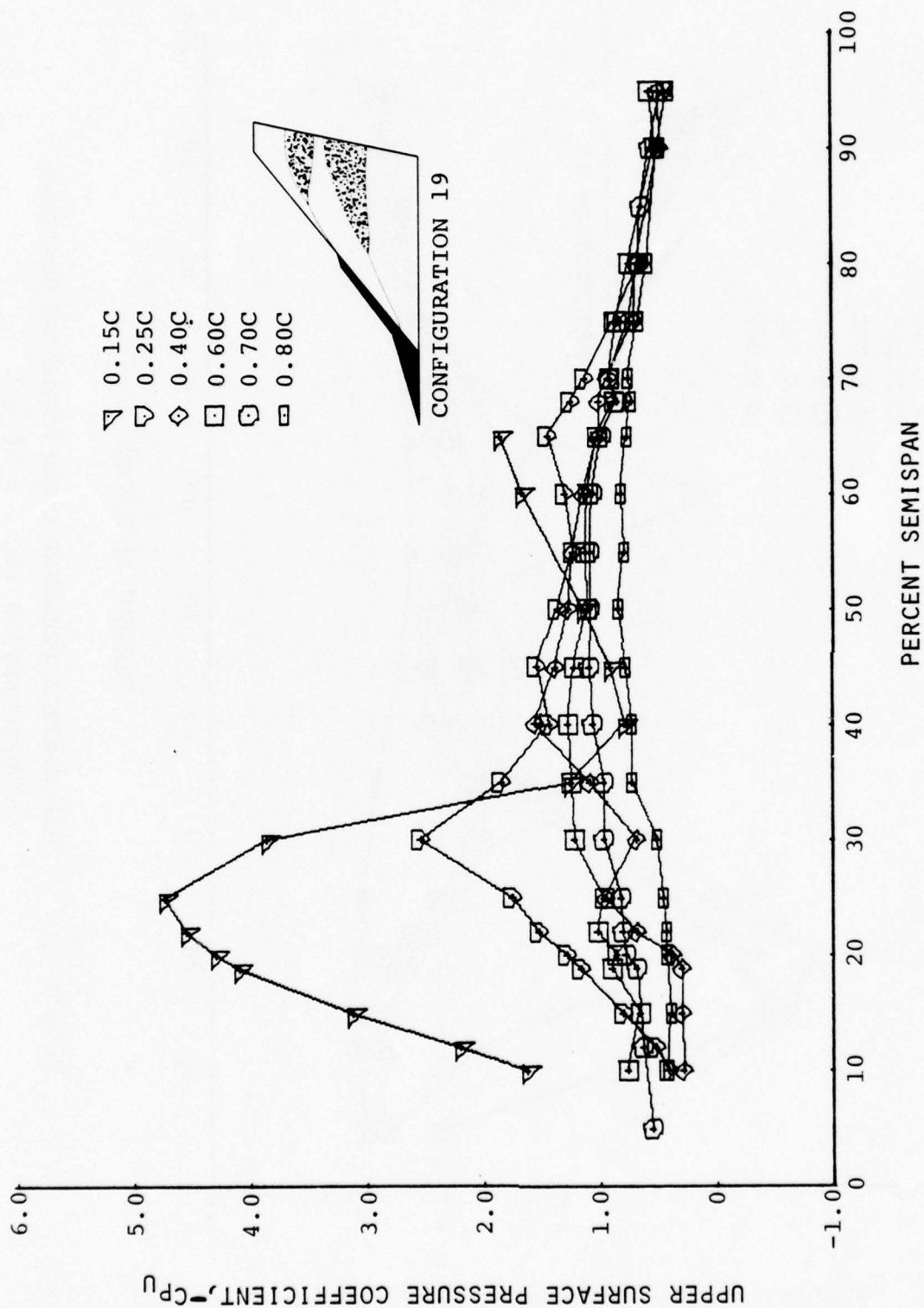


FIGURE 43b. UPPER SURFACE PRESSURE COEFFICIENT VS SEMISPAN.
(CONFIGURATION 19, $\alpha = 26.1^\circ$)

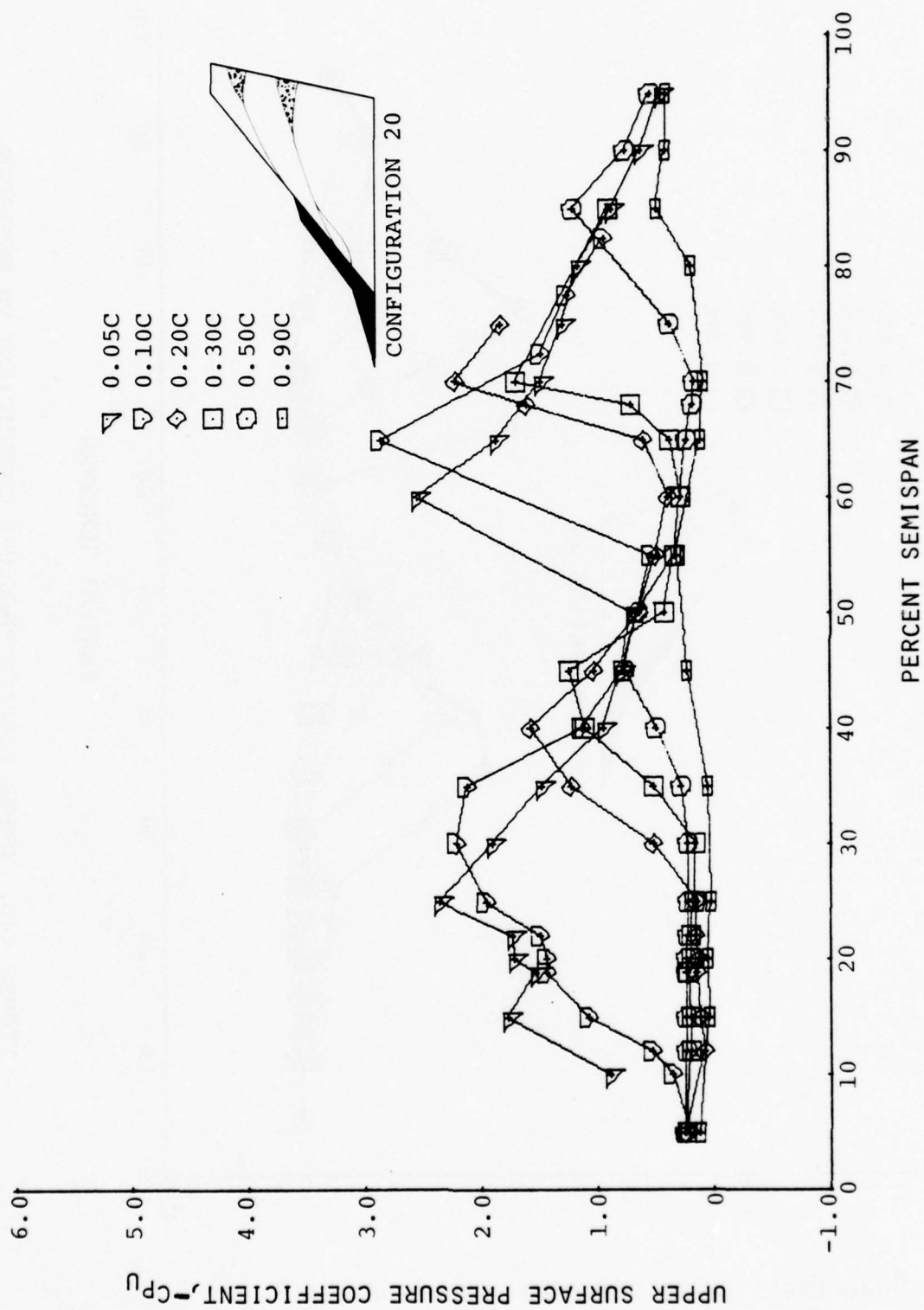


FIGURE 44a. UPPER SURFACE PRESSURE COEFFICIENT VS SEMISPAN.
(CONFIGURATION 20, $\alpha = 12.0^\circ$)

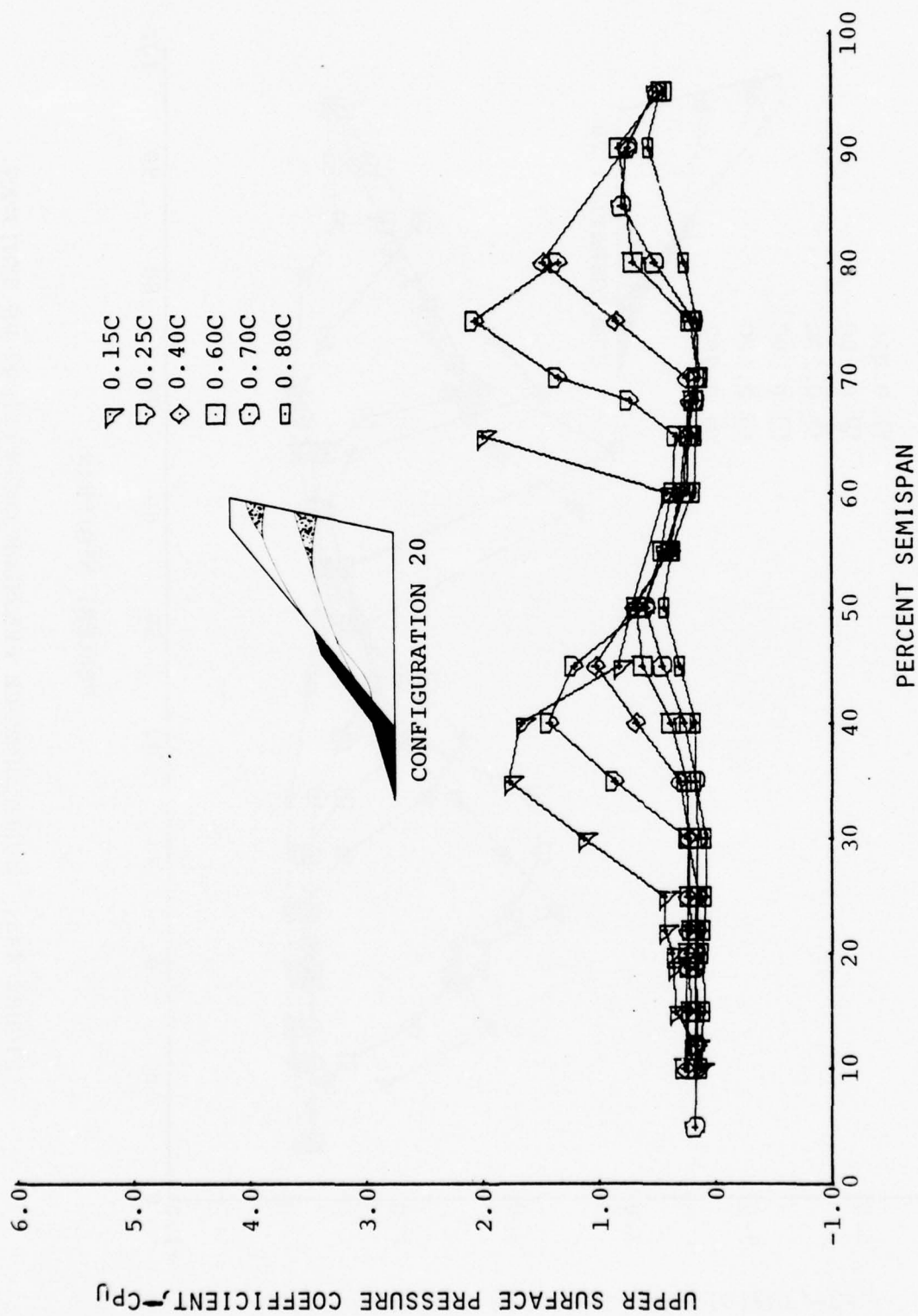


FIGURE 44b. UPPER SURFACE PRESSURE COEFFICIENT VS SEMISPAN.
(CONFIGURATION 20, $\alpha = 12.0^\circ$)

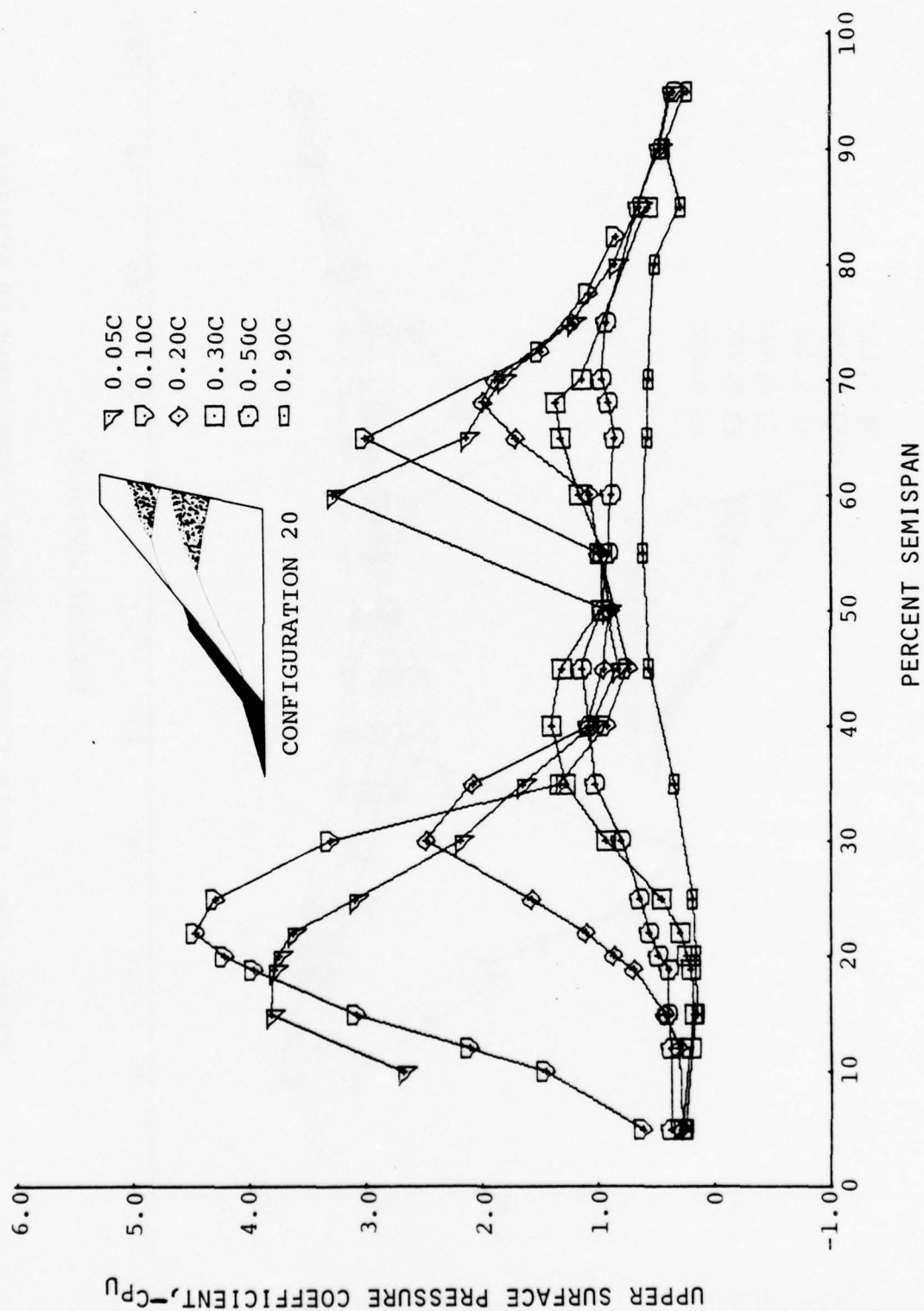


FIGURE 45a. UPPER SURFACE PRESSURE COEFFICIENT VS SEMISPAN.
 (CONFIGURATION 20, $\alpha = 20.0^\circ$)

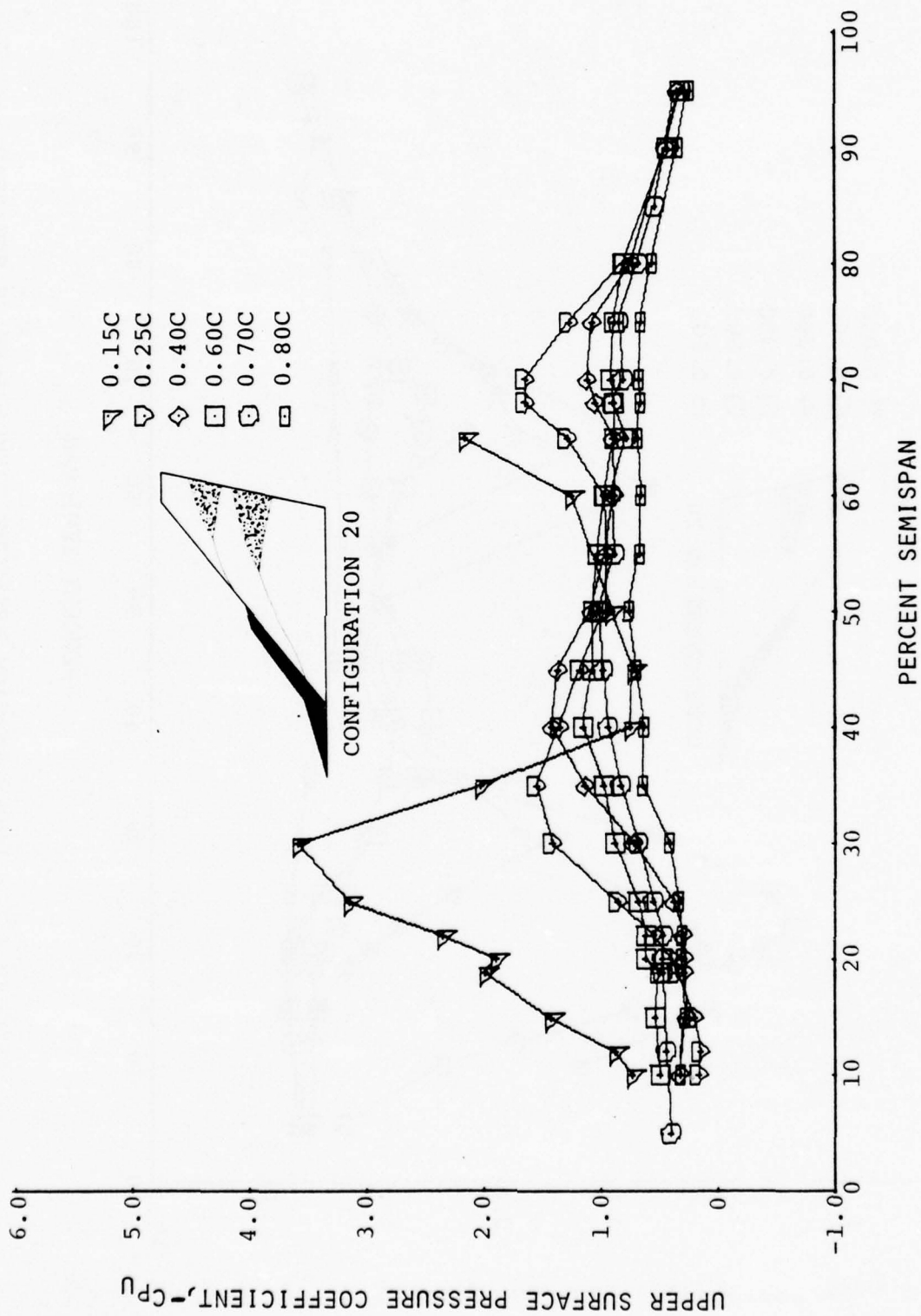


FIGURE 45b. UPPER SURFACE PRESSURE COEFFICIENT VS SEMISPAN.
(CONFIGURATION 20, $\alpha = 20.0^\circ$)

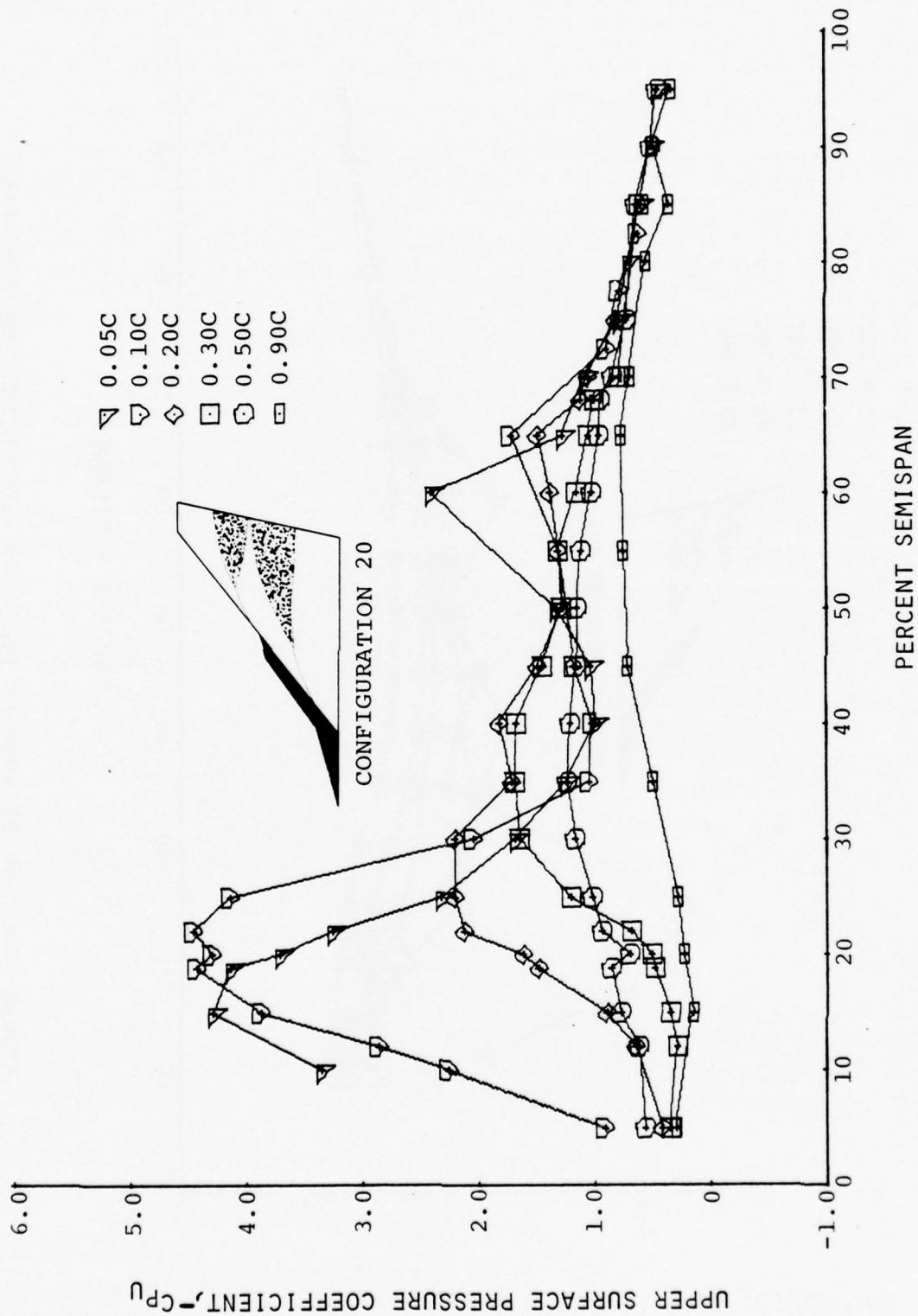


FIGURE 46a. UPPER SURFACE PRESSURE COEFFICIENT VS SEMISPAN.
(CONFIGURATION 20, $\alpha = 24.0^\circ$)

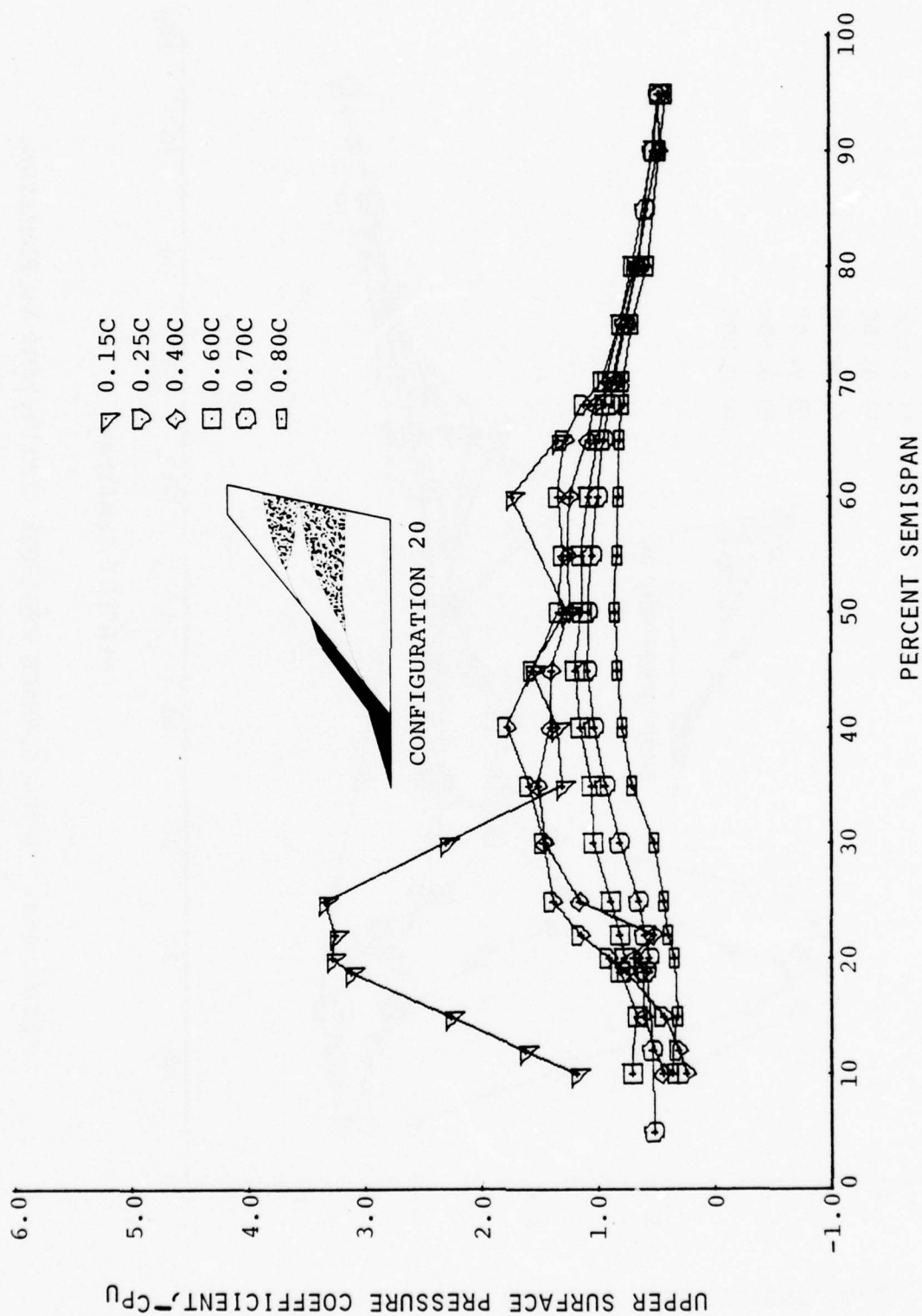
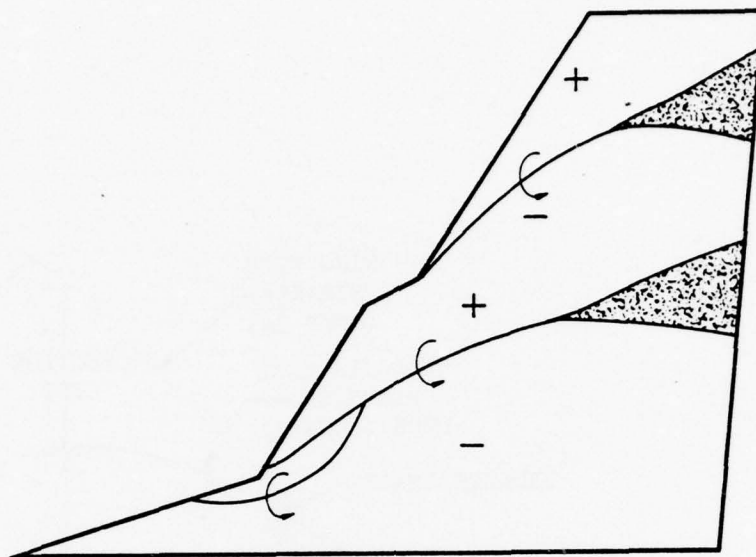
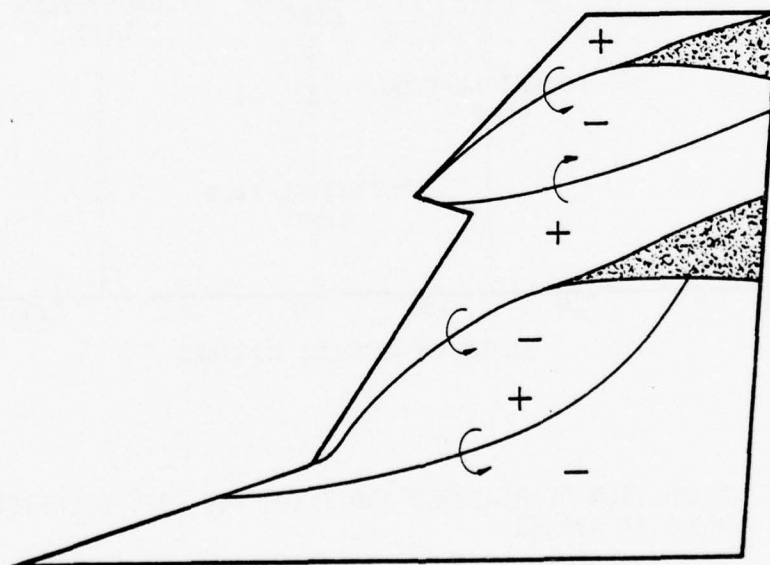


FIGURE 46b. UPPER SURFACE PRESSURE COEFFICIENT VS SEMISPAN.
 (CONFIGURATION 20, $\alpha = 24.0^\circ$)



Configurations 19 and 20



Proposed Configuration

FIGURE 47. EFFECT OF VORTEX INDUCED VELOCITIES
ON ANGLE OF ATTACK

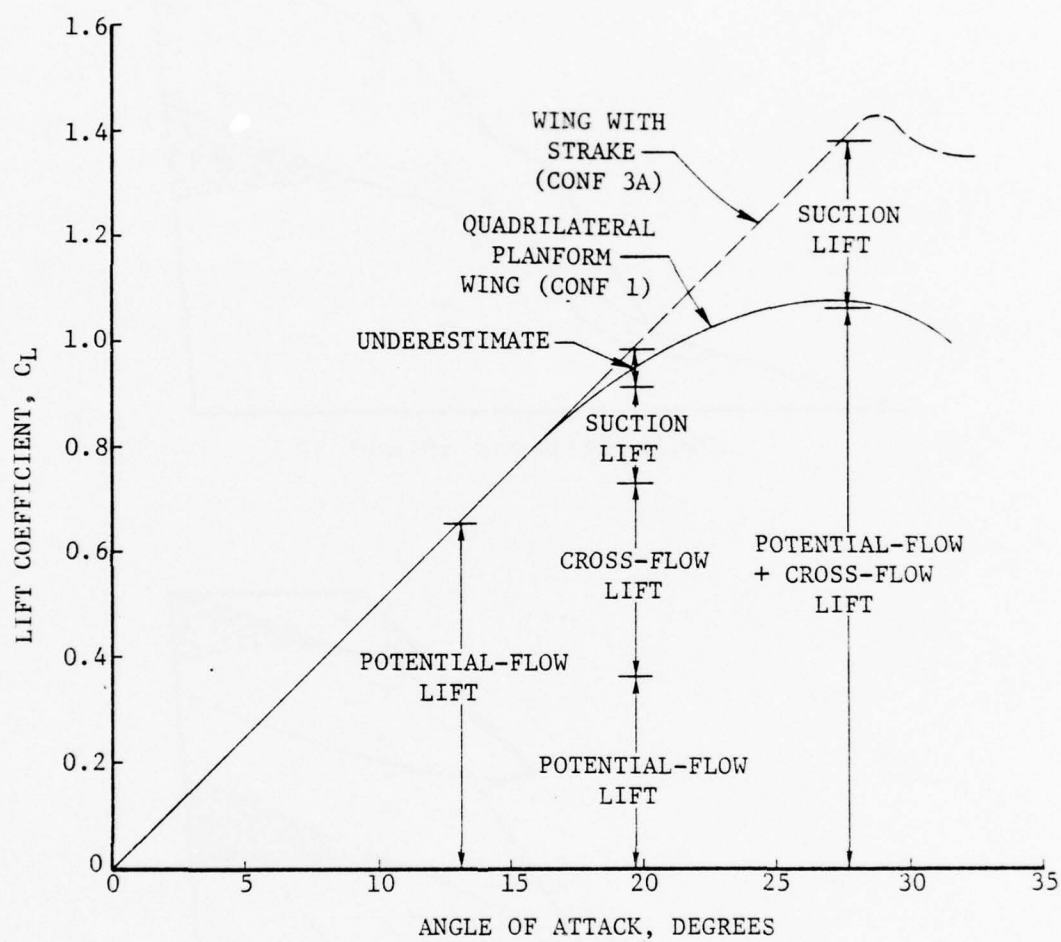


FIGURE 48. COMPARISON OF MEASURED AND PREDICTED LIFT COEFFICIENT VS. ANGLE OF ATTACK

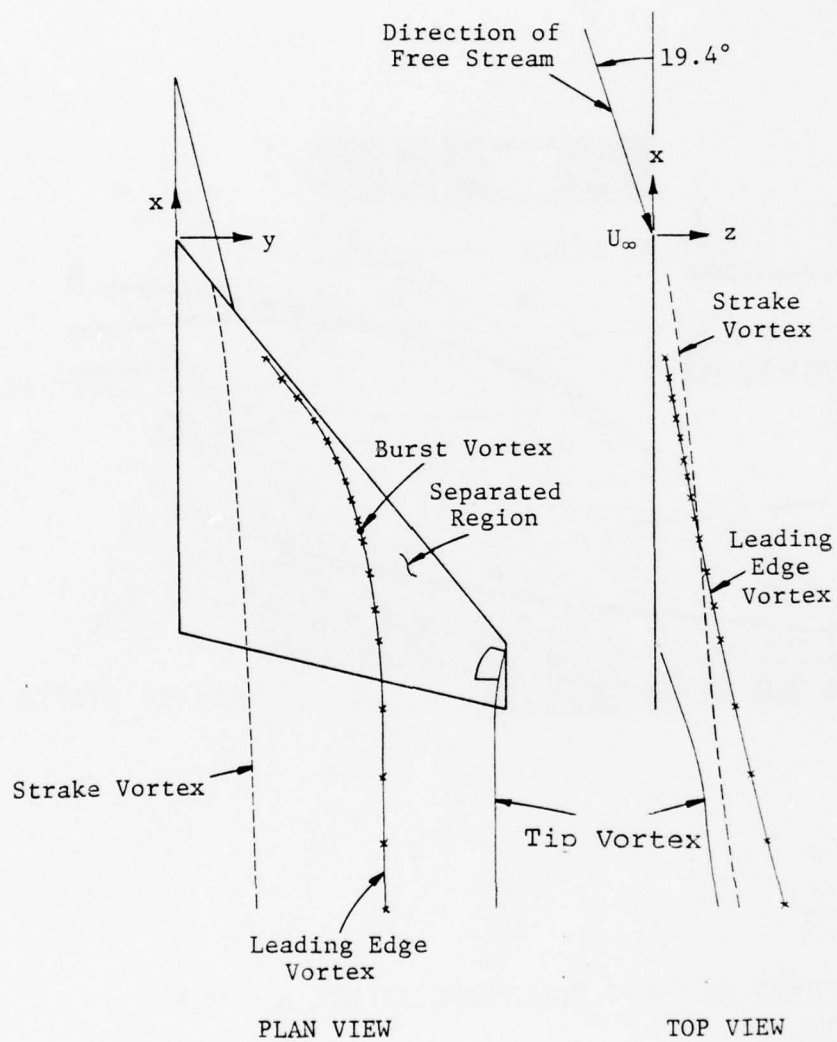


FIGURE 49. PREDICTED VORTEX GEOMETRY, $\alpha = 19.4^\circ$

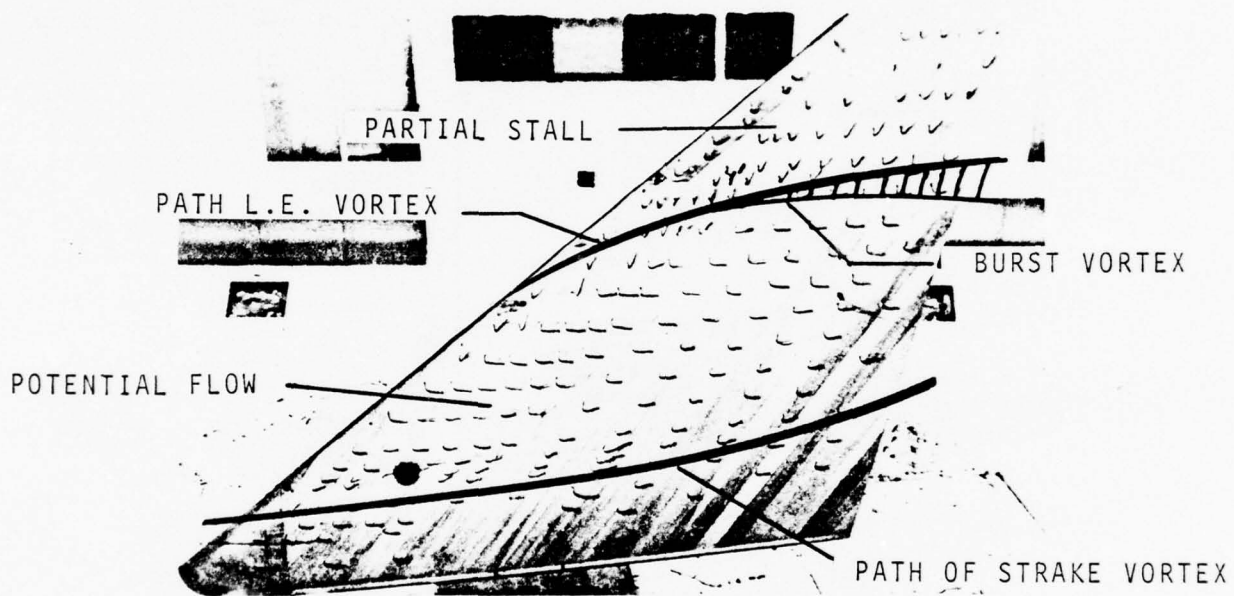


FIGURE 50. TUFT FLOW VISUALIZATION, $\alpha = 19.4^\circ$

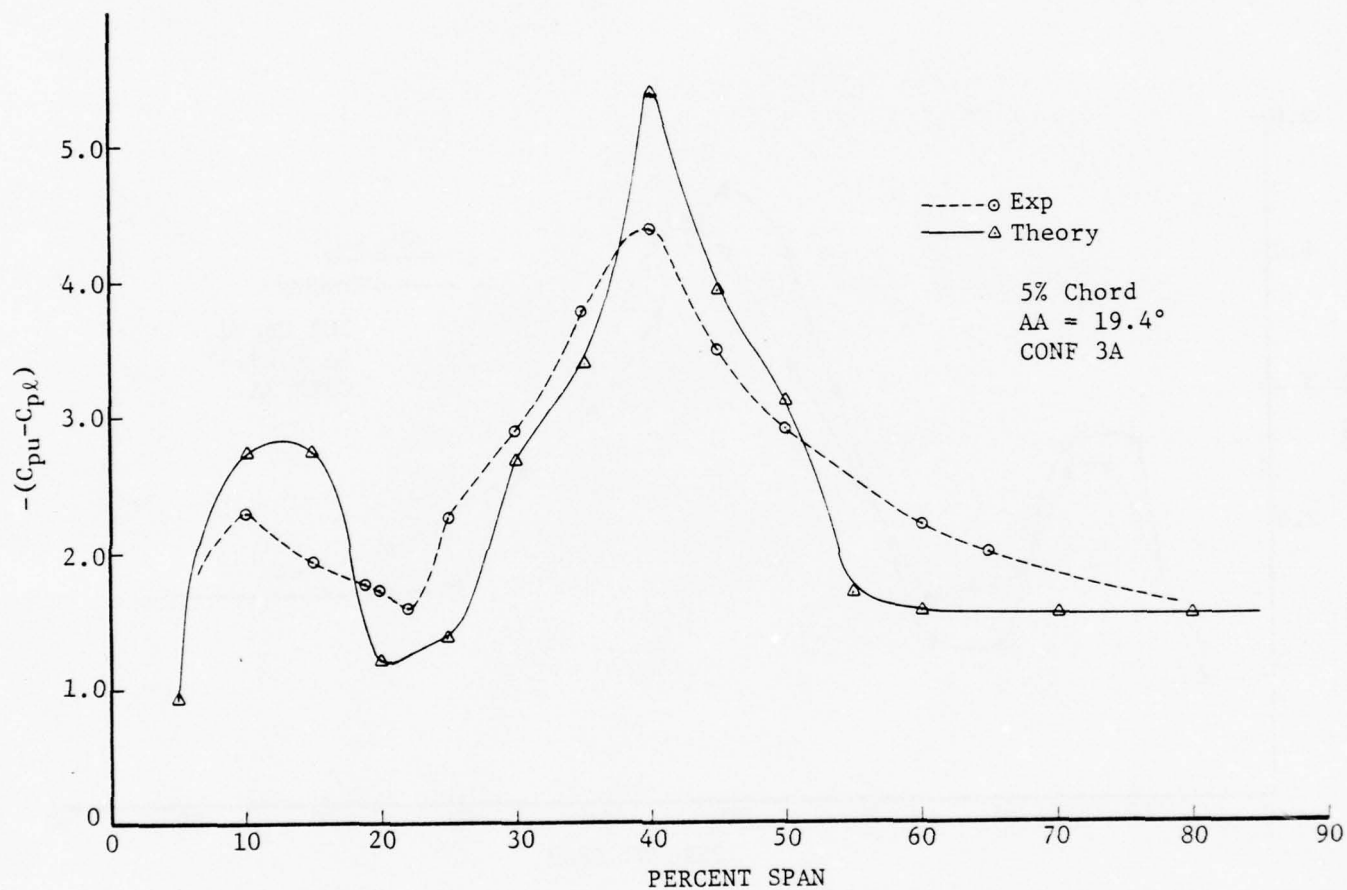


FIGURE 51a. COMPARISON OF MEASURED AND PREDICTED SPANWISE PRESSURE DISTRIBUTION AT 5% CHORD, $\alpha = 19.4^\circ$

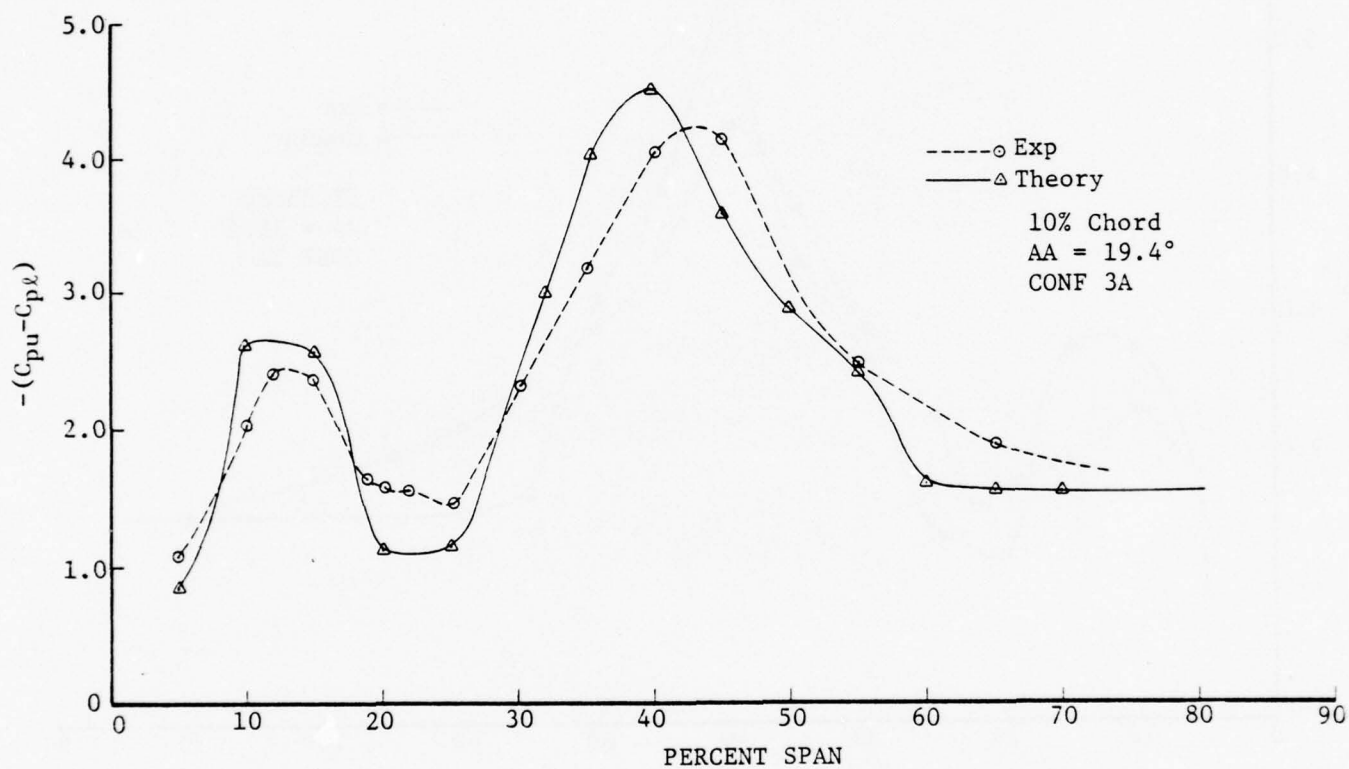


FIGURE 51b. COMPARISON OF MEASURED AND PREDICTED SPANWISE PRESSURE DISTRIBUTIONS AT 10% CHORD, $\alpha = 19.4^\circ$

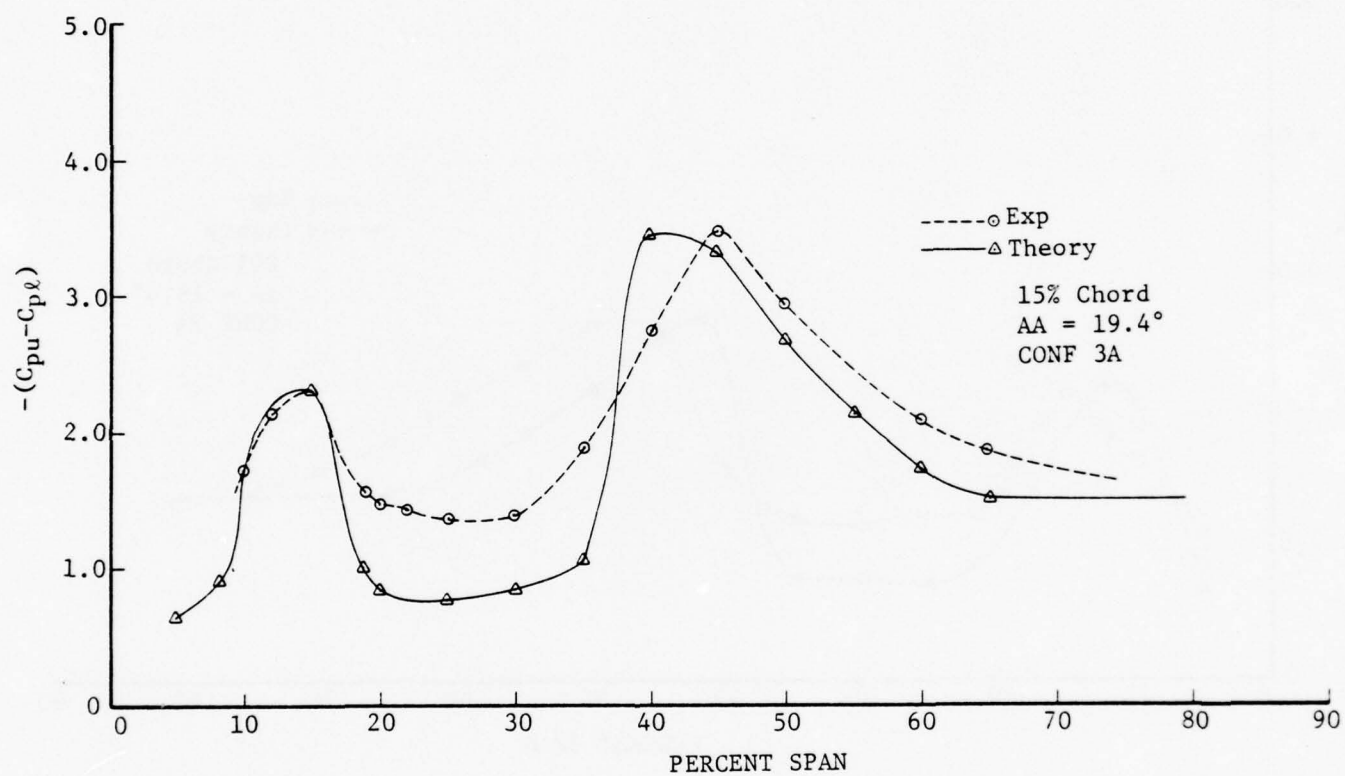


FIGURE 51c. COMPARISON OF MEASURED AND PREDICTED SPANWISE PRESSURE DISTRIBUTIONS AT 15% CHORD, $\alpha = 19.4^\circ$

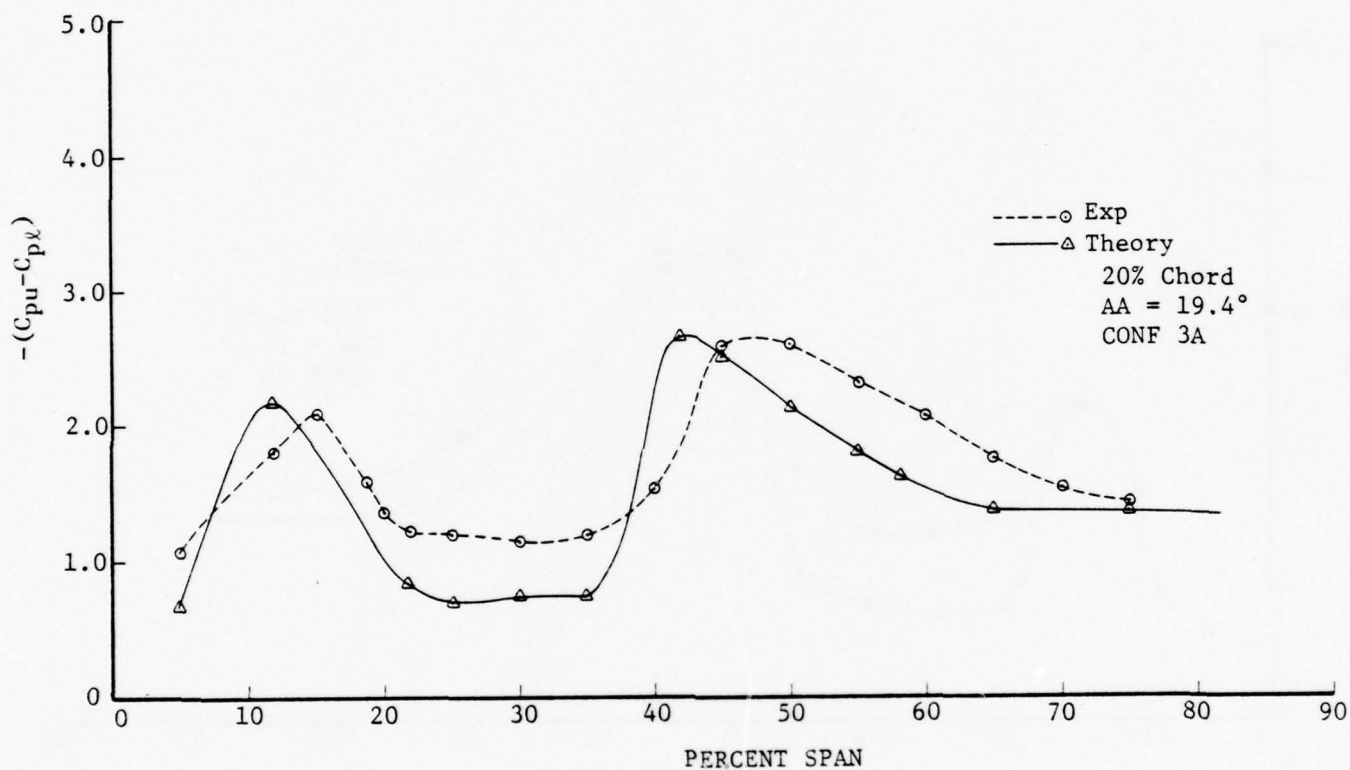


FIGURE 51d. COMPARISON OF MEASURED AND PREDICTED SPANWISE PRESSURE DISTRIBUTIONS AT 20% CHORD, $\alpha = 19.4^\circ$

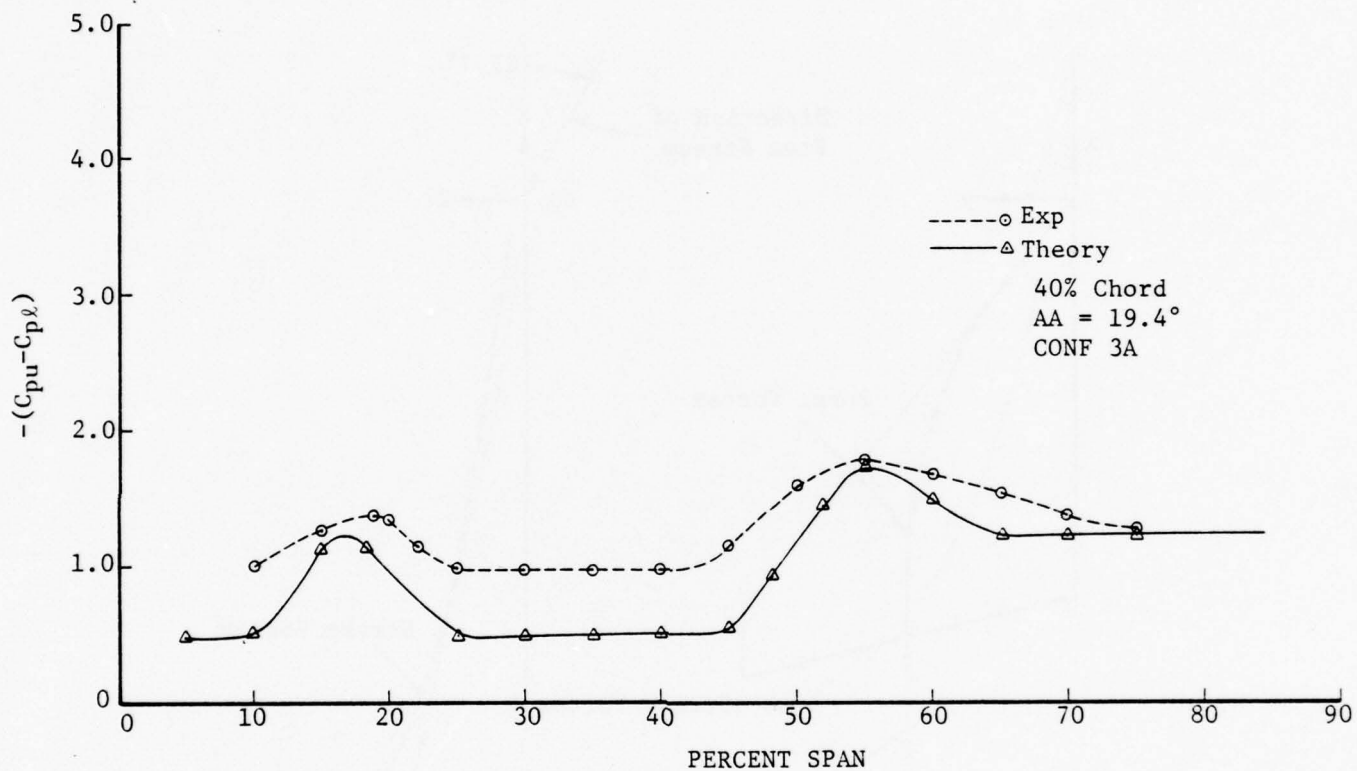


FIGURE 51e. COMPARISON OF MEASURED AND PREDICTED SPANWISE PRESSURE DISTRIBUTIONS AT 40% CHORD, $\alpha = 19.4^\circ$

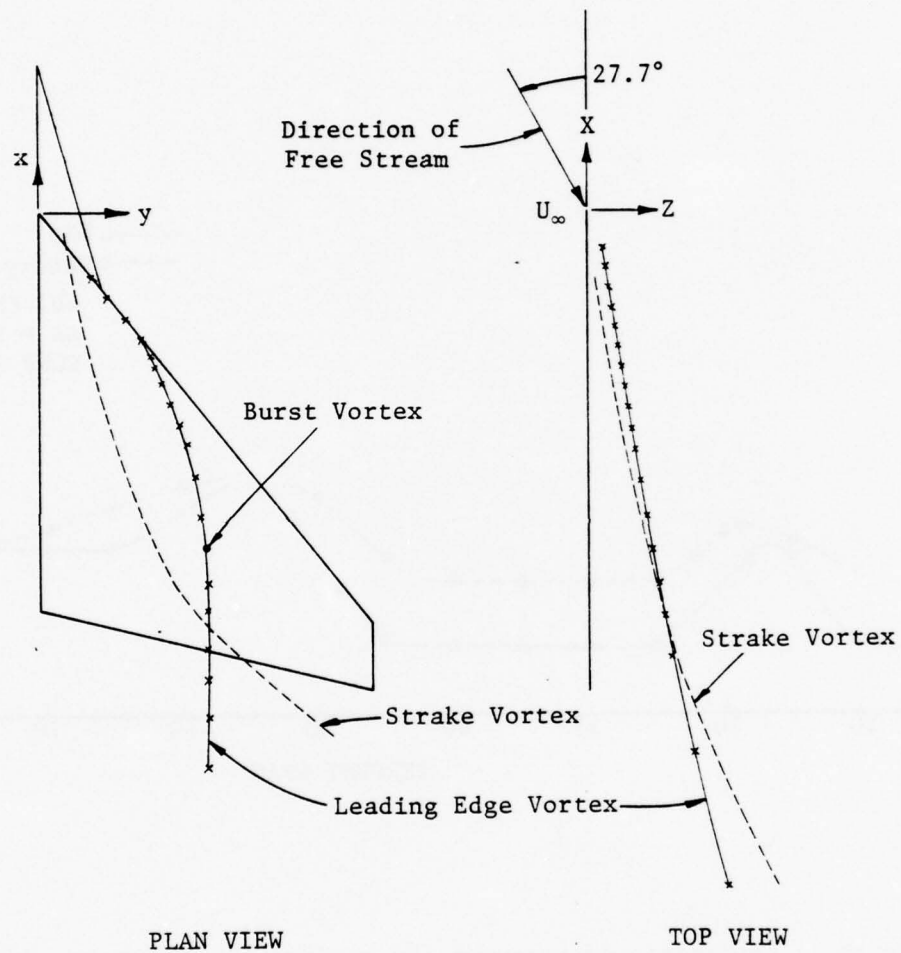


FIGURE 52. PREDICTED VORTEX GEOMETRY, $\alpha = 27.7^\circ$

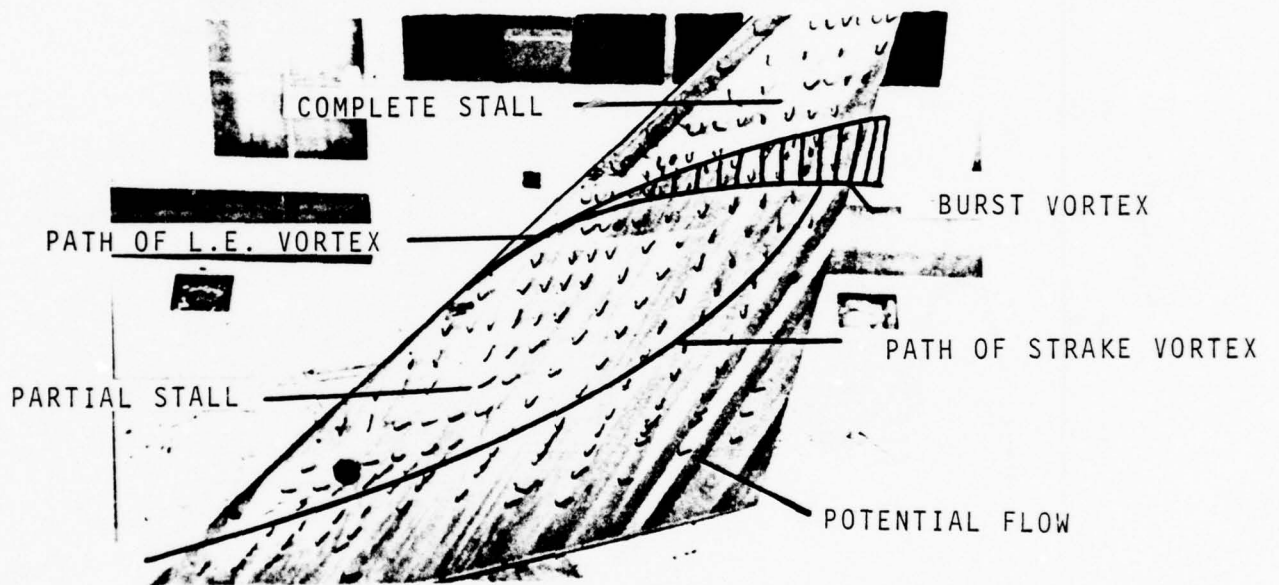


FIGURE 53. TUFT FLOW VISUALIZATION $\alpha = 27.7^\circ$

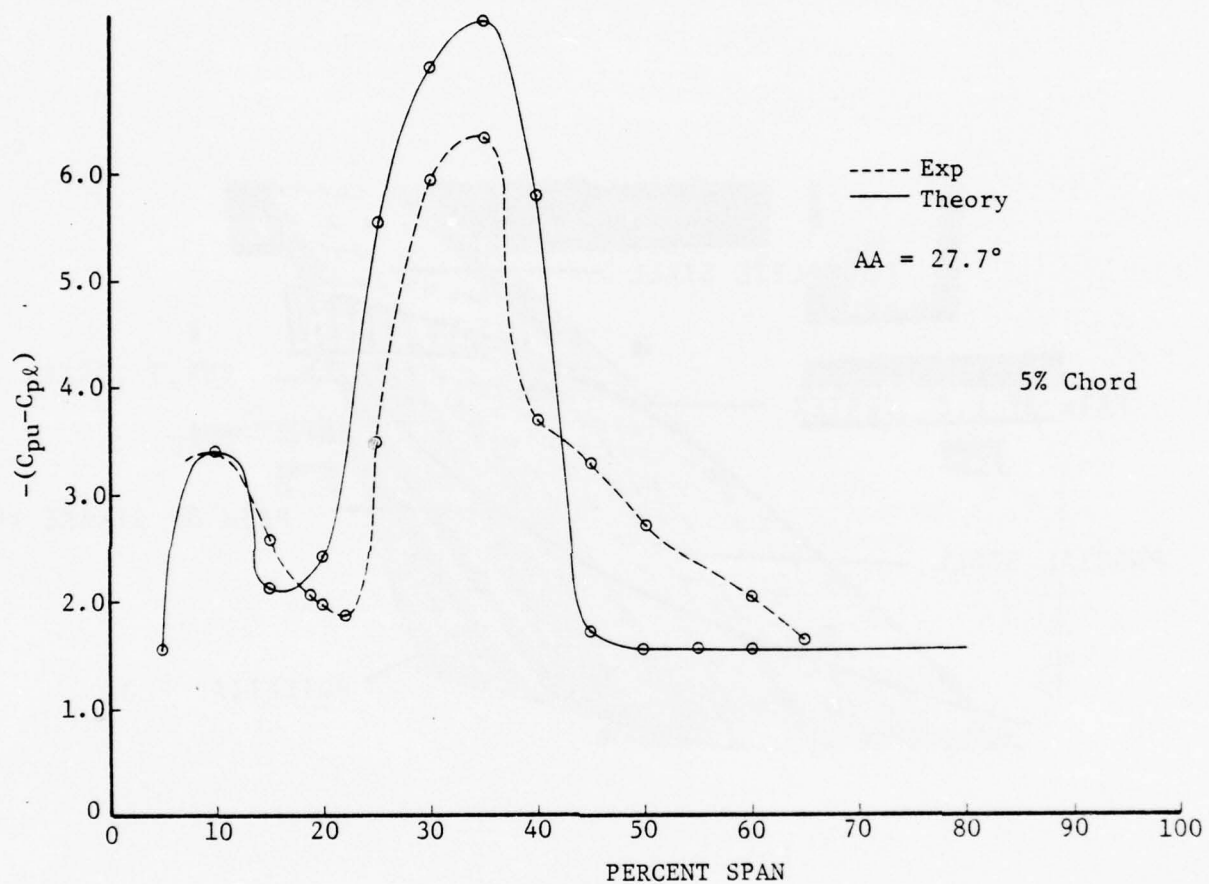


FIGURE 54a. COMPARISON OF MEASURED AND PREDICTED SPANWISE PRESSURE DISTRIBUTIONS AT 5% CHORD, $\alpha = 27.7^\circ$

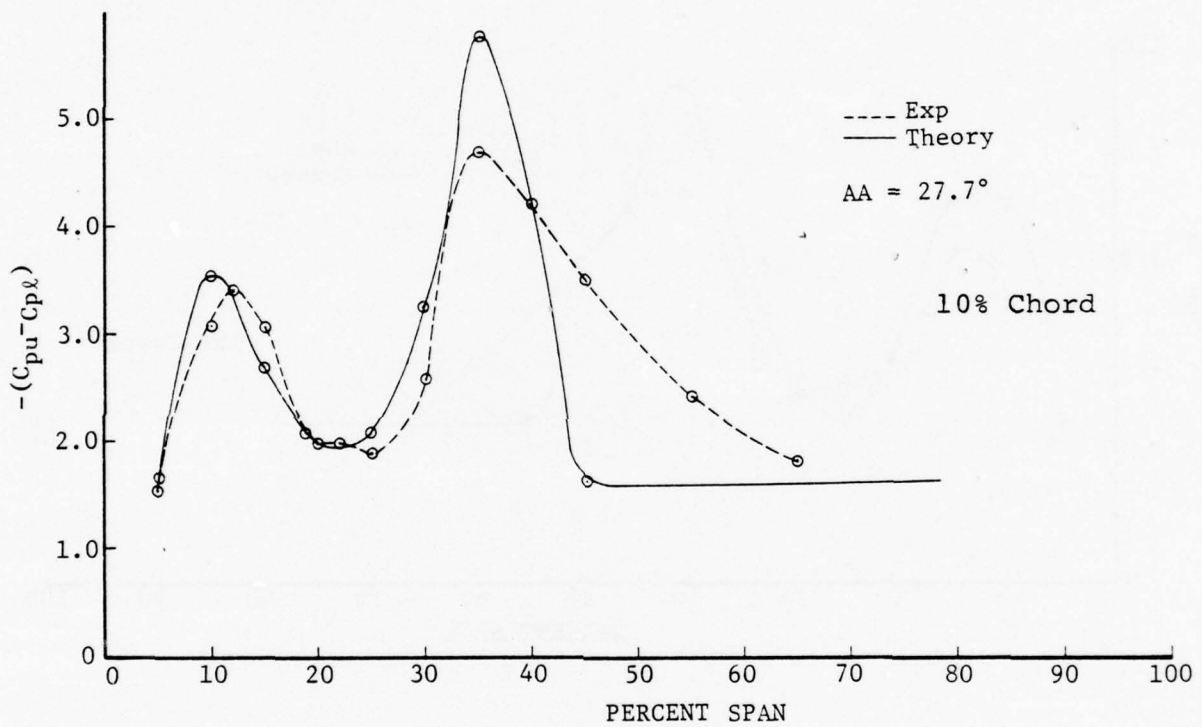


FIGURE 54b. COMPARISON OF MEASURED AND PREDICTED SPANWISE PRESSURE DISTRIBUTIONS AT 10% CHORD, $\alpha = 27.7^\circ$

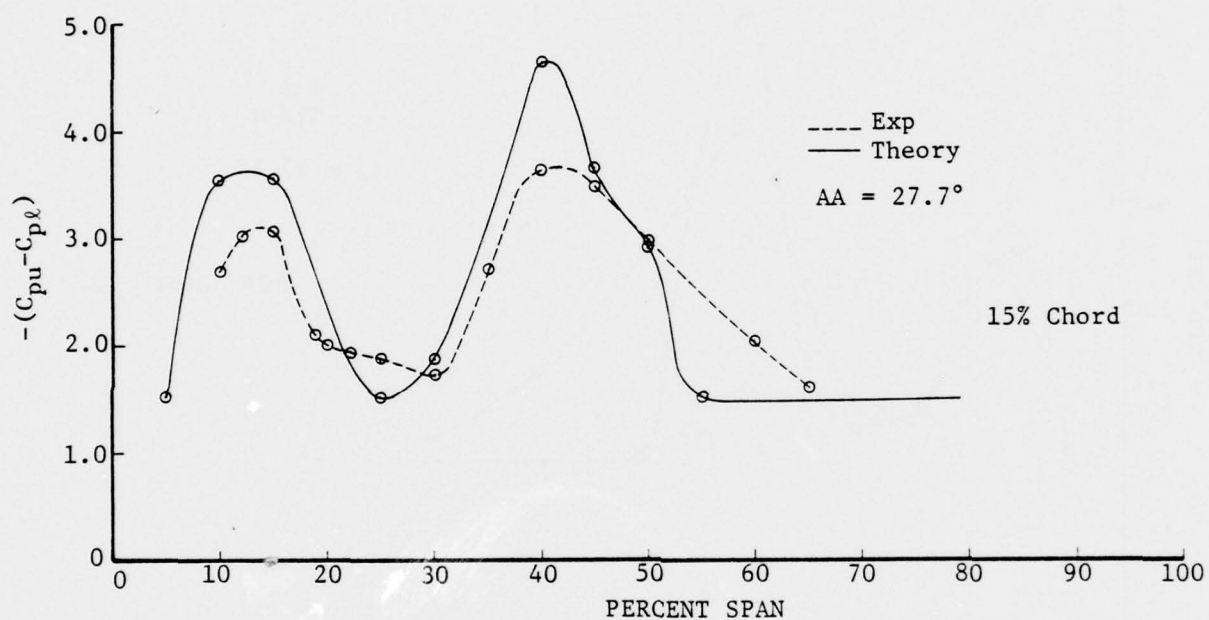


FIGURE 54c. COMPARISON OF MEASURED AND PREDICTED SPANWISE PRESSURE DISTRIBUTIONS AT 15% CHORD, $\alpha = 27.7^\circ$

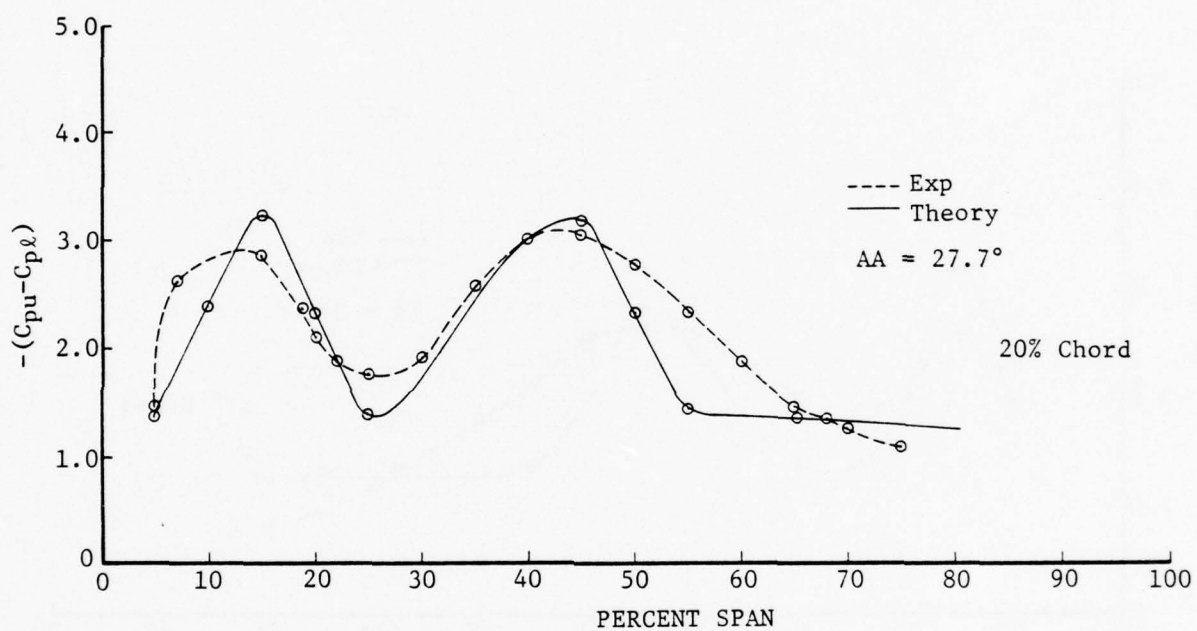


FIGURE 54d. COMPARISON OF MEASURED AND PREDICTED SPANWISE PRESSURE DISTRIBUTIONS AT 20% CHORD, $\alpha = 27.7^\circ$

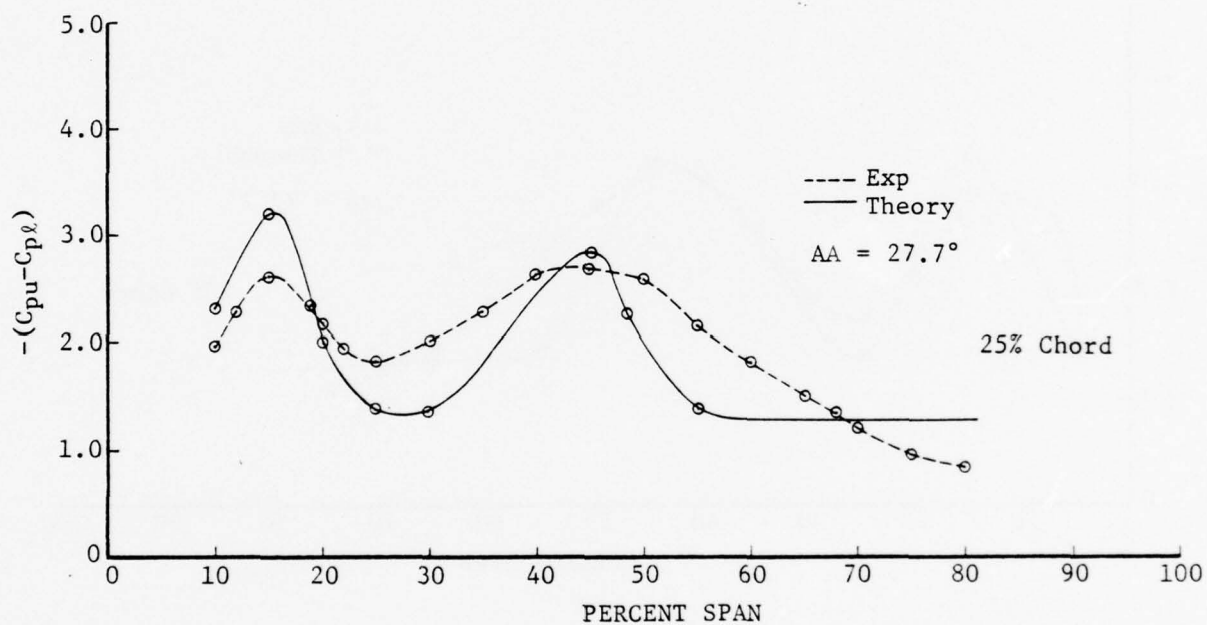


FIGURE 54e. COMPARISON OF MEASURED AND PREDICTED SPANWISE PRESSURE DISTRIBUTIONS AT 25% CHORD, $\alpha = 27.7^\circ$

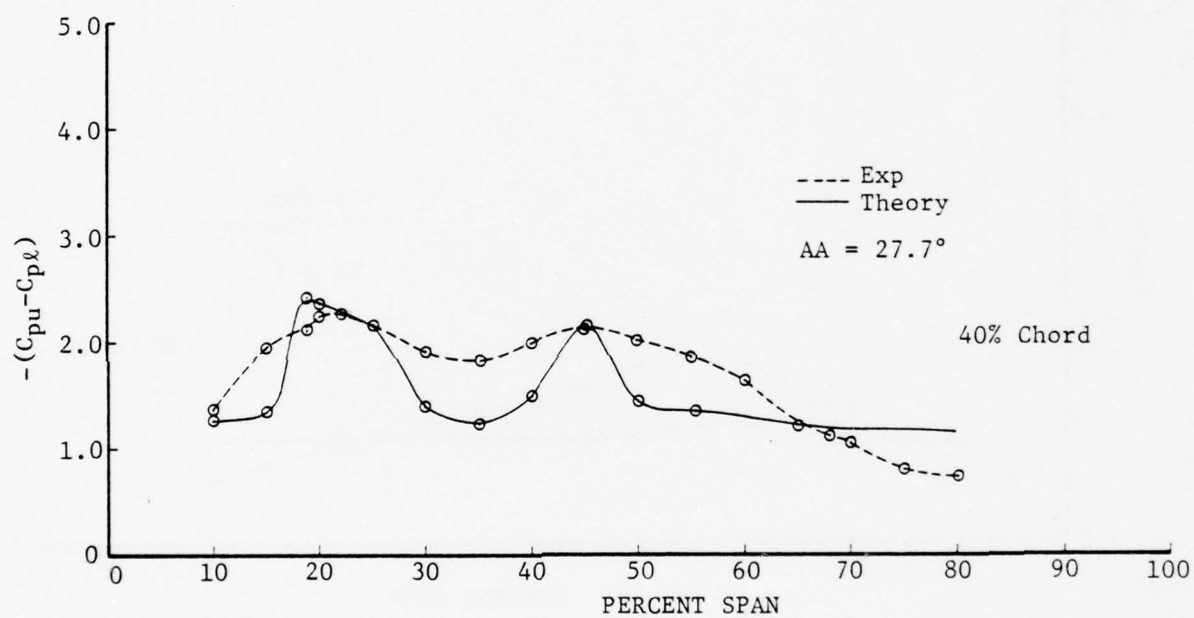


FIGURE 54f. COMPARISON OF MEASURED AND PREDICTED SPANWISE PRESSURE DISTRIBUTIONS AT 40% CHORD, $\alpha = 27.7^\circ$

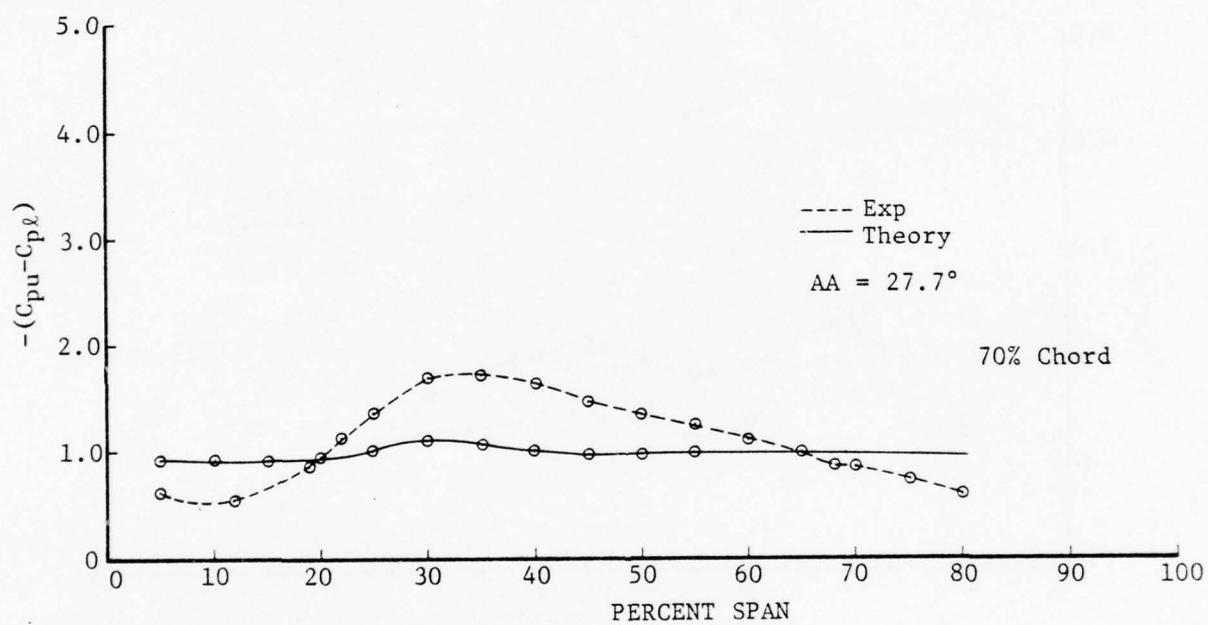


FIGURE 54g. COMPARISON OF MEASURED AND PREDICTED SPANWISE PRESSURE DISTRIBUTIONS AT 70% CHORD, $\alpha = 27.7^\circ$

APPENDIX

SUMMARY OF WIND
TUNNEL BALANCE DATA

LIST OF SYMBOLS
(APPENDIX)

AA,	angle of attack, degrees
AY	yaw angle (not relevant)
C	mean aerodynamic chord
C CP	chordwise center of pressure, percent of mean aerodynamic chord
CD,	drag coefficient
CL,	lift coefficient
CM,	pitching moment coefficient about the MAC
CN,	drag moment coefficient
CRM	rolling moment coefficient
CY	side force coefficient (not relevant)
L D	lift-to-drag ratio
Q,	dynamic pressure, lb/ft^2
RN,	Reynolds number
S CP	spanwise center of pressure, percent of span
V	wind tunnel test velocity, ft/sec

APPENDIX A
SUMMARY OF WIND TUNNEL
BALANCE DATA

RUN NO.	CONFIGURATION NO.	RUN NO.	CONFIGURATION NO.
1	3A	14	17
2	6	15	4A
3	5A	16	15
4	5B	17	14
5	5C	18	18
6	7A	29	9C1
7	8AC	30	5C
8	9A2	31	6
9	9A1	32	20
10	9C1	33	14
11	10	34	18
12	11	35	19
13	12		

NO BALANCE DATA WERE TAKEN FOR RUNS 19 THROUGH 28

RUNS 19 THROUGH 23 WERE HELIUM-BUBBLE FLOW STUDIES
RUNS 24 THROUGH 28 WERE TUFT-FLOW STUDIES

UNIVERSITY OF MARYLAND
WIND TUNNEL OPERATIONS DEPT.

CONFIGURATION 3A RUN NO TEST NO Q V RN WIND AXES 04/14/76
1 729 011.89 100.00 02.563 01 03 01 01 00 00 00 1

AA	AY	CL	CD	CM	CN	CRM	CY	C CP	L D	S CP
-004.3	000.0	-00.214	0.0146	00.021	-0.0506	00.0775	00.008	00.098	-14.657	-00.343
-003.3	000.0	-00.161	0.0113	00.016	-0.0518	00.0577	00.006	00.099	-14.247	-00.339
-002.2	000.0	-00.105	0.0092	00.012	-0.0513	00.0357	00.000	00.114	-11.413	-00.320
-001.1	000.0	-00.054	0.0081	00.010	-0.0504	00.0178	00.000	00.185	-06.666	-00.311
-000.0	000.0	-00.006	0.0074	00.005	-0.0522	00.0004	00.002	00.833	-00.810	-00.066
001.1	000.0	00.048	0.0075	00.003	-0.0515	-00.0186	00.002	-00.062	06.400	-00.366
002.2	000.0	00.101	0.0093	-00.001	-0.0519	-00.0385	00.002	00.009	10.860	-00.361
003.2	000.0	00.151	0.0120	-00.003	-0.0520	-00.0553	00.013	00.019	12.583	-00.346
004.3	000.0	00.209	0.0158	-00.009	-0.0528	-00.0756	00.013	00.043	13.227	-00.341
006.5	000.0	00.325	0.0270	-00.014	-0.0531	-00.1183	00.026	00.042	12.037	-00.342
008.7	000.0	00.439	0.0453	-00.007	-0.0487	-00.1591	00.036	00.015	09.690	-00.339
010.9	000.0	00.546	0.0750	00.001	-0.0397	-00.1960	00.043	-00.001	07.280	-00.336
013.1	000.0	00.669	0.1187	00.001	-0.0244	-00.2300	00.054	-00.001	05.636	-00.322
015.2	000.0	00.754	0.1664	-00.002	-0.0094	-00.2431	00.058	00.002	04.531	-00.301
017.4	000.0	00.877	0.2329	-00.009	0.0081	-00.2737	00.065	00.009	03.765	-00.290
019.5	000.0	00.980	0.3048	00.002	0.0726	-00.2892	00.061	-00.001	03.215	-00.289
021.7	000.0	01.067	0.3840	00.013	0.0936	-00.2999	00.052	-00.011	02.778	-00.276
023.9	000.0	01.180	0.4685	00.019	0.1087	-00.3212	00.057	-00.014	02.518	-00.266
026.1	000.0	01.327	0.5953	00.018	0.0870	-00.3470	00.064	-00.012	02.229	-00.240
026.1	000.0	01.341	0.6093	00.038	0.0910	-00.3539	00.039	-00.025	02.200	-00.243

UNIVERSITY OF MARYLAND
WIND TUNNEL OPERATIONS DEPT.

CONFIGURATION 3A		RUN NO	TEST NO	Q	V	RN	WIND AXES		04/14/76		
AA	AY	1	729	011.89	100.00	02.563	01	03	01 01 00 00 00 00 1		
			CD	CL	CM	CN	CRM	CY	C CP	L D	S CP
028.1	000.0		0.6641	01.339	00.051	0.1012	-00.3307	00.056	-00.034	02.016	-00.227
030.0	000.0		0.7112	01.300	00.076	0.1531	-00.3122	00.041	-00.052	01.827	-00.234
032.1	000.0		0.7982	01.312	00.065	0.1758	-00.3284	00.026	-00.042	01.643	-00.242
015.2	000.0		0.1715	00.764	-00.013	0.0451	-00.2500	00.061	00.016	04.454	-00.323

UNIVERSITY OF MARYLAND
WIND TUNNEL OPERATIONS DEPT.

CONFIGURATION 6 RUN NO TEST NO Q V RN WIND AXES 04/14/76
2 729 011.89 100.00 02.563 01 12 01 01 00 00 00 2

AA	AY	CL	CD	CM	CN	CRM	CY	C CP	L D	S CP
-004.3	000.0	-00.211	0.0188	00.015	0.0034	00.0710	00.011	00.070	-11.223	-00.334
-003.2	000.0	-00.151	0.0136	00.012	0.0009	00.0495	00.005	00.079	-11.102	-00.327
-002.2	000.0	-00.102	0.0107	00.010	-0.0002	00.0324	00.006	00.098	-09.532	-00.317
-001.1	000.0	-00.050	0.0091	00.009	0.0012	00.0179	00.005	00.180	-05.494	-00.358
-000.0	000.0	00.001	0.0086	00.004	0.0005	-00.0016	-00.001	-04.000	00.116	-01.600
001.1	000.0	00.055	0.0098	00.004	0.0008	-00.0222	-00.001	-00.072	05.612	-00.403
002.2	000.0	00.106	0.0116	00.001	0.0004	-00.0394	00.002	-00.009	09.137	-00.371
003.2	000.0	00.158	0.0142	00.001	-0.0002	-00.0570	00.011	-00.006	11.126	-00.360
004.3	000.0	00.219	0.0193	-00.002	0.0011	-00.0795	00.012	00.009	11.347	-00.360
006.6	000.0	00.353	0.0405	-00.007	0.0086	-00.1282	00.014	00.019	08.716	-00.361
008.7	000.0	00.477	0.0710	-00.010	0.0184	-00.1679	00.019	00.020	06.718	-00.350
011.0	000.0	00.621	0.1151	-00.006	0.0319	-00.2158	00.019	00.009	05.395	-00.345
013.2	000.0	00.767	0.1721	00.006	0.0463	-00.2516	00.019	-00.007	04.456	-00.325
015.3	000.0	00.837	0.2193	00.030	0.0579	-00.2587	00.022	-00.034	03.816	-00.306
017.4	000.0	00.918	0.2774	00.042	0.0690	-00.2685	00.023	-00.043	03.309	-00.288
019.6	000.0	00.996	0.3434	00.053	0.0853	-00.2812	00.026	-00.050	02.900	-00.278
021.7	000.0	01.074	0.4178	00.062	0.0994	-00.2884	00.026	-00.053	02.570	-00.264
023.8	000.0	01.174	0.5072	00.072	0.0687	-00.3107	00.025	-00.056	02.314	-00.243
025.9	000.0	01.204	0.5691	00.074	0.0763	-00.3061	00.015	-00.055	02.115	-00.231

UNIVERSITY OF MARYLAND
WIND TUNNEL OPERATIONS DEPT.

CONFIGURATION 6		RUN NO	TEST NO	Q	V	RN	WIND AXES		04/14/76	
		2	729	011.89	100.00	02.563	01 12 01 01 00 00 00	00 00 00	2	
AA	AY	CL	CD	CM	CN	CRM	CY	C CP	L D	S CP
027.9	000.0	01.200	0.6246	00.074	0.1281	-00.2979	00.000	-00.054	01.921	-00.238
029.9	000.0	01.220	0.6995	00.076	0.1475	-00.3024	-00.004	-00.054	01.744	-00.238
031.9	000.0	01.217	0.7446	00.072	0.1494	-00.3019	-00.011	-00.050	01.634	-00.234

UNIVERSITY OF MARYLAND
WIND TUNNEL OPERATIONS DEPT.

WIND AXES 04/14/76
01 08 01 01 00 00 00 3

RUN NO TEST NO Q V RN
3 729 011.89 100.00 02.563

CONFIGURATION 5A

AA	AY	CL	CD	CM	CN	CRM	CY	C CP	L D	S CP
-004.3	000.0	-00.208	0.0165	00.018	-0.0481	00.0716	00.004	00.086	-12.606	-00.324
-003.2	000.0	-00.157	0.0123	00.013	-0.0506	00.0558	00.004	00.082	-12.764	-00.336
-002.2	000.0	-00.100	0.0098	00.012	-0.0507	00.0323	00.004	00.120	-10.204	-00.303
-001.1	000.0	-00.052	0.0087	00.009	-0.0491	00.0174	00.002	00.173	-05.977	-00.317
-000.0	000.0	-00.001	0.0076	00.005	-0.0502	-00.0002	00.000	05.000	-00.131	00.200
001.1	000.0	00.055	0.0085	00.003	-0.0505	-00.0219	00.000	-00.054	06.470	-00.380
002.2	000.0	00.106	0.0105	-00.000	-0.0507	-00.0397	00.006	00.000	10.095	-00.355
003.2	000.0	00.157	0.0131	-00.002	-0.0500	-00.0579	00.011	00.012	11.984	-00.350
004.3	000.0	00.206	0.0175	-00.005	-0.0510	-00.0739	00.011	00.024	11.771	-00.337
006.5	000.0	00.326	0.0320	-00.009	-0.0480	-00.1172	00.020	00.027	10.187	-00.339
008.7	000.0	00.432	0.0538	-00.015	-0.0422	-00.1525	00.024	00.034	08.029	-00.331
010.9	000.0	00.547	0.0831	-00.012	-0.0334	-00.1880	00.029	00.021	06.582	-00.322
013.0	000.0	00.662	0.1291	-00.011	-0.0197	-00.2235	00.038	00.016	05.127	-00.316
015.2	000.0	00.773	0.1821	-00.005	-0.0045	-00.2453	00.039	00.006	04.244	-00.296
017.4	000.0	00.883	0.2435	00.003	0.0593	-00.2712	00.043	-00.003	03.626	-00.302
019.5	000.0	00.924	0.2969	00.029	0.0716	-00.2602	00.034	-00.029	03.112	-00.277
021.6	000.0	01.041	0.3824	00.033	0.0901	-00.2826	00.037	-00.029	02.722	-00.266
024.0	000.0	01.267	0.5167	00.020	0.0706	-00.3498	00.040	-00.014	02.452	-00.254
026.1	000.0	01.327	0.6024	00.038	0.0900	-00.3501	00.038	-00.026	02.202	-00.242
026.1	000.0	01.341	0.6093	00.038	0.0910	-00.3539	00.039	-00.025	02.200	-00.243

UNIVERSITY OF MARYLAND
WIND TUNNEL OPERATIONS DEPT.

CONFIGURATION 5A RUN NO 3 TEST NO 729 Q 011.89 V 100.00 RN 02.563 WIND AXES 01 07 01 01 00 00 00 00 04/14/76 3

AA	AY	CL	CD	CM	CN	CRM	CY	C CP	L D	S CP
028.1	000.0	01.324	0.6600	00.067	0.1394	-00.3302	00.030	-00.045	02.006	-00.241
030.0	000.0	01.267	0.7015	00.079	0.1514	-00.3128	00.028	-00.054	01.806	-00.239
019.5	000.0	00.957	0.3097	00.031	0.0734	-00.2710	00.037	-00.030	03.090	-00.278
021.7	000.0	01.057	0.3852	00.033	0.0921	-00.2899	00.043	-00.029	02.744	-00.269
024.0	000.0	01.262	0.5207	00.017	0.0718	-00.3435	00.038	-00.012	02.423	-00.251
026.1	000.0	01.327	0.6062	00.038	0.0895	-00.3489	00.036	-00.026	02.189	-00.241

UNIVERSITY OF MARYLAND
WIND TUNNEL OPERATIONS DEPT.

CONFIGURATION 5B RUN NO 4 TEST NO 729 Q 011.89 V 100.00 RN 02.563 WIND AXES 01 06 01 01 00 00 00 00 04/14/76 4

AA	AY	CL	CD	CM	CN	CRM	CY	C CP	L D	S CP
-004.3	000.0	-00.211	0.0164	00.019	0.0026	00.0722	00.010	00.089	-12.865	-00.340
-003.2	000.0	-00.158	0.0122	00.015	-0.0004	00.0534	00.001	00.094	-12.950	-00.337
-002.2	000.0	-00.103	0.0096	00.012	-0.0003	00.0328	-00.001	00.116	-10.729	-00.318
-001.1	000.0	-00.053	0.0083	00.010	0.0009	00.0184	-00.001	00.188	-06.385	-00.347
-000.0	000.0	-00.003	0.0073	00.005	-0.0004	00.0003	-00.004	01.666	-00.410	-00.100
001.1	000.0	00.051	0.0089	00.003	0.0006	-00.0185	-00.004	-00.058	05.730	-00.362
002.2	000.0	00.103	0.0106	-00.002	0.0003	-00.0378	-00.000	00.019	09.716	-00.366
003.2	000.0	00.156	0.0132	-00.003	-0.0003	-00.0565	00.003	00.019	11.818	-00.361
004.3	000.0	00.215	0.0180	-00.006	-0.0001	-00.0778	00.013	00.027	11.944	-00.359
006.5	000.0	00.329	0.0324	-00.013	0.0033	-00.1180	00.018	00.039	10.154	-00.356
008.7	000.0	00.443	0.0543	-00.016	0.0094	-00.1562	00.023	00.035	08.158	-00.349
010.9	000.0	00.546	0.0836	-00.017	0.0178	-00.1913	00.034	00.030	06.531	-00.346
013.0	000.0	00.661	0.1267	-00.015	-0.0204	-00.2215	00.033	00.022	05.217	-00.314
015.2	000.0	00.772	0.1797	-00.009	-0.0045	-00.2467	00.041	00.011	04.296	-00.299
017.4	000.0	00.877	0.2383	00.003	0.0104	-00.2707	00.042	-00.003	03.680	-00.287
019.5	000.0	00.954	0.2963	00.017	0.0727	-00.2757	00.044	-00.017	03.219	-00.284
021.7	000.0	01.056	0.3747	00.023	0.0911	-00.2906	00.047	-00.020	02.818	-00.271
023.9	000.0	01.199	0.4870	00.022	0.0697	-00.3367	00.045	-00.017	02.462	-00.259
026.1	000.0	01.345	0.6007	00.027	0.0888	-00.3559	00.045	-00.018	02.239	-00.243

UNIVERSITY OF MARYLAND
WIND TUNNEL OPERATIONS DEPT.

CONFIGURATION 5B		RUN NO	TEST NO	Q	V	RN	WIND AXES	04/14/76		
AA	AY	CL	CD	CM	CN	CRM	CY	C CP	L D	S CP
028.1	000.0	01.315	0.6492	00.056	0.0975	-00.3351	00.045	-00.038	02.025	-00.232
030.0	000.0	01.305	0.7010	00.070	0.1507	-00.3249	00.031	-00.047	01.861	-00.240
032.0	000.0	01.288	0.7567	00.073	0.1634	-00.3174	00.021	-00.048	01.702	-00.238

UNIVERSITY OF MARYLAND
WIND TUNNEL OPERATIONS DEPT.

WIND AXES 04/14/76
01 05 01 01 00 00 00 5

CONFIGURATION 5C 5 729 011.89 100.00 02.563
RUN NO TEST NO Q V RN

AA	AY	CL	CD	CM	CN	CRM	CY	C CP	L D	S CP
-004.3	000.0	-00.210	0.0170	00.020	0.0023	00.0672	00.005	00.094	-12.352	-00.318
-003.2	000.0	-00.155	0.0121	00.016	-0.0006	00.0510	00.006	00.103	-12.809	-00.328
-002.2	000.0	-00.105	0.0097	00.013	-0.0009	00.0362	00.003	00.123	-10.824	-00.343
-001.1	000.0	-00.052	0.0082	00.010	0.0002	00.0171	00.004	00.192	-06.341	-00.328
-000.0	000.0	-00.003	0.0077	00.006	-0.0008	00.0016	-00.002	02.000	-00.389	-00.533
001.1	000.0	00.054	0.0092	00.003	-0.0004	-00.0212	-00.002	-00.055	05.869	-00.392
002.2	000.0	00.105	0.0105	-00.002	0.0001	-00.0399	00.004	00.019	10.000	-00.380
003.2	000.0	00.157	0.0131	-00.004	-0.0000	-00.0582	00.005	00.025	11.984	-00.370
004.3	000.0	00.213	0.0172	-00.007	-0.0003	-00.0775	00.011	00.032	12.383	-00.361
006.5	000.0	00.332	0.0311	-00.012	0.0029	-00.1225	00.020	00.036	10.675	-00.366
008.7	000.0	00.444	0.0516	-00.018	0.0072	-00.1625	00.032	00.040	08.604	-00.361
010.9	000.0	00.557	0.0790	-00.021	0.0143	-00.1968	00.041	00.037	07.050	-00.348
013.1	000.0	00.674	0.1182	-00.021	0.0274	-00.2322	00.051	00.030	05.702	-00.340
015.2	000.0	00.775	0.1756	-00.014	0.0446	-00.2522	00.050	00.017	04.413	-00.321
017.4	000.0	00.872	0.2308	-00.000	0.0587	-00.2684	00.050	00.000	03.778	-00.303
019.5	000.0	00.978	0.2994	00.002	0.0703	-00.2890	00.049	-00.001	03.266	-00.289
021.6	000.0	01.042	0.3761	00.015	0.0901	-00.2926	00.052	-00.013	02.770	-00.275
023.8	000.0	01.143	0.4847	00.021	0.1272	-00.3147	00.051	-00.016	02.358	-00.273
026.1	000.0	01.324	0.5832	00.023	0.0876	-00.3607	00.058	-00.015	02.270	-00.250

UNIVERSITY OF MARYLAND
WIND TUNNEL OPERATIONS DEPT.

CONFIGURATION 5C										WIND AXES					04/14/76				
RUN NO		TEST NO		Q		V		RN											
5		729		011.89		100.00		02.563											
AA	AY	CL	CD	CM	CN	CRM	CY	C CP	L D	S CP									
028.1	000.0	01.354	0.6634	00.051	0.0910	-00.3439	00.049	-00.033	02.041	-00.229									
030.1	000.0	01.310	0.7087	00.067	0.1513	-00.3188	00.040	-00.044	01.848	-00.236									
032.0	000.0	01.298	0.7674	00.067	0.1598	-00.3164	00.029	-00.044	01.691	-00.234									
029.0	000.0	01.304	0.6734	00.066	0.1381	-00.3117	00.044	-00.044	01.936	-00.231									

UNIVERSITY OF MARYLAND
WIND TUNNEL OPERATIONS DEPT.

CONFIGURATION 7A										WIND AXES				04/14/76			
RUN NO TEST NO Q V RN										01 14 01 01 00 00 00 00 6							
6 729 011.89 100.00 02.563																	
AA	AY	CL	CD	CM	CN	CRM	CY	C CP	L D	S CP							
-004.3	000.0	-00.210	0.0194	00.014	-0.0058	00.0716	-00.000	00.066	-10.824	-00.336							
-003.2	000.0	-00.155	0.0140	00.010	-0.0086	00.0526	-00.001	00.064	-11.071	-00.335							
-002.2	000.0	-00.103	0.0111	00.010	-0.0088	00.0352	-00.003	00.097	-09.279	-00.337							
-001.1	000.0	-00.052	0.0093	00.008	-0.0082	00.0180	-00.003	00.153	-05.591	-00.342							
-000.0	000.0	-00.003	0.0089	00.007	-0.0087	00.0011	-00.005	02.333	-00.337	-00.366							
001.1	000.0	00.051	0.0101	00.004	-0.0082	-00.0197	-00.005	-00.078	05.049	-00.382							
002.2	000.0	00.102	0.0118	00.002	-0.0085	-00.0379	-00.003	-00.019	08.644	-00.367							
003.2	000.0	00.155	0.0147	00.002	-0.0084	-00.0564	00.003	-00.012	10.544	-00.357							
004.3	000.0	00.215	0.0213	00.001	-0.0071	-00.0759	00.003	-00.004	10.093	-00.347							
006.5	000.0	00.346	0.0406	-00.006	-0.0018	-00.1272	00.008	00.017	08.522	-00.362							
008.7	000.0	00.459	0.0700	-00.008	0.0086	-00.1653	00.011	00.017	06.557	-00.354							
010.9	000.0	00.583	0.1061	-00.004	-0.0291	-00.2012	00.016	00.006	05.494	-00.324							
013.1	000.0	00.697	0.1541	00.015	-0.0170	-00.2315	00.019	-00.021	04.523	-00.310							
015.3	000.0	00.843	0.2255	00.027	0.0017	-00.2581	00.016	-00.030	03.738	-00.286							
017.5	000.0	00.924	0.2860	00.050	0.0618	-00.2715	00.018	-00.051	03.230	-00.286							
019.6	000.0	01.005	0.3506	00.062	0.0761	-00.2884	00.016	-00.058	02.866	-00.279							
021.7	000.0	01.099	0.4350	00.068	0.0972	-00.3045	00.014	-00.057	02.526	-00.269							
023.9	000.0	01.184	0.5080	00.074	0.1082	-00.3210	00.012	-00.057	02.330	-00.261							
025.9	000.0	01.213	0.5834	00.082	0.0765	-00.3088	00.011	-00.060	02.079	-00.231							

UNIVERSITY OF MARYLAND

WIND TUNNEL OPERATIONS DEPT.

WIND AXES 04/14/76

RUN NO TEST NO Q V RN

01 14 01 01 00 00 00 6

02.563

CONFIGURATION 7A

6

729

011.89

100.00

02.563

AA	AY	CL	CD	CM	CN	CRM	CY	C CP	L D	S CP
027.9	000.0	01.240	0.6273	00.080	0.1224	-00.3179	-00.010	-00.057	01.976	-00.243
029.9	000.0	01.220	0.6824	00.085	0.1352	-00.3161	-00.009	-00.060	01.787	-00.244
013.1	000.0	00.703	0.1563	00.016	0.0322	-00.2318	00.015	-00.022	04.497	-00.323

UNIVERSITY OF MARYLAND
WIND TUNNEL OPERATIONS DEPT.

CONFIGURATION 8AC										WIND AXES				04/14/76			
RUN NO TEST NO Q V RN										01 08 01 01 00 00 00 7							
7 729 011.89 100.00 02.563																	
AA	AY	CL	CD	CM	CN	CRM	CY	C CP	L D	S CP							
-004.3	000.0	-00.210	0.0168	00.016	0.0026	00.0721	00.010	00.075	-12.500	-00.341							
-003.2	000.0	-00.152	0.0128	00.013	0.0003	00.0519	00.003	00.085	-11.875	-00.340							
-002.2	000.0	-00.101	0.0101	00.011	-0.0008	00.0323	00.003	00.108	-10.000	-00.318							
-001.1	000.0	-00.051	0.0087	00.008	0.0010	00.0170	00.001	00.156	-05.862	-00.333							
-000.0	000.0	-00.003	0.0077	00.004	-0.0001	-00.0002	-00.001	01.333	-00.389	00.066							
001.1	000.0	00.050	0.0087	00.001	0.0001	-00.0184	-00.001	-00.020	05.747	-00.368							
002.2	000.0	00.104	0.0107	-00.000	0.0004	-00.0383	00.002	00.000	09.719	-00.368							
003.2	000.0	00.155	0.0138	-00.001	0.0002	-00.0565	00.008	00.006	11.231	-00.363							
004.3	000.0	00.212	0.0185	-00.004	0.0001	-00.0765	00.017	00.018	11.459	-00.358							
006.5	000.0	00.331	0.0338	-00.007	0.0037	-00.1197	00.025	00.021	09.792	-00.358							
008.7	000.0	00.445	0.0561	-00.010	0.0103	-00.1592	00.025	00.022	07.932	-00.354							
010.9	000.0	00.562	0.0876	-00.011	0.0202	-00.1952	00.036	00.019	06.415	-00.344							
013.1	000.0	00.678	0.1357	-00.009	0.0348	-00.2260	00.032	00.013	04.996	-00.329							
015.2	000.0	00.788	0.1882	-00.002	0.0470	-00.2499	00.033	00.002	04.187	-00.312							
017.4	000.0	00.886	0.2456	00.009	0.0614	-00.2715	00.036	-00.009	02.607	-00.301							
019.5	000.0	00.937	0.3038	00.033	0.0724	-00.2657	00.025	-00.033	03.084	-00.279							
021.7	000.0	01.071	0.3903	00.033	0.0946	-00.2982	00.033	-00.028	02.744	-00.273							
024.0	000.0	01.255	0.5205	00.025	0.0767	-00.3462	00.037	-00.018	02.411	-00.255							
026.1	000.0	01.320	0.5946	00.057	0.0843	-00.3490	00.028	-00.039	02.219	-00.242							
026.1	000.0	01.341	0.6093	00.038	0.0910	-00.3539	00.029	-00.025	02.200	-00.243							

UNIVERSITY OF MARYLAND
WIND TUNNEL OPERATIONS DEPT.

CONFIGURATION 8AC		RUN NO	TEST NO	Q	V	RN	WIND AXES		04/14/76	
		7	729	011.89	100.00	02.563	01 08 01 01 00 00 00	00 00 00	7	
AA	AY	CL	CD	CM	CN	CRM	CY	C CP	L D	S CP
028.0	000.0	01.256	0.6254	00.076	0.0883	-00.3159	00.022	-00.054	02.008	-00.228
030.0	000.0	01.248	0.6888	00.078	0.1479	-00.3076	00.017	-00.054	01.811	-00.238
026.0	000.0	01.291	0.5967	00.056	0.0936	-00.3385	00.025	-00.039	02.163	-00.242
013.1	000.0	00.673	0.1357	-00.010	0.0348	-00.2219	00.030	00.014	04.959	-00.326
-021.7	000.0	-01.071	0.3707	00.000	0.0575	00.3019	00.031	00.000	-02.889	-00.266
-023.9	000.0	-01.220	0.4733	00.005	0.0860	00.3411	00.026	00.003	-02.577	-00.265
-026.1	000.0	-01.311	0.5657	-00.008	0.1495	00.3657	00.027	-00.005	-02.317	-00.276
-028.0	000.0	-01.248	0.5805	-00.045	0.1457	00.3289	00.017	-00.032	-02.149	-00.261
-026.0	000.0	00.007	-0.0031	00.000	-0.0019	-00.0028	-00.007	-00.000	-02.258	-00.412

UNIVERSITY OF MARYLAND
WIND TUNNEL OPERATIONS DEPT.

WIND AXES 04/14/76
01 10 01 01 00 00 00 8

RUN NO TEST NO Q V RN
8 729 011.69 100.00 02.563

CONFIGURATION 9A2

AA	AY	CL	CD	CM	CN	CRM	CY	C CP	L D	S CP
-004.3	000.0	-00.212	0.0181	00.019	0.0030	00.0742	00.009	00.089	-11.712	-00.348
-003.2	000.0	-00.157	0.0132	00.013	-0.0004	00.0530	00.005	00.082	-11.893	-00.336
-002.2	000.0	-00.101	0.0103	00.012	-0.0007	00.0328	00.003	00.118	-09.805	-00.324
-001.1	000.0	-00.050	0.0089	00.009	0.0010	00.0162	00.001	00.180	-05.617	-00.324
-000.0	000.0	-00.004	0.0080	00.005	-0.0004	-00.0010	-00.001	01.250	-00.500	00.250
001.1	000.0	00.048	0.0091	00.003	0.0003	-00.0181	-00.001	-00.062	05.274	-00.377
002.2	000.0	00.104	0.0106	-00.001	-0.0011	-00.0390	00.000	00.009	09.811	-00.374
003.2	000.0	00.153	0.0136	-00.002	-0.0005	-00.0560	00.009	00.013	11.250	-00.365
004.3	000.0	00.215	0.0198	-00.006	0.0013	-00.0791	00.011	00.027	10.858	-00.365
006.5	000.0	00.341	0.0374	-00.003	0.0067	-00.1261	00.011	00.008	09.117	-00.367
008.7	000.0	00.461	0.0636	00.003	0.0161	-00.1686	00.019	-00.006	07.248	-00.363
010.9	000.0	00.555	0.0953	-00.003	0.0255	-00.1930	00.026	00.005	05.823	-00.345
013.1	000.0	00.673	0.1362	-00.011	0.0347	-00.2287	00.028	00.016	04.941	-00.336
015.2	000.0	00.774	0.1896	00.002	0.0509	-00.2465	00.031	-00.002	04.082	-00.315
017.4	000.0	00.878	0.2468	00.014	0.0628	-00.2670	00.036	-00.015	03.557	-00.300
019.5	000.0	00.946	0.3046	00.029	0.0765	-00.2792	00.032	-00.029	03.105	-00.290
021.6	000.0	01.048	0.3793	00.032	0.0927	-00.2937	00.031	-00.028	02.762	-00.275
023.9	000.0	01.231	0.5089	00.025	0.0680	-00.3387	00.041	-00.018	02.418	-00.253
026.1	000.0	01.343	0.6061	00.040	0.0933	-00.3665	00.032	-00.027	02.215	-00.251

WIND AXES 04/14/76
01 10 01 01 00 00 00 00 8

RUN NO	TEST NO	Q	V	RN
CONFIGURATION 9A2				
8	729	011.89	100.00	02.563

155

UNIVERSITY OF MARYLAND
WIND TUNNEL OPERATIONS DEPT.

WIND AXES 04/14/76
01 10 01 01 00 00 00 9

RUN NO TEST NO Q V RN
9 729 011.89 100.00 02.563

CONFIGURATION 9A1.

AA	AY	CL	CD	CM	CN	CRM	CY	C CP	L D	S CP
-004.3	000.0	-00.199	0.0165	00.014	-0.0000	00.0673	00.003	00.070	-12.060	-00.335
-003.2	000.0	-00.150	0.0133	00.011	-0.0012	00.0488	00.002	00.073	-11.278	-00.324
-002.2	000.0	-00.102	0.0106	00.010	-0.0006	00.0332	00.023	00.098	-09.622	-00.325
-001.1	000.0	-00.051	0.0088	00.008	0.0009	00.0171	00.000	00.156	-05.795	-00.335
-000.0	000.0	00.000	0.0080	00.006	-0.0005	-00.0020	-00.002		00.000	
001.1	000.0	00.051	0.0090	00.004	-0.0004	-00.0195	-00.002	-00.078	05.666	-00.382
002.2	000.0	00.098	0.0109	00.002	-0.0005	-00.0355	-00.001	-00.020	08.990	-00.362
003.2	000.0	00.155	0.0142	00.001	-0.0004	-00.0559	00.002	-00.006	10.915	-00.360
004.3	000.0	00.209	0.0193	00.001	-0.0008	-00.0781	00.010	-00.004	10.829	-00.370
006.5	000.0	00.321	0.0356	00.001	0.0025	-00.1126	00.018	-00.003	09.016	-00.347
008.7	000.0	00.451	0.0612	-00.002	0.0101	-00.1614	00.020	00.004	07.369	-00.353
010.9	000.0	00.551	0.0961	00.005	0.0196	-00.1852	00.025	-00.008	05.733	-00.331
013.1	000.0	00.701	0.1502	00.017	0.0337	-00.2263	00.027	-00.023	04.667	-00.317
015.2	000.0	00.791	0.2027	00.036	0.0474	-00.2447	00.025	-00.044	03.902	-00.304
017.4	000.0	00.902	0.2719	00.048	0.0627	-00.2718	00.027	-00.050	03.317	-00.295
019.6	000.0	00.991	0.3372	00.036	0.0778	-00.2877	00.027	-00.034	02.938	-00.283
021.7	000.0	01.096	0.4185	00.117	0.0909	-00.3054	00.022	-00.099	02.618	-00.270
023.9	000.0	01.183	0.5019	00.118	0.0597	-00.3108	00.023	-00.091	02.357	-00.239
025.9	000.0	01.241	0.5849	00.109	0.0758	-00.3148	00.018	-00.079	02.121	-00.230

UNIVERSITY OF MARYLAND
WIND TUNNEL OPERATIONS DEPT.

CONFIGURATION 9A1										WIND AXES			04/14/76	
RUN NO TEST NO Q V RN										01 10 01 01 00 00 00 00 9				
9 729 011.89 100.00 02.563														
AA	AY	CL	CD	CM	CN	CRM	CY	C CP	L D	S CP				
027.9	000.0	01.207	0.6389	00.110	0.1230	-00.2954	00.003	-00.080	01.889	-00.233				
029.9	000.0	01.214	0.6839	00.109	0.1342	-00.2966	00.000	-00.078	01.775	-00.232				
026.0	000.0	01.248	0.5764	00.111	0.1223	-00.3154	00.013	-00.080	02.165	-00.245				
013.1	000.0	00.700	0.1504	00.015	0.0346	-00.2287	00.024	-00.020	04.654	-00.321				

UNIVERSITY OF MARYLAND
WIND TUNNEL OPERATIONS DEPT.

WIND AXES 04/14/76
01 10 01 01 00 00 00 1

RUN NO TEST NO Q V RN
10 729 011.89 100.00 02.563

CONFIGURATION 9C1

AA	AY	CL	CD	CM	CN	CRM	CY	C CP	L D	S CP
-004.3	000.0	-00.209	0.0186	00.013	0.0025	00.0710	00.009	00.061	-11.236	-00.338
-003.2	000.0	-00.154	0.0134	00.011	-0.0003	00.0511	00.008	00.071	-11.492	-00.331
-002.2	000.0	-00.103	0.0111	00.010	-0.0009	00.0322	00.004	00.097	-09.279	-00.311
-001.1	000.0	-00.052	0.0094	00.009	0.0007	00.0216	00.005	00.173	-05.531	-00.415
-000.0	000.0	-00.001	0.0085	00.007	-0.0000	-00.0005	00.005	07.000	-00.117	00.500
001.1	000.0	00.045	0.0093	00.003	-0.0010	-00.0144	00.000	-00.066	04.838	-00.320
002.2	000.0	00.099	0.0117	00.001	-0.0004	-00.0356	00.003	-00.010	08.461	-00.359
003.2	000.0	00.152	0.0143	00.001	-0.0007	-00.0531	00.009	-00.006	10.629	-00.348
004.3	000.0	00.208	0.0198	00.001	-0.0001	-00.0704	00.011	-00.004	10.505	-00.335
006.5	000.0	00.329	0.0361	-00.000	0.0039	-00.1149	00.019	00.000	09.113	-00.346
008.7	000.0	00.437	0.0628	00.003	0.0115	-00.1481	00.020	-00.006	06.958	-00.335
010.9	000.0	00.568	0.1011	00.011	0.0242	-00.1905	00.030	-00.019	05.618	-00.332
013.1	000.0	00.720	0.1587	00.018	-0.0114	-00.2295	00.013	-00.024	04.536	-00.299
015.3	000.0	00.809	0.2135	00.039	0.0030	-00.2449	00.029	-00.046	03.789	-00.283
017.4	000.0	00.908	0.2733	00.048	0.0647	-00.2668	00.074	-00.050	03.322	-00.288
019.5	000.0	00.984	0.3386	00.058	0.0779	-00.2795	00.029	-00.055	02.906	-00.278
021.7	000.0	01.078	0.4173	00.065	0.0966	-00.2807	00.024	-00.056	02.583	-00.256
023.8	000.0	01.155	0.4976	00.076	0.0603	-00.2938	00.020	-00.060	02.321	-00.233
025.9	000.0	01.203	0.5763	00.081	0.0747	-00.3011	00.023	-00.060	02.087	-00.227

UNIVERSITY OF MARYLAND
WIND TUNNEL OPERATIONS DEPT.

AA	AY	CL	CD	CM	CN	CRM	CY	C CP	L D	S CP	WIND AXES	04/14/76
027.9	000.0	01.214	0.6303	00.075	0.0814	-00.2962	00.010	-00.054	01.926	-00.219	01 05 01 01 00 00 00 00 1	
029.9	000.0	01.229	0.7050	00.078	0.1476	-00.2996	00.002	-00.055	01.743	-00.235		
025.9	000.0	01.225	0.5851	00.079	0.0766	-00.3091	00.018	-00.058	02.093	-00.229		
017.4	000.0	00.918	0.2919	00.052	0.0675	-00.2689	00.030	-00.054	03.256	-00.288		

UNIVERSITY OF MARYLAND
WIND TUNNEL OPERATIONS DEPT.

CONFIGURATION 10										WIND AXES				04/14/76			
RUN NO TEST NO Q V RN										01 02 01 01 00 00 00 00 11							
11 729 011.89 100.00 02.563																	
AA	AY	CL	CD	CM	CN	CRM	CY	C CP	L D	S CP							
-000.0	000.0	00.003	0.0090	00.005	0.0002	-00.0041	-00.002	-01.666	00.333	-01.366							
002.2	000.0	00.107	0.0119	-00.001	0.0006	-00.0386	00.006	00.009	08.991	-00.360							
004.4	000.0	00.228	0.0201	-00.010	0.0017	-00.0819	00.007	00.043	11.343	-00.357							
006.6	000.0	00.372	0.0405	-00.022	0.0097	-00.1361	00.013	00.058	09.185	-00.364							
008.8	000.0	00.491	0.0679	-00.026	0.0205	-00.1721	00.021	00.052	07.231	-00.349							
011.0	000.0	00.611	0.1056	-00.025	0.0345	-00.2095	00.023	00.040	05.785	-00.342							
013.1	000.0	00.718	0.1503	-00.026	0.0498	-00.2377	00.033	00.035	04.777	-00.331							
015.3	000.0	00.811	0.2010	-00.026	0.0652	-00.2583	00.040	00.031	04.034	-00.318							
017.4	000.0	00.908	0.2559	-00.028	0.0810	-00.2783	00.037	00.029	03.548	-00.307							
019.5	000.0	00.984	0.3184	-00.027	0.0947	-00.2882	00.040	00.026	03.090	-00.293							
021.6	000.0	01.030	0.3839	-00.044	0.1103	-00.2844	00.031	00.040	02.682	-00.277							
023.7	000.0	01.075	0.4655	-00.075	0.1239	-00.2900	00.010	00.064	02.309	-00.269							
025.6	000.0	01.027	0.4865	-00.100	0.1279	-00.2773	00.003	00.088	02.110	-00.268							
027.6	000.0	01.002	0.5136	-00.107	0.1359	-00.2715	00.000	00.095	01.950	-00.269							
029.5	000.0	00.952	0.5366	-00.112	0.0385	-00.2569	-00.017	00.102	01.767	-00.244							
025.6	000.0	01.043	0.4946	-00.102	0.1291	-00.2824	00.003	00.088	02.108	-00.268							
013.1	000.0	00.710	0.1474	-00.025	0.0490	-00.2342	00.054	00.034	04.816	-00.329							

UNIVERSITY OF MARYLAND
WIND TUNNEL OPERATIONS DEPT.

CONFIGURATION 11										WIND AXES				04/14/76			
RUN NO		TEST NO		Q		V		RN									
12		729		011.89		100.00		02.563				01 01 01 01 00 00 12					
AA	AY	CL	CD	CM	CN	CRM	CY	C CP	L D	S CP							
-000.0	000.0	-00.003	0.0076	00.005	-0.0008	00.0005	00.001	01.666	-00.394	-00.166							
004.4	000.0	00.224	0.0169	-00.013	0.0007	-00.0792	00.014	00.057	13.254	-00.351							
008.7	000.0	00.471	0.0503	-00.039	0.0115	-00.1746	00.047	00.082	09.363	-00.368							
013.1	000.0	00.705	0.1136	-00.062	0.0402	-00.2504	00.073	00.087	05.205	-00.355							
017.4	000.0	00.898	0.2206	-00.066	0.0833	-00.2851	00.081	00.071	04.070	-00.321							
021.6	000.0	01.045	0.3514	-00.071	0.1122	-00.3061	00.068	00.064	02.973	-00.296							
025.7	000.0	01.093	0.4844	-00.096	0.1367	-00.2916	00.039	00.080	02.256	-00.269							
029.7	000.0	01.053	0.5848	-00.126	0.1001	-00.2839	00.011	00.104	01.800	-00.246							

AA
028.1
030.0
032.0

UNIVERSITY OF MARYLAND
WIND TUNNEL OPERATIONS DEPT.

CONFIGURATION										WIND AXES				04/14/76			
12										01 11 01 01 00 00 00 00 13				00 00 00 00 13			
13										02.563							
RUN NO										Q				V			
TEST NO										729				100.00			
13										011.89				02.563			
AA	AY	CL	CD	CM	CN	CRM	CY	C CP	L D	S CP							
-000.0	000.0	00.008	0.0082	00.005	-0.0007	00.0403	00.003	-00.625	00.975	05.037							
002.2	000.0	00.100	0.0106	00.002	-0.0006	00.0071	00.006	-00.020	09.433	00.071							
004.3	000.0	00.209	0.0186	00.002	-0.0013	-00.0299	00.010	-00.009	11.236	-00.141							
006.5	000.0	00.325	0.0358	00.001	0.0041	-00.0713	00.020	-00.003	09.078	-00.218							
008.7	000.0	00.435	0.0609	00.006	0.0114	-00.1019	00.024	-00.013	07.142	-00.233							
010.9	000.0	00.562	0.1000	00.012	-0.0259	-00.1432	00.024	-00.021	05.620	-00.237							
013.1	000.0	00.709	0.1549	00.023	-0.0091	-00.1820	00.023	-00.031	04.577	-00.241							
015.3	000.0	00.805	0.2088	00.039	0.0026	-00.2025	00.023	-00.046	03.855	-00.235							
017.4	000.0	00.894	0.2702	00.048	0.0654	-00.2185	00.032	-00.051	03.308	-00.244							
019.6	000.0	01.000	0.3461	00.057	0.0830	-00.2493	00.023	-00.053	02.889	-00.248							
021.7	000.0	01.098	0.4253	00.070	0.0990	-00.2584	00.026	-00.059	02.581	-00.235							
023.9	000.0	01.179	0.5066	00.076	0.0650	-00.2705	00.023	-00.059	02.327	-00.213							
025.9	000.0	01.217	0.5783	00.080	0.0783	-00.2726	00.018	-00.059	02.104	-00.207							
027.9	000.0	01.210	0.6361	00.076	0.1368	-00.2744	00.000	-00.055	01.902	-00.224							
029.9	000.0	01.208	0.7013	00.078	0.1449	-00.2582	-00.001	-00.055	01.722	-00.211							
025.9	000.0	01.199	0.5758	00.079	0.0907	-00.2655	00.017	-00.059	02.082	-00.209							
015.3	000.0	00.809	0.2115	00.040	0.0519	-00.2041	00.025	-00.047	03.825	-00.251							
017.4	000.0	00.913	0.2693	00.043	0.0658	-00.2770	00.038	-00.045	03.390	-00.298							

UNIVERSITY OF MARYLAND
WIND TUNNEL OPERATIONS DEPT.

CONFIGURATION 17													WIND AXES				04/14/76
RUN NO 14													01 05 01 01 00 00 00 14				
TEST NO 729													02.563				
Q 011.89													100.00				
V 100.00													02.563				
RN 02.563																	
AA	AY	CL	CD	CM	CN	CRM	CY	C CP	L D	S CP							
-000.0	000.0	-00.001	0.0084	00.005	-0.0007	-00.0010	-00.001	05.000	-00.119	01.000							
002.2	000.0	00.104	0.0111	00.000	-0.0012	-00.0371	00.000	-00.000	09.369	-00.355							
004.3	000.0	00.215	0.0190	-00.001	-0.0024	-00.0750	00.011	00.004	11.315	-00.345							
006.5	000.0	00.338	0.0360	-00.001	0.0015	-00.1196	00.006	00.002	09.388	-00.350							
008.7	000.0	00.447	0.0630	00.002	0.0095	-00.1535	00.025	-00.004	07.095	-00.339							
010.9	000.0	00.572	0.1009	00.006	0.0211	-00.1900	00.027	-00.010	05.668	-00.327							
013.1	000.0	00.720	0.1578	00.020	0.0365	-00.2309	00.026	-00.027	04.562	-00.316							
015.3	000.0	00.837	0.2180	00.039	0.0520	-00.2583	00.023	-00.045	03.839	-00.303							
017.5	000.0	00.933	0.2860	00.048	0.0672	-00.2717	00.023	-00.049	03.262	-00.286							
019.6	000.0	01.039	0.3536	00.055	0.0797	-00.3069	00.029	-00.050	02.928	-00.287							
021.8	000.0	01.123	0.4317	00.068	0.0967	-00.3072	00.021	-00.056	02.601	-00.266							
023.9	000.0	01.182	0.5170	00.077	0.0645	-00.3064	00.018	-00.059	02.286	-00.237							
026.0	000.0	01.256	0.5936	00.084	0.0743	-00.3220	00.015	-00.060	02.115	-00.231							
028.0	000.0	01.263	0.6513	00.081	0.1260	-00.3106	00.008	-00.057	01.929	-00.234							
030.0	000.0	01.272	0.7162	00.081	0.1425	-00.3205	00.002	-00.055	01.771	-00.236							
026.0	000.0	01.243	0.5923	00.083	0.1087	-00.3153	00.012	-00.060	02.098	-00.240							
015.3	000.0	00.840	0.2202	00.040	0.0517	-00.2550	00.026	-00.046	03.814	-00.299							

UNIVERSITY OF MARYLAND
WIND TUNNEL OPERATIONS DEPT.

CONFIGURATION 4A												WIND AXES				04/14/76
RUN NO				TEST NO		G		V		RN		01 04 01 01 00 00 00 15				
15				729		011.89		100.00		02.563						
AA	AY	CL	CD	CM	CN	CRM	CY	C CP	L D	S CP						
002.2	000.0	00.111	0.0103	-00.001	-0.0003	-00.0401	00.012	00.009	10.776	-00.361						
-000.0	000.0	00.009	0.0071	00.004	0.0007	-00.0046	00.015	-00.444	01.267	-00.511						
-002.2	000.0	-00.099	0.0091	00.010	0.0013	00.0370	00.012	00.101	-10.879	-00.373						
-004.3	000.0	-00.209	0.0154	00.019	0.0022	00.0766	00.026	00.090	-13.571	-00.366						
-006.5	000.0	-00.319	0.0277	00.028	0.0061	00.1187	00.031	00.087	-11.516	-00.370						
-008.7	000.0	-00.431	0.0486	00.033	0.0125	00.1579	00.041	00.076	-08.868	-00.364						
-010.9	000.0	-00.560	0.0783	00.039	0.0223	00.2017	00.043	00.069	-07.151	-00.357						
-013.0	000.0	-00.665	0.1215	00.035	0.0355	00.2317	00.047	00.051	-05.473	-00.346						
-015.2	000.0	-00.762	0.1716	00.030	0.0505	00.2484	00.049	00.038	-04.440	-00.324						
-017.4	000.0	-00.870	0.2282	00.026	0.0658	00.2707	00.054	00.028	-03.812	-00.309						
-019.5	000.0	-00.973	0.2944	00.020	0.0811	00.2913	00.062	00.019	-03.305	-00.297						
-021.7	000.0	-01.084	0.3779	00.014	0.0510	00.3112	00.048	00.012	-02.868	-00.268						
-024.0	000.0	-01.267	0.4924	00.023	0.0803	00.3619	00.060	00.016	-02.573	-00.267						
-026.2	000.0	-01.385	0.5939	00.017	0.1518	00.3786	00.064	00.011	-02.332	-00.270						
-028.1	000.0	-01.362	0.6209	-00.031	0.1509	00.3600	00.053	-00.020	-02.193	-00.260						
-030.0	000.0	-01.297	0.6602	-00.056	0.1558	00.3199	00.038	-00.038	-01.964	-00.244						
-032.0	000.0	-01.273	0.7166	-00.064	0.1703	00.3121	00.031	-00.043	-01.776	-00.243						
-034.0	000.0	-01.246	0.8052	-00.047	0.1753	00.3080	-00.014	-00.031	-01.547	-00.238						

UNIVERSITY OF MARYLAND

WIND TUNNEL OPERATIONS DEPT.

WIND AXES
01 09 01 01 00 00 00 16

RUN NO TEST NO Q V RN
16 729 011.89 100.00 02.563

CONFIGURATION 15

AA	AY	CL	CD	CM	CN	CRM	CY	C CP	L D	S CP
002.2	000.0	00.110	0.0110	00.001	-0.0006	-00.0378	00.010	-00.009	10.000	-00.342
-000.0	000.0	00.007	0.0081	00.005	0.0006	-00.0028	00.009	-00.714	00.864	-00.400
-002.1	000.0	-00.095	0.0102	00.009	0.0015	00.0349	00.011	00.094	-09.313	-00.367
-004.3	000.0	-00.205	0.0172	00.013	0.0020	00.0713	00.021	00.063	-11.918	-00.345
-006.5	000.0	-00.326	0.0326	00.016	0.0074	00.1196	00.026	00.048	-10.000	-00.365
-008.7	000.0	-00.455	0.0574	00.016	0.0144	00.1671	00.032	00.034	-07.926	-00.365
-010.9	000.0	-00.558	0.0905	00.012	0.0254	00.1957	00.034	00.021	-06.165	-00.348
-013.1	000.0	-00.682	0.1394	00.005	0.0398	00.2233	00.033	00.007	-04.892	-00.325
-015.3	000.0	-00.807	0.1961	-00.009	0.0567	00.2480	00.030	-00.010	-04.115	-00.306
-017.4	000.0	-00.898	0.2550	-00.020	0.0720	00.2701	00.035	-00.021	-03.521	-00.299
-019.5	000.0	-00.986	0.3243	-00.029	0.0888	00.2776	00.037	-00.027	-03.040	-00.280
-021.7	000.0	-01.080	0.3946	-00.041	0.1022	00.2997	00.030	-00.035	-02.736	-00.275
-023.8	000.0	-01.170	0.4736	-00.047	0.0723	00.3124	00.031	-00.037	-02.470	-00.249
-025.9	000.0	-01.222	0.5462	-00.055	0.0759	00.3175	00.016	-00.041	-02.237	-00.238
-028.0	000.0	-01.246	0.6182	-00.055	0.1379	00.3070	00.007	-00.039	-02.015	-00.241
-030.0	000.0	-01.283	0.6955	-00.060	0.1543	00.3237	00.002	-00.041	-01.844	-00.245
-032.0	000.0	-01.287	0.7547	-00.064	0.1691	00.3325	-00.017	-00.042	-01.705	-00.249
-034.0	000.0	-01.246	0.8052	-00.047	0.1753	00.3080	-00.014	-00.031	-01.547	-00.238
-030.0	000.0	-01.271	0.6923	-00.055	0.1575	00.3067	00.002	-00.038	-01.835	-00.237
-017.4	000.0	-00.895	0.2575	-00.023	0.0726	00.2643	00.033	-00.024	-03.475	-00.294

UNIVERSITY OF MARYLAND

WIND TUNNEL OPERATIONS DEPT.

CONFIGURATION 14 RUN NO TEST NO Q V RN WIND AXES 04/14/76

17 729 011.89 100.00 02.563 01 12 01 01 00 00 00 17

AA	AY	CL	CD	CM	CN	CRM	CY	C CP	L D	S CP
-000.0	000.0	00.006	0.0085	00.004	0.0001	-00.0028	-00.005	-00.666	00.705	-00.466
002.2	000.0	00.107	0.0114	00.001	-0.0001	-00.0406	-00.000	-00.009	09.385	-00.379
004.3	000.0	00.217	0.0187	-00.002	0.0003	-00.0787	00.004	00.009	11.604	-00.360
006.5	000.0	00.339	0.0367	-00.008	0.0072	-00.1234	00.007	00.023	09.237	-00.361
008.7	000.0	00.462	0.0661	-00.010	0.0159	-00.1604	00.016	00.021	06.989	-00.345
010.9	000.0	00.587	0.1037	-00.004	0.0288	-00.2009	00.022	00.006	05.660	-00.340
013.2	000.0	00.737	0.1551	00.006	-0.0105	-00.2429	00.022	-00.007	04.751	-00.310
015.3	000.0	00.845	0.2216	00.026	0.0094	-00.2592	00.022	-00.029	03.813	-00.289
017.5	000.0	00.942	0.2780	00.043	0.0689	-00.2833	00.024	-00.043	03.388	-00.296
019.6	000.0	01.018	0.3466	00.047	0.0824	-00.2895	00.019	-00.043	02.937	-00.279
021.7	000.0	01.105	0.4299	00.062	0.1038	-00.3010	00.023	-00.052	02.570	-00.268
023.9	000.0	01.197	0.5022	00.071	0.0660	-00.3221	00.022	-00.054	02.383	-00.247
025.9	000.0	01.210	0.5715	00.054	0.0797	-00.3026	00.012	-00.040	02.117	-00.229
027.9	000.0	01.214	0.6329	00.120	0.1319	-00.3047	00.001	-00.087	01.918	-00.241
029.9	000.0	01.218	0.6839	00.121	0.1410	-00.3112	-00.000	-00.086	01.780	-00.243
031.9	000.0	01.218	0.7559	00.119	0.1545	-00.2971	-00.011	-00.083	01.611	-00.233
-002.2	000.0	-00.107	0.0115	00.007	-0.0490	00.0381	-00.004	00.065	-09.304	-00.338
-004.3	000.0	-00.209	0.0198	00.012	-0.0452	00.0710	00.002	00.057	-10.555	-00.320
-006.5	000.0	-00.335	0.0386	00.018	-0.0350	00.1186	00.001	00.053	-08.678	-00.337

UNIVERSITY OF MARYLAND
WIND TUNNEL OPERATIONS DEPT.

CONFIGURATION 14										WIND AXES				04/14/76			
RUN NO		TEST NO		Q	V	RM	L D		S CP	01 12 01 01 00 00 00 17		04/14/76					
17		729		011.89	100.00	02.563											
AA	AY	CL	CD	CM	CN	CRM	CY	C CP	L D	S CP							
-008.7	000.0	-00.474	0.0687	00.020	-0.0237	00.1689	00.002	00.041	-06.899	-00.340							
-010.9	000.0	-00.595	0.1054	00.016	-0.0101	00.1960	00.010	00.029	-05.645	-00.315							
-013.1	000.0	-00.709	0.1522	00.006	0.0518	00.2102	00.012	00.008	-04.658	-00.298							
-015.3	000.0	-00.815	0.2079	-00.011	0.0685	00.2367	00.013	-00.013	-03.920	-00.292							
-017.4	000.0	-00.910	0.2628	-00.011	0.0836	00.2505	00.008	-00.011	-03.462	-00.278							
-019.6	000.0	-00.996	0.3352	-00.031	0.0524	00.2592	00.011	-00.029	-02.971	-00.249							
-021.7	000.0	-01.101	0.4053	-00.040	0.0628	00.3019	00.003	-00.034	-02.716	-00.258							
-023.8	000.0	-01.177	0.4707	-00.050	0.1122	00.3053	00.007	-00.039	-02.458	-00.255							
-025.9	000.0	-01.228	0.5576	-00.058	0.0878	00.3157	00.002	-00.043	-02.202	-00.239							
-027.9	000.0	-01.234	0.6236	-00.056	0.1008	00.3273	-00.013	-00.040	-01.978	-00.243							

UNIVERSITY OF MARYLAND
WIND TUNNEL OPERATIONS DEPT.

WIND AXES 04/14/76
01 12 01 01 00 00 00 18

RUN NO TEST NO Q V RN
18 729 011.89 100.00 02.563

CONFIGURATION 18

AA	AY	CL	CD	CM	CN	CRM	CY	C CP	L D	S CP
-000.0	000.0	-00.000	0.0085	00.007	0.0017	-00.0008	00.007		-00.000	
-002.1	000.0	-00.094	0.0093	00.011	0.0018	00.0337	00.014	00.117	-10.107	-00.350
-004.2	000.0	-00.195	0.0142	00.015	0.0019	00.0672	00.023	00.076	-13.732	-00.344
-006.5	000.0	-00.307	0.0269	00.022	0.0048	00.1128	00.033	00.071	-11.412	-00.365
-008.7	000.0	-00.436	0.0503	00.024	0.0128	00.1584	00.034	00.054	-08.667	-00.361
-010.9	000.0	-00.542	0.0819	00.017	0.0253	00.1867	00.039	00.031	-06.617	-00.343
-013.0	000.0	-00.644	0.1242	00.011	0.0399	00.2110	00.042	00.016	-05.185	-00.327
-015.2	000.0	-00.774	0.1750	00.005	0.0539	00.2546	00.050	00.006	-04.402	-00.327
-017.4	000.0	-00.923	0.2500	00.007	0.0723	00.2835	00.040	00.007	-03.692	-00.305
-019.6	000.0	-00.995	0.3185	00.033	0.0909	00.2915	00.044	00.031	-03.124	-00.292
-021.7	000.0	-01.079	0.3852	00.047	0.1048	00.2974	00.046	00.041	-02.801	-00.275
-023.8	000.0	-01.152	0.4560	00.051	0.0752	00.3170	00.038	00.041	-02.515	-00.258
-025.9	000.0	-01.216	0.5383	00.063	0.1333	00.3187	00.028	00.047	-02.258	-00.259
-028.0	000.0	-01.260	0.6122	00.061	0.1543	00.3713	00.020	00.043	-02.090	-00.282
-028.0	000.0	-01.264	0.6108	00.062	0.1503	00.3144	00.022	00.044	-02.069	-00.248
-030.0	000.0	-01.296	0.6901	00.061	0.1636	00.3402	00.016	00.041	-01.877	-00.256
-032.0	000.0	-01.292	0.7429	00.066	0.1737	00.3432	-00.003	00.044	-01.739	-00.257
002.2	000.0	00.102	0.0127	00.003	0.0009	-00.0366	00.006	00.029	08.031	-00.358
004.4	000.0	00.230	0.0253	00.003	0.0054	-00.0863	00.011	00.012	09.090	-00.374

UNIVERSITY OF MARYLAND
WIND TUNNEL OPERATIONS DEPT.

CONFIGURATION 18		RUN NO		TEST NO		Q		V		RN		WIND AXES		04/14/76	
		18		729		011.89		100.00		02.563		01 12 01 01 00 00 00 18			
AA	AY	CL	CD	CM	CN	CRM	CY	C CP	L D	S CP					
006.6	000.0	00.355	0.0480	-00.005	0.0129	-00.1229	00.006	00.013	07.395	-00.344					
008.8	000.0	00.508	0.0841	-00.006	0.0230	-00.1774	00.009	00.011	06.040	-00.347					
011.0	000.0	00.633	0.1289	00.002	0.0369	-00.2104	00.009	-00.003	04.910	-00.330					
013.2	000.0	00.744	0.1785	00.019	0.0480	-00.2353	00.012	-00.024	04.168	-00.313					
015.3	000.0	00.833	0.2275	00.035	0.0566	-00.2506	00.011	-00.040	03.661	-00.297					
017.4	000.0	00.900	0.2865	00.047	0.0697	-00.2566	00.009	-00.049	03.141	-00.281					
019.6	000.0	01.007	0.3603	00.056	0.0843	-00.2794	00.008	-00.052	02.794	-00.272					
021.7	000.0	01.091	0.4262	00.065	0.0696	-00.2916	00.007	-00.055	02.547	-00.253					

UNIVERSITY OF MARYLAND
WIND TUNNEL OPERATIONS DEPT.

CONFIGURATION 9C1		RUN NO	TEST NO	Q	V	RN	WIND AXES		04/14/76	
		29	729	011.89	100.00	02.563	01	10 01 01 00 00 00	29	
AA	AY	CL	CD	CM	CN	CRM	CY	C CP	L D	S CP
008.7	000.0	00.458	0.0670	00.002	0.0150	-00.1572	00.020	-00.004	06.835	-00.340
013.1	000.0	00.720	0.1616	00.017	0.0418	-00.2241	00.021	-00.023	04.455	-00.308
017.4	000.0	00.919	0.2828	00.045	0.1207	-00.2717	00.024	-00.046	03.249	-00.307
021.7	000.0	01.114	0.4303	00.066	0.1518	-00.3061	00.020	-00.055	02.588	-00.285
025.9	000.0	01.199	0.5761	00.076	0.1319	-00.3017	00.011	-00.057	02.081	-00.247

UNIVERSITY OF MARYLAND
WIND TUNNEL OPERATIONS DEPT.

CONFIGURATION 5C		RUN NO	TEST NO	Q	V	RN	WIND AXES		04/14/76	
		30	729	011.89	100.00	02.563	01 05 01 01 00 00 00 00	00 00 00 00 00 00 00 00	3	
AA	AY	CL	CD	CM	CN	CRM	CY	C CP	L D	S CP
008.7	000.0	00.446	0.0524	00.003	0.0070	-00.1611	00.035	-00.006	08.511	-00.357
013.1	000.0	00.685	0.1314	-00.006	-0.0195	-00.2359	00.044	00.008	05.213	-00.323
017.4	000.0	00.904	0.2549	-00.005	0.0599	-00.2740	00.048	00.005	03.546	-00.297
021.8	000.0	01.133	0.4227	00.012	0.0972	-00.3076	00.040	-00.009	02.680	-00.266
025.9	000.0	01.179	0.5411	00.070	0.0707	-00.2976	00.031	-00.053	02.178	-00.230

UNIVERSITY OF MARYLAND
WIND TUNNEL OPERATIONS DEPT.

CONFIGURATION 6		RUN NO	TEST NO	Q	V	RN	WIND AXES			04/14/76
		31	729	011.89	100.00	02.563	01	12	01	01 00 00 00 31
AA	AY	CL	CD	CM	CN	CRM	CY	C CP	L D	S CP
008.8	000.0	00.487	0.0729	-00.010	0.0193	-00.1750	00.019	00.020	06.680	-00.357
013.2	000.0	00.769	0.1751	00.005	0.0483	-00.2505	00.021	-00.006	04.391	-00.323
017.4	000.0	00.921	0.2860	00.045	0.0707	-00.2691	00.023	-00.046	03.220	-00.288
021.7	000.0	01.101	0.4306	00.039	0.0992	-00.2993	00.019	-00.032	02.556	-00.266
025.9	000.0	01.219	0.5846	00.062	0.0734	-00.3086	00.012	-00.045	02.084	-00.228

UNIVERSITY OF MARYLAND
WIND TUNNEL OPERATIONS DEPT.

CONFIGURATION 20										WIND AXES				04/14/76			
RUN NO TEST NO Q V RN										01 15 01 01 00 00 00 32							
32 729 011.89 100.00 02.563																	
AA	AY	CL	CD	CM	CN	CRM	CY	C CP	L D	S CP							
-000.0	000.0	00.007	0.0073	00.004	-0.0006	-00.0029	-00.000	-00.571	00.958	-00.414							
002.2	000.0	00.096	0.0108	00.002	-0.0007	-00.0339	00.001	-00.020	08.888	-00.353							
004.3	000.0	00.199	0.0185	00.001	-0.0016	-00.0701	00.009	-00.005	10.756	-00.349							
006.5	000.0	00.319	0.0340	00.003	0.0014	-00.1120	00.015	-00.009	09.382	-00.347							
008.7	000.0	00.430	0.0585	00.007	0.0085	-00.1485	00.022	-00.016	07.350	-00.341							
010.9	000.0	00.551	0.0955	00.014	0.0216	-00.1867	00.026	-00.025	05.769	-00.335							
013.0	000.0	00.651	0.1446	00.024	0.0358	-00.2095	00.031	-00.035	04.502	-00.317							
015.2	000.0	00.787	0.1991	00.037	0.0576	-00.2459	00.034	-00.045	03.952	-00.311							
017.4	000.0	00.864	0.2528	00.047	0.1028	-00.2567	00.032	-00.052	03.417	-00.306							
019.5	000.0	00.980	0.3355	00.060	0.1234	-00.2774	00.035	-00.057	02.921	-00.292							
021.8	000.0	01.133	0.4187	00.074	0.1432	-00.3322	00.036	-00.061	02.705	-00.299							
023.9	000.0	01.188	0.5013	00.093	0.1575	-00.3126	00.037	-00.072	02.369	-00.271							
026.0	000.0	01.265	0.5967	00.110	0.1225	-00.3221	00.031	-00.078	02.119	-00.245							
028.0	000.0	01.265	0.6593	00.115	0.1697	-00.3096	00.018	-00.080	01.918	-00.247							
030.0	000.0	01.258	0.7136	00.104	0.1750	-00.3090	00.004	-00.071	01.762	-00.245							
013.1	000.0	00.670	0.1442	00.024	0.0508	-00.2186	00.035	-00.035	04.646	-00.327							
021.7	000.0	01.080	0.4127	00.074	0.1513	-00.2976	00.038	-00.064	02.616	-00.287							
025.9	000.0	01.217	0.5800	00.108	0.1271	-00.2972	00.028	-00.080	02.098	-00.239							

UNIVERSITY OF MARYLAND
WIND TUNNEL OPERATIONS DEPT.

CONFIGURATION 14		RUN NO	TEST NO	Q	V	RN	WIND AXES		04/14/76	
AA	AY	CL	CD	CM	CN	CRM	CY	C CP	L D	S CP
008.7	000.0	00.470	0.0677	-00.012	0.0148	-00.1659	00.012	00.025	06.942	-00.349
013.2	000.0	00.747	0.1613	00.006	0.0419	-00.2511	00.017	-00.007	04.631	-00.332
017.5	000.0	00.930	0.2786	00.043	0.1175	-00.2760	00.026	-00.044	03.338	-00.307
021.8	000.0	01.145	0.4381	00.066	0.1505	-00.3111	00.018	-00.053	02.613	-00.281
025.9	000.0	01.212	0.5691	00.075	0.1219	-00.3111	00.006	-00.056	02.129	-00.248

UNIVERSITY OF MARYLAND
WIND TUNNEL OPERATIONS DEPT.

CONFIGURATION 18		RUN NO	TEST NO	Q	V	RN	WIND AXES		04/14/76	
		34	729	011.89	100.00	02.563	01	12	01 01 00 00 00 34	
AA	AY	CL	CD	CM	CN	CRM	CY	C CP	L D	S CP
008.8	000.0	00.506	0.0854	-00.008	0.0231	-00.1747	-00.003	00.015	05.925	-00.343
013.2	000.0	00.737	0.1755	00.015	0.0481	-00.2344	00.000	-00.019	04.199	-00.315
017.4	000.0	00.922	0.2910	00.046	0.1194	-00.2623	00.001	-00.047	03.168	-00.295
021.7	000.0	01.104	0.4306	00.065	0.1444	-00.2962	-00.004	-00.054	02.563	-00.277

UNIVERSITY OF MARYLAND
WIND TUNNEL OPERATIONS DEPT.

WIND AXES 04/14/76
01 13 01 01 00 00 00 35

WIND AXES 04/14/76
01 13 01 01 00 00 00 35

CONFIGURATION 19

AA	AY	CL	CD	CM	CN	CRM	CY	C CP	L D	S CP
000.0	000.0	00.005	0.0085	00.005	-0.0054	-00.0026	00.000	-01.000	00.588	-00.520
002.2	000.0	00.098	0.0116	-00.000	-0.0063	-00.0355	00.003	00.000	08.448	-00.359
004.3	000.0	00.210	0.0192	-00.001	-0.0080	-00.0752	00.014	00.004	10.937	-00.352
006.5	000.0	00.322	0.0346	-00.001	-0.0033	-00.1153	00.020	00.003	09.306	-00.352
008.7	000.0	00.435	0.0588	-00.002	0.0038	-00.1513	00.029	00.004	07.397	-00.341
010.9	000.0	00.553	0.0968	00.003	0.0167	-00.1857	00.029	-00.005	05.712	-00.330
013.1	000.0	00.697	0.1450	00.017	0.0270	-00.2283	00.038	-00.023	04.806	-00.320
015.2	000.0	00.790	0.1991	00.030	0.0417	-00.2465	00.034	-00.036	03.967	-00.305
017.4	000.0	00.883	0.2537	00.041	0.0530	-00.2642	00.044	-00.044	03.480	-00.291
019.6	000.0	01.003	0.3439	00.056	0.0755	-00.2885	00.038	-00.052	02.916	-00.280
021.8	000.0	01.121	0.4273	00.068	0.0468	-00.3072	00.042	-00.056	02.623	-00.252
023.9	000.0	01.189	0.5016	00.084	0.0585	-00.3085	00.033	-00.065	02.370	-00.236
026.0	000.0	01.261	0.5858	00.095	0.0746	-00.3238	00.035	-00.068	02.152	-00.232
028.0	000.0	01.269	0.6652	00.099	0.1362	-00.3078	00.028	-00.069	01.907	-00.234
030.0	000.0	01.254	0.7072	00.097	0.1352	-00.3008	00.007	-00.067	01.773	-00.228
025.9	000.0	01.242	0.5885	00.095	0.0836	-00.3033	00.033	-00.069	02.110	-00.225
021.7	000.0	01.099	0.4202	00.067	0.0948	-00.3001	00.036	-00.056	02.615	-00.266
017.4	000.0	00.913	0.2693	00.043	0.0658	-00.2770	00.038	-00.045	03.390	-00.298
013.1	000.0	00.699	0.1504	00.020	0.0384	-00.2272	00.041	-00.027	04.647	-00.321
008.7	000.0	00.446	0.0623	-00.003	0.0174	-00.1554	00.028	00.006	07.158	-00.347